

Aus dem Adolf-Butenandt-Institut der
Ludwig-Maximilians-Universität München
Lehrstuhl: Stoffwechselbiochemie
Vorstand: Prof. Dr. rer. nat. Dr. h.c. Christian Haass

The FTLD risk factor TMEM106B controls lysosomal trafficking and dendrite outgrowth

- Dissertation -

zum Erwerb des Doktorgrades der Naturwissenschaften (Dr. rer. nat.)
an der Medizinischen Fakultät der Ludwig-Maximilians-Universität München



vorgelegt von
Benjamin Michael Schwenk
aus Augsburg

2014

Gedruckt mit Genehmigung der Medizinischen Fakultät der Ludwig-Maximilians-Universität
München

Betreuer: Prof. Dr. rer. nat. Dr. h.c. Christian Haass

Zweitgutachter: PD Dr. rer. nat. Ingrid Boeckhoff

Dekan: Prof. Dr. med. Dr. h.c. Maximilian Reiser, FACR, FRCR

Tag der mündlichen Prüfung: 26.03.2015

Eidesstattliche Versicherung

Ich erkläre hiermit an Eides statt, dass ich die vorliegende Dissertation mit dem Thema *The FTLD risk factor TMEM106B controls lysosomal trafficking and dendrite outgrowth* selbständig verfasst, mich außer der angegebenen keiner weiteren Hilfsmittel bedient und alle Erkenntnisse, die aus dem Schrifttum ganz oder annähernd übernommen sind, als solche kenntlich gemacht und nach ihrer Herkunft unter Bezeichnung der Fundstelle einzeln nachgewiesen habe.

Ich erkläre des Weiteren, dass die hier vorgelegte Dissertation nicht in gleicher oder in ähnlicher Form bei einer anderen Stelle zur Erlangung eines akademischen Grades eingereicht wurde.

München, _____

Benjamin Michael Schwenk

Life is what happens while you are busy making other plans.

John Lennon

Summary

Frontotemporal dementia is the second most common neurodegenerative disease in people younger than 65 years. Patients suffer from behavioral changes, language deficits and speech impairment. Unfortunately, there is no effective treatment available at the moment. Cytoplasmic inclusions of the DNA/RNA-binding protein TDP-43 are the pathological hallmark in the majority of FTLD cases, which are accordingly classified as FTLD-TDP. Mutations in *GRN*, the gene coding for the trophic factor progranulin, are responsible for the majority of familiar FTLD-TDP cases. The first genome-wide association study performed for FTLD-TDP led to the identification of risk variants in the so far uncharacterized gene *TMEM106B*. Initial cell culture studies revealed intracellular localization of TMEM106B protein in lysosomes but its neuronal function remained elusive.

Based on these initial findings, I investigated the physiological function of TMEM106B in primary rat neurons during this thesis. I demonstrated that endogenous TMEM106B is localized to late endosomes and lysosomes in primary neurons, too. Notably, knockdown of the protein does neither impair general neuronal viability nor the protein level of FTLD associated proteins, such as GRN or TDP-43. However, shRNA-mediated knockdown of TMEM106B led to a pronounced withering of the dendritic arbor in developing and mature neurons. Moreover, the strong impairment of dendrite outgrowth and maintenance was accompanied by morphological changes and loss of dendritic spines. To gain mechanistic insight into the loss-of-function phenotypes, I searched for coimmunoprecipitating proteins by LC-MS/MS. I specifically identified the microtubule-binding protein MAP6 as interaction partner and was able to validate binding. Strikingly, overexpression of MAP6 in primary neurons phenocopied the TMEM106B knockdown effect on dendrites and loss of MAP6 restored dendritic branching in TMEM106B knockdown neurons, indicating functional interaction of the two proteins. The link between a lysosomal and a microtubule-binding protein made me study the microtubule dependent transport of dendritic lysosomes. Remarkably, live cell imaging studies revealed enhanced movement of dendritic lysosomes towards the soma in neurons devoid of TMEM106B. Again, MAP6 overexpression phenocopied and MAP6 knockdown rescued this effect, strengthening the functional link. The MAP6-

5

independent rescue of dendrite outgrowth by enhancing anterograde lysosomal movement provided additional evidence that dendritic arborization is directly controlled by lysosomal trafficking.

From these findings I suggest the following model: TMEM106B and MAP6 together act as a molecular brake for the retrograde transport of dendritic lysosomes. Knockdown of TMEM106B and (the presumably dominant negative) overexpression of MAP6 release this brake and enhance the retrograde movement of lysosomes. Subsequently, the higher protein turnover and the net loss of membranes in distal dendrites may cause the defect in dendrite outgrowth. The findings of this study suggest that lysosomal misrouting in *TMEM106B* risk allele carrier might further aggravate lysosomal dysfunction seen in patients harboring *GRN* mutations and thereby contribute to disease progression.

Taken together, I discovered the first neuronal function for the FTLTDP risk factor TMEM106B: This lysosomal protein acts together with its novel, microtubule-associated binding partner MAP6 as molecular brake for the dendritic transport of lysosomes and thereby controls dendrite growth and maintenance.

Zusammenfassung

Frontotemporale Demenz ist die zweithäufigste Form neurodegenerativer Erkrankungen bei Menschen unter 65 Jahren. Patienten leiden an Verhaltensauffälligkeiten und Sprach- sowie Artikulationsstörungen. Leider steht zurzeit keine wirksame medikamentöse Therapie zur Verfügung. Das pathologische Hauptmerkmal der meisten FTLD-Fälle sind zytoplasmatische Einschlüsse des DNA/RNA-bindenden Proteins TDP-43. Diese Fälle werden entsprechend als FTLD-TDP klassifiziert. Für einen Großteil der familiären FTLD-TDP Fälle sind Mutationen in *GRN*, dem für den Wachstumsfaktor Progranulin kodierenden Gen, verantwortlich. Die erste für FTLD-TDP durchgeführte genomweite Assoziationsstudie führte zur Entdeckung von genetischen Varianten im bis dato uncharakterisierten Gen *TMEM106B*. Diese Varianten sind mit einem erhöhten Risiko an FTLD zu erkranken assoziiert. Initiale Studien in Zellkultur zeigten eine Lokalisierung des *TMEM106B* Proteins in Lysosomen, die Frage nach der neuronalen Funktion des Proteins blieb allerdings bisher unbeantwortet.

Auf diesen ersten Ergebnissen aufbauend untersuchte ich während meiner Dissertation die physiologische Funktion von *TMEM106B* in primären Rattenneuronen. Ich konnte zeigen, dass endogenes *TMEM106B* auch in primären Neuronen in späten Endosomen und Lysosomen lokalisiert ist. Beachtenswerterweise verminderte die Herunterregulierung (shRNA-vermittelter Gen-Knockdown) des Proteins weder das generelle Überleben der Neuronen noch die Level von anderen FTLD-assoziierten Proteinen, wie *GRN* oder *TDP-43*. Die Herunterregulierung von *TMEM106B* führte jedoch zu einem ausgeprägten Verlust von Dendriten in sich entwickelnden und ausgereiften Neuronen. Des Weiteren war die starke Beeinträchtigung dendritischen Wachstums und Aufrechterhaltung von einer morphologischen Veränderung und dem Verlust der Dornfortsätze begleitet. Um den Mechanismus dieser Phänotypen zu erklären, suchte ich nach *TMEM106B* coimmunopräzipitierenden Proteinen mittels Massenspektrometrie. Ich konnte das Mikrotubuli bindende Protein *MAP6* als spezifischen Bindungspartner identifizieren und die Interaktion beider Proteine validieren. Hervorzuheben ist, dass die Überexpression von *MAP6* in primären Neuronen den Effekt der Herunterregulation von *TMEM106B* auf die Dendriten kopierte und die Herunterregulation von *MAP6*

die dendritischen Verästelungen in TMEM106B depletierten Neuronen sogar wiederherstellen konnte. Diese Ergebnisse legen eine funktionelle Interaktion beider Proteine nahe. Die Verbindung zwischen einem lysosomalen und einem an die Mikrotubuli bindenden Protein brachte mich dazu, den Mikrotubuli abhängigen Transport von dendritischen Lysosomen zu untersuchen. Bemerkenswerterweise zeigten mittels Lebendzellmikroskopie erzeugte Aufnahmen eine erhöhte Bewegung dendritischer Lysosomen Richtung Zellsoma in TMEM106B depletierten Neuronen. Auch in diesem Kontext konnte die Überexpression von MAP6 den Effekt kopieren und die Herunterregulation von MAP6 den Effekt aufheben und somit die These einer funktionellen Interaktion festigen. Die MAP6 unabhängige Wiederherstellung des dendritischen Wachstums durch die Erhöhung des lysosomalen Transports in anterograder Richtung lieferte einen zusätzlichen Beweis dafür, dass das dendritische Wachstum direkt von lysosomalem Transport abhängt.

Ausgehend von diesen Ergebnissen schlage ich folgendes Modell vor: TMEM106B und MAP6 wirken zusammen als molekulare Bremse für den retrograden Transport dendritischer Lysosomen. Die Herunterregulation von TMEM106B und die (wahrscheinlich dominant negative wirkende) Überexpression von MAP6 lösen diese Bremse und verstärken die retrograde Bewegung von Lysosomen. Daraufhin könnten der gestiegene Proteinumsatz und der Verlust von Plasmamembranbestandteilen zu einem Fehler im dendritischen Wachstum führen. Die Ergebnisse dieser Arbeit legen nahe, dass fehlerhafter, lysosomaler Transport in TMEM106B Risikoallelträgern zu einer Verstärkung der lysosomalen Fehlfunktion in Patienten mit GRN Mutation führt und dabei zur Krankheitsentwicklung beiträgt.

Zusammengefasst habe ich die erste neuronale Funktion für den FTLTDP Risikofaktor TMEM106B entdeckt: Dieses lysosomale Protein wirkt zusammen mit seinem neuentdeckten, Mikrotubuli assoziierten Bindungspartner MAP6 als molekulare Bremse für den dendritischen Transport von Lysosomen und kontrolliert dadurch Wachstum und Aufrechterhaltung von Dendriten.

Table of contents

Eidesstattliche Versicherung	2
Summary	5
Zusammenfassung	7
Table of contents	9
List of figures	11
List of abbreviations	12
I. Introduction.....	15
1. FTLD	15
1.1 Clinical presentation.....	15
1.2 Molecular genetics of the FTLD subtypes	19
1.3 TMEM106B	25
2. Lysosomes and lysosomal transport.....	28
2.1 Function – degradative and non degradative.....	28
2.2 Biogenesis	29
2.3 Regulation	31
3. Microtubules and Microtubule-dependent transport	32
3.1 Microtubules.....	32
3.2 Microtubule dependent transport.....	34
3.3 Microtubule associated proteins (MAPs)	37
II. Aim of the study	40
III. Materials and Methods	41
1. Materials.....	41
1.1 Equipment	41
1.2 Chemicals, enzymes and antibodies.....	45
1.2.6 Antibodies	49
1.3 DNA oligonucleotides and plasmids	51
1.4 Buffer	55
1.5 Services	59
1.6 Software and Online tools	59
1.7 Cell lines and bacteria strains.....	60
2. Methods.....	61
2.1 Molecular Biology.....	61
2.2 Cell biology	67
2.3 Protein biochemistry.....	71
2.4 Imaging techniques.....	77
2.5 Mass spectrometry (in collaboration with Sebastian Hög).....	80

2.6 Statistical analysis	81
IV. Results	82
1. Generation and validation of TMEM106B shRNA and antibodies.....	82
2. Effects of TMEM106B knockdown in primary neurons.....	84
2.1 TMEM106B knockdown does not affect viability of primary neurons	84
2.2 TMEM106B is mainly localized in dendritic lysosomes	85
2.3 TMEM106B knockdown does not change lysosomal parameters	88
3. Effect of TMEM106B knockdown on neuronal morphology	91
3.1 TMEM106B knockdown inhibits dendritic branching.....	91
3.2 TMEM106B knockdown impairs spines and synaptic markers.....	95
3.3 TMEM106B knockdown increases axonal length.....	96
4. TMEM106B interacts with MAP6	99
4.1 Identification of MAP6 as TMEM106B binding partner in rat brain.....	99
4.2 Mapping of the MAP6/TMEM106B interaction domain in HEK293 cells	103
5. MAP6 function in dendrites	105
5.1 MAP6 affects dendritic branching.....	105
5.2 MAP6 depletion rescues TMEM106B knockdown phenotype.....	108
6. Role of TMEM106B in lysosomal Transport.....	110
6.1 TMEM106B knockdown affects lysosomal transport.....	110
6.2 MAP6 affects lysosomal transport	117
6.3 MAP6 depletion rescues TMEM106B knockdown effect on lysosomal transport	118
6.4 Overexpressed MAP6 co-migrates with dendritic lysosomes.....	121
6.5 Low dose Nocodazole rebalances lysosomal trafficking and partially rescues dendrite withering	123
6.6 Enhancing anterograde transport by dnRILP stimulates dendrite growth and rescues TMEM106B knockdown phenotype.....	126
V. Discussion.....	130
1. Genome-wide association study identified <i>TMEM106B</i> risk variants.....	130
2. Neuronal Phenotype: Loss of TMEM106B impairs dendrite and spine growth and maintenance ...	130
3. Interaction of TMEM106B with MAP6	133
4. Dendritic trafficking of lysosomes is affected by TMEM106B and MAP6.....	134
5. Axonal phenotype.....	137
6. Model.....	138
7. Implications for FTLN and other neurodegenerative diseases	141
8. Summary, open questions and future perspectives.....	143
VI. References	146
VII. Acknowledgements.....	167
VIII. Publications	169

List of figures

Figure 1: molecular and pathological Classification of FTLD.....	19
Figure 2: Domain structure and topology of TMEM106B.....	27
Figure 3: Secretory and endocytic pathway.....	30
Figure 4: Microtubule assembly and dynamics.....	33
Figure 5: Domain structure and isoforms of MAP6.....	38
Figure 6: Validation of polyclonal TMEM106B antibodies.....	83
Figure 7: TMEM106B knockdown does not affect general neuron viability.....	84
Figure 8: TMEM106B is localized in late endosomes / lysosomes of primary neurons.....	86
Figure 9: TMEM106B is also occurring in axons of primary neurons.....	88
Figure 10: Lysosomal morphology is unchanged upon TMEM106B knockdown.....	89
Figure 11: Lysosomal pH-value is unchanged upon TMEM106B knockdown.....	91
Figure 12: TMEM106B knockdown impairs dendrite branching and maintenance.....	92
Figure 13: Validation of the TMEM106B knockdown phenotype by expression of a shRNA resistant mutant.....	93
Figure 14: TMEM106B knockdown increases length of the main dendrite.....	94
Figure 15: dominant-negative Rab7a impairs dendritic arborization.....	95
Figure 16: Changes in spine and axon morphology upon TMEM106B knockdown.....	98
Figure 17: MAP6 peptides identified by mass-spec.....	100_Toc391898130
Figure 18: TMEM106B interacts with MAP6 in rat brain.....	101
Figure 19: TMEM106B and MAP6 peak in the lysosomal fraction of a density gradient.....	103
Figure 21: TMEM106B N-terminus binds to MAP6 C-terminus.....	104
Figure 22: Effects of MAP6 overexpression and knockdown on dendritic branching.....	106
Figure 23: Knockdown of MAP6 in primary neurons.....	106
Figure 24: Validation of MAP6 shRNA using human MAP6.....	107
Figure 25: MAP6 knockdown rescues the branching effect of TMEM106B knockdown.....	108
Figure 26: Validation of the specificity of shMAP6 rescue using shMap2.....	109
Figure 27: TMEM106B controls retrograde trafficking of dendritic late endosomes/lysosomes.....	111
Figure 28: TMEM106B knockdown enhances retrograde movement of late endosomes/lysosomes.....	112
Figure 29: Reintroduction of shRNA resistant TMEM106B rescues impaired trafficking.....	114
Figure 30: TMEM106B knockdown does not change trafficking of axonal lysosomes.....	115
Figure 31: TMEM106B knockdown does not change mitochondrial transport in dendrites.....	116
Figure 32: MAP6 regulates retrograde trafficking of late endosomes / lysosomes in dendrites.....	118
Figure 33: MAP6 knockdown rebalances lysosomal trafficking in TMEM106B knockdown neurons....	120
Figure 34: MAP6-GFP comigrates with LAMP1-RFP in dendrites.....	122
Figure 35: Nocodazole treatment rebalances lysosomal trafficking in TMEM106B knockdown neurons	124
Figure 36: Nocodazole treatment rescues the branching effect of TMEM106B knockdown.....	125
Figure 37: Overexpression of dominant negative RILP increases anterograde movement of lysosomes.	127
Figure 38: dn RILP restores dendritic branching in TMEM106B knockdown neurons.....	128
Figure 39 Model of the effects of TMEM106B and MAP6 on lysosomal transport.....	140
Table 1: unique peptides for MAP6 identified by LC-MS/MS.....	101

List of abbreviations

AChEI	acetylcholinesterase inhibitor
AD	Alzheimer's disease
ADP/GDP	adenosine/guanidine -diphosphate
ALS	Amyotrophic lateral sclerosis
ANOVA	analysis of variance
AP1-4	adaptin1-4
APOE	apolipoprotein E
APS	ammonium persulfate
ARMD	age-related macular degeneration
ATP/GTP	adenosine/guanidine-triphosphate
BIBD	basophilic inclusion body disease
BS3	Bis-sulfosuccinimidyl suberate
BSA	bovine serum albumin
bvFTD	behavioral variant FTD
C9orf72	C9 open reading frame 72
Ca	constitutive active
cDNA	complementary DNA
CHMP2B	Charged multivesicular body protein 2b
CID	collision-induced dissociation
CIP	calf intestine phosphatase
CLEAR	coordinated lysosomal expression and regulation
CMT2B	Charcot-Marie-Tooth-Type 2B
COX8	cyclooxygenase 8
CSF	cerebral spinal fluid
CT	C-terminus
CTR	C-terminal repeat
DIV	days <i>in vitro</i>
DMSO	Dimethylsulfoxide
dn	dominant negative
DNA	deoxyribonucleic acid
DPR	di-peptide-repeat
DTI	diffusion tensor imaging
DTT	dithiothreitol
E18	embryonic day 18
E.coli	Escherichia coli
ECL	enhanced chemiluminescence
EDTA	ethylenediaminetetraacetic acid
EEG	electro encephalogram
EMCCD	electron-multiplying charged coupled device
ER	endoplasmic reticulum
EWS	Ewing sarcoma protein
fcMRI	functional connectivity MRI
FCS	fetal calf serum
FDA	US food and drug administration
FDG-PET	fluorodesoxyglucose-positron emission tomography
FDR	false discovery rate

FET	FUS, EWS, TAF15
FTD	frontotemporal dementia
FTLD(-U)	frontotemporal lobar degeneration (with ubiquitin pathology)
FUS/TLS	Fused-in-sarcoma/Translocated-in-liposarcoma
GFP/EGFP	green fluorescent protein/enhanced GFP
GluA2	ionotropic AMPA glutamate receptor 2
GRIP	glutamate receptor interacting protein
GRN	Progranulin
GST	glutathione-S-transferase
GWAS	genome-wide association study
HBSS	Hank's balanced salt solution
HEK293 cells	human embryonic kidney cells
HOPS complex	homotypic fusion and protein sorting complex
HRP	horse radish peroxidase
IB	immunoblot
IF	immunofluorescence
IP	immunoprecipitation
IPTG	Isopropyl β -D-1-thiogalactopyranoside
kDa	kilodalton
KIF	kinesin superfamily proteins
LAMP1	lysosomal-associated membrane protein 1
LB	lysogeny broth
LC-MS/MS	Liquid chromatography-tandem mass spectrometry
LD	linkage disequilibrium
LOAD	late onset AD
LRO	Lysosomal related organelles
M6PR	Mannose-6-phosphate receptor
MAP	microtubule-associated protein
MAPT	microtubule-associated protein Tau
MARK	MAP/microtubule affinity-regulating kinase
MBP	Mannose-binding protein
MND	motor neuron disease
MRI	magnetic resonance imaging
MT	microtubule
MTOC	microtubule organization center
mTORC1	mammalian target of rapamycin complex1
NA	numeric aperture
NCL	neuronal ceroid lipofuscinosis
NEAA	non-essential amino acids
NIFID	neuronal intermediate filament inclusion disease
NMDAR	N-Methyl-D-aspartic acid receptor
NT	N-terminus
OD280	optical density
PABA	poly(A)-binding protein
PBS	phosphate-buffered saline
PCR	polymerase chain reaction
PDL	poly-D-lysine

PFA	paraformaldehyde
PNFA	progressive nonfluent aphasia
PPA	primary progressive aphasia
PSD-95	post-synaptic density protein 95
PVDF	polyvinylidene difluoride
PY-NLS	proline-tyrosine nuclear localization signal
qPCR	quantitative PCR
RAB	member RAS oncogene family
RAN translation	repeat associated non-ATG translation
RFP	red fluorescent protein
RILP	Rab-interacting lysosomal protein
(m)RNA	(messenger) ribonucleic acid
RT	room temperature
RT-PCR	reverse-transcriptase PCR
SD	semantic dementia
SDS-PAGE	sodium dodecyl sulfate- polyacrylamide gel electrophoresis
shRNA	short hairpin RNA
SNARE	soluble NSF attachment protein receptor
SNP	single nucleotide polymorphism
SOD1	superoxide dismutase 1
SPECT	single-photon emission computed tomography
SSRI	selective serotonin reuptake inhibitor
(E-/F-/N-) STOP	(early-/fibroblastic- /neuronal-) stable tubule-only polypeptide
SV2	synaptic vesicle glycoprotein 2
TAF-15	TATA box-binding protein (TBP)-associated factor 68 kDa
TARDBP/ TDP-43	transactive response DNA-binding protein 43
TEMED	tetramethylethylenediamin
TFEB	transcription factor EB
TfR	Transferrin receptor
TGN	trans-golgi network
TIA1	cytotoxic granule-associated RNA binding protein 1
+TIP	microtubule plus-end tracking protein
TMD	transmembrane domain
TMEM106B	transmembrane protein 106B
TOM20	translocase of outer membrane 20
UBQLN2	ubiquilin2
UPS	ubiquitin-proteasome system
UV	ultraviolet
VAMP7	vesicle-associated membrane protein 7
VCP	valosin containing protein
VPS10	vacuolar protein sorting homolog receptor 10
wt	wild-type
XTT	2,3-bis-(2-methoxy-4-nitro-5-sulfophenyl)-2H-tetrazolium-5-carboxanilide
YWHAZ	tyrosine 3-monooxygenase/tryptophan 5-monooxygenase activation protein, zeta

I. Introduction

1. FTLD

1.1 Clinical presentation

Frontotemporal dementia (FTD) was first described by Czech neurologist and psychiatrist Arnold Pick in 1892. The patient, a 71-year old man, presented with gradual mental retardation and speech disturbances, autopsy revealed cerebral atrophy primarily in the left hemisphere (Pick, 1892). Two decades later, Alois Alzheimer found and stained characteristic inclusions in these patients, henceforth called Pick bodies (Alzheimer, 1911). However, not until the last 20 years pathological and mechanistic findings helped researchers to understand disease mechanisms and provided potential drug targets.

1.1.1 Clinical Symptoms of FTLD

Frontotemporal lobar degeneration (FTLD) is the pathological syndrome underlying a group of diseases classified by the overarching term of frontotemporal dementia. In the following the term FTLD is used to designate both disease and pathology. FTLD is a presenile neurodegenerative disease with an average onset of 58 years (Johnson et al., 2005). The clinical presentation of FTLD is subclassified into behavioral variant of FTD (bvFTD), progressive non fluent aphasia (PNFA) and semantic dementia (SD). More than 50 % of all cases group into the first category. Patients suffering from bvFTD usually present with changes in behavior and personality (disinhibition, apathy, loss of empathy and social competence, stereotypic behavior) while learning and memory are preserved (Rascovsky et al., 2011). PNFA and SD as of late combined in the term ‘primary progressive aphasia’ (PPA) both occur in approximately similar probability in the rest of the patients (Gorno-Tempini et al., 2011). Main symptoms in patients suffering from PNFA are ‘non fluent’, agrammatic speech and anomia. These are often accompanied by apraxia of speech, which designates the inability to plan and coordinate the movements necessary for speech (Josephs et al., 2011). In contrast, patients affected by semantic dementia develop impaired comprehension, impaired conceptual

knowledge and anomia while speech production is still functional (Sieben et al., 2012).

1.1.2 Epidemiology of FTLD

FTLD is the second most common neurodegenerative disease in people under the age of 65 years (Harvey et al., 2003). The disease has a prevalence of 10-20 patients per 100,000 people and an incidence of 3.5-4.1 per 100,000 / year in the age group of 45 – 64 years (reviewed in (Van Langenhove et al., 2012)). FTLD has a strong genetic component, as between 30-50 % of all patients have at least one relative with similar clinical symptoms. And in up to 25 % of patients the disease actually segregates with an autosomal dominant pattern. Proteins whose underlying genes are found to be mutated in patients, often aggregate in the brain and exhibit the characteristic neuropathology (Goldman et al., 2007; Goldman et al., 2005). Interestingly, aggregates of these proteins are also found in sporadic cases without known mutations rendering these proteins a likely cause of the disease (Dormann and Haass, 2011). Moreover, just recently variants in the so far undescribed gene *transmembrane protein 106B* (*TMEM106B*) were discovered to increase the risk for a subclass of sporadic and familial cases of FTLD (Van Deerlin et al., 2010).

FTLD has a pronounced overlap with another presenile neurodegenerative disease, amyotrophic lateral sclerosis (ALS). Both diseases share many genetic and pathological features. Transactive response (TAR)-DNA-binding protein 43 (TDP-43) and Fused-in-sarcoma (FUS) inclusions are found in both diseases and *TARDBP* and *FUS* mutations – usually a cause for ALS – lead in rare cases to FTLD. And with the discovery of the C9orf72 hexanucleotide-repeat-expansion a common genetic denominator was found that can cause either disease or a combined form. Moreover, 15 % of ALS patient develop FTLD symptoms and vice versa thus suffering from a hybrid forms both diseases (Ringholz et al., 2005; Wheaton et al., 2007). Remarkably, in up to 75 % of ALS patients cognitive symptoms are found in late stages of the disease (Strong et al., 2009). However, pure genetic forms of the disease are observed as well. For example progranulin (GRN) mutations lead exclusively to FTLD while superoxide dismutase 1 (SOD1) mutations cause always ALS. These observations render FTLD and ALS a disease continuum with the pure

forms as distinct ends (Ling et al., 2013; Morris et al., 2012; Van Langenhove et al., 2012).

1.1.3 Pathology of FTLD

The gross pathological changes seen in almost all patients are selective atrophy in the frontal and temporal lobe, with neuronal degeneration or neuron loss, spongy changes of the brain structure, neuroinflammation, gliosis and intracellular proteinaceous inclusions. However, apart from the clinical sub-classification the disease can also be sub-grouped according to the aggregating proteins and the neuropathology seen in affected brain. FTLD-TAU, the subgroup which is defined by inclusions of hyperphosphorylated Tau protein accounts for approximately 40% of all FTLD cases (Joachim et al., 1987). Most of the remaining patients present with Tau-negative, ubiquitin-positive inclusions and thus are diagnosed with FTLD-U. These cases can be further subdivided in mainly FTLD-TDP – patients show TDP-43 positive inclusions, and rarer cases of FTLD-FUS and FTLD-UPS – patients show FUS inclusions respectively inclusions whose only known constituents are components of the ubiquitin-proteasome system (UPS) such as p62. Other types or even dementia lacking distinctive histopathology are found but are very rare (Pan and Chen, 2013). An association between neuropathological and the clinical subtype is observed but is not very strict: FTLD-TDP mainly leads to bvFTD or SD whereas FTLD-Tau causes usually PNFA. If patients are additionally diagnosed with motor neuron disease (MND), it is very likely that a TDP-43 or FUS proteinopathy is observed (reviewed in (Pan and Chen, 2013; Rademakers et al., 2012)).

1.1.4 Diagnosis of FTLD

Consensus diagnostic criteria for FTLD were originally defined in 1998 by Neary and colleagues and later partially revised by Rascovsky et al., based on clinical inclusion and exclusion features, neuropsychological investigations and brain imaging. Core diagnostic features include insidious onset and gradual progression for each of the three subgroups of FTLD. Decline in social conduct and emotional blunting are key symptoms for bvFTD, non-fluent spontaneous speech for PNFA and language and perceptual disorder for SD. Furthermore clinicians examine patients

with neuropsychological examinations especially for frontal lobe function, speech and language abilities (Neary et al., 1998; Rascovsky et al., 2011). In contrast to patients suffering from stroke, individuals affected by FTLD have normal activity in the electroencephalography (EEG) but structural and functional brain imaging reveals often asymmetrical abnormalities and atrophy in the frontal or temporal lobe. While structural and functional magnetic resonance imaging (MRI) help to define the areas of atrophy, functional connectivity MRI (fcMRI) and diffusion tensor imaging (DTI) are used to sub-classify FTLD and to establish a differential diagnosis of bvFTD. Other imaging techniques such as fluorodesoxyglucose-positron emission tomography (FDG-PET) and single-photon emission computed tomography (SPECT) can help to distinguish FTLD from other dementias (McGinnis, 2012).

1.1.5 Therapy of FTLD

So far no FDA approved treatment for FTLD exists, even though several studies are ongoing e.g. with the N-methyl-D-aspartic acid receptor (NMDAR) antagonist memantine, typically used for Alzheimer's disease (AD) (Boxer et al., 2009). In the past also other AD drugs as the acetylcholinesterase inhibitors (AChEI) donepezil and rivastigmine were tested but with largely negative outcome (Mendez, 2009). Apart from that, FTLD patients primarily receive symptomatic treatment with psychotropic drugs as selective serotonin reuptake inhibitors (SSRI) or atypical antipsychotics for behavioral abnormalities (Mendez, 2009). Additional non-pharmacological interventions, such as education, behavioral management and interventions, are an important relief for patients and caregivers (Manoochehri and Huey, 2012). Future, more causal treatment strategies may include interference with the expression and splicing of disease related proteins, the regulation of microtubule stability, the prevention of protein aggregation and the restoration of the cellular degradation systems (Trojanowski et al., 2008; Vossel and Miller, 2008).

1.2 Molecular genetics of the FTLD subtypes

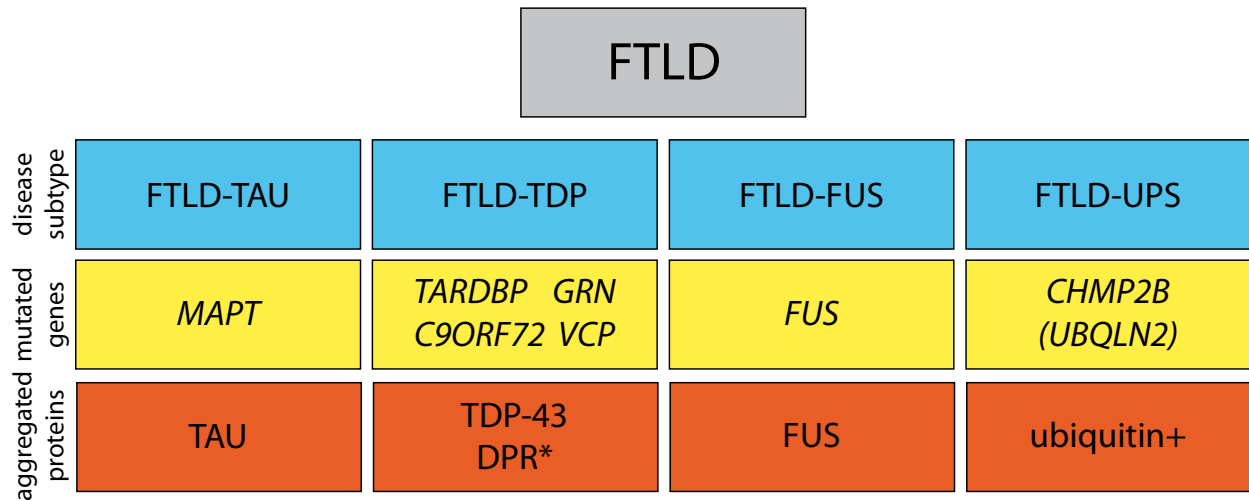


Figure 1: Genetic and pathological Classification of FTLD

The disease is subcategorized according to the aggregating proteins. Disease subtypes are depicted in blue boxes, underlying mutations in yellow boxes and aggregating proteins in orange boxes. Gene in parentheses has no definite association with FTLD. Asterisk denotes that rare DPR-positive cases are observed without TDP-43 pathology. Adapted from (Dormann and Haass, 2013).

1.2.1 FTLD-TAU

The first gene identified causing FTLD was *Microtubule-associated protein Tau* (*MAPT*). Mutations in the *MAPT* gene result in hyperphosphorylated intracellular inclusions (neurofibrillary tangles) of the Tau protein and almost exclusively to FTLD-TAU (Hutton et al., 1998). Tau is a microtubule-binding protein expressed primarily in the nervous system. Apart from the stabilization of microtubules its main functions lie in regulation of microtubule-dependent transport and scaffolding of signaling complexes thereby controlling their activity (Morris et al., 2011). Most pathogenic *MAPT* mutations cluster around exon 9 to 13, which encode the microtubule binding domains of the protein. These mutations either change the ratio of the *MAPT* splice variants which consequentially leads to impaired microtubule binding of Tau or directly affect the binding. Numerous studies report that reduced binding to the cytoskeleton causes altered microtubule stability and disturbed

microtubule-dependent axonal transport by now unbound and eventually mis-localized Tau (reviewed in (Pan and Chen, 2013; Rademakers et al., 2004; Sieben et al., 2012)). Additionally, aggregated Tau protein – depending on its phosphorylation status – as well as dendritically redistributed soluble tau seems to mediate toxic signaling (Haass and Mandelkow, 2010; Ittner et al., 2010).

1.2.2 FTLD-TDP

1.2.2.1 GRN

The first causative gene for Tau negative FTLD was independently described by two groups in 2006. Interestingly, the mutations were found in *GRN*, a gene located close to the *MAPT* locus on chromosome 17 (Baker et al., 2006; Cruts et al., 2006). *GRN* mutations lead exclusively to and are one of the major causes of FTLD-TDP pathology (Nicholson et al., 2012). *GRN* is a secreted glycoprotein that can be further cleaved by extracellular proteases into 7.5 cysteine-rich granulin peptides. Although general, trophic functions of *GRN* in wound healing and tumorigenesis as well as its anti-inflammatory capacity are relatively well understood, the exact role in brain is not completely clear (He and Bateman, 2003). In dissociated neurons *GRN* seems to promote neurite outgrowth and neuronal survival (Gass et al., 2012; Van Damme et al., 2008). Especially the role of the small granulin peptides remains mostly elusive. They seem to antagonize some aspects of *GRN* function as they are proinflammatory (Zhu et al., 2002), but may act similarly to the full length protein in terms of neurite outgrowth and neuronal survival (Gass et al., 2012). Moreover, every granulin peptide acts differently and they seem to inhibit and antagonize each other (Cenik et al., 2012). *GRN* mutations are inherited in an autosomal dominant pattern. Most heterozygous mutations are null mutations due to nonsense mediated RNA decay, thus leading to *GRN* haploinsufficiency in patients. In rarer cases, mutations rather lead to mislocalization, reduced expression or impaired secretion of the protein than to a complete loss of the mRNA. The genetic findings argue for a loss of function pathogenesis in *GRN* mutation carriers (reviewed in (Nicholson et al., 2012; Ward and Miller, 2011)).

To study the impact of *GRN* loss on FTLD, *GRN* knockout mice were generated. Similar to FTLD patients, mice show decreased survival and behavioral

abnormalities. Further phenotypes include pronounced microgliosis, especially in hippocampus and cortex and ubiquitinated protein aggregates in neurons (Kayasuga et al., 2007; Yin et al., 2010). More comprehensive analysis of the knockout animals revealed Cathepsin D pathology and lipofuscin aggregates in the brain – typically a sign of lysosomal deficiency (Ahmed et al., 2010; Wils et al., 2012). Strikingly, just recently two human siblings with homozygous *GRN* loss of function mutations have been identified. Both suffer from adult neuronal ceroid lipofuscinosis (NCL), a lysosomal storage disease, instead of FTLN-TDP as seen in heterozygous carriers (Smith et al., 2012). Another link between *GRN* and the lysosome is the recent identification of sortilin as scavenger receptor for the protein in neurons. Upon binding to sortilin, *GRN* is re-endocytosed and rapidly transported to the lysosome. In line with these findings, *GRN* level are elevated in the brain of sortilin knockout mice (Hu et al., 2010).

In 2010, *TMEM106B* was identified as the first genetic risk factor for FTLN-TDP with *GRN* mutations. *TMEM106B* risk variants elevate the penetrance of *GRN* mutations and decrease the age of onset in mutation carriers (Van Deerlin et al., 2010). It was suggested that these risk variant influence *GRN* mRNA or protein level (Cruchaga et al., 2011; Finch et al., 2011), but the physiological function of *TMEM106B* was unclear.

1.2.2.2 TDP-43

Although TDP-43 is the eponymous protein for FTLN-TDP, mutations in its coding gene *TARDBP* usually lead to ALS-TDP. Only in very rare cases these mutations cause FTLN-TDP ((Benajiba et al., 2009; Borroni et al., 2009; Gitcho et al., 2009; Tamaoka et al., 2010). TDP-43 is a DNA/RNA-binding protein with functions in transcription, RNA-splicing and microRNA processing (Sieben et al., 2012). *TARDBP* mutations cluster in the C-terminal glycine-rich domain involved in protein-protein interaction (Pesiridis et al., 2009). Major pathological hallmark of FTLN-TDP are TDP-43-positive, ubiquitin-positive, α -Synuclein-negative, Tau-negative inclusions in neurons and glia cells (Arai et al., 2006; Neumann et al., 2006). These inclusions contain full-length and C-terminal fragments of hyperphosphorylated and ubiquitinated TDP-43 as well as proteins responsible for

stress granule formation, such as poly(A)-binding protein (PABA) and cytotoxic granule-associated RNA binding protein 1 (Tia1) (Fujita et al., 2008; Liu-Yesucevitz et al., 2010). These findings suggest a possible pathomechanism: stress granules might be precursors of the insoluble aggregates and mediate toxicity (Dormann and Haass, 2011). Another possible disease mechanism leading to neurotoxicity of TDP-43 mutations are deficits in RNA splicing or metabolism as the inclusion bearing cells are mostly devoid of intra-nuclear TDP-43 (Arai et al., 2006; Neumann et al., 2006). Notably, pronounced toxicity was observed in overexpression and knockout animal models (Feiguin et al., 2009; Johnson et al., 2009). Therefore the question arises if loss of TDP-43 function or toxic gain of function of the aggregates is the disease causing mechanism. So far neither animal models nor cell culture experiments could answer this question satisfactorily (Slegers et al., 2010).

1.2.2.3 *C9orf72*

The most common genetic cause for FTL-D-TDP (as well as for ALS-TDP and overlapping forms of the disease) are mutations in *C9orf72*, coding for a so far uncharacterized protein. A GGGGCC hexanucleotide-repeat expansion in the promoter region or the first intron, depending on the transcript, was found in patients. In healthy controls 0 - 20 GGGGCC repeats are observed, whereas up to several thousand exist in patients. The classical FTL-D-TDP pathology is accompanied by RNA foci and a reduction of the mRNA level of the longer isoform of *C9orf72* (DeJesus-Hernandez et al., 2011; Renton et al., 2011). In most hexanucleotide-repeat-expansion carriers TDP-43-positive, p62-positive, Tau-negative neuronal and glial inclusions in the cortex, the hippocampus and remarkably also the cerebellum – usually free of other aggregates in FTL-D – are found (Al-Sarraj et al., 2011). Strikingly, many aggregates in the brain of *C9orf72*-patients are TDP-43-negative and consist mainly of di-peptide-repeat-proteins (DPRs) which are ATG-independently translated from the repeat mRNA (Ash et al., 2013; Mori et al., 2013c). So far three independent but not mutually exclusive scenarios for the pathomechanism of the *C9orf72* hexanucleotide-repeat expansion have been proposed: haplo-insufficiency thus loss of function of the *C9orf72* protein

(DeJesus-Hernandez et al., 2011; Gijssels et al., 2012), RNA mediated toxicity by sequestration of RNA binding proteins by the repeat RNA (Mori et al., 2013b) and ATG-independent translation of the repeat into aggregating dipeptide repeat proteins and DPR-toxicity (Mori et al., 2013c). Interestingly, so-called repeat associated non-ATG (RAN) translation was first described in another neurodegenerative disease, spinocerebellar ataxia type 8 (SCA8), where polyalanin, polyglutamine and polyserine peptides are translated from a trinucleotide-repeat expansion (Zu et al., 2011). Rare *C9orf72* FTLD cases without TDP-43 pathology suggest that primarily TDP-43 independent mechanisms cause disease in *C9orf72*-patients. Moreover, DPR aggregation might be a potential prerequisite for TDP-43 pathology in the *C9orf72* cases (Brettschneider et al., 2012; Mori et al., 2013a; Proudfoot et al., 2014).

1.2.3 FTLD-FUS

Another rare subgroup of FTLD cases was redefined in 2009 as FTLD-FUS with the discovery of FUS aggregates as a common pathological hallmark in patients with atypical FTLD with ubiquitin pathology (aFTLD-U), basophilic inclusion body disease (BIBD) and neuronal intermediate filament inclusion diseases (NIFID) (Mackenzie et al., 2010). Similar to TDP-43, FUS is a DNA/RNA-binding protein with main functions in transcriptional regulation, mRNA transport and splicing (Dormann and Haass, 2013). Although rare cases of FTLD-FUS with *FUS/TLS* mutations have been reported (Kwiatkowski et al., 2009; Vance et al., 2009), they usually cause ALS-FUS. FUS inclusions in FTLD are mainly observed in sporadic cases without mutations (Munoz et al., 2009; Neumann et al., 2009). *FUS* mutations causing FTLD or ALS cluster in the C-terminal region of the gene. This region encodes the non-canonical PY-nuclear localization signal (PY-NLS) whose function is consequently impaired by a reduced affinity to the nuclear import factor transportin (Dormann et al., 2010). Hence, redistribution of FUS from the nucleus to the soma and cytoplasmic aggregation of the protein is observed in patient brains. So far known constituents of the ubiquitinated, p62-positive inclusions are the other two members of the FET family of proteins Ewing sarcoma protein (EWS) and TATA box-binding protein (TBP)-associated factor 15 (TAF-15) (Neumann et al., 2011) and stress granule marker (Dormann et al., 2010). Nuclear clearance of FUS

and FUS aggregation in turn opens the question whether the pathomechanism of FTLD-FUS comprises loss of nuclear function of FUS or toxic gain of function of the aggregates. Similar to FTLD with TDP-43 pathology, the answer remains elusive. Loss-of-function studies suggest FUS as an important regulator of neuronal health (Fujii et al., 2005). Deficits seen in knockout neurons and animals may be due to an impairment of alternative splicing events since the level and splicing of many mRNAs are affected by depletion of FUS (Ishigaki et al., 2012; Lagier-Tourenne et al., 2012; Rogelj et al., 2012). The misregulated mRNAs are enriched for neuronal targets, among them Tau, a protein already implicated in the pathogenesis of FTLD (Orozco et al., 2012).

1.2.4 FTLD-UPS

Other mutations leading to pure FTLD or ASL-FTLD have been reported in the genes coding for valosin containing protein (*VCP*) (Watts et al., 2004), charged multivesicular body protein 2b (*CHMP2B*) (Momeni et al., 2006b) and ubiquilin2 (*UBQLN2*) (Deng et al., 2011; Synofzik et al., 2012). Since all these proteins are implicated in protein sorting and degradation, the dysfunction of the ubiquitin-proteasome system leading to impaired protein degradation might be one of the key pathomechanisms of FTLD. Consequentially, all remaining cases, devoid of TDP-43, FUS or Tau pathology but positive for ubiquitin and p62 aggregates, are summarized in the term FTLD-UPS (Mackenzie et al., 2010).

In summary three main pathomechanisms become evident for the FTLD-continuum: disturbed RNA-metabolism, toxicity of the aggregating proteins and dysfunction of the cellular degradation system.

1.3 TMEM106B

1.3.1 Identification as risk factor

In 2010, a single linkage disequilibrium (LD) block on chromosome 7p21 was identified as the first risk locus for FTLD. Three single nucleotide polymorphisms (SNPs) clustering in and around *TMEM106B*, a gene of unknown function, reached genome-wide significance. These variants increased the risk of developing FTLD-TDP, especially in individuals with *GRN* mutations (GRN+/FTLD-TDP) (Van Deerlin et al., 2010). Most replication studies confirmed the association of *TMEM106B* SNPs with GRN+/FTLD-TDP risk (Cruchaga et al., 2011; Finch et al., 2011; van der Zee et al., 2011). Homozygosity for the protective minor allele CC of the most statistically significant SNP rs1990622 - 7kb downstream of *TMEM106B* – was found in 2.6 % of patients and 19.1 % of controls (Finch et al., 2011). Some studies found even a correlation of the risk variants with disease age of onset or GRN plasma levels. The increased risk especially in GRN mutation carriers, changed GRN mRNA level and the additionally reported correlation between *TMEM106B* protein and GRN mRNA level strongly point to a functional relationship of both proteins (Cruchaga et al., 2011; Finch et al., 2011; Rollinson et al., 2011; van der Zee et al., 2011). The impact of the risk SNPs on *TMEM106B* mRNA or protein levels is still under debate. The original study showed elevated *TMEM106B* mRNA levels in risk SNP carriers whereas replications in other patient cohorts did not confirm this (Van Deerlin et al., 2010; van der Zee et al., 2011). Nicholson and colleagues reported that the protein level of the protective *TMEM106B* T185S variant is decreased compared to the wild-type (wt) protein. However, the SNP leading to the amino-acid exchange in the protein, although in perfect LD with rs1990622, is itself not statistically significant towards the risk of FTLD-TDP (Nicholson et al., 2013). Several recent studies suggest a role for *TMEM106B* not only in FTLD but also in broader field of neurodegeneration: Although *TMEM106B* risk variants are not genetically associated with ALS per se, they decrease the cognitive abilities in these patients (Vass et al., 2011). Furthermore, the protective allele of rs1990622 reduced the risk for TDP-43 pathology and hippocampal sclerosis in AD patients (Rutherford et al., 2012).

Interestingly, the same polymorphism seems to influence – in interaction with apolipoprotein E (APOE) variant $\epsilon 4$ – the risk of late onset Alzheimer's disease (LOAD) in a big Chinese population (Lu et al., 2013).

1.3.2 Localization and function

Busch et al. demonstrated that TMEM106B is expressed in neurons, glia and endothelial cells in cortex and parts of the hippocampus, but not in the dentate gyrus and the cerebellum of the human brain (Busch et al., 2013). Cell culture studies revealed that TMEM106B is an integral type 2 transmembrane protein which is highly N- but not O-glycosylated. Endoglycosidase-H-resistant complex glycosylation suggest transport of the protein beyond the early Golgi apparatus into the late secretory pathway. The glycosylation pattern influences targeting of the protein as mutations in the different glycosylation sites either led to retention in the ER or transport to the plasma membrane. Immunofluorescence (IF) studies in cell-lines revealed that overexpressed as well as endogenous TMEM106B is located mainly in Lamp1-positive late-endosomes and lysosomes. Inhibiting lysosomal proteases by leupeptine or inhibiting the acidification of the lysosome by Bafilomycin A1 leads to an accumulation of TMEM106B, providing further proof of lysosomal targeting (Lang et al., 2012). Overexpression of TMEM106B is reported to increase lysosomal size and change lysosomal morphology. Additionally, lysosomal acidification and thus their degradative capacity are reduced (Brady et al., 2013; Chen-Plotkin et al., 2012). Interestingly, degradation of the wild type TMEM106B seems to be slower compared to protective T185S variant. The increased protein stability argues for elevated TMEM106B levels in risk SNP carrier since messenger RNA (mRNA) level remain similar. Nicholson and colleagues ascribe this effect to a different glycosylation pattern at the N-glycosylation site affected by the amino-acid exchange (Nicholson et al., 2013).

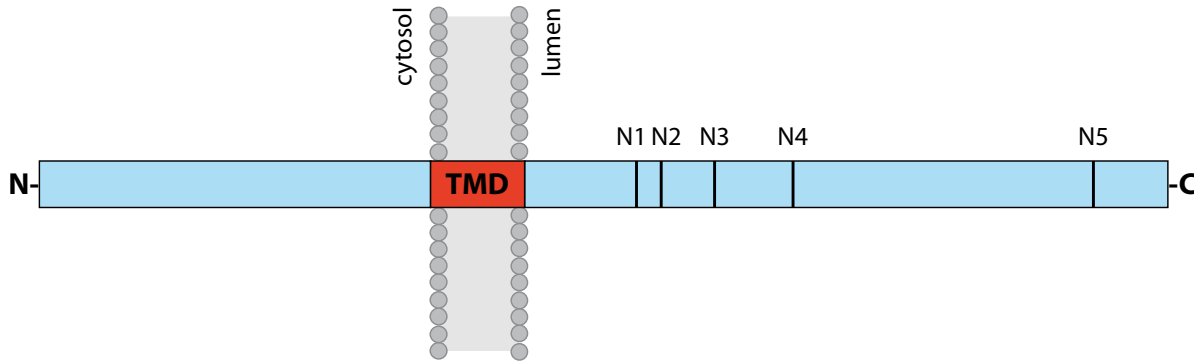


Figure 2: Domain structure and topology of TMEM106B

Schematic representation of the domain structure and topology of the type-two transmembrane protein TMEM106B. TMD: transmembrane domain; N1-N5: confirmed N-glycosylation sites; Adapted from (Lang et al., 2012).

Despite the genetic association, the effect of TMEM106B on GRN is not entirely clear. Although several studies reported an elevated GRN protein level or changes in GRN localization upon exogenous TMEM106B expression, this is possibly an unspecific effect attributed to lysosomal impairment as knockdown of TMEM106B does not influence GRN levels at all. Moreover, no differential effect of the TMEM106B T185S variant could be detected regarding these findings (Brady et al., 2013; Chen-Plotkin et al., 2012; Lang et al., 2012; Nicholson et al., 2013).

In FTLT-TDP patients with *GRN* mutations TMEM106B mRNA and protein levels are up-regulated and intracellular localization of the protein seems to be affected. The protein appears to be more disorganized and accumulated in the soma and the primary dendrites arguing for transport deficits of TMEM106B containing vesicles (Busch et al., 2013; Chen-Plotkin et al., 2012).

Although the genetic association of TMEM106B to FTLT-TDP is undisputed and the intracellular localization of the protein is elucidated, only minor progress was made in unravelling the physiological function of the protein. Especially the role of the protein at the lysosome and the probable participation in cellular functions already implicated in the disease need further studies.

2. Lysosomes and lysosomal transport

Lysosomes are an important part of the intracellular degradation system (Saftig and Klumperman, 2009). Deficits in this system are highly associated with neurodegenerative disease in general and FTLN in particular (Nixon, 2013; Pan and Chen, 2013). This association becomes especially apparent as TMEM106B a protein whose genetic variants influence the risk of many neurodegenerative diseases (Lu et al., 2013; van Blitterswijk et al., 2014; Van Deerlin et al., 2010) is demonstrated to localize to the lysosomal compartment (Lang et al., 2012).

2.1 Function – degradative and non degradative

The lysosome is the primary degradative compartment of the cell. More than 50 different hydrolases degrade proteins, lipids, polysaccharides and nucleic acids. Extracellular substrates reach the lysosome through endocytosis, phagocytosis or pinocytosis, intracellular material through autophagy. Three types of autophagy are known: 1. Microautophagy, the direct engulfment of cytoplasm by the lysosome (Mijaljica et al., 2011); 2. Chaperone-mediated autophagy, the direct delivery of proteins by hsc70 and subsequent lysosomal degradation (Kaushik and Cuervo, 2012); 3. Macroautophagy, the fusion of lysosomes with autophagosomes containing the material marked for degradation to autolysosomes (Ravikumar et al., 2010). Lysosomes control the ratio between biosynthesis and degradation thus overall cell metabolism, by regulating mammalian target of rapamycin complex 1 (mTORC1) (one of the key regulator of cell growth and autophagy (Laplante and Sabatini, 2012)) activity and signaling (Sancak et al., 2010). However, lysosomes are implicated in other important cellular functions such as cholesterol homeostasis, tissue remodeling, pathogen defense as well as cell death (reviewed in (Saftig and Klumperman, 2009)), Moreover, lysosomal exocytosis is a crucial step in plasma membrane repair (Rao et al., 2004; Reddy et al., 2001). Lysosomal exocytosis was long thought to be specific to secretory cells, that contain so called lysosome related organelles (LROs), but one and a half decades ago it was demonstrated that any cell can perform this task (Rodriguez et al., 1997). For example, the delivery of new

membranes to neurites in developing neurons relies on this process (Arantes and Andrews, 2006).

2.2 Biogenesis

Lysosomes are single membrane bounded vesicles with an acidic pH-optimum (pH: 4.5-5) in which most biomolecules of the cell are degraded. The resident proteome of lysosomes consists of two major classes of proteins. The first category of lysosomal proteins is soluble hydrolases responsible for the degradation of specific substrates. Apart from their catabolic activity they play a role in antigen processing and initiation of apoptosis (Conus and Simon, 2008). The second group are integral lysosomal membrane proteins responsible for the acidification of the lysosomal lumen, protein import and export and membrane fusion and trafficking (Eskelinen et al., 2003).

The biogenesis of lysosomes is a coordinated process arising from the endocytic and biosynthetic pathway. Newly synthesized lysosomal proteins are delivered directly through the trans-Golgi network (TGN) to the endocytic system and further to the lysosome. This direct pathway functions mainly through mannose-6-phosphate receptors (M6PR) trafficking (Kornfeld and Mellman, 1989). Proteins become tagged with Mannose-6-phosphate residues in the early Golgi, are recognized by M6PR in the TGN and are transported to endosomes. Other pathways involve indirect delivery through exocytosis at the plasma membrane and subsequent endocytosis and the targeting of lysosomal hydrolases by vacuolar protein sorting homolog receptor 10 (VPS10) family proteins such as sortilin (Canuel et al., 2009).

The formation of the actual membrane vesicle is a continuous process. Early endosomes that bud from the TGN mature stepwise to late endosomes and lysosomes through a spatiotemporal sequence of intermediates. During the maturation a continuous exchange of cargo, membranes and regulating proteins occurs while the intraluminal pH value drops gradually from around 6 in early endosomes to 4.5 – 5 in lysosomes (reviewed in (Saftig and Klumperman, 2009)). The lysosomal pH gradient is established and maintained mainly by v-Type H⁺ ATPases (Mindell, 2012).

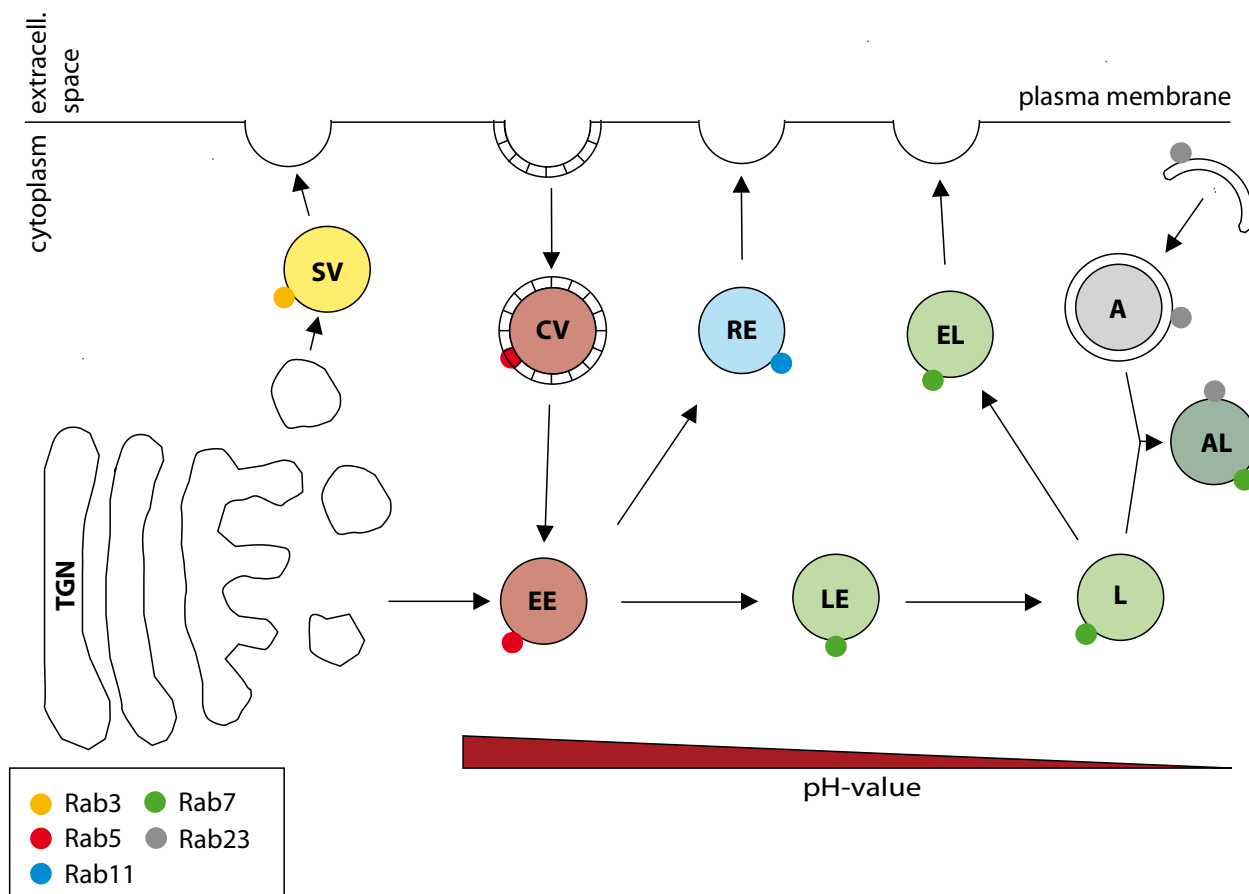


Figure 3: Secretory and endocytic pathway

A cell with its secretory and endocytic transport pathways which build a complex network of vesicular trafficking and the localizations of selected Rab-GTPases. Secretory vesicles bud from the TGN and go directly to the plasma membrane to release their content into the extracellular space. Early endosomes receive their contents from endocytosis or from the TGN. During their life cycle, EE go through a continuous process of fusion events i.e. with clathrin-coated vesicles or other endosomal vesicles. The endosomes end up either as recycling endosomes and release their cargo again in the extracellular space or gradually develop an acidic environment and become late endosomes than lysosomes. Lysosomes in the end either fuse with the plasma membrane and release their contents in the extracellular space as well or fuse with autophagosomes to become autolysosomes one of the most important degradative compartments of the cell. Most transport and fusion events are mediated by distinct RAB-GTPases.

TGN: Trans-Golgi-network; SV: secretory vesicle; EE: early endosome; CV: clathrin-coated vesicle; RE: recycling endosome; LE: late endosome; L: lysosome; EL: exocytosed lysosome; A: autophagosome; AL: autolysosome; Adapted from (Galvez et al., 2012; Lamb et al., 2013; Schwartz et al., 2007; Stenmark, 2009).

2.3 Regulation

Several classes of signaling molecules and regulatory proteins control endosomal or lysosomal fusion events and lysosomal maturation. Examples are the assembly/adaptor complexes adaptin 1-4 (AP1-4), which mediate vesicle formation, soluble N-ethylmaleimide-sensitive-factor attachment receptor (SNARE) proteins (e.g. Vesicle-associated membrane protein 7 (VAMP7) and synaptotagmin 7), which mediate vesicle fusion, and member RAS-oncogene family-GTPases (RAB-GTPases), important regulators of vesicle transport (Ohya et al., 2009). Moreover, v-type ATPases are required for cargo transport into the lysosome in addition to their role to maintain the intravesicular pH (Reviewed in (Bagshaw et al., 2005)).

Rab-GTPases are master regulators of membrane trafficking and vesicle fusion and fission events. Interestingly, Rab7 is the only lysosomal Rab-GTPase known so far. As for all other Rab-GTPases, GTP hydrolysis provides the biological energy for its downstream effects (Pfeffer, 1994). For lysosomal fusion, Rab7 acts in concert with the tethering homotypic fusion and protein sorting complex (HOPS) consisting of several VPS proteins (Zhu et al., 2009). In contrast, distribution and transport of lysosomes is controlled by the interaction of Rab7 with Rab-interacting lysosomal protein (RILP) and the dynein/dynactin complex (Jordens et al., 2001). The importance of tight lysosomal regulation becomes apparent through the functional or genetic link of Rab7 to a variety of neurological and non-neurological diseases (e.g. AD, Charcot-Marie-Tooth Type 2B (CMT2B) and cancer) (reviewed in (Zhang et al., 2009a)). Just recently, the main switch for the regulation of lysosomal processes was discovered: transcription factor EB (TFEB) promotes transcription of the coordinated lysosomal expression and regulation (CLEAR) network proteins which share a common target sequence in their promoter region. Almost all CLEAR network proteins are implicated in lysosomal biosynthesis, maintenance and function. By that TFEB provides a global transcriptional control of the coordinated synthesis and action of lysosomal proteins (Sardiello et al., 2009). Furthermore, TFEB promotes the transcription of proteins that are involved in the broader process of endosomal, autophagosomal and lysosomal function (Settembre et al., 2011).

Remarkably, both *TMEM106B* and *GRN* have one or more CLEAR target sequences in their predicted promoter regions (Sardiello et al., 2009).

3. Microtubules and Microtubule-dependent transport

Microtubules (MT) are important mediators of intracellular transport events and most organelles are transport along them through the cell. Already early in the research on neurodegeneration, malfunction of MT-dependent transport processes were implicated in the pathogenesis of various diseases (Breuer et al., 1987; Gajdusek, 1985; Praprotnik et al., 1996). In this thesis I could demonstrate that the FTLT-TDP risk factor *TMEM106B* affects the microtubule dependent transport in primary neurons. *TMEM106B* acts together with its novel interactor microtubule-associated protein 6 (MAP6) as a molecular brake for lysosomes in dendrites. Lysosomes are already strongly implicated in the pathogenesis of FTLT and the misrouting of these organelles may further aggravate neurodegeneration in patients.

3.1 Microtubules

Microtubules form together with actin filaments and intermediate filaments the cytoskeleton of a cell. Fundamental cellular processes such as mitosis or organelle transport critically depend on microtubules. In neurons, microtubules act as rail tracks for directed intracellular transport into axons and dendrites. Moreover, they are regulators of neuronal polarization and differentiation and have a crucial role in spine remodeling and synaptic function (Jaworski et al., 2009). Microtubules are hollow fibers assembled from α - and β -tubulin heterodimers. These dimers polymerize in a GTP consuming process end-to-end into long chains. Thirteen of these so called protofilaments form the actual microtubule, which can reach a length of up to 100 μ m in axons. Microtubule nucleation starts from a γ -tubulin ring complex, the microtubule-organizing center (MTOC). Due to its heterodimeric composition, microtubules have distinct ends, a fast-growing plus-end, and a slow growing minus-end. Usually, elongation proceeds to the plus-end. However, this is a dynamic process - growth (rescue) and shrinkage (catastrophe) of microtubules are in a balanced ratio (Amos and Schlieper, 2005). The structure of microtubules is the

same in neuronal and non-neuronal cells. However, organization is different and much more complex in neurons, especially owed to their highly polarized shape and their complex function (Kapitein and Hoogenraad, 2011). The dynamics and organization of microtubules is tightly regulated by the expression of different tubulin isotypes, their post-translational modifications and microtubule-associated proteins (MAPs) (Amos and Schlieper, 2005).

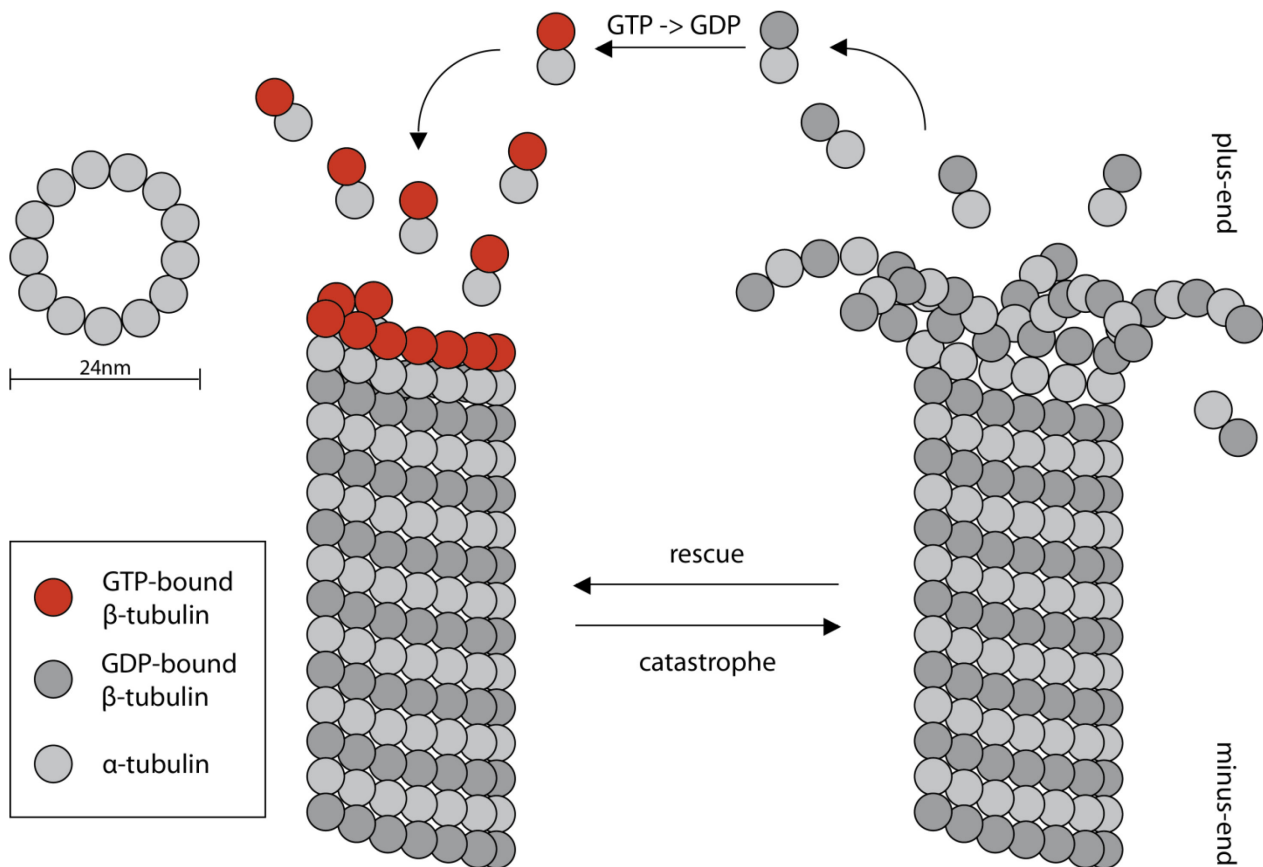


Figure 4: Microtubule assembly and dynamics

Schematic representation of microtubule structure and dynamics. Microtubules are comprised of 13 protofilaments that form a 24 nm wide hollow structure. They are polar structures due to the head to tail assembly of the $\alpha\beta$ -tubulin heterodimers. GTP bound tubulin dimers bind to the fast growing plus-end of microtubules and form the fiber (rescue). The last β -tubulin layer retains its GTP cap to maintain stability. All other layers hydrolyze the bound GTP during or directly after polymerization. As soon as the outer GTP cap is lost, microtubules depolymerize at the plus-end (catastrophe). Rescue and catastrophe are alternating and dynamic processes. Adapted from (Conde and Caceres, 2009)

Microtubules are located in the soma, the axon and dendrites and transiently in the actin rich spines (Hu et al., 2008). Axonal microtubules are uniformly orientated with all plus-ends to the tip, whereas dendritic microtubules have a mixed orientation but for the very distal part (Baas et al., 1988). However, this is not an irreversible process as neurons losing their axon can develop a new one out of an already existing dendrite, a process requiring major cytoskeletal reorganization (Bradke and Dotti, 2000). In mature neurons two distinct populations of microtubules exist: stable microtubules with a half live of several hours that are resistant to cold shock and depolymerizing drugs such as nocodazole and dynamic microtubules, prone to catastrophe with a half live of just minutes (Baas and Black, 1990; Sahenk and Brady, 1987). Both populations differ in the way tubulins are posttranslationally modified (Song et al., 2013) and in the abundance of cofactors such as MAP6 (Slaughter and Black, 2003).

3.2 Microtubule dependent transport

3.2.1 Motor and adaptor proteins

Directed cargo transport is apart from maintenance of cell structure and shape one of the main function of microtubules. In mammalian cells three classes of transport proteins exist which carry organelles, proteins and RNAs in an ATP dependent manner along the microtubules: myosins, kinesins and cytoplasmic dyneins.

Myosins are responsible for short range, actin-filament dependent transport. In neurons these transport events take place in dynamic structures as spines, presynaptic buttons and growth cones. There, myosins influence such important processes as remodeling of the actin cytoskeleton, synaptic plasticity or spine growth but also interact with MT-dependent events (Kneussel and Wagner, 2013). In contrast, kinesins and dyneins account for long-range microtubule-dependent transport.

Kinesin superfamily proteins (KIFs) mainly promote microtubule plus-end-directed transport. In axons with their unipolar (plus-end out) microtubules, KIFs mediate anterograde trafficking of their respective cargos. All family members share a similar globular motor domain but have different class-specific cargo binding

domains (Akhmanova and Hammer, 2010). The different KIFs form homo- or heterodimers and in rare cases also monomeric KIFs exist (Hirokawa and Takemura, 2005).

Cytoplasmic dyneins exclusively promote microtubule minus-end-directed transport, and thereby mediate retrograde transport in axons. The multiprotein transport complex consists of heavy, intermediate, intermediate-light and light chains (Akhmanova and Hammer, 2010). All dynein family members have very similar isotypes however they interact with a variety of different adaptor proteins as dynactin, dynamitin, p150^{glued} which are responsible for specific cargo recognition and interaction (Vallee et al., 2004). In dendrites, where microtubules are of mixed orientation, it is still unclear what transport complex conveys certain cargos in which direction. Although often the same motor proteins are used, distinct cargos have their specific adaptor proteins.

Temporal and spatial control of cargo transport is a multifactorial process but the exact regulatory mechanisms are heavily debated: Microtubule stability, influenced by microtubule-associated proteins and posttranslational modification of tubulin, regulate motor protein activity (Westermann and Weber, 2003). Furthermore the availability of cargo and motor itself (Coy et al., 1999) and the cargo-motor interaction have an impact on microtubule-dependent transport: some motor proteins bind directly to their cargo e.g. membrane lipids or internalized receptors (Tai et al., 1999), others can only bind via specific adaptor proteins such as scaffolding proteins (glutamate receptor-interacting protein (GRIP) for glutamate receptor 2 (GluA2) (Setou et al., 2002) or RAB GTPases (RAB7/RILP for lysosomes (Jordens et al., 2001). Additional factors such as ion concentration affect transport locally, for example mitochondrial movement in axons is reduced upon Ca²⁺ influx (Chang et al., 2006) (or reviewed in (Akhmanova and Hammer, 2010; Schlager and Hoogenraad, 2009)).

3.2.2 Bidirectional transport

Bidirectional transport in neurites with frequent stopping and alternation between anterograde and retrograde transport is observed for almost all types of cargos. In axons with their unipolar microtubules, transport requires both, kinesins and

dyneins. In contrast, in dendrites bidirectional transport could also work with only one type of motor proteins due to the mixed polarity of microtubules. However, also in dendrites both protein families mediate bidirectional transport. Two possibilities have been proposed for these bidirectional transport events. On the one hand, the “tug-of-war”-model: kinesins and dyneins are simultaneously attached to the same cargo and pull in different directions. This leads to stalling of transport or saltatory movement in both directions where the stronger motor proteins determine the net direction (Muller et al., 2008; Soppina et al., 2009). On the other hand, the coordination-model also assumes both motors to be attached simultaneously to the cargo. However, one motor is shut off when the opposing motor is active. This theory is supported by the fact that either kinesin or dynein knockdown in cells leads to an impairment of both retrograde and anterograde transport (Jolly and Gelfand, 2011). Nevertheless, it is unclear at the moment which models or even both are physiological relevant. In conclusion, much evidence arose that bidirectional trafficking is a complex mechanism controlled by multiprotein complexes binding to adaptor proteins and the transported cargos (RAB GTPases, scaffolding proteins, kinases,...) (Franker and Hoogenraad, 2013).

3.2.3 Neurite selective transport

Selective sorting of cargo into axons and dendrites is important to maintain neuronal polarity. This is guaranteed by selective transport into or selective retention from the respective neurite depending on the cargo involved (Hirokawa and Takemura, 2005). Motor and adaptor proteins determine the fate of the cargo as well: most kinesins steer to the axon, dyneins usually to the dendrites. The cytoskeletal organization in the axonal initial segment additionally serves as a control element (Kapitein et al., 2010; Song et al., 2009; van Spronsen et al., 2013).

The complex and tight regulation of microtubule dependent transport is most important in highly polarized cells such as neurons where axons grow up to 1 m long. Especially since crucial processes as neuronal polarity, axonal guidance and outgrowth or synaptic plasticity are directly dependent on a highly efficient and dynamic transport system (Franker and Hoogenraad, 2013).

3.3 Microtubule associated proteins (MAPs)

3.3.1 MAPs in general

Microtubule-associated proteins directly interact with microtubules and regulate their dynamic and organization. They are grouped into microtubule dependent motor proteins, which were already discussed above, microtubule plus-end tracking proteins (+TIPs) and structural MAPs. +TIPs typically bind to the plus-end of growing microtubules and mediate interaction and binding of microtubules to other proteins or cellular structures (Akhmanova and Steinmetz, 2010). Structural MAPs assist microtubule nucleation, regulate growth and stability, and control the ratio between catastrophe and rescue. The most abundant structural MAPs in neurons are dendritic MAP2 and mainly axonal tau. Their activity and localization is regulated by post-translational modification e.g. phosphorylation by MAP/microtubule affinity-regulating kinases (MARKs). Both proteins are thought to maintain microtubule spacing. MAP2 is further implicated in dendritic remodeling and synaptic plasticity, whereas Tau is involved in axonal transport. Hyperphosphorylated Tau inclusions are the hallmark of a variety of so called tauopathies including Alzheimer's disease and FTLN (Reviewed in (Hoogenraad and Bradke, 2009; Jordan and Wilson, 2004; Kapitein and Hoogenraad, 2011)).

3.3.2 The microtubule-associated protein MAP6/STOP

3.3.2.1 MAP6 structure

MAP6/STOP (stable tubule-only polypeptide) is a microtubule-stabilizing protein located both in axons and dendrites of neurons. Similar to other microtubule-binding proteins like Tau and MAP2, several different splice variants of MAP6 exist. These are differentially expressed depending on cell type and in the case of neurons also on the developmental state of the cell. The most widely studied homologue of the protein is rat MAP6. In very young rodent neurons only isoform 2 (E-STOP (early STOP): NP_001041632.1) is expressed, later on the longer isoform 1 (N-STOP (neuronal STOP): NP_034967.2) becomes upregulated, too. In non-neuronal cells the shortest variant, isoform 3 (F-STOP (fibroblastic STOP): NP_001036820.2) is the major isoform (Denarier et al., 1998). Although all three isoforms mediate

microtubule stability to a similar extent, only the neuronal isoforms 1 and 2 seem to bind constitutively to the cytoskeleton under physiological conditions (Bosc et al., 2003). The longest isoform consists of four distinct domains: The N-terminal domain, the central penta-repeat domain, a linker region and the C-terminal repeat domain with several 11 amino acid long imperfect repeats which is lacking in the shorter isoform 2 (Bosc et al., 1996). For human tissue, only two isoforms are annotated corresponding to mouse isoforms one and two. However, both isoforms have lost four of the five central repeats (Bosc et al., 2003). The microtubule stabilizing sites, thus probably also microtubule-binding sites are mainly located in the N-terminal and the central repeat domain. All these sites overlap with calmodulin-binding sites and upon interaction with Ca^{2+} /calmodulin MAP6 loses its ability to mediate microtubule cold resistance (Bosc et al., 2001).

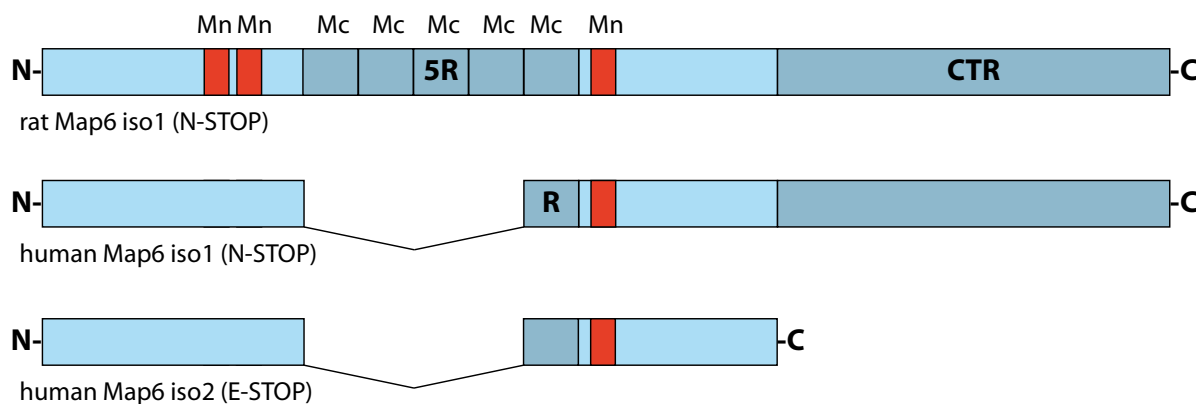


Figure 5: Domain structure and isoforms of MAP6

Schematic representation of the domain structure of rat (A) and human (B) isoforms of MAP6/STOP. 5R: penta-repeat domain; CTR: C-terminal repeat domain; R: single repeat in human orthologous; Adapted from (Bosc et al., 2001).

3.3.2.2 MAP6 function

The main functions of MAP6 are maintaining microtubule stability and their protection from cold induced depolymerization (Andrieux et al., 2002; Bosc et al., 1996). However, MAP6 additionally interacts with the actin cytoskeleton e.g. at spines, dendritic branch points and the Golgi apparatus arguing for additional,

microtubule-independent functions of the protein. This interaction depends on post-translational modifications as phosphorylation and palmitoylation and the overall protein level of MAP6 (Baratier et al., 2006; Gory-Faure et al., 2006). In line with these findings, recent studies implicate MAP6 in the control of cellular morphology and endocytosis (Arama et al., 2012; Morderer et al., 2012).

MAP6/STOP knockout mice are used as a model for schizophrenia as the behavioral profile of these animals is reminiscent of this neurological disease. The transgenic mice have a lower synaptic vesicle density, thereby an impaired glutamate release resulting in decreased synaptic plasticity (Andrieux et al., 2002; Brenner et al., 2007). Additionally, knockout animals show an imbalance in serotonergic and dopaminergic neurotransmission, leading to reduced anxiety but increased depressive behavior (Bouvrais-Veret et al., 2008; Fournet et al., 2010). Neuropathological examinations revealed enlarged ventricles in the knockout animals leading to a decrease in the size of the cortex, thalamus and striatum however not the hippocampus (Powell et al., 2007). Atypical antipsychotics seem to alleviate the cognitive deficits on the molecular as well as the behavioral level in MAP6 knockout mice (Delotterie et al., 2010). However, it is still not clear how loss of a microtubule-binding protein and reduced microtubule stability cause these neurological phenotypes.

II. Aim of the study

Genetic variants in the so far uncharacterized gene *TMEM106B* increase the risk of developing FTLD-TDP especially in individuals harboring *GRN* mutations (Cruchaga et al., 2011; Finch et al., 2011; Van Deerlin et al., 2010). However, the exact mechanism behind and the physiological function of the encoded protein remained unknown.

Based on these genetic findings, the aim of my thesis was to evaluate the physiological role of *TMEM106B* in primary neurons by knockdown studies.

First, I aimed to confirm the lysosomal localization of *TMEM106B* previously described in cancer cells (Lang et al., 2012) also in primary neurons and to examine general neuronal viability and lysosomal function upon *TMEM106B* knockdown. Since neurite loss, intracellular transport deficits and changes in synaptic transmission are early signs of pathology in most neurodegenerative diseases (Luebke et al., 2010; Masliah et al., 2001; Millecamps and Julien, 2013), I focused on these incidents in the next steps of my work. Accordingly, the second aim of my thesis was the phenotypical characterization of *TMEM106B* knockdown neurons focusing on the morphological analysis of dendrites, axons and spines by confocal microscopy and the study of intracellular transport of lysosomes by live cell imaging. Moreover, to shed light on the cellular context of *TMEM106B*'s function and to interpret the identified neuronal phenotypes I purposed to find and validate novel *TMEM106B*-interacting proteins by LC-MS/MS analysis. Last, I intended to validate the interaction functionally, seeking shared phenotypes of *TMEM106B* and its interaction partners and rescuing them by simultaneous knockdown or coexpression. These experiments may help to integrate *TMEM106B* into cellular pathways already implicated in the pathogenesis of FTLD.

Together, these insights might one day help to treat or even cure patients from this devastating disease.

III. Materials and Methods

1. Materials

1.1 Equipment

1.1.1 General equipment

equipment	supplier
analytical balance (0.0001 – 200 g)	Mettler-Toledo
autoclave	Systec
balance (0.01 – 2000 g)	Mettler-Toledo
fridge	Santo electronic
freezer (-20°C)	Liebherr
freezer (-80°C)	Heraeus
glassware	VWR
gloves (Latex)	Semperit
gloves (Nitrile)	Meditrade
Milli Q plus filtration system	Merck Millipore
Parafilm “M“	Pechiney Plastic Packaging
pH meter	Thermo Scientific
pH indicator strips	Merck Millipore
pipette boy	Integra
pipettes	Gilson, Raynon
pipette tips (10 µl, 200 µl, 1000 µl)	Sarstedt, VWR
serological pipettes (2 ml, 5 ml, 10 ml, 25 ml)	Sarstedt
thermomixer	Eppendorf
tubes (1.5 ml, 2 ml)	Sarstedt
tubes (15 ml, 50 ml)	Sarstedt
vortex	Scientific Industries
microsurgical instruments (Dumont forceps and scissors)	FST
Scanner	Epson

1.1.2 Centrifuges

equipment	supplier
5417R cooling centrifuge	Eppendorf
Megafuge 40R	Heraeus
Megafuge 1.0	Heraeus
Avanti J-20 XP centrifuge	Beckmann Coulter
Optima LE-80K ultracentrifuge	Beckmann Coulter
Optima MAX-XP ultracentrifuge	Beckmann Coulter
rotor (SW-41)	Beckmann Coulter
rotor (JA25.50)	Beckmann Coulter
rotor (TLA-55)	Beckmann Coulter
rotor (JA10)	Beckmann Coulter
rotor (TH-641)	Sorvall
centrifuge tubes (1.5 ml for TLA-55)	Beckmann Coulter
centrifuge tubes (30 ml for JA25.50)	Nalgene
centrifuge tubes	Nalgene

1.1.3 Molecular biology

equipment	supplier
electrophoresis	Thermo Scientific
incubator	B. Braun Biotech International
microwave	Sharp
Mastercycler Pro	Eppendorf
PCR tubes, strips, 96 well plates	Sarstedt
CFX384 Real-Time System	Bio-Rad
384 well plates	Bio-Rad
Power supply	Bio-Rad
ultraviolet (UV) Lamp	Intas
Nano Drop	Implen
heating cabinet	Binder

1.1.4 Protein biochemistry

equipment	supplier
Filter paper	Schleicher & Schüll
Heating block MR Hei-Tec	Heidolph instrument
Glass plates for electrophoresis gels	Bio-Rad
Immobilon-P membrane, PVDF, 0.45 µM	Merck Millipore
Electrophoresis gel casting system	Bio-Rad
Electrophoresis system (Mini-PROTEAN Tetra Cell)	Bio-Rad
Electrophoresis Transfer Cell (Mini-PROTEAN Trans-Blot)	Bio-Rad
Foam Pads	Bio-Rad
dynabead magent	Life technologies
power supply	Major Science
shaker	Edmund Bühler GMBH
Developer	CaWo
X-ray films	Fuji
X-ray film chamber	G. Kisker
scanner	Epson
Automated Potter Multifix Record	Johann Gg Bachhofer
Digital Sonifier 250	Branson

1.1.5 Cell culture

equipment	supplier
Cell culture hood	Heraeus
rubber policemen	Corning Incorporated
Bunsen burner	Heraeus
cell culture dish (3.5 cm, 6 cm, 10 cm)	Nunc
cell culture plate (12 well, 96 well)	Nunc
CO ₂ -incubator	Thermo Scientific

oven	Memmert
glass bottom dish ($d_{\text{glass}} = 20 \text{ mm}$, 3.5 cm)	Mattek
Hemocytometer	Optik Labor
N ₂ -tank	Messer Griesheim
PES membrane filter (0.45 μm)	VWR International
water bath	GFL

1.1.6 Imaging

equipment	supplier
Confocal laser scanning microscope (LSM 510, LSM 710)	Carl Zeiss
Spinning disc microscope (Cellobserver SD)	Carl Zeiss
Epifluorescence microscope (Axiovert.A2)	Carl Zeiss
Objective (LD LCI Plan Apochromat, 25x/0.8 Oil, W, Gly) – LSM710	Carl Zeiss
Objective (Plan Apochromat, 40x/1.3 Oil DICII) – LSM510	Carl Zeiss
Objective (Plan Apochromat, 40x/1.4 Oil DICII) – LSM710	Carl Zeiss
Objective (Plan Apochromat, 63x/1.4 Oil DICII) – LSM710	Carl Zeiss
Objective (Plan Apochromat, 63x/1.4 Oil DIC) – Cellobserver SD	Carl Zeiss
Objective (Plan Neofluar 40x/1.3 oil Ph3) – Axiovert.A2	Carl Zeiss
climate chamber	Pecon
light microscope (Wilovert S)	Hund Wetzlar
Powerwave XS plate reader	BioTek

1.1.7 Mass spectrometry

equipment	supplier
Proxeon Easy nLCII liquid chromatograph	Thermo Scientific

2.4 μm C18 beads	Dr. Maisch GmbH
TQ Velos Orbitrap mass spectrometer	Thermo Scientific

1.1.8 Kits

Kit	supplier
Amaya primary culture kit P3	Lonza
Cell Proliferation Kit II (XTT)	Roche applied science
NOVEX Colloidal Blue Staining Kit	Life Technologies
NucleoBond Plasmid kit	Machery Nagel
NucleoBond Xtra Midi EF kit	Machery Nagel
NucleoSpin Gel and PCR cleaning kit	Machery Nagel
RNeasy Mini Kit	Qiagen
TaqMan MicroRNA Reverse Transcription Kit	Applied Biosystems
SsoFast™ EvaGreen Supermix	Bio-Rad

1.2 Chemicals, enzymes and antibodies

1.2.1 Molecular biology

Name	company
Agarose Ultrapure	Life Technologies
restriction enzymes	NEB
Ampiciline	Boehringer Mannheim
deoxyribonucleic acid (DNA) polymerase (Pfu)	Agilent
DNA polymerase (Pwo)	Roche Applied Science
DNA polymerase (Taq)	Roche Applied Science
DNA polymerase (Pfu II Ultra)	Agilent
tetracycline	Sigma-Aldrich
dNTPs	Roche Applied Sciences
DNA ladder	Life Technologies

Ethidiumbromide	ROTH
T4-Ligase	NEB
calf intestine phosphatase (CIP)	NEB

1.2.2 Cell culture

Name	company
DMEM glutamax-I	Life Technologies
Neurobasal	Life Technologies
Fetal calf serum (FCS)	Life Technologies
l-glutamine	Sigma-Aldrich
l-glutamate	Sigma-Aldrich
DNase	Sigma-Aldrich
poly-D-lysine (PDL)	Sigma-Aldrich
laminine	Roche Applied Science
trypsin-EDTA	Life Technologies
trypsin (2.5 %)	Life Technologies
Penicillin/Streptomycin	Life Technologies
Non-essential amino acids (NEAA)	Life Technologies
Lipofectamine2000	Life Technologies
B27	Life Technologies
Bovine serum albumin (BSA)	Sigma-Aldrich
Nocodazole	Sigma-Aldrich
OptiMEM	Life Technologies

1.2.3 Biochemistry

Name	Company
proteinase inhibitor	Sigma-Aldrich
phosphatase inhibitor	Sigma-Aldrich
ammonium persulfate (APS)	Roche

tetramethylethyldiamin (TEMED)	USB
Acrylamid (19:1 / 40 % (w/v))	Bio-Rad
β -mercaptoethanol	Merck Millipore
SeaBlue Prestained Protein Ladder Plus 2	Life Technologies
myc-beads	Sigma-Aldrich
Protein G Dynabeads	Life Technologies
Protein A sepharose beads	GE Healthcare
iodixanol	Sigma-Aldrich
lysozyme	Merck Millipore
Isopropyl- β -D-1-thiogalactopyranoside (IPTG)	ROTH
glutathion sepharose 4B	GE Healthcare
Maltose beads	
Bis-sulfosuccinimidyl suberate (BS3)	Sigma-Aldrich
enhanced chemiluminescence (ECL)	Thermo Scientific
ECL plus	Thermo Scientific
I-Block	Tropix
dithiothreitol (DTT)	Sigma-Aldrich

1.2.4 Microscopy

Name	Company
vectahield H-1000 mounting medium	Vectorlabs
Immersol 518 F	Carl Zeiss
Microscope Cover glasses (18 mm, 20 mm)	VWR
Microscope slides Superfrost plus	Thermo Scientific

1.2.5 General chemicals

Name	Company
acetonitrile	Merck Millipore

acetic acid	Merck Millipore
Bromophenol blue	Merck Millipore
boric acid	Merck Millipore
dimethyl sulfoxide (DMSO)	Roth
ethylenediaminetetraacetic acid (EDTA)	USB
Ethanol	Sigma-Aldrich
formic acid	Millipore
gelatin powder	Sigma-Aldrich
Glycerol	USB
Glycine	Biomol
Hepes	Biomol
Isopropanol	Merck Millipore
KCl	USB
KH ₂ PO ₄	Merck Millipore
β-mercaptoethanol	ROTH
methanol	Merck Millipore
Na ₂ [B ₄ O ₅ (OH) ₄]	Sigma-Aldrich
NaCl	Merck Millipore
NH ₄ HCO ₃	Merck Millipore
Na ₂ HPO ₄	Merck Millipore
NaH ₂ PO ₄	Sigma-Aldrich
NaOH	Merck Millipore
NaN ₃	Merck Millipore
paraformaldehyde (PFA)	Sigma-Aldrich
sodium dodecylsulfate (SDS)	Roth
sucrose	Sigma-Aldrich
Staurosporine	Sigma-Aldrich
Tris	AppliChem
TritonX100	Merck Millipore
Tryptone	BD Biosciences
Yeast extract	BD Biosciences

1.2.6 Antibodies

Primary antibodies

Antigen	Supplier	Species	Clone	Dilution
β -actin	Sigma-Aldrich	mouse monoclonal	AC-15	WB: 1:5,000
γ -adaptin	BD Biosciences	mouse monoclonal	88/Adaptin γ	WB: 1:500
calnexin	Enzo Life Sciences	rabbit polyclonal		WB: 1:10,000
FUS	Bethyl	mouse monoclonal	A300-292A	WB: 1:500
green fluorescent protein (GFP)	Neuromab	mouse monoclonal	N86/38	IF: 1:500
LAMP1	Enzo Life Sciences	mouse monoclonal	Ly1C6	IF: 1:50
Map6 (rat amino acids 793 – 952 according to NP_058900)	Immunization at Eurogentec	rabbit polyclonal		IF: 5 μ g / ml, WB: 1 μ g / ml
MAP6	Cell Signaling Technologies	mouse monoclonal	175	IF: 1:50, WB: 1:500
MAP6	Abcam	mouse monoclonal	ab78077	IF: 1:50, WB 1:500
Myc	Santa-Cruz- Biotechnology	mouse monoclonal	9E10	IF: 1:250, WB: 1:1,000
Na ⁺ /K ⁺ -ATPase	Developmental Studies Hybridoma Bank	mouse monoclonal	a2F	WB: 1:1,000
postsynaptic density protein 95 (PSD-95)	Neuromab	mouse monoclonal	K28/43	WB: 1:1,000

Rab7	Cell Signaling Technologies	mouse monoclonal	2094	WB: 1:500
Synaptophysin	Millipore	mouse monoclonal	SY38	WB: 1:1,000
synaptic vesicle glycoprotein 2 (SV2)	Developmental Studies Hybridoma Bank	mouse monoclonal	SP2/0	WB: 1:2,000
Tau	Dako	rabbit polyclonal	A 0024	WB: 1:10,000
Tau-1	Millipore	mouse monoclonal	PC1C6	IF: 1:500
TDP-43	Cosmo Bio	rabbit polyclonal	405-414	WB: 1:1,000
translocase of outer membrane 20 (TOM20)	Santa-Cruz-Biotechnology	rabbit polyclonal	FL-145	WB: 1:500
TMEM106B (rat amino acids 1-91)	Immunization at Eurogentec	rabbit polyclonal	344	IF: 5 µg / ml
TMEM106B (rat amino acids 1-91)	Immunization at Eurogentec	rabbit polyclonal	345	WB: 1 µg / ml
Transferrin receptor (TfR)	Life Technology	mouse monoclonal	H68.4	WB: 1:500
βIII-tubulin	Sigma-Aldrich	mouse monoclonal	SDL.3D10	IF: 1:500, WB: 1:10,000
Cathepsin D	Santa-Cruz-Biotechnology	mouse monoclonal	C-20	WB: 1:1000

Secondary antibodies

Antigen	Supplier	Species	Labeled	Dilution
mouse IgG (H+L)	Life technologies	goat	Alexa488, 555 or 647	IF: 1:500
rabbit IgG (H+L)	Life technologies	goat	Alexa488, 555 or 647	IF: 1:500
rat IgG (H+L)	Life technologies	goat	Alexa488, 555 or 647	IF: 1:500
mouse IgG (H+L)	Promega	goat	horse radish peroxidase (HRP)	WB: 1:5,000
rabbit IgG (H+L)	Promega	goat	HRP	WB: 1:5,000
rat IgG (H+L)	Santa-Cruz-Biotechnology	goat	HRP	WB: 1:5,000

1.3 DNA oligonucleotides and plasmids**1.3.1 Primer for cloning**

primer	sequence sense	sequence antisense
rat TMEM106B	GGATCCGCCACCATGGGAAAGT CTCTTTCTCATTTACC	CATGAATTCATTGTTGTGGCTG AAGGACATTTAGATAC
shRNA resistant rat TMEM106B*	GGGCACTGTGTAGTCGATCTGC TTTTTCATATCAAGTGGGCCAAT G	GCAGATCGACTACACAGTGCCC ACAGTTATTGCCGAGG
	GCGGCCGCAACACTACGTACCA GTTGGCCCAGTCTG	GGTACGTAGTGTGCGGCCGCA GTCAACATACTGGTACCTCTCC
rat MAP6 isoform 1	GTGAGATCTGCCACCATGGCGT GGCCGTGCATCACTAGG	TGTGTGACCTCCATGGCATT CAAGGGAATCAAGG
human dnRILP (c33AA 201-401)	TAAGTCGACCCGGGCACCAGC ACGGACAGGAG	CATGAATTCTAAGTCAGGCCTCTG GGGCGGCTGAG
human RAB7a-GFP	AAAGGCGCGCCTATGACCTCTA GGAAGAAAGTGTGCTGAAGG	CGAGAATTCTTAGCAACTGCAG CTTCTGCCGAGG
human RAB7a-GFP	GATTCTGGAGTTGGTAAAGCTT CACTCATGAACCAAGTATG	CATACTGGTTCATGAGTGAATT CTTACCAACTCCAGAATC

(dominant negative T22N)		
human RAB7a-GFP (constitutive active Q67L)	CTGGGACACAGCAGGCCTAGAA CGGTTCCAGTCCCTTG	CAAGGGACTGGAACCGTTCTAG GCCTGCTGTGTCCCAG
GFP-TMEM-NT primer	CCGCTCGAGCTGGAAAGTCTCT TTCTCATTGTC	CGCGGATCCTTATGTTCTTCTT GGCCTTAATCTCTG
human Map6 isoform 1	CTAGTCTAGAGCCACCATGGCG TGGCCGTG	TTCCGCGGCCGCTATGGCCGAC GTCGACTCAAGGGGAGCTCTCA ATGTATTC
human MAP6 isoform 2	CTAGTCTAGAGCCACCATGGCG TGGCCGTG	TTCCGCGGCCGCTATGGCCGAC GTCGACTCACTCTTTCGCCTCA GCCAG

1.3.2 Short hairpin RNA (shRNA)

Primers for shRNA cloning (BglII/HindIII into pSuper or pSuperSub), 19mer target sequence is marked in bold, reverse complement of target sequence in italic

target	sequence sense	sequence antisense
rm- shTMEM106B#1	gatcccc GCAGATTGATTATACGGTA ttcaagaga <i>TACCGTATAATCAATCT</i> GCtttttgaaa	agcttttccaaaa GCAGATTGATTA TACGGTA <i>tctcttgaaTACCGTATAA</i> <i>TCAATCTGC</i> ggg
rm- shTMEM106B#2	gatcccc GTGGAAGGAACACGACTTA ttcaagaga <i>TAAGTCGTGTTCCCTTCC</i> ACtttttgaaa	agcttttccaaaa GTGGAAGGAACA CGACTTA <i>tctcttgaaTAAGTCGTGT</i> <i>TCCCTCCAC</i> ggg
r-shMAP6	gatcccc GGTGCAGATCAGCGTGACA ttcaagaga <i>TGTCACGCTGATCTGCA</i> CCtttttgaaa	agcttttccaaaa GGTGCAGATCAG CGTGACA <i>tctcttgaaTGTCACGCTG</i> <i>ATCTGCACC</i> ggg
shLuc	gatcccc CGTACGCGGAATACTTCGA ttcaagaga <i>TCGAAGTATTCCGCGTA</i> CGtttttgaaa	agcttttccaaaa CGTACGCGGAAT ACTTCGA <i>tctcttgaaTCGAAGTATT</i> <i>CCGCTACG</i> ggg
r-shMAP2	gatcccc CGAGAGGAAAGACGAAGGA ttcaagaga <i>TCCTTCGTCTTTCCTCT</i> CGtttttgaaa	agcttttccaaaa CGAGAGGAAAGA CGAAGGA <i>tctcttgaaTCCTTCGTCT</i> <i>TTCTCTCG</i> ggg

1.3.3 qPCR primers

target	sequence sense	sequence antisense
rm-TMEM106B	actggaagagatagtgtcacttgtccca	agccaatccagacaggagcaggc
rm-YWHAZ	tgagcagaagacggaaggtgctg	tctgatgggggtgtgtcggctgc

1.3.4 Plasmids

β -actin-EGFP (XX3 – empty vector)	Dieter Edbauer
FhSynRedW-mCherry	Dieter Edbauer
FhSynW-rTMEM106B* (resistant to shTMEM106B #1 and #2)	EcoRI/ BamHI into AD149
GW1.2b-myc-rMAP6	BglII/SalI into XX7
FhSynW-myc-rMAP6	AscI/EcoRV from GW1.2b-myc-rMap6 into AD538 FhsynW1-myc
pSUPER-mr-shTMEM106B#1	oligos BglII/HindIII into pSUPER
pLL3.7-hSyn-shTMEM106B#1-pTag-RFP	XbaI/XhoI from pSuper into AD425
pSUPER-mr-shTMEM106B#2	oligos BglII/HindIII into pSUPER
pLL3.7-hSyn-shTMEM106B#2-pTag-RFP	XbaI/XhoI from pSuper into AD425
pSUPERsub-r-shMAP6	oligos BglII/HindIII into pSUPERsub
pLL3.7-hSyn-shMAP6-pTag-RFP	XbaI/XhoI from pSUPERsub into AD425
pSUPER-shLuc	oligos BglII/HindIII into pSUPER
pSUPERsub-shLuc	oligos BglII/HindIII into pSUPERsub
pLL3.7-hSyn-shLuc-pTag-RFP	XbaI/XhoI from pSUPER in AD425
GFP-TMEM-NT	XhoI/BamHI Into pEGFP-C1 by Christina Lang
hMap6 isoform 1	XbaI/SalI in XX7
hMap6 isoform 2	XbaI/SalI in XX7
hRab7a-GFP	AscI/EcoRI in XX7
MAP6-GFP	GFP from XX8 AflII/AscI into GW1.2b-

	myc-rMap6
Mito-RFP: mitochondrial targeting sequence of cyclooxygenase 8 (COX8) fused to red fluorescent protein (RFP)	Anna Pils
dnRilp c33	Sall/EcoRI into XX7
GW1.2b-CMV-myc (XX7 – empty vector)	Dieter Edbauer
GW1.2b-CMV-EGFP (XX8 – empty vector)	Dieter Edbauer
Rab7a pEGFP-C1	Capell lab
dn hRab7a-GFP (T22N)	AscI/EcoRI in XX7
ca hRab7a-GFP (Q67L)	AscI/EcoRI in XX7
pEYFP-C1	Sabina Tahirovic
Lamp1-RFP	Capell lab
FhSynW2- Δ Zeo (AD149 – empty vector)	Dieter Edbauer
AD538 FhsynW1-myc (AD538 – empty vector)	Dieter Edbauer
pSUPER (empty vector – H1 promoter for expression of shRNAs)	Dieter Edbauer
pLL3.7-hSyn-pTag-RFP (AD425 – empty vector for lentiviral expression of shRNAs)	Dieter Edbauer
FhSynW-rTMEM106B	EcoRI, BamHI into AD149
pSUPERsub (empty vector – H1 promoter for expression of shRNAs)	Dieter Edbauer
pSPAX2	(Salmon and Trono, 2007)
pVSVg	(Kuhn et al., 2010)

1.4 Buffer

If not stated otherwise, components of buffers are dissolved in MilliQ water.

1.4.1 Buffer for antibody generation

buffer	composition
homogenization buffer	0.32 M sucrose, 4 mM Hepes, 2 mM EDTA pH 7.4
STE-buffer	10 mM Tris-HCl 150 mM NaCl 1 mM EDTA pH 8.0
conjugation buffer	20 mM Na ₂ HPO ₄ 0.15 M NaCl pH 8.0
column buffer	0.2 M Tris-HCl 0.5 M NaCl pH 8.0
glycine elution buffer	0.1 M Glycine-HCl 0.5 M NaCl pH 2.5
neutralization buffer	1 M Tris pH 9.5

1.4.2 Buffer for Molecular Biology:

buffer	composition
lysogeny broth (LB) medium	1 % Tryptone 0.5 % Yeast extract 86 mM NaCl

LB agar	1.5 % agar in LB medium
5x DNA loading buffer	50 % Glycerol 50 mM Na ₂ EDTA 0.05 % Bromophenol blue pH 8.0
Sodium borate buffer	5mM Na ₂ [B ₄ O ₅ (OH) ₄] x 10 H ₂ O pH 8.0 (adjusted with H ₃ BO ₃)

1.4.3. Buffer for cell culture

buffer	composition
phosphate-buffered saline (PBS)	0.14 M NaCl 10 mM Na ₂ HPO ₄ 2.8 mM KH ₂ PO ₄ 2.7 mM KCl pH 7.4
Hepes buffer	0.3 M Hepes pH 7.3
Hank's buffered salt solution (HBSS)	0.14 M NaCl 5.4 mM KCl 0.25 mM Na ₂ HPO ₄ 5.6 mM glucose 0.44 mM KH ₂ PO ₄ 1.3 mM CaCl ₂ 1.0 mM MgSO ₄ 4.2 mM NaHCO ₃
borate buffer	40 mM boric acid 10 mM sodium tetra borate pH 8.5

1.4.4 Buffer for protein biochemistry

buffer	composition
4x Lämmli sample buffer	4% SDS, 20% glycerol, 5% β -mercaptoethanol, 200 mM Na_2HPO_4 pH 7.4
RIPA buffer	50 mM TrisHCl 150 mM NaCl 2 mM EDTA 1% NP-40 0.1% SDS pH 7.4
stacking gel buffer	0.5 M Tris 0.4 % (w/v) SDS pH 6.8
separating gel buffer	1.5 M Tris 0.4 % (w/v) SDS pH 8.8
running buffer	25 mM Tris 0,2 M Glycine 0.1 % SDS
blotting buffer	25 mM Tris 0,2 M Glycine
TBSTx	20 mM Tris 0.14 M NaCl 0.2 % TritonX100 pH 7.6
Coomassie fixing solution	10 % acetic acid 50 % methanol
Coomassie staining solution	20 % stainer A (Colloidal Blue

	Staining Kit) 5 % stainer B (Colloidal Blue Staining Kit) 20 % methanol
--	---

1.4.5 Buffer for immunofluorescence

buffer	composition
4 % PFA fixing solution	4 % PFA 0.15 mM NaOH 0.13 mM NaH ₂ PO ₄ 0.12 mM sucrose pH 7.6
2x GDB buffer	0.2 % Gelatine powder 0.33 M Na ₂ HPO ₄ 0.9 M NaCl 0.6 % TritonX100 pH 7.4
HBSS/Hepes buffer	7 mM Hepes in HBSS

1.4.6 Buffer for mass spectrometry

buffer	composition
ammonium bicarbonate buffer	100 mM NH ₄ HCO ₃
Coomassie destaining solution	50 % ammonium bicarbonate buffer 50 % acetonitrile
tryptic digest solution	13 ng / µl trypsin 10 mM NH ₄ HCO ₃ 10 % acetonitrile
extraction buffer	1.7 % formic acid 67 % acetonitrile

1.5 Services

Service	Supplier
DNA Sequencing	GATC Biotech AG
Antibody production	Eurogentec SA
Oligonucleotide synthesis	Sigma-Aldrich

1.6 Software and Online tools

Software	Supplier
ImageJ / Fiji	National Institutes of Health
MS Office	Microsoft
GraphPad Prism	GraphPad Software
Adobe Photoshop CS5	Adobe
Adobe Acrobat Professional	Adobe
MetaMorph	Molecular Devices
Carl Zeiss Axiovision	Carl Zeiss
CLC Main Workbench 6	CLC bio
BioRad CFX manager	Bio-Rad
NCBI databases (http://www.ncbi.nlm.nih.gov)	National Institutes of Health
ensembl (http://www.ensembl.org)	EMBL-EBI and Wellcome Trust Sanger Institute
APE – A plasmid editor v1.17	Wayne Davis
i-score designer (http://www.med.nagoya-u.ac.jp/neurogenetics/i_Score/i_score.html)	(Ichihara et al., 2007)
Spidey web tool (http://www.ncbi.nlm.nih.gov/spidey/).	National Institutes of Health
Primer3 web tool (http://bioinfo.ut.ee/primer3/)	(Untergasser et al., 2007)
Proteome Discoverer 1.2	Thermo Scientific
The International Protein Index database	EMBL-EBI and Wellcome Trust

for rat (version 3.87)	Sanger Institute
------------------------	------------------

1.7 Cell lines and bacteria strains

	supplier
DH5 α chemically competent <i>Escherichia coli</i> (<i>E. coli</i>)	Life Technologies
TOP10 Chemically competent <i>E.coli</i>	Life Technologies
HEK293-FT	Life Technologies

2. Methods

2.1 Molecular Biology

2.1.1 Molecular cloning

Cloning strategy

For cloning of complete complementary DNAs (cDNAs) or cDNA fragments, the region of interest was either excised with restriction enzymes from a plasmid based vector or PCR amplified from a cDNA library or a plasmid based vector. Restriction sites in the donor construct for subcloning or sites attached with primers to PCR products were chosen according to the available restriction sites in the acceptor plasmid. For cloning of shRNAs, oligonucleotides containing the desired sequence were ordered and hybridized as follows:

Component	amount
Forward oligonucleotide (100 μ M)	1 μ l
Reverse oligonucleotide (100 μ M)	1 μ l
NEB buffer 4	2 μ l
MilliQ water	Ad 20 μ l

The mixture was incubated at 95°C for 4 min and let cool down slowly to RT. The acceptor plasmid was digested with the corresponding restriction enzymes but not dephosphorylated prior to ligation with the annealed oligonucleotides.

shRNA design

Oligonucleotides with a length of 25 nucleotides binding to ideally unique seed region on the target of interest were designed using the iScore designer (http://www.med.nagoyau.ac.jp/neurogenetics/i_Score/i_score.html) and the NCBI Blast web tool (<http://blast.ncbi.nlm.nih.gov/Blast.cgi>). Usually, shRNAs were initially tested in HEK293-FT cells coexpressing an overexpression construct. Knockdown efficiency was tested on protein level using immunoblotting. All constructs were verified by DNA sequencing.

Polymerase chain reaction (PCR)

For standard PCR reaction Pfu DNA polymerase was used and the PCR mix was set as follows:

Component	amount
DNA template	100 ng
Forward primer (20 μ M)	1 μ l
Reverse primer (20 μ M)	1 μ l
dNTPs (10 mM each)	1 μ l
10x Pfu buffer	5 μ l
Pfu DNA polymerase	1 μ l
MilliQ water	ad 50 μ l

Standard protocol comprised 30 PCR cycles, annealing temperature $T_a = T_{m(\text{primer})} - 5^\circ\text{C}$ and elongation time of 1 min per 1000 base pairs.

Step	Temperature [$^\circ\text{C}$]	Time	# of cycles
Initial denaturation	95	2 min	1
Denaturation	95	20 s	30
Annealing	$T_{m(\text{primer})} - 5$	20 s	
Extension	72	1 min / 1kb	
Final Extension	72	8 min	1

For special applications other polymerases (Taq, PWO, Pfu II Ultra) were used according to the manufacturer's instructions.

Restriction digest and dephosphorylation

Plasmid based vectors (3 μ g) were cut with the respective restriction enzymes typically at 37 $^\circ\text{C}$ for 1 h. PCR products were cut typically at 37 $^\circ\text{C}$ overnight. The amount of the restriction enzymes, conditions and buffer system was chosen according the manufacturer's instruction or the NEB double digest finder

(<https://www.neb.com/tools-and-resources/interactive-tools/double-digest-finder>).

The ends of plasmid backbones were dephosphorylated with calf intestine phosphatase (CIP) for 1 hour at 37°C after the restriction digest in order to prevent self-ligation. To purify the digested and dephosphorylated DNA, the plasmid was subjected to agarose gel electrophoresis, the respective bands excised, purified and eluted in 50µl MilliQ water (see chapter: *Agarose-gel electrophoresis*).

Ligation

The digested, dephosphorylated vector backbone was incubated with the digested PCR product or vector fragment, Ligase buffer and Ligase added for at least 1 hour at room temperature. The ligation mix was set as follows:

Component	amount
vector backbone	3 µl
PCR product / plasmid fragment	9 µl
10x ligase buffer	2 µl
ligase	2 µl
MilliQ water	ad 20 µl

Transformation

The complete ligation mixture was gently mixed with 100 µl freshly thawed chemical competent DH5α *E. coli* bacteria. Bacteria were incubated for 25 min on ice, heat shocked for 1 min at 42°C to facilitate uptake of the DNA and put back on ice for 1 min. Afterwards, 500 µl LB medium was added and the transformation mix incubated at 37°C under gentle shaking for 1 h. After incubation, the whole ligation mix was plated on LB plates containing selection antibiotics and incubated for 8 to 12 h at 37°C.

DNA preparation

To prepare DNA from *E.coli* bacteria, single clones were picked with sterile pipette tips and added to 5 ml antibiotics containing LB medium (miniprep) or to 100 ml antibiotic containing LB medium (midiprep). The liquid culture was incubated under

gentle shaking at 37°C overnight. Afterwards, the culture was centrifuged with xx g for 5 min (miniprep) or 10 min (midiprep) at 4°C and the supernatant discarded. The bacteria pellet was resuspended and plasmid DNA was purified with the NucleoBond Plasmid kit (miniprep) or the NucleoBond Xtra Midi EF kit (midiprep) according to the manufacturer's instructions.

Control digestion

To verify successful cloning purified plasmids were control digested. One or several restriction enzymes were chosen to ensure a distinct restriction pattern. The amount of the restriction enzymes, conditions and buffer system was chosen according the manufacturer's instruction or the NEB double digest finder (<https://www.neb.com/tools-and-resources/interactive-tools/double-digest-finder>).

Agarose-gel electrophoresis

To purify digested plasmid fragments or PCR products, to separate several DNA fragments from a single digestion mix or to visualize the restriction pattern after control digestion one dimensional electrophoresis was used. DNA was mixed with the respective amount of 5x DNA loading buffer and applied to agarose gels (0.7 % to 2 % agarose in SB buffer) containing 0.2 µg/ml ethidiumbromide. Electrophoresis was performed in sodium borate buffer at a constant voltage of 300 V. Gels were examined under UV light (xx nm).

Sequencing

To further verify successful cloning and check for small deletions, insertions or point mutations in the insert purified plasmids were sequenced at GATC Biotech AG (Konstanz). One or several primers which bound to or upstream of the region of interest were used to sequence each construct.

2.1.2 Reverse transcription and quantitative PCR (RT-qPCR)

RNA isolation

RNA from primary neurons was isolated using the Qiagen RNAeasy kit following the manufacturer's instructions. For storage RNA was kept at -80°C. To avoid

interference of residual genomic DNA, a DNase digest step was performed during RNA extraction, according to manufacturer's instructions.

Reverse transcription-PCR (RT-PCR)

To generate complementary DNA (cDNA) isolated RNA was reversely transcribed with random hexamer primers (N6) using TaqMan MicroRNA Reverse Transcription Kit following the manufacturer's instructions. For the cDNA standard curve, equal amounts of all RNA samples were pooled and the mixture was serially diluted in a 1:10 ratio. The reaction mix was set as follows. For each reaction the RNA sample was diluted in 15µl nuclease-free H₂O and combined with 30µL reaction mix.

Component	amount
100 mM dNTPs	0.45 µl
MultiScribe™ Reverse Transcriptase (50 U/µL)	3 µl
RNase inhibitor	0.56 µl
10X RT buffer	4.5 µl
N6 primer (50 ng/µl)	4.5 µl
diluted RNA	15 µl
nuclease-free H ₂ O	ad 45 µl

The standard program for the RT-PCR reaction was:

time	temperature
30 min	16 °C
30 min	42 °C
5 min	85 °C
hold	4 °C

Quantitative PCR (qPCR)

The qPCR reaction was performed using the SsoFast™ EvaGreen (BioRad) reaction mix according to the manufacturer's instructions. cDNA was diluted in a ratio of 1:1 in nuclease free H₂O, was mixed with the reaction mix and gene specific primers

were added. Tyrosine 3-monooxygenase/tryptophan 5-monooxygenase activation protein, zeta (YWHAZ) was usually as housekeeping gene. The relative mRNA expression was calculated using the BioRad CFX manager software with the $\Delta\text{-}\Delta\text{-}C_t$ method. The reaction mix was set as follows:

Component	amount
SsoFast™ EvaGreen	2.5 μ l
Forward primer (400 nM)	0.05 μ l
Reverse primer (400 nM)	0.05 μ l
cDNA template	2 μ l
Nuclease free H ₂ O	ad 5 μ l

The qPCR was performed in a CFX384 Real-Time System quantitative PCR (BioRad) with the following program:

Step	Temperature [°C]	Time	# of cycles
Initial denaturation	95	30 s	1
Denaturation	95	5 s	50
Annealing and extension	60	5 s	
Extension	95	10 s	
Melt curve	65 - 95	5 s (increment 0.5 °C)	1

Quantitative PCR primer design

qPCR primers were design based on the genomic and mRNA sequences of the gene of interest provided by the NCBI database. A multiple alignment between sequences was generated using the Spidey web tool (<http://www.ncbi.nlm.nih.gov/spidey/>). To avoid detection of genomic DNA, intron spanning primers (intron size >1000 bp) were selected using the Primer3 web tool (<http://bioinfo.ut.ee/primer3/>). Primers were chosen for a product size of 200-300 bp and for PCR temperature of 60°C.

2.2 Cell biology

2.2.1 HEK293 cells

Cultivation of HEK293 cells

Human embryonic kidney cells (HEK293FT) were cultivated in DMEM-Glutamax medium supplemented with 10% FCS, 1% Penicillin/streptomycin and 1% NEAA at 37°C / 5 % CO₂. At a confluency of 80-90% HEK293FT cells were split in a ratio of 1:1 to 1:10. For that purpose the medium was removed, cells were washed once with PBS, 2ml 0.05% Trypsin/EDTA was added and cells were incubated for 1 min at 37°C. Afterwards, 2 ml medium was added to stop trypsin activity, cells were carefully detached and centrifuged for 5 min at 1000 rpm. The cell pellet was resuspended in 10 ml medium and plated in the desired concentration in cell culture dishes.

Transfection of HEK293 cells

For transfection HEK293FT cells were split in a ratio of 1:1 on day one. On day two, 1,000,000 - 2,000,000 cells were plated in a 10 cm dish and transfected with Lipofectamin 2000 on day three following the manufacturer's instruction:

Component	Amount
Total DNA	10 µg
in OptiMEM	1.5 ml
After 5 min combine with:	
Lipofectamin 2000	30 µl
in OptiMEM	1.5 ml

The transfection mix incubated for 20 min at room temperature. Meanwhile, medium was removed from the cells and replaced by 5 ml prewarmed OptiMEM. After incubation, the transfection mix was added to the cells for 4 to 8 h before OptiMEM was replaced by normal culture medium. Cells were harvested and analyzed 36 to 48 h later.

Lentivirus production

For production of lentivirus, low passage HEK293FT cells were used as packaging cell line. Full confluency of HEK293-FT cells was avoided to increase virus titer. Three 10 cm dishes per virus with 5.5 million cells each were plated 24 hours prior to transfection with Lipofectamin 2000. Transfection mix was set as follows:

Component	Amount
LTR vector	18.6 µg
pSPAX2	11 µg
pVSVg	6.4 µg
Total DNA	36 µg
in OptiMEM	4.5 ml
After 5 min combine with:	
Lipofectamin 2000	108 µl
in OptiMEM	4.5 ml

LTR vector contains the lentiviral expression construct, pSPAX2 and pVSVg allow packaging of the virus particles. Transfection mix was incubated for 20 min at room temperature. In the meantime, media was exchanged with 5 ml OptiMEM supplemented with 10 % FCS per 10 cm dish. After incubation, 3 ml transfection mix was added drop-wise to each plate. After 24 h incubation, the medium was changed to DMEM Glutamax supplemented with 10 % FCS, 1 % penicillin /streptomycin, 1 % NEAA and 1.3 % BSA for another 24 hours and collected subsequently. The virus containing medium was centrifuged with 600 g for 10 min at room temperature (RT) and the resulting supernatant filtered through a sterile 0.45 µm PES membrane filter. The filtrate was centrifuged with 66,000 g for 2 h at 4°C, the supernatant discarded and the resulting virus containing pellet resuspended in 160 µl Neurobasal medium. Virus was stored in aliquots at -80°C until usage.

2.2.2 Primary neuron culture*Preparation of neurons*

Embryonic day 18 (E18) to E19 pregnant Sprague-Dawley rats were sacrificed with CO₂ treatment and subsequent cervical dislocation. The abdomen of the mother was

opened, pubs were removed, decapitated and the heads placed in ice cold HBSS. The brain was detached from the skull, the meninges were removed and hippocampi and cortices prepared and washed four times with ice cold HBSS under a cell culture hood. Hippocampi were incubated for 15 min at 37°C with 150 µl 2.5 % trypsin in 5 ml HBSS. Cortices were incubated for 20 min at 37°C with 300 µl 2.5 % trypsin and 500 µl DNase (2,000 U/mg) in 5 ml HBSS. Afterwards, hippocampi and cortices were washed four times with prewarmed HBSS and neurons dissociated by gently pipetting up and down several times. The concentration of neurons was determined in a hemocytometer and 85,000 hippocampal neurons respectively 400,000 cortical neurons in 1 ml medium for 12 well plates, 14,000 hippocampal neurons in 100 µl medium for 96 well plates or 50,000 hippocampal neurons in 3 ml medium for 3.5 cm glass bottom dishes were plated. Following electroporation 500,000 hippocampal neurons for a 6 cm dish were plated on astrocyte feeder cells in N2 medium.

Preparation of coverslips

18 mm coverslips were treated with 65 % nitric acid for 2 days to remove lipids and washed four times with milliQ-water afterwards. For subsequent sterilization, coverslips were incubated at least 6 h at more than 200°C in a heating cabinet.

Preparation of cell culture dishes

Plastic dishes were coated with 1.5% PDL in 0.1 M borate buffer glass bottom dishes and dishes with cover slips with 1.5% PDL and 0.625% laminin in 0.1 M borate buffer for at least 4 h. After coating, dishes were washed four times with sterile MilliQ water and equilibrated with neurobasal medium in the cell culture incubator until plating the neurons.

Cultivation of primary neurons

Primary rat neurons were cultivated with Neurobasal medium supplemented with 2 % B27, 1% Penicillin/streptomycin, 0.25 % glutamine (cortical neurons) respectively Neurobasal medium supplemented with 2 % B27, 1% Penicillin/streptomycin, 0.25 % glutamine, 0.125% glutamate (hippocampal neurons) at 37°C / 5 % CO₂. After seven days in culture or one day prior to transfection neurons were fed: 300 µl medium was exchanged with 500 µl fresh

medium per well for 12 well plates or 100 μ l fresh medium was added per well for 96 well plates.

Transfection of primary neurons

Neurons were transfected with Lipofectamin 2000. Transfection mix was set as follows and incubated for 20 min:

Component	Amount
Total DNA	1.8 μ g
in OptiMEM	100 μ l
After 5 min combine with:	
Lipofectamin 2000	3.2 μ l
in OptiMEM	100 μ l

In the meantime, coverslips with neurons were dipped once in prewarmed Neurobasal medium and transferred to a new well with 1 ml prewarmed Neurobasal medium supplemented with 1 % Penicillin/streptomycin and 0.25% glutamine. After incubation, 200 μ l transfection mix was added drop-wise to the coverslips. After 45 min, coverslips were dipped twice in prewarmed Neurobasal medium and transferred back into the original medium. Neurons were analyzed three or five days after transfection.

Transduction of primary neurons

For neurons grown in 12 well plates, 500 μ l medium was withdrawn and stored in the cell culture incubator to avoid pH value changes. The desired amount of virus was added to the neurons and incubated for 6 to 8 h. Thereafter, medium was discarded and replaced by the previously withdrawn medium. 500 μ l of freshly prepared Neurobasal medium supplemented with 2 % B27, 1% Penicillin/streptomycin, 0.25 % glutamine was added to each well. Neurons were analyzed five or six days after transduction. For rescue experiments with TMEM106B virus, transduction was performed one day prior to transfection.

Electroporation of primary neurons

Neurons were electroporated with the Amaxa 4D-Nucleofector and the primary culture kit P3 according to the manufacturer's instructions prior to plating. Briefly, 500,000 neurons were centrifuged for 5 min with 80 g at room temperature. Supernatant was removed and replaced by 100 μ l Amaxa Rat Neuron Nucleofector Solution, up to 5 μ g DNA was added and neurons were resuspended. After transfer to the cuvette, neurons were electroporated with the program EM110, resuspended in 500 μ l prewarmed N2 medium and plated.

Nocodazole treatment

Neurons were treated every 36 h with 10 nM freshly thawed nocodazole (stock solution: 10 μ M in DMSO) or the same volume of DMSO as control.

2.2.3 Cell viability Assay

XTT-assay

For the 2,3-bis-(2-methoxy-4-nitro-5-sulfophenyl)-2H-tetrazolium-5-carboxanilide (XTT)-assay, hippocampal neurons were cultivated in a 96 well plate. The assay was performed according to the manufacturer's instructions: freshly thawed XTT labeling reagent and Electron-coupling reagent were mixed in the ratio of 50:1. 50 μ l of the mix was added per well and the plate incubated for 18 to 24 h in the cell culture incubator. Absorbance was measured in a plate reader at a wavelength of 480 nm and a reference wavelength at 650 nm. Relative cell viability was calculated by subtraction of $A_{650\text{nm}}$ from $A_{480\text{nm}}$. Untreated or control treated neurons were set as 100 % viable, while staurosporine treatment (1 μ M for 4 h) was used as positive control.

2.3 Protein biochemistry

2.3.1 Generation and affinity purification of rabbit polyclonal antibodies

Antigen purification for immunization

For affinity purification with the corresponding maltose-binding-protein (MBP)-fusion protein, 800 ml LB liquid culture of *E.coli* bacteria transformed with MBP tagged antigen coding vectors was expanded and induced with 1 mM IPTG 30°C

when bacteria suspension reached an $OD_{600} = 0.6$. After centrifugation with 600 g for 10 min at 4°C the resulting pellet was resuspended in STE buffer. 100 µg / ml lysozyme was added and incubated for 15 min on ice to disrupt the cells and extract the antigen. Afterwards, 5 mM DTT was added and the lysate sonicated for 1 min. After centrifugation with 10,000 g for 10 min at 4°C the supernatant was incubated with 4 ml maltose beads under vigorous shaking for 30 min. Afterwards beads were washed three times with STE buffer. Antigen was eluted using. The antigen was eluted with glycine elution buffer and collected in 1 ml fractions. Fractions were neutralized with 100 µl 1M Tris pH 9.5. Protein concentration was measured using OD_{280} . Samples from all steps of the purification protocol were taken to check purity of the antigen by SDS-PAGE and subsequent commassie staining (see sections 2.4.2 and 2.4.4). Protease and phosphatase inhibitor were present in all steps of the purification.

Antibody production

Polyclonal antibodies were generated by immunizing rabbits with MBP-tagged antigens at Eurogentec SA, Belgium. The serum of several large bleeds and the final bleed were collected and stored at -20°C until affinity purification of the antibodies

Antibody	antigen for immunization
polyclonal TMEM106B antibodies 344 and 345	MBP fused with rat TMEM106B AA1-91: MGKSLSHLPLHSNKEDGYDGVSTSTDNMR NGLVSSEVRNEDGRSGDVSQFPYVEFTG RDSVTCPTCQGTGRIPRGQENQLVALIP YSDQRLR
for polyclonal MAP6 antibody	MBP fused with rat MAP6 AA793-952: NASIMASLKNEAPVASESVKNQGLGGPE PAKDTGTDLKGHGSVFVAPVKSQGPVVP EPTKGQDPIIPALAKDQGPIPEPPKNQ GPPVVLGPIKNQDPVIVPVLKGQDPVVP APTKDPGPTAPDPLKSQGPRGPQLPTVS PSPPVMIPTVPHAHEYIEGSP*

Antigen generation and crosslinking for affinity purification

For affinity purification of the antibodies glutathione-S-transferase (GST)-fusion proteins with the corresponding antigen were generated. 800 ml LB liquid culture of E.coli bacteria transformed with GST tagged antigen coding vectors was expanded and induced with 1 mM IPTG 30°C when bacteria suspension reached an $OD_{600} = 0.6$. After centrifugation with 600 g for 10 min at 4°C the resulting pellet was resuspended in STE buffer. 100 µg / ml lysozyme was added and incubated for 15 min on ice to disrupt the cells and extract the antigen. Afterwards, 5 mM DTT and 1 % TritonX100 was added and the lysate sonicated for 1 min. After centrifugation with 10,000 g for 10 min at 4°C the supernatant was incubated with 4 ml glutathione beads under vigorous shaking for 30 min. Afterwards beads were washed three times with 0.5 % TritonX100 in STE buffer. Washed beads were poured into a column, washed another four times with conjugation buffer and crosslinked to the antigen with 5 mM BS3. Protease and phosphatase inhibitor were present in all steps of the purification.

Antibody purification

For affinity purification, serum from immunized rabbits was diluted 1:1 with PBS and passed three times over the column described above. Beads were washed three times with column buffer. The antibody was eluted with glycine elution buffer and collected in 1 ml fractions. Fractions were neutralized with 100 µl 1M Tris pH 9.5. Protein concentration was measured using OD_{280} . Samples from all steps of the purification protocol were taken to check purity of the antibody by western blotting.

2.3.2 Immunoblotting

Lysate preparation

Neurons in 12 well plates were washed with PBS, directly lysed in 250 µl 2x Lämmli sample buffer and boiled for 10 min at 96°C. HEK293FT cells were scraped in PBS, centrifuged with 5000 rpm for 5 min at 4°C. The cell pellet was lysed in RIPA buffer or 1% TritonX100 in PBS for 15 min at 4°C. The lysate was

centrifuged with 17,000 *g* for 20 min at 4°C, the supernatant subsequently diluted with 2x Lämmli sample buffer in a ratio of 1:1 and boiled at 96°C for 10 min.

SDS-polyacrylamide gel electrophoresis (SDS-PAGE)

Proteins in the cell lysate were separated under denaturizing conditions using a discontinuous SDS polyacrylamide gel electrophoresis system. Acrylamide concentration was 4% for the stacking gel and 7.5 to 12.5 % for the separating gel depending on the hydrodynamic radius of the denatured proteins. Gels were cast as described below (mixture for 4 10 % gels):

Stacking gel	6.5 ml H ₂ O 2.5 ml stacking gel buffer 1 ml acrylamide added for polymerization: 100 µl 10% APS 10 µl TEMED
Seperating gel	10 ml H ₂ O 5 ml separating gel buffer 5 ml acrylamide added for polymerization: 200 µl 10% APS 20 µl TEMED

Between 10 µl and 15 µl total protein lysate was used per lane. Electrophoresis was carried out in running buffer with a voltage of 90 V for the first 15 min and 120 to 180 V until the dye front reached the end of the gel.

Immunoblotting (IB)

For immunodetection, proteins separated by SDS-PAGE were blotted onto previously ethanol activated polyvinylidene difluoride (PVDF) membranes. Protein transfer was performed in methanol free blotting buffer at a constant current of 400 mA per blotting chamber for 75 min.

Immunodetection of proteins

PVDF membranes were blocked in 0.8 % I-Block in TBSTx for at least 1 h and incubated with primary antibodies in 0.8 % I-Block in TBSTx overnight at 4°C. After five washing steps with TBSTx for ten min each, a HRP coupled secondary antibody in 0.8 % I-Block in TBSTx, appropriate for the species of the primary antibody used, was incubated for 1 h at room temperature. Membranes were washed another five times with TBSTx and incubated with 2 ml of the chemiluminescence substrates ECL or ECLplus depending on the expected intensity of the emitted signal. For detection of the signal, X-ray films were exposed to the membrane in complete darkness and developed using a CaWo X-ray film processor. Signals on the films were quantified densitometrically using ImageJ software.

2.3.3 Immunoprecipitation (IP)

Immunoprecipitation from rat brain

Three P15 Sprague-Dawley rat brains were extracted and immediately snap frozen. The frozen brains were homogenized with an automated potter cell homogenizer in 20 ml homogenization buffer and centrifuged with 1,000 g for 10 min in a JA25.50 rotor at 4°C. The supernatant S1 was further centrifuged with 75,465 g for 30 min at 4°C, the resulting pellet P2 (membrane fraction) resuspended in 15 ml PBS and after addition of 1 % Triton X100 lysed for 15 min on ice. The lysate was centrifuged with 100,000 g for 20 min rotor at 4°C in a TLA55. The supernatant was immunoprecipitated with 10 µg of the respective antibodies crosslinked with BS3 to 50 µl protein G dynabeads for 1.5 h at room temperature. Input was taken right before the immunoprecipitation. Beads were washed five times for 5 min each with lysis buffer at 4°C. Protein was eluted for 5 min with 30 µl glycine elution buffer at room temperature, diluted in a ratio of 1:1 with 4x Lämmli sample buffer and boiled for 10 min at 96°C. Samples were subjected to SDS-PAGE and either western blotting or colloidal Coomassie staining and subsequent mass spectrometric analysis. Protease and phosphatase inhibitors were present in all steps of the immunoprecipitation.

Immunoprecipitation from HEK293FT cells

HEK293FT cells were washed and scraped in PBS, centrifuged with 5000 rpm for 5 min at 4°C and lysed in 1% Triton X100 in PBS for 15 min at 4°C. The lysate was centrifuged with 17,000 g for 40 min at 4°C, the resulting supernatant subsequently diluted with PBS to a concentration of 0.5 % TritonX100 and precleared with protein A sepharose beads for 30 min at 4°C under light agitation. The cleared lysate was subjected to immunoprecipitation with 30 µl myc-agarose beads for 1 h at 4°C. Input samples were taken directly before beginning the immunoprecipitation. Beads were washed five times for 5 min each with 0.5 % Triton X100 in PBS at 4°C and boiled in 2x Lämmli sample buffer for 10 min at 96°C to elute the proteins. Samples were subjected to SDS-PAGE and western blotting. Protease and Phosphatase inhibitors were present in all steps of the immunoprecipitation.

2.3.4 Other protein biochemistry techniques

Colloidal Coomassie

For detection of total proteins, SDS polyacrylamide gels were stained with the NOVEX Colloidal Blue Staining Kit according to the manufacturer's instruction. Gels were lightly agitated in fixing solution for at least 2 h, incubated with staining solution for 3 h and washed several times with MilliQ water until protein bands appeared.

Subcellular fractionation

The brain of an adult female Sprague-Dawley rat was extracted and immediately snap frozen. The frozen brain was homogenized with a manual potter cell homogenizer in 20 ml homogenization buffer and centrifuged with 1,500 g for 10 min at 4°C. The postnuclear supernatant was further centrifuged in a TH641 rotor with 100,000 g for 30 min at 4°C and the pellet (membrane fraction) was resuspended in homogenization buffer. A 10 % volume fraction was loaded on 15 ml of a discontinuous iodixanol gradient (2.5 %, 5 %, 7.5 %, 10 %, 12.5 %, 15 %, 17.5 %, 20 %, 30 % in homogenization buffer). The gradient was centrifuged at 274,044 g for 2.5 h at 4°C in a TH-641 rotor. Fractions (1 ml each) were collected manually

by puncturing the bottom of the centrifugation tube with a needle and further processed for SDS-PAGE and western blotting as described above.

2.4 Imaging techniques

2.4.1 Immunofluorescence

Fixation

Hippocampal neurons grown on coverslips were washed with PBS and fixed with 4% PFA fixing solution for 15 min at RT.

Immunostaining

Fixed neurons were washed three times for at least 5 min each with PBS. Neurons were incubated with the respective primary antibody in 1x GDB buffer overnight at 4°C. After additional three washing steps with PBS, neurons were incubated with the appropriate Alexa-488, Alexa-555 or Alexa-647 coupled secondary antibody in 1x GDB buffer for 1 h at RT and washed another three times with PBS. If necessary, nuclei were stained with 1:1000 TO-PRO 3 in PBS for 10 min at room temperature directly before mounting the immunostained coverslips. All incubation steps were conducted in a light-protected, humidified incubation chamber.

Mounting

Directly after staining, coverslips were dipped in MilliQ water and mounted on microscope slides with Vectashield mounting medium. Excess mounting medium was aspirated and coverslips were sealed with clear nail polish.

Image acquisition

Confocal images were taken on a confocal laser scanning Carl Zeiss LSM510 or LSM710 system. 40x or 63x oil immersion objectives (NA=1.3/1.4) were used. Pinhole was set to 1 Airy unit for the longest wavelength used and maintained for all other wavelengths. For filter sets, excitation and emission wavelengths precast parameters for the respective Alexa dyes were used. Laser intensity and detector gain was chosen that all pixels were in linear range and not oversaturated. Distance between two adjacent confocal planes of a z stack was set that every pixel was covered by two confocal planes to get an optimal resolution in z direction. The x-y-

Resolution of confocal images was set to at least 1024 x 1024 pixels. Scanning speed was chosen according to the purpose of the experiment. For quantitative and semi quantitative measurements all settings were maintained for every image of the respective experiment.

For analysis of axonal length, images were taken on a Carl Zeiss Axio imager.A2 epifluorescence microscope with a 40x oil immersion objective (NA=1.3).

2.4.2 Live imaging

Movie acquisition

For Time-lapse microscopy a Carl Zeiss Cell observer SD spinning disc system was used. Images were taken with a 63x oil immersion objective (NA=1.4) on an air cooled Evolve 512 electron-multiplying charged-coupled device (EMCCD) camera with a frame rate of 1 Hz for 5 min. For filter sets, excitation and emission wavelengths precast parameters for the respective fluorescent proteins were used. Velocity of the spinning disc was 5000 rpm. Laser intensity and gain was set that all pixels in the region of interest were in linear range and not oversaturated. The x-y resolution of the images was set to 512 x 512 pixels due to camera limitations. For live imaging Neurons were grown in 3.5 cm glass bottom dishes and imaged either in their normal culture medium or in prewarmed and equilibrated HBSS/Hepes buffer. During image acquisition neurons were kept at 37°C/5 % CO₂ in a climate chamber.

2.4.3 Image analysis

Image processing

Confocal images were processed with ImageJ software. Z-stacks and color channels were separated and if required a maximum intensity projection from a z-stack or a merged image from different color channels generated.

Quantitative analysis of colocalization

Colocalization of pixels in different channels of the same confocal plane of an image was analyzed using the JaCoP plugin of ImageJ software (Bolte and Cordelieres, 2006). As quantitative parameter for the correlation of two channels Pearson's coefficient R_r was used:

$$R_r = \frac{\sum(R_i - \bar{R}) * (G_i - \bar{G})}{\sqrt{\sum(R_i - \bar{R})^2 * \sum(G_i - \bar{G})^2}}$$

For every pixel i in the images, R and G are intensities of the red and green channel respectively. At which $R_r = 1$ denotes perfect colocalization, $R_r = 0$ denotes random localization and $R_r = -1$ denotes perfect exclusion.

Morphological analysis

For the analysis of axonal length, the longest tau1 positive neurite of a developing neuron kept 4 days *in vitro* (DIV4) was chosen. Its length was measured using the Carl Zeiss Axio Vision software. For the analysis of the length of the longest dendrite mature neurons (DIV19) were analyzed. The longest dendrites were identified morphologically and measured using ImageJ software.

Sholl analysis (Sholl, 1953) was used to assess the complexity of the total dendritic arbor of a growing (DIV12) or mature (DIV19) neuron. To that end, a mask with nine concentric circles in distances between 12.5 μm and 112.5 μm (12.5 μm intervals) was laid around the center of the cell soma in MetaMorph software. For each circle the number of dendrite crossings was counted and plotted against the respective distance to the soma.

Spine length, width and density (spine number per 100 μm) was measured using MetaMorph software. Two dendrite segments per neuron (DIV19) with preferably no axonal crossings and a total length of at least 150 μm were chosen. Maximal length and width and the total number of every structure below 10 μm on these segments were determined with the software.

All analysis were done manually and blinded to the experimental conditions

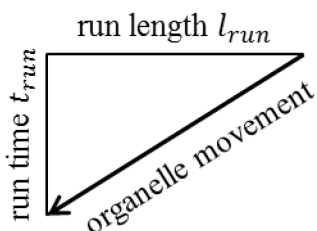
2.4.4 Movie analysis

Generation of kymographs

5 min time laps movies from single neurons were used to analyze organelle movement with ImageJ software. Kymographs were generated along a line (width: 3 pixels) from dendrite tip to soma in at least four dendritic segments per neuron. The Kymograph-plugin (http://www.embl.de/eamnet/html/body_kymograph.html) was used to generate the kymographs.

Analysis of organelle dynamics

The dynamics of organelle movement was manually analyzed in kymographs. The numbers of stationary (horizontal lines in the kymograph), moving (sloped lines in the kymograph) and the total number of organelles were determined. The direction of moving organelles was assigned and classified as retrograde movement (net movement to the soma), anterograde movement (net movement to the dendrite tip) or no net movement. Speed ($v = \frac{l_{run}}{t_{run}}$) and run length l_{run} of all movement events longer than 5 μm was determined as shown below and mean values calculated.



Co-migration assay

For co-migration assays of two fluorescently labeled proteins time laps movies with two different wavelengths were acquired. Kymographs were generated as explained above for each wavelength individually and merged images generated.

2.5 Mass spectrometry (in collaboration with Sebastian Høgl)

Sample preparation

Bands cut from colloidal Coomassie stained SDS-polyacrylamide gels were excised and tryptic in-gel digestion of the proteins was performed (Shevchenko et al., 2006). Gel fragments were destained with 100 μl 100 mM ammonium bicarbonate/acetonitrile (1:1, v/v) for 30 min and subsequent addition of 500 μl acetonitrile. After withdrawal of the destaining solution at least 50 μl trypsin buffer were added and incubated for 2 h on ice to saturate the gel pieces. To cover the gel piece up to 20 μl ammonium bicarbonate buffer was added and the whole mixture was incubated at 37°C overnight for the tryptic digest. To extract the digested

proteins 100 μ l extraction buffer was added, incubated for 15 min at 37°C under light agitation. The supernatant was withdrawn and analyzed.

Liquid chromatography-tandem mass spectrometry (LC-MS/MS)

The trypsin digested peptides were analyzed on a LC-MS/MS setup. A Proxeon Easy nLCII (Thermo Fisher Scientific) with 15 cm columns (2.4 μ m C18 beads, Dr. Maisch GmbH) was coupled to a LTQ Velos Orbitrap mass spectrometer (Thermo Fisher Scientific). A bilinear gradient of 60 to 85 min was applied for peptide separation. MS1 scans were acquired in the orbitrap mass analyzer applying a target value of 1,000,000 and a resolution of 60,000. Subsequently, collision induced dissociation (CID) fragmentation was performed for the 14 most intensive ions of the MS1 spectrum using an isolation width of 2 Da. Centroid MS2 spectra were acquired for the TOP 14 peptides in the linear ion trap with a target value of 10,000 in the normal scanning mode. Enabled charge state screening, a monoisotopic precursor selection, 35% normalized collision energy, an activation time of 10 ms, wide band activation and a dynamic exclusion list were applied.

Data analysis

Peptide identification was performed using the Proteome Discoverer 1.2 software with the embedded SEQUEST algorithm. The International Protein Index database for rat (version 3.87) was used for the database search with carbamidomethylation of cysteine as a static and oxidation of methionine as a dynamic modification. Only full tryptic peptides with a maximum of 2 missed cleavages and an false discovery rate (FDR) below 5 % were included in the analysis.

2.6 Statistical analysis

Statistical analysis with Student's t-test were calculated with MS Excel software, analysis with One-way and Two-way Analysis of Variance (ANOVA)-tests were calculated with GraphPad Prism software. Statistical significance was indicated as: * $p < 0.05$, ** $p < 0.01$, *** $p < 0.001$.

IV. Results

1. Generation and validation of TMEM106B shRNA and antibodies

In order to investigate the role of TMEM106B in primary neurons, I used shRNA mediated knockdown of the endogenous protein using either transfection or lentiviral transduction. I generated two shRNAs against TMEM106B and compared the knockdown efficiency to a control shRNA (shLuc). qPCR analysis of transduced neurons (DIV7+5) demonstrated a knockdown of almost 90% for shT106b#1 and more than 95% for shT106b#2 (Figure 6A). Moreover, it was essential for all localization and functional studies to use antibodies which reliably detect the endogenous protein in immunoblot and immunofluorescence. Thus, polyclonal antibodies specific for the N-terminus of rat TMEM106B were generated. To this end, two rabbits were immunized with a peptide consisting of the first 91 amino acids of rat TMEM106B fused to MBP. The antibodies were affinity purified from rabbit serum with a homologous GST fusion protein (compare method section). In order to test the antibodies, primary cortical neurons (DIV7+5) were transduced with a shRNA against TMEM106B or a control shRNA. In the immunoblot, the signal for endogenous TMEM106B was drastically reduced for in TMEM106B knockdown samples compared to control samples (Figure 6B). In order to test the TMEM106B antibody additionally in immunofluorescence, primary hippocampal neurons (DIV7+5) were transfected with two different shRNAs against TMEM106B or the control shRNA. In shT106b transfected neurons – identified by cotransfected EGFP – TMEM106B staining was strongly reduced whereas a strong staining was still visible in the control cells. These experiments confirm good specificity of the antibodies in immunoblot and immunofluorescence (Figure 6C).

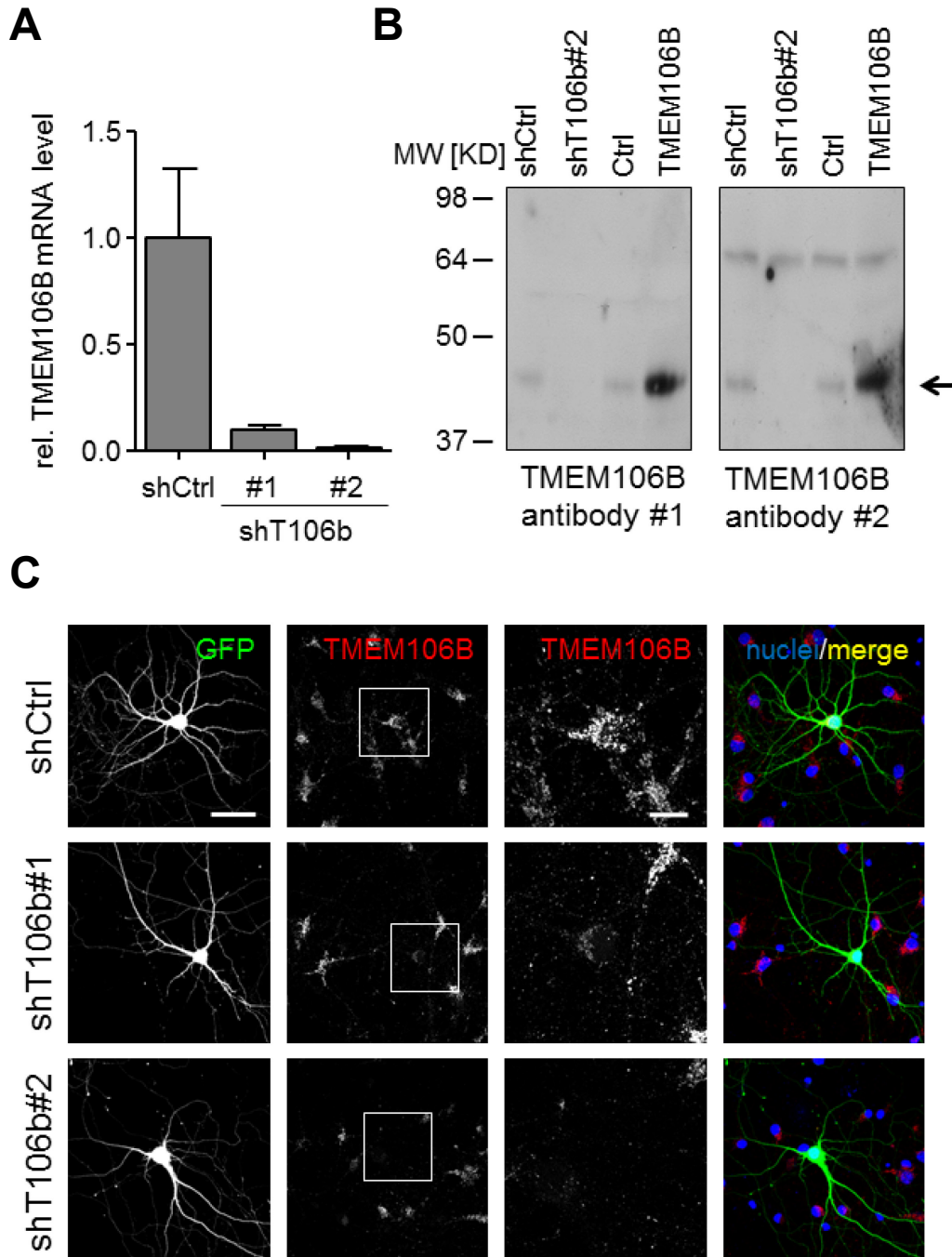


Figure 6: Validation of polyclonal TMEM106B antibodies

(A) Primary rat cortical neurons (DIV7+5) were transduced with a lentivirus expressing control shRNA (shCtrl), TMEM106B shRNA (shT106b#2), empty vector control or rat TMEM106B. Immunoblots with two different polyclonal antibodies against the first 91 N-terminal amino acids of rat TMEM106B. Arrow points to correct bands. (B) Primary hippocampal neurons were transfected with a control shRNA, shT106b#1 or shT106b#2 and GFP as transfection marker. Neurons were stained with an antibody against TMEM106B (red). Staining confirms TMEM106B knockdown in the two dimensional projection. Scale bar represents 50 μ m in the overview or 10 μ m in the magnification of the nucleus.

2. Effects of TMEM106B knockdown in primary neurons

2.1 TMEM106B knockdown does not affect viability of primary neurons

Next, I tested whether the knockdown of TMEM106B had any influence on FTLD related proteins. As above, I transduced cortical neurons (DIV7) with TMEM106B shRNA #1, #2 or the control shRNA for 6 days and assessed the levels of GRN, TDP-43, FUS and Tau by immunoblotting. No change was detected in the overall expression levels comparing knockdown cell lysates with the control lysates. Moreover, the protein levels of the important neuronal marker β -III-tubulin remained unchanged, too (Figure 7A).

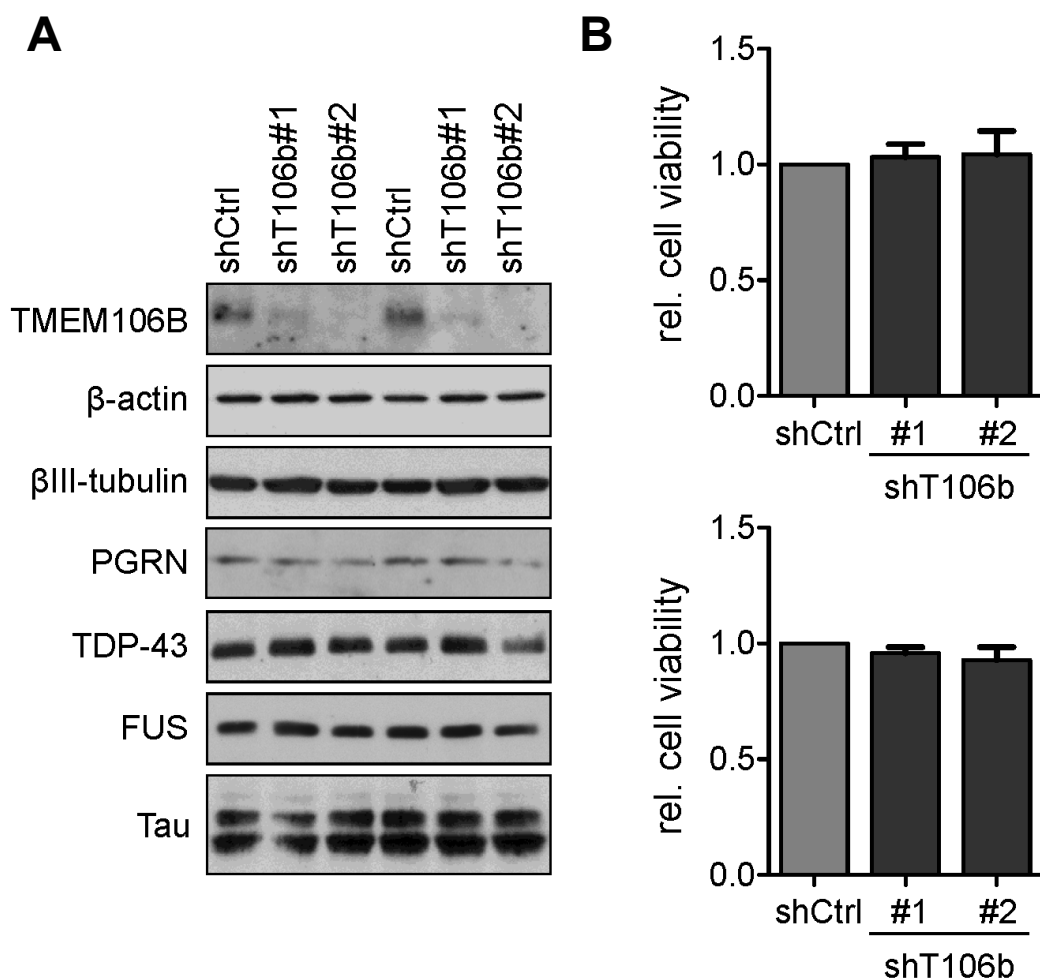


Figure 7: TMEM106B knockdown does not affect general neuron viability

(A) Primary rat cortical neurons (DIV7+6) were transduced with a lentivirus expressing either TMEM106B shRNA (shT106b) #1 or #2 or a control shRNA (shCtrl). Immunoblots with the indicated antibodies for neuronal marker proteins or FTLD associated proteins. Protein levels are not changed. (B)

Primary rat cortical neurons (DIV7+6 or DIV 14+6) were transduced with the indicated lentivirus. Cell viability upon TMEM106B knockdown was measured using an XTT assay. TMEM106B knockdown had no statistically significant effect (one-way ANOVA). $n \geq 3$ independent experiments, mean \pm SEM.

Additionally, I performed a metabolic-based XTT-cell-viability assay, to assess if the knockdown of TMEM106B had any influence on neuronal survival. Young neurons (DIV7+5) as well as fully mature neurons (DIV14+5) were transduced with both shRNAs for TMEM106B and the control shRNA and incubated with the XTT reagents. Notably, loss of TMEM106B protein exhibited no obvious toxicity in this context (Figure 7B). Altogether this data demonstrates that loss of TMEM106B protein in primary neuronal culture influences neither the protein levels of several FTLN-associated proteins nor the general viability of the cell and thus likely contributes to FTLN pathogenesis by other mechanisms.

2.2 TMEM106B is mainly localized in dendritic lysosomes

In order to determine the subcellular compartment of TMEM106B in a disease relevant cell type, I performed colocalization experiments for the endogenous protein in primary hippocampal neurons. Hence, I stained untransfected neurons after seven days in vitro with antibodies against TMEM106B and several organelle marker among them, lysosomal-associated membrane protein 1 (LAMP1). Endogenous TMEM106B showed a vesicular pattern which overlapped to a high extent with the lysosomal marker LAMP1. In the merged image a substantial overlap of the two color signals verifies the predominantly late endosomal / lysosomal localization (Figure 8A). The TMEM106B staining was especially abundant in soma and the main dendrites. This finding could be confirmed later on by others in tumor cell lines and primary neuronal culture (Brady et al., 2013; Chen-Plotkin et al., 2012; Lang et al., 2012)

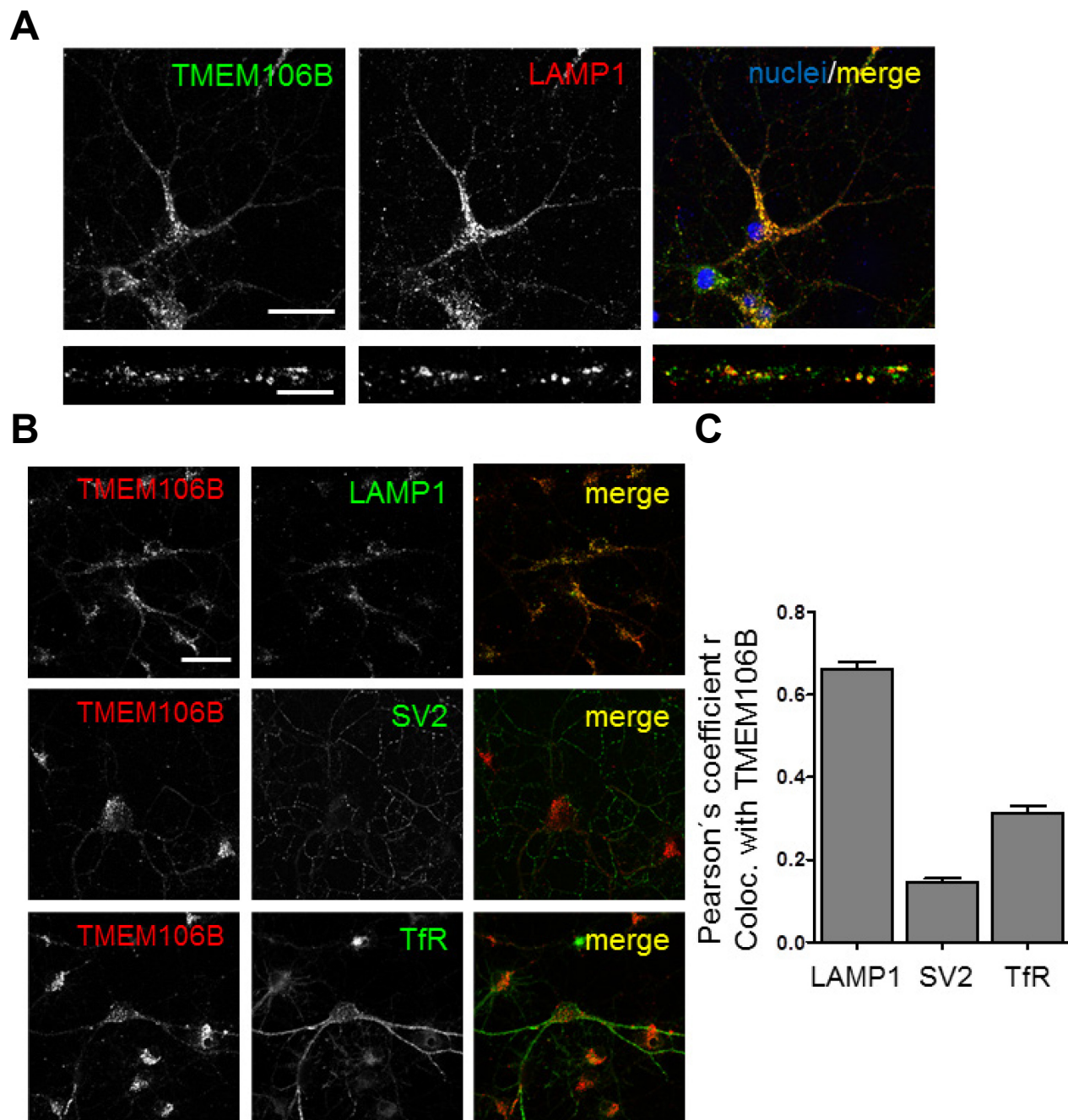


Figure 8: TMEM106B is localized in late endosomes / lysosomes of primary neurons

(A) Primary rat hippocampal neurons (DIV12) were stained with antibodies against TMEM106B (green) and the lysosomal marker LAMP1 (red). Scale bar represents 50 μm in the overview or 10 μm in dendrite segments. Merged image indicates widespread co-localization in a single confocal plane. (B) Primary hippocampal neurons (DIV12) were stained with antibodies against TMEM106B (red) and LAMP1 for lysosomes, SV2 for synaptic vesicles or transferrin receptor TfR for early endosomes (green). Scale bar represents 50 μm . The amount of colocalization was analyzed in at least 15 confocal fields using the JaCoP plugin of ImageJ. (C) Quantitative analysis of colocalization using the Pearson's coefficient. (Mean \pm SEM). Substantial Colocalization was detected only for TMEM106B with the lysosomal marker LAMP1.

In order to confirm this observation I quantified the amount of colocalization between TMEM106B and various organelle markers. To this end, I stained primary hippocampal neurons with an antibody against TMEM106B and antibodies against LAMP1, against SV2, a marker for synaptic vesicles or against Transferrin Receptor (TfR), a marker for early- and recycling-endosomes. The correlation of the intensity distribution between the individual color channels was calculated using the Pearson's coefficient R_r . The correlation coefficient between TMEM106B and LAMP1 staining was in the expected range for a pronounced colocalization ($R_r = 0.66 \pm 0.02$) (Zinchuk and Grossenbacher-Zinchuk, 2011) and thereby significantly higher than the correlation between TMEM106B and the other two vesicular marker proteins ($R_r = 0.15 \pm 0.01$ for SV2 and $R_r = 0.31 \pm 0.02$ for TfR) (Figure 8B and 8C).

Axonal architecture is quite complex in mature neurons and it is often impossible to trace the full length of an axon. Thus I focused the analysis of TMEM106B localization in axons on an earlier time-point (DIV4) when functional dendrites are not established yet but the axon is already formed. Axons were defined morphologically as the longest neurite or by the presence of a gradient of unphosphorylated tau (Tau-1 staining) (Mandell and Banker, 1996). Costaining of TMEM106B with Tau-1 or LAMP1 showed clear overlap of the signals, indicating that TMEM106B is also found in axonal lysosomes, although to a lesser extent compared to dendritic lysosomes (Figure 9).

Taken together these findings demonstrate a strong late endosomal / lysosomal localization of TMEM106B in neurons especially in the soma and the main dendrites and to a lesser extent in the axonal compartment.

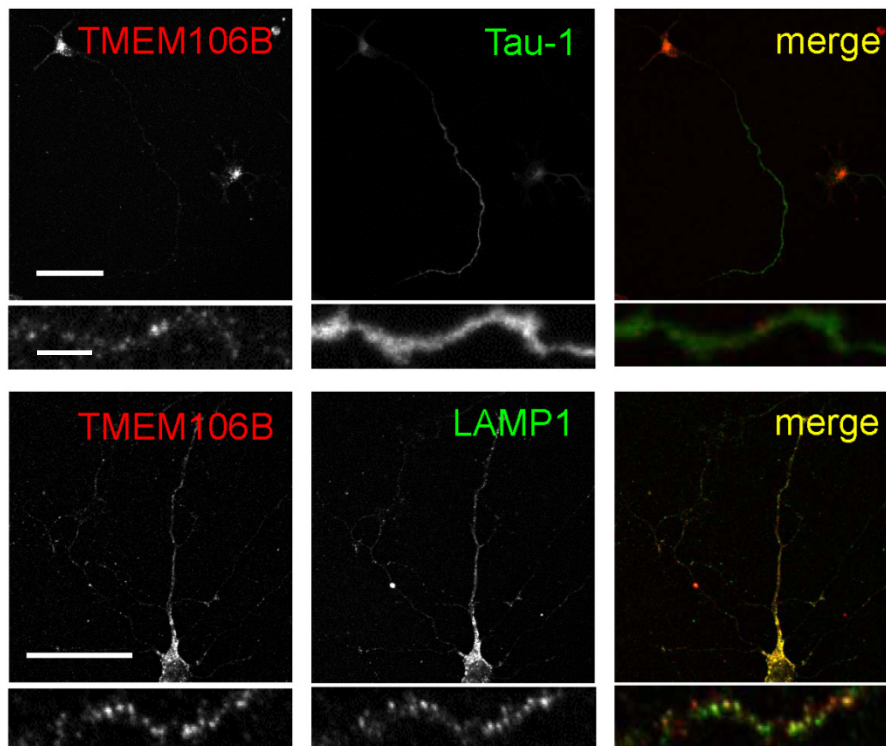


Figure 9: TMEM106B is also occurring in axons of primary neurons

Primary rat hippocampal neurons (DIV4) were stained with antibodies against TMEM106B (red) and the axonal marker Tau-1 (green) or the lysosomal marker LAMP1 (green). Scale bar represents 50 μm in the overview or 10 μm in axonal segments. Merged images indicate widespread co-localization in a single confocal plane.

2.3 TMEM106B knockdown does not change lysosomal parameters

Since it was previously described that overexpression of TMEM106B in HeLa and N2a cells resulted in enlarged lysosomes and vacuolar structure (Brady et al., 2013; Chen-Plotkin et al., 2012), I aimed to test morphology, localization and degradative function of lysosomes in primary neuronal culture. However, plasmid-based overexpression of TMEM106B in neurons leads to large vacuoles with TMEM106B aggregates in soma and dendrites with little resemblance to endogenous staining (data not shown). Thus, I used shRNA mediated knockdown to examine the influence of TMEM106B on lysosomal parameters. TMEM106B shRNA transfected hippocampal neurons (DIV7+5) were stained with an antibody against the lysosomal

marker LAMP1. There was no obvious change visible in the appearance and size of the vesicles in comparison to control transfected neurons (Figure 10).

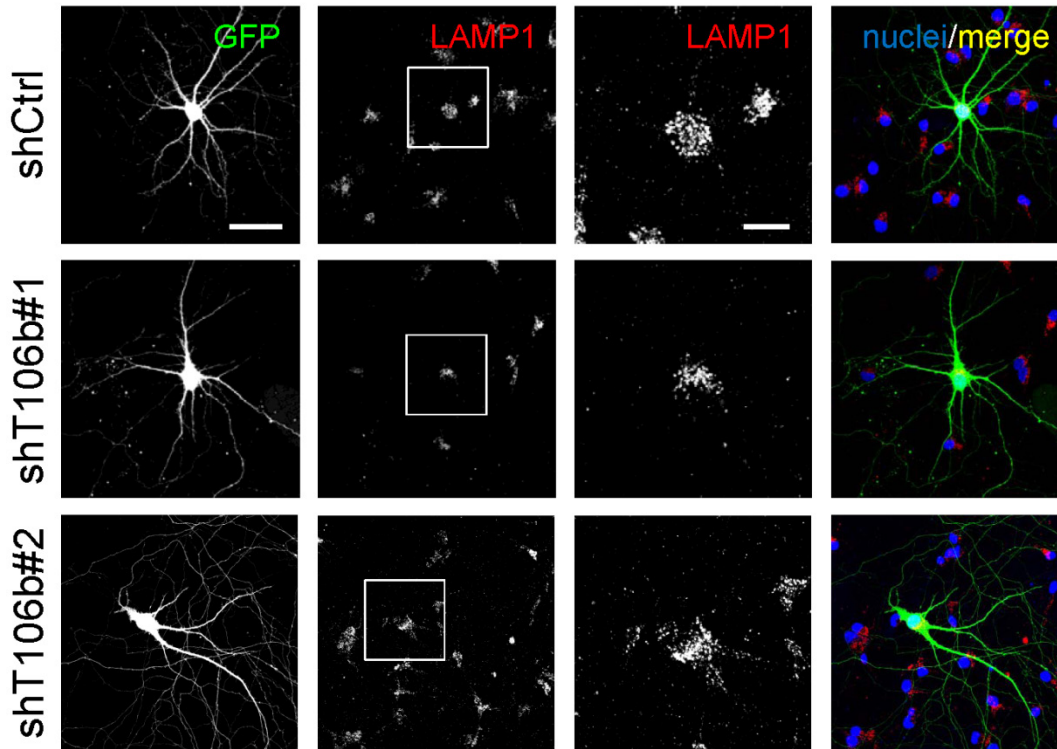


Figure 10: Lysosomal morphology is unchanged upon TMEM106B knockdown

Primary rat hippocampal neurons (DIV7+5) were cotransfected with shCtrl, shT106b#1 or shT106#2 and GFP as transfection marker. Immunofluorescence of neurons stained with an antibodies against LAMP1 (red). Scale bar represents 50 μm in the overview or 10 μm in the magnification of the soma. No obvious change in morphology and a slight tendency to perinuclear distribution of lysosomes was detected.

Next, I assessed lysosomal function by measurement of the intravesicular pH value directly with LysoTracker staining and indirectly by measuring the pH-dependent maturation of the lysosomal protease Cathepsin D. Live labeling of lysosomes revealed bright LysoTracker staining in shT106B#2 transfected neurons as well as in control neurons demonstrating acidic environment under both conditions (Figure 11A). Additional evidence for working lysosomes was provided by the unaltered pH dependent proteolytic processing of Cathepsin D. Total lysates of TMEM106B shRNA and control transduced neurons showed no difference in the band pattern on immunoblot (Figure 11B). Taken together, my results show no obvious difference in

lysosomal localization and function in TMEM106B knockdown neurons and thereby rather argue for other defects than in lysosomal degradation.

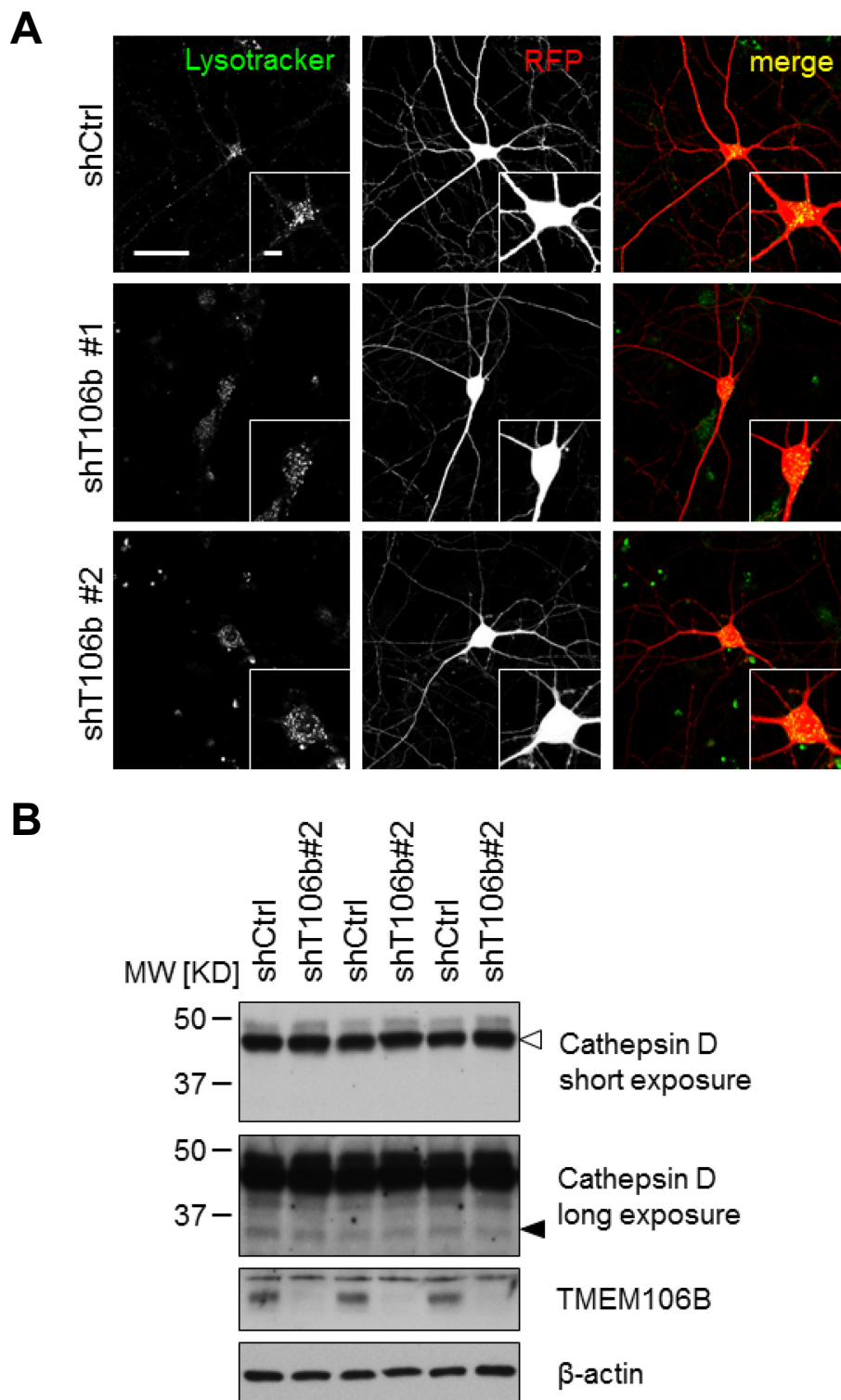


Figure 11: Lysosomal pH-value is unchanged upon TMEM106B knockdown

(A) Primary rat hippocampal neurons (DIV7+5) were cotransfected with shCtrl, shT106b#1 or shT106#2 and RFP as transfection marker. Neurons were live labeled with LysoTracker green and imaged immediately. Scale bar represents 50 μm in the overview or 10 μm in the magnification of the soma. No obvious change in LysoTracker staining was detected. (B) Primary cortical neurons (DIV7+6) were lentivirally transduced with shCtrl or shT106b#2. Immunoblot with the indicated antibodies. No change in the pH-dependent maturation of Cathepsin D was detected.

3. Effect of TMEM106B knockdown on neuronal morphology**3.1 TMEM106B knockdown inhibits dendritic branching**

Interestingly, knocking down TMEM106B in primary neurons, although not toxic, led to a dramatic reduction in dendritic branching (compare Figure 6B). To examine this observation in more detail and to quantify the effect I utilized Sholl analysis, a technique which analyzes dendritic complexity by combined measurement of dendrite length and branching (Sholl, 1953). For this analysis, Hippocampal neurons were transfected at DIV7 with the TMEM106B shRNAs or the control shRNA and a filler protein (EGFP) to visualize neuron morphology. Five days after transfection, neurons were fixed and confocal images of individual cells acquired. On each image nine concentric circles at intervals of 12.5 μm were placed around the cell soma and the number of crossings between the dendrites and each circle was counted. The quantification clearly confirmed the initial impression: with both shRNAs, dendrite branching is drastically reduced compared to control transfected neurons, especially in the proximal part of the dendrite (Figure 12A and 12B). Next, I set out to elucidate if this effect reflects a deficiency only in dendrite outgrowth – which indicates the phenotype seen in the still developing neurons at DIV7+5 – or also a deficit in dendrite maintenance. Therefore mature neurons (DIV14+5) were transfected likewise with TMEM106B shRNAs or the control shRNA. Again, the complexity of the dendritic arbor was drastically reduced with both shRNAs compared to control shRNA transfected neurons (Figure 12C and 12D), clearly pointing to impairment in both, dendrite outgrowth and maintenance.

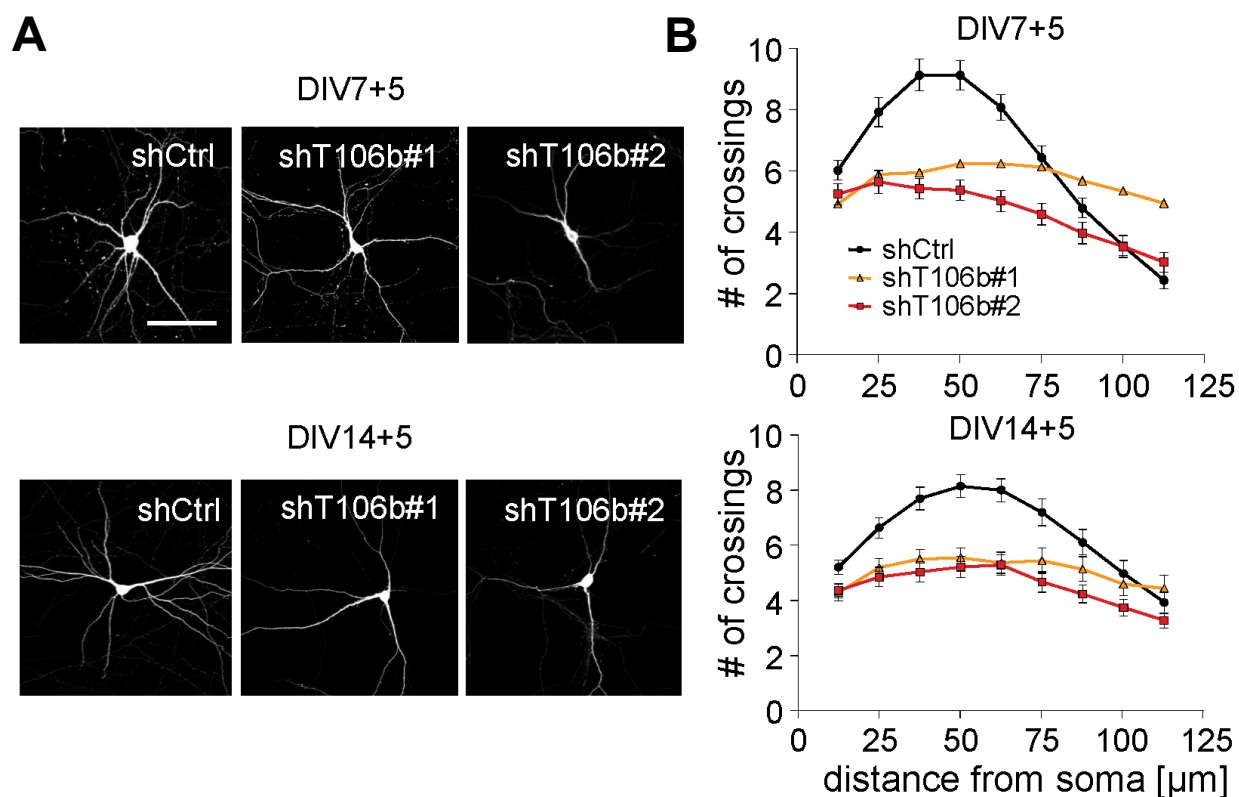


Figure 12: TMEM106B knockdown impairs dendrite branching and maintenance

(A, B) Primary rat hippocampal neurons (DIV7+5 and DIV14+5) were cotransfected with the indicated shRNAs and GFP to visualize cell morphology. Dendritic arborization was quantified manually and blinded to the experimental condition by Sholl analysis using MetaMorph software. Neurons transfected with either TMEM106B shRNA #1 or #2 show significantly reduced branching pattern compared to control shRNA transfected cells (Analysis at DIV7+5: shT106b#1: from 25 μm to 62.5 μm radius $p < 0.001$, 100 μm and 112.5 μm $p < 0.001$; shT106b#2: from 25 μm to 75 μm $p < 0.001$; Analysis at DIV14+5: shT106b#1: from 37.5 μm to 62.5 μm $p < 0.001$, at 75 μm $p < 0.05$; shT106b#2: 37.5 μm to 62.5 μm $p < 0.001$, at 25 μm and 87.5 μm $p < 0.05$). $n > 38$ neurons per condition, 3 independent experiments, mean \pm SEM. Two-way ANOVA. Scale bar represents 100 μm .

In order to exclude that the dendritic phenotype is due to off-target effects of the short hairpin, I used two shRNAs with different target sites which both led to the same phenotype (Figure 12A-12D). Moreover, I generated a TMEM106B overexpression construct (TMEM106B*) with silent mutations rendering the mRNA resistant to both TMEM106B shRNAs used, to perform rescue experiments. Since already mild overexpression of TMEM106B in the neurons leads to unphysiological aggregation of the exogenously expressed protein (Brady et al., 2013; Chen-Plotkin

et al., 2012), I used lentivirus to titrate the shRNA resistant construct back to endogenous protein levels (Figure 13A). This careful reintroduction of TMEM106B into shT106b transfected neurons prevented unphysiological aggregation of the exogenous protein. Under these conditions, I achieved a complete prevention of the dendrite loss for shRNA #1 and a partial prevention for the more potent shRNA #2 (Figure 13B and 13C, compare Figure 6), confirming the specificity of the short hairpin sequences used.

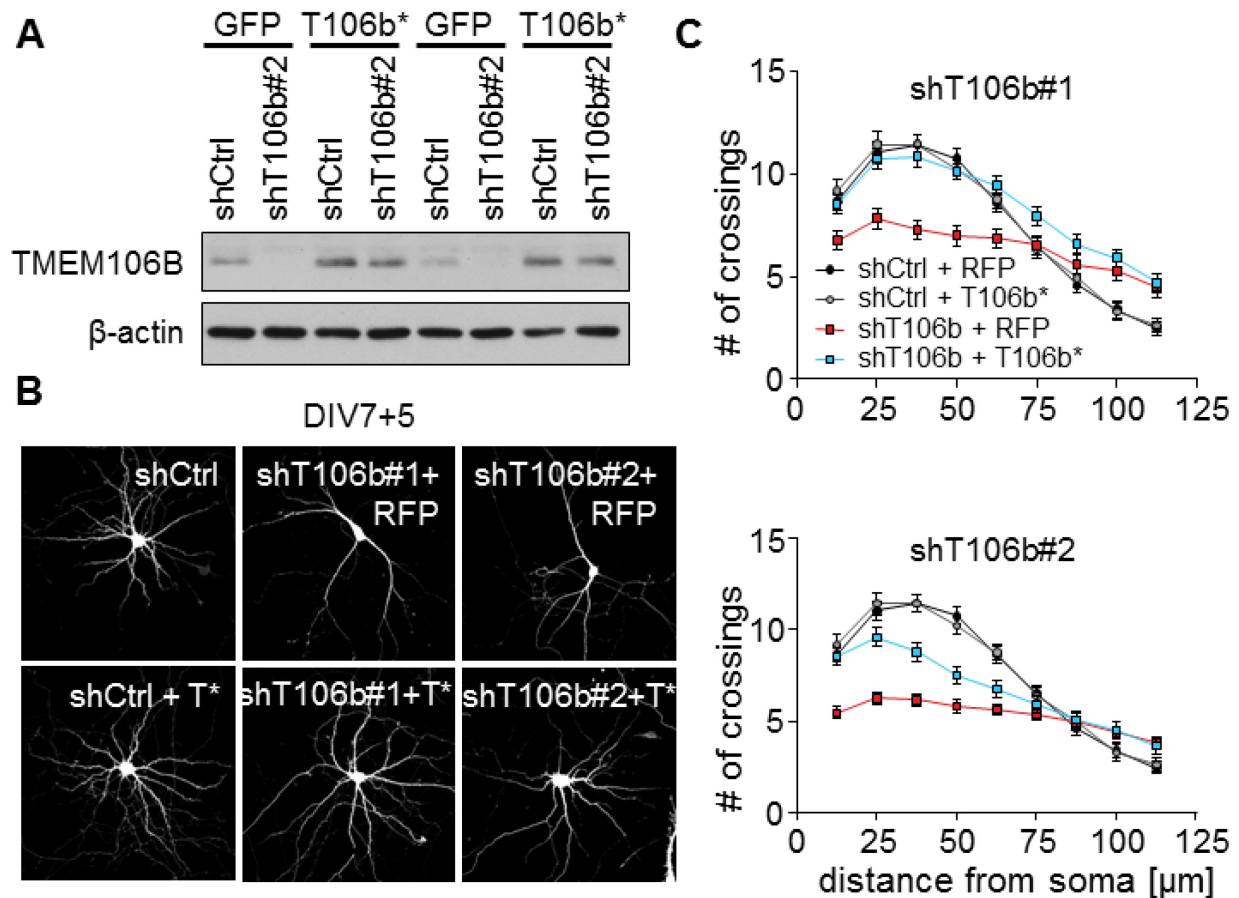


Figure 13: Validation of the TMEM106B knockdown phenotype by expression of a shRNA resistant mutant

(A) Primary cortical neurons (DIV7+6) were transduced with a shRNA-expressing lentivirus (shCtrl or shT106b#2) and a lentivirus expressing shRNA-resistant TMEM106B (T106b*) or GFP as control to titrate TMEM106B expression. (B, C) Primary rat hippocampal neurons were virally infected (DIV6) with either mCherry (RFP) or shRNA-resistant TMEM106B mutant (T106b*) and cotransfected (DIV7+5) with either a control shRNA or the indicated TMEM106B shRNA and GFP to outline neuron morphology. Sholl analysis was done as above. ShRNA-resistant TMEM106B overexpression fully rescued the phenotype of the less potent TMEM106B shRNA #1 and partially rescued the more potent shRNA #2. (Analysis of shT106b#1: shCtrl+RFP vs. shT106b+RFP: from 25 μ m to 50 μ m $p < 0.001$, shT106b+RFP vs. shT106b+T106b*: 25 μ m and 62.5 μ m $p < 0.05$, 37.5 μ m and 50 μ m $p < 0.001$; Analysis of shT106b#2:

shCtrl+RFP vs. shT106b+GFP: from 12.5 μm to 50 μm $p < 0.001$, shT106b+RFP vs. shT106b+T106b*: from 12.5 μm to 25 μm $p < 0.001$, at 37.5 μm $p < 0.05$). $n > 38$ neurons per condition, three independent experiments, mean \pm SEM, two-way ANOVA. Scale bar represents 100 μm .

Since the observed dendrite loss affected primarily the proximal arborization (see Figure 12B and 12D), I specifically tested if the length of the main (longest) dendrite was also affected upon TMEM106B knockdown. Notably, the main dendrite of shTMEM106B #1 or #2 transfected neurons (DIV14+5) was about 30 % longer than the main dendrite of shCtrl transfected neurons (Figure 14), suggesting that especially secondary and higher order dendrites are affected by the loss of TMEM106B.

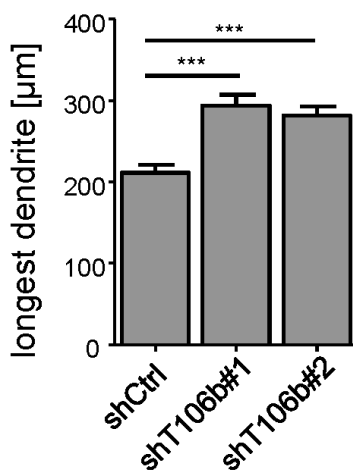


Figure 14: TMEM106B knockdown increases length of the main dendrite

Primary hippocampal neurons (DIV7+5) were transfected with either of the two shRNAs against TMEM106B or a control shRNA and GFP to visualize the cell morphology. In projections of confocal z-stacks the length of the longest dendrite of each neuron was measured using ImageJ software. Image acquisition and analysis was done blinded to the experimental condition. Dendrites of shRNA treated neurons were significantly longer than of ctrl treated neurons. 40 neurons per condition were analyzed. Mean \pm SEM, one-way ANOVA: *** denotes $p < 0.001$.

Since I observed a strong dendritic phenotype upon knockdown of a lysosomal protein, I set out to test if general defects in lysosomal activity can alter dendritic architecture. I expressed the dominant negative mutant of RAB7A to block of lysosomal function. This GDP/GTP exchange factor is important for cargo transport to the lysosome, endosomal/lysosomal fusion events and lysosomal biogenesis in general. The T22N mutation of the protein, which impairs the affinity for GTP and the nucleotide exchange acts dominant negative and inhibits these functions (Bucci et al., 2000; Mukhopadhyay et al., 1997; Spinoso et al., 2008). Primary hippocampal neurons (DIV7+5) were transfected with either wild type (wt) RAB7A, dominant negative (dn) RAB7A T22A or constitutive active (ca) RAB7A Q67L together with

EGFP as transfection marker and to outline neuronal morphology. The dendritic branching of these transfected neurons was assessed with Sholl analysis as described above. Whereas neurons expressing constitutive active RAB7A had only a slightly but not significantly increased dendrite complexity compared to wt RAB7A overexpressing neurons, neurons expressing RAB7A T22N showed a significant decrease in dendrite branching (Figure 15A and 15B). This finding argues for a causal link between lysosomal function and the growth and maintenance of dendrites.

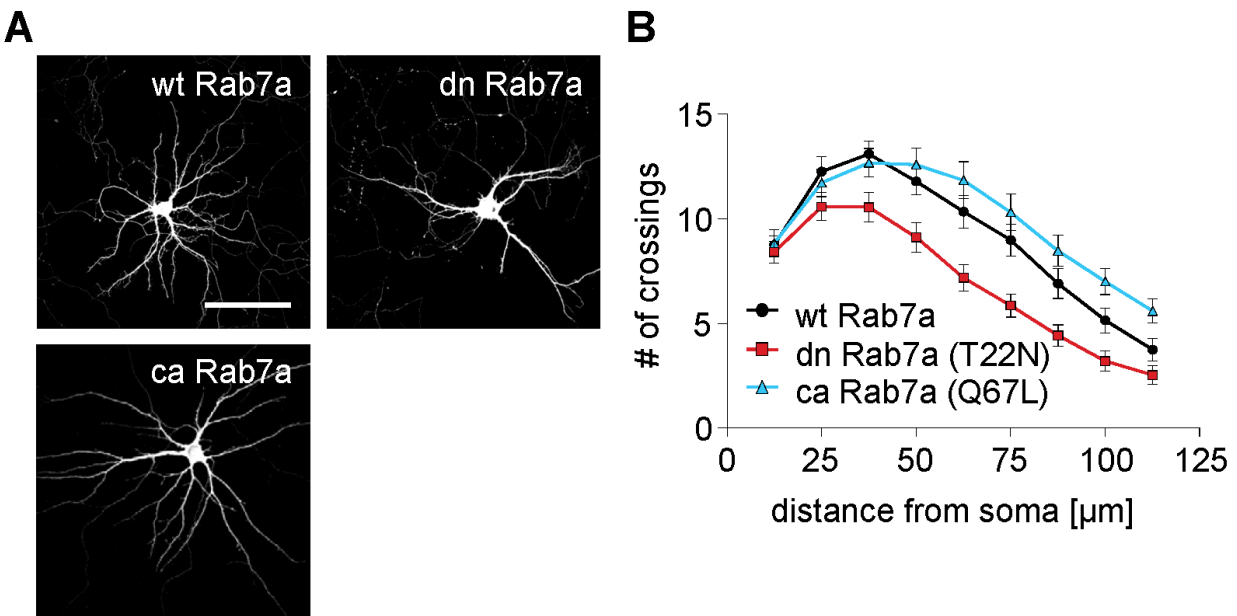


Figure 15: Dominant-negative RAB7a impairs dendritic arborization

(B, C) Primary rat hippocampal neurons (DIV7+5) were cotransfected with the indicated RAB7a wild-type or mutant constructs and GFP to visualize the neuronal morphology. Dendritic arborization was quantified by Sholl analysis as above. Neurons transfected with dominant negative RAB7a T22N (dn) are significantly different from wild-type RAB7a (wt) or constitutive active RAB7a Q67L (ca) transfected cells (wt RAB7a vs. dn RAB7a: from 50 μm to 75 μm radius $p < 0.05$). $n > 40$ neurons per condition, three independent experiments, mean \pm SEM, two-way ANOVA. Scale bar represents 100 μm .

3.2 TMEM106B knockdown impairs spines and synaptic markers

Since changes in dendrite morphology and function are often accompanied by alterations in dendritic protrusions / spines (Koleske, 2013), the previous findings raised the question if also spine morphology is affected by TMEM106B knockdown

in primary neurons. Hence, I analyzed spine density and morphology in mature neurons (DIV14+5) treated with shRNA against TMEM106B. On these images I quantified the overall density of dendritic spines as well as their width and length from a total of 100-200 / μm dendrite segments per neuron. Spine size and morphology is a good correlate of their function. The width of the spine head is proportional to the number of postsynaptic receptors and thereby to the strength of the transmission. Especially mushroom-shaped protrusions are a sign for strong synaptic activity (Hering and Sheng, 2001). As can be seen on the representative images (Figure 16A), the control shRNA transfected neurons exhibited normal spine density and most protrusions were mushroom shaped. In contrast, spines in shTMEM106B #1 or #2 transfected neurons were significantly less dense and were much thinner and more filopodia like – a sign for reduced synaptic strength (Figure 16A and 16B). Again, this effect was more pronounced in neurons treated with the stronger shRNA #2. Moreover, also the length of the protrusions was reduced by approximately 20 percent upon TMEM106B knockdown (Figure 16B).

Next, I confirmed these findings on a biochemical level. Cortical neurons (DIV7+6) were transduced with a lentivirus expressing either TMEM106B shRNA #2 or the control shRNA. The levels of the presynaptic marker protein synaptophysin and the postsynaptic density protein PSD-95 were analyzed by immunoblotting (Figure 16C). Synaptophysin and PSD-95 levels, normalized on the housekeeping protein β -actin, were reduced by 60 percent and 40 percent, respectively, upon TMEM106B knockdown (Figure 16D) corroborating the morphological data.

3.3 TMEM106B knockdown increases axonal length

For a complete picture of neuronal morphology upon TMEM106B knockdown, axonal length was measured additionally. For axonal analysis, neurons were used at an early stage of development to avoid the complex architecture at later time points, which hinders tracing of neurites (compare Figure 9B). Neurons were nucleofected with the shRNA constructs directly before plating and axonal length was measured four days later. The criteria for identifying axons were the same as described above (see chapter 2.2). ShT106b#2 nucleofected neurons had about 30 percent longer

axons than control shRNA nucleofected neurons (Figure 16E and 16F). Together with the data from the XTT-assay (compare Figure 7B) and the increased length of the main dendrite (compare Figure 14D), the above finding provides an additional sign for unaltered neuronal viability since decrease in axonal length is often an early sign of toxicity in neurons.

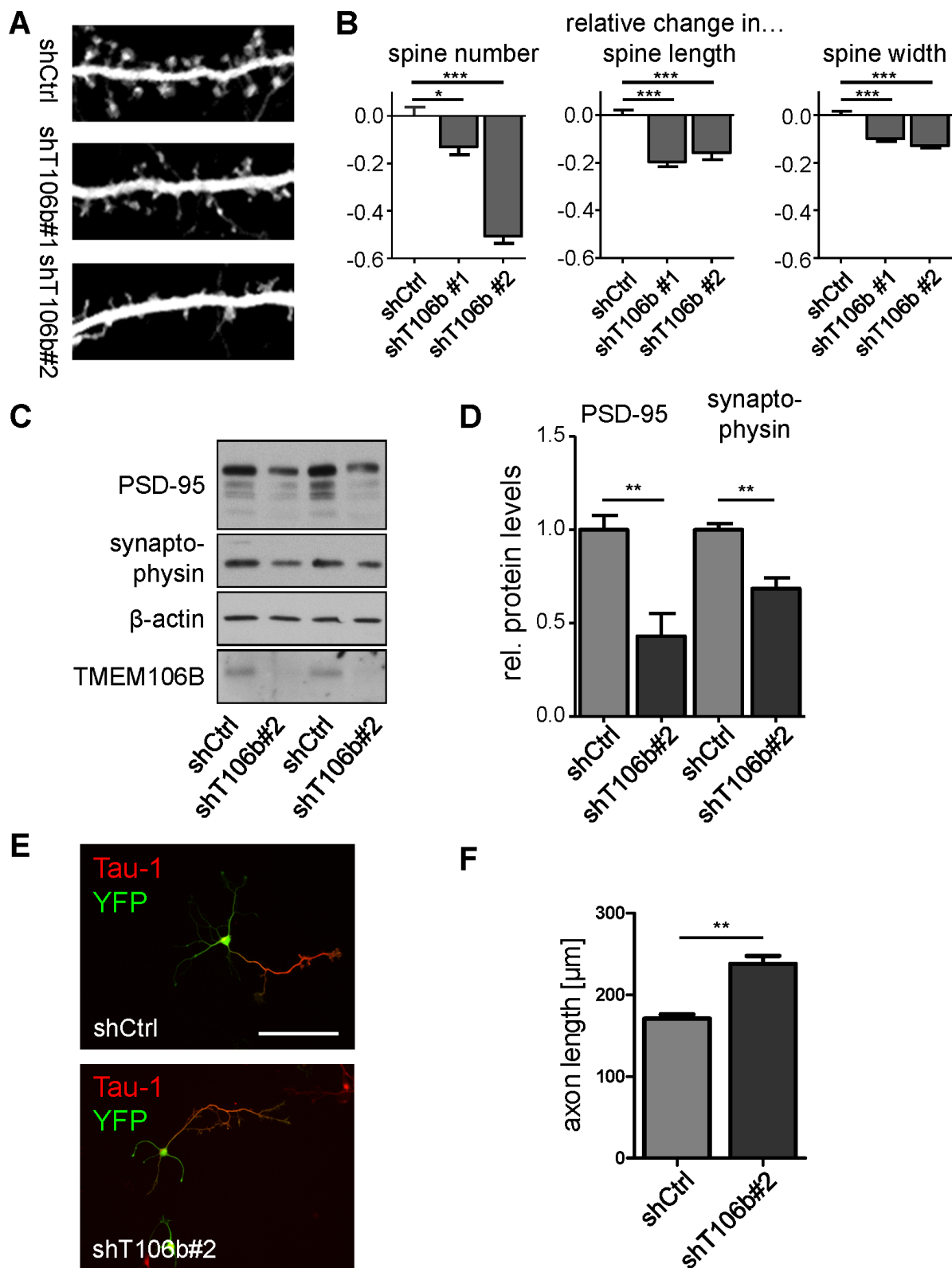


Figure 16: Changes in spine and axon morphology upon TMEM106B knockdown

(A, B) Hippocampal neurons were co-transfected with the indicated shRNAs and GFP (DIV14+5). Spine morphology (length and width) and density was assessed manually and blinded to the experimental condition

using MetaMorph software. Neurons show shorter, thinner and less dense dendritic protrusions upon TMEM106B knockdown. ($n > 38$ per condition; one-way ANOVA; *: $p < 0.05$, ***: $p < 0.001$). (C) Primary cortical neurons were transduced with the lentivirus expressing the indicated shRNAs. Immunoblots with antibodies against presynaptic synaptophysin and postsynaptic PSD-95 show a reduction of protein levels upon TMEM106B knockdown. (D) Quantification of the immunoblots from (C) normalized to β -actin. ($n = 4$, mean \pm SEM, Student's t-test, ** denotes $p < 0.01$). Reduction of synaptic marker proteins corroborates synapse loss at the biochemical level. (E, F) Primary rat hippocampal neurons were nucleofected with either TMEM106B shRNA #2 or control shRNA together with YFP to outline neuron morphology prior to plating (DIV0+4). Neurons were immunostained with antibodies against YFP (green) and the axonal marker Tau-1 (red). Axonal length was measured using AxioVision software blinded to the experimental condition. Increased axonal length in TMEM106B knockdown cells indicates that TMEM106B knockdown does not cause unspecific toxicity. ($n > 80$ per condition, three independent experiments; Student's t-test, ** denotes $p < 0.01$). Scale bar represents 100 μ m.

Taken together I was able to demonstrate that knockdown of TMEM106B in primary neurons leads to a pronounced inhibition of dendritic branching and maintenance. Although this is accompanied by dramatic changes in spine morphology and density, no overall neurotoxicity is observed. This point is further strengthened by the increase in the length of the developing axon and the main dendrite observed upon loss of TMEM106B.

4. TMEM106B interacts with MAP6

4.1 Identification of MAP6 as TMEM106B binding partner in rat brain

To further elucidate the cellular context of TMEM106Bs function and to identify the underlying mechanisms of the dendrite loss I set out to identify TMEM106B interacting proteins. Thus, I established a protocol for immunoprecipitation from rat brain samples. The protein was immunoprecipitated from the lysate (1% Triton X100) of a crude membrane fraction by the polyclonal TMEM106B antibody cross-linked to magnetic protein-G-coupled beads. The eluted precipitates were subjected to SDS-PAGE and the proteins thereon stained with colloidal coomassie dye (Figure 17A). TMEM106B-IP specific bands and their corresponding areas in the control lanes were excised, the containing proteins subjected to tryptic digest and subsequently identified by LC-MS/MS. The only protein found specifically in TMEM106B immunoprecipitates in all three independent experiments (with a total

of five biological replicates) was the MT-binding protein MAP6. This protein, also referred to as stable tubule-only polypeptide (STOP), is known to mainly interact with and stabilize microtubules (Bosc et al., 1996). However, additional targeting to the actin cytoskeleton and the Golgi apparatus is reported (Baratier et al., 2006; Gory-Faure et al., 2006). LC-MS/MS specifically identified eleven unique peptides (table 1) of the protein with a total sequence coverage of 23 % in IP samples (Figure 17B).

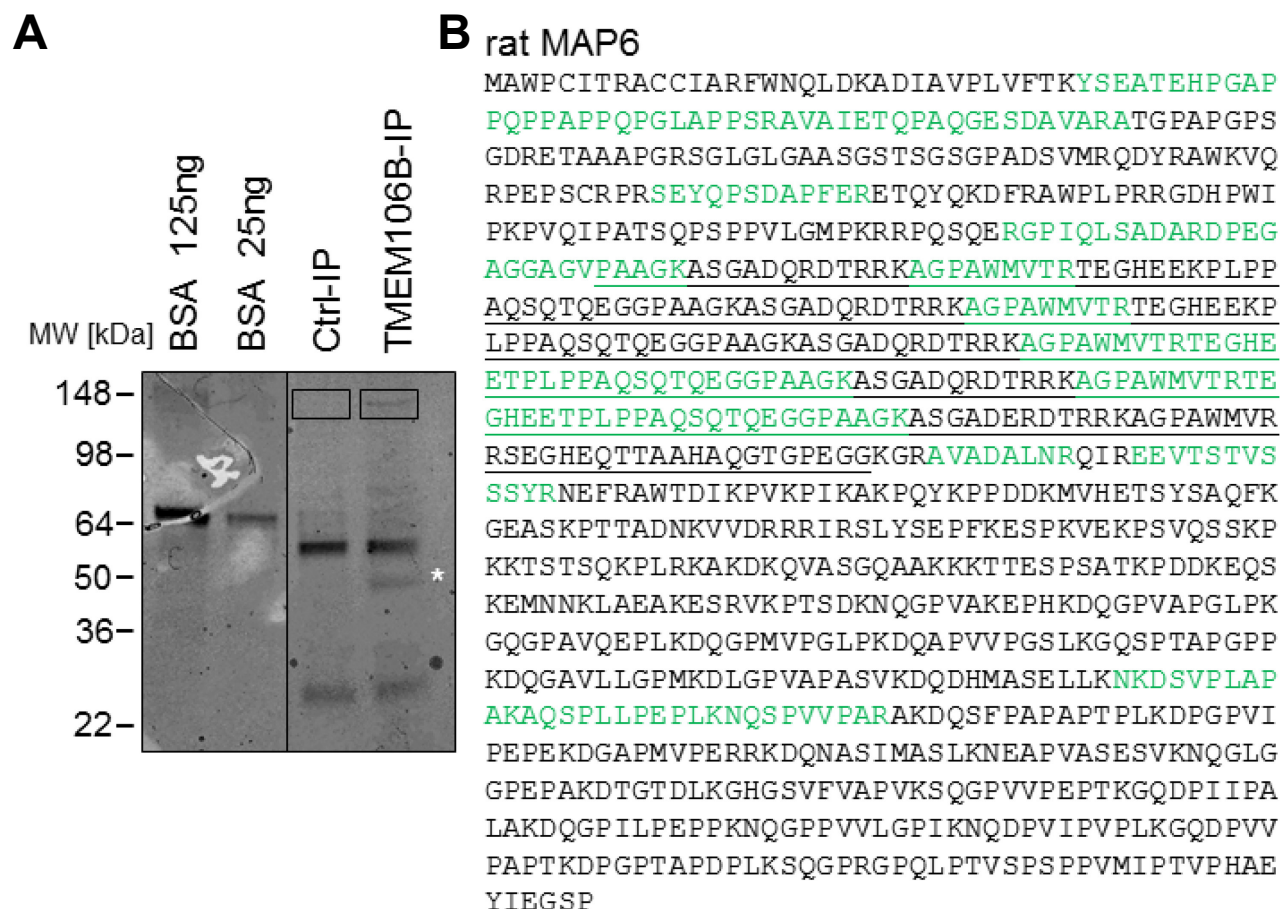


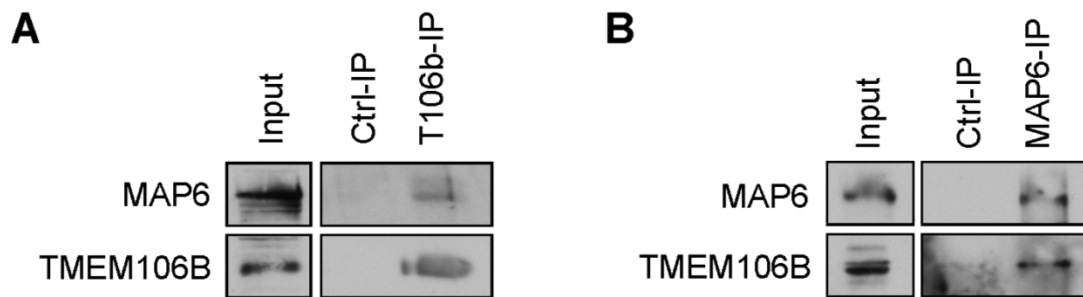
Figure 17: MAP6 peptides identified by LC-MS/MS

(A) Proteins coimmunoprecipitating with TMEM106B in rat brain (P15) were analyzed. Colloidal coomassie stained SDS-PA gel of control and TMEM106B immunoprecipitates. Boxed regions were cut out and further processed for LC-MS/MS. BSA served as marker for amount of recovered protein. Asterisk denotes TMEM106B band. Brightness/contrast in the image was adjusted in a linear manner to better identify bands on the gel. (B) Proteins coimmunoprecipitating with TMEM106B in rat brain (P15) were analyzed by LC-MS/MS. MAP6 was identified by 11 peptides highlighted in green throughout the whole protein sequence. The region with five tandem repeats binding microtubules is underlined. Mass spectrometry was performed by Sebastian Hög.

Table 1: Unique peptides for MAP6 identified by LC-MS/MS

peptide sequence	charge	m/z [Da]	MH+ [Da]
TEGHEETPLPPAQSQTQEGGPAAGK	3	839.73142	2517.17969
AVAIETQPAQGESDAVAR	2	906.95901	1812.91074
YSEATEHPGAPPQPPAPPQGLAPPSR	3	916.12646	2746.36484
GPIQLSADARDPEGAGGAGVPAAGK	3	754.72241	2262.15268
DPEGAGGAGVPAAGK	2	627.31016	1253.61304
AQSPLLPEPLKNQSPVVPAR	3	714.40826	2141.21024
SEYQPSDAPFER	2	713.32019	1425.63310
NKDSVPLPAK	2	570.32367	1139.64006
EEVTSTVSSSYR	2	672.81799	1344.62871
AGPAWMVTR	2	494.75421	988.50115
AVADALNR	2	415.23001	829.45275

Moreover, the endogenous interaction of both proteins could also be corroborated on immunoblot level. With this method, I confirmed the specific interaction of TMEM106B and MAP6 in both directions (Figure 18A and 18B).

**Figure 18: TMEM106B interacts with MAP6 in rat brain**

TMEM106B (A) and MAP6 (B) were immunoprecipitated from P15 rat brain. Immunoblots with the indicated antibodies demonstrate MAP6 coimmunoprecipitating in TMEM106B IP and TMEM106B coimmunoprecipitating in MAP6 IP.

In order to provide further evidence for the interaction of TMEM106B and MAP6 in a shared cellular compartment, subcellular fractionation from adult rat brain was performed. The 100,000 g membrane fraction of homogenized brain was further separated via a discontinuous iodixanol density gradient. Mitochondrial and endoplasmic reticulum (ER) components (identified by their marker proteins translocase of outer mitochondrial membrane 20 (TOM20) and calnexin respectively) accumulated in denser fractions of the gradient whereas plasma membrane components ($\text{Na}^+\text{-K}^+\text{-ATPase}$) and remaining microtubule components ($\beta\text{III-tubulin}$) accumulated in light fractions. Remarkably, TMEM106B and MAP6 peaked together with markers for the secretory and endocytic pathway ($\gamma\text{-adaplin}$ for the Golgi apparatus and RAB7 for late-endosomes and lysosomes) in the middle fractions (Figure 19). This finding suggests close contact between TMEM106B and MAP6 in the same subcellular compartments, including lysosomes.

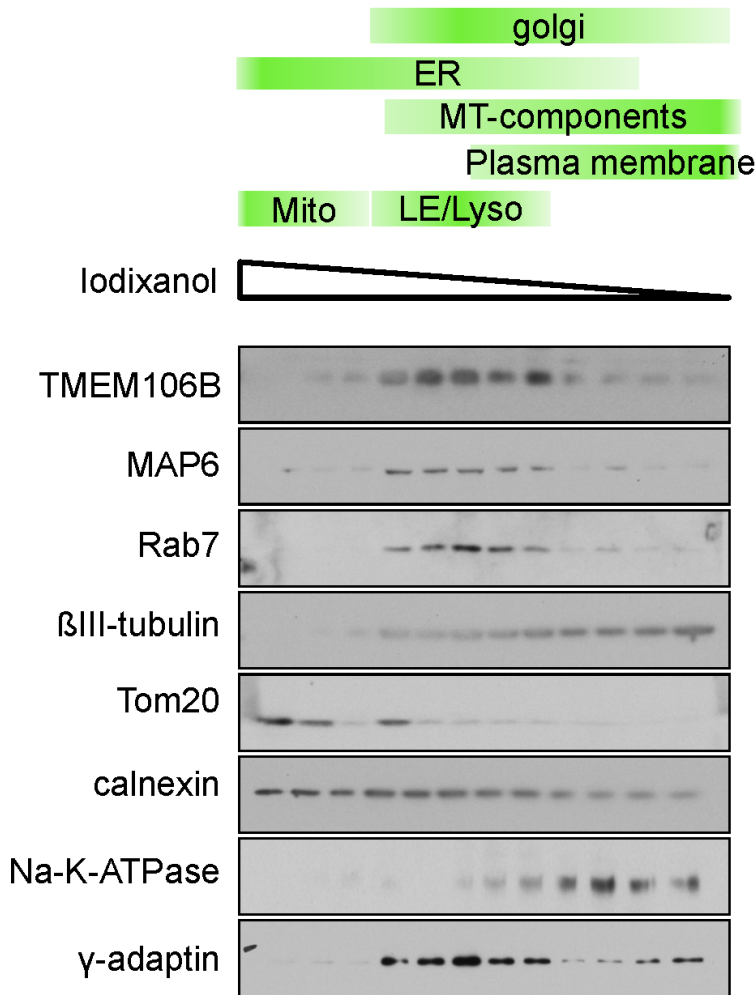


Figure 19: TMEM106B and MAP6 peak in the lysosomal fraction of a density gradient

Subcellular compartments from adult rat brain were fractionated using a discontinuous iodixanol density gradient (2.5 – 30%). Immunoblots of 1 ml fractions with the indicated antibodies. TMEM106B and MAP6, both peak in the same, RAB7-positive fractions.

4.2 Mapping of the MAP6/TMEM106B interaction domain in HEK293 cells

In the next step, I aimed to map the protein domains crucial for the interaction of TMEM106B and MAP6. For that purpose several deletion mutants were generated and expressed in HEK293 cells. Due to the type II transmembrane topology of TMEM106B (Lang et al., 2012), it was predicted that only the extravesicular N-terminal part (AA 1-97) of the protein is able to take part in the binding. For better expression and stability a GFP-tagged human TMEM106B N-terminal fragment (GFP-TMEM106B-NT, AA1-93) was cloned. Additionally, three different myc-tagged MAP6 constructs were generated as potential binding partner: full length rat MAP6 (NP_058900.1), human MAP6 isoform 1 (NP_149052.1) lacking four of the five central repeats and human isoform 2 (NP_997460.1) lacking additionally the c-

terminal repeat domain (Figure 18C). As expected, full length rat MAP6 co-immunoprecipitated GFP-TMEM106B-NT that was co-expressed in HEK293 cells. The same was true for coIP experiments with human MAP6 isoform 1. However, the shorter, c-terminally truncated isoform two of human MAP6 did not bind to the TMEM106B N-terminal domain. This result indicates binding of the cytoplasmic N-terminus of TMEM106B to the C-terminal repeat region of MAP6 (Figure 18C and 18D). Taken together these results confirm the interaction of TMEM106B and MAP6 which is mediated by the N-terminus of TMEM106B and the C-terminus of the MAP6.

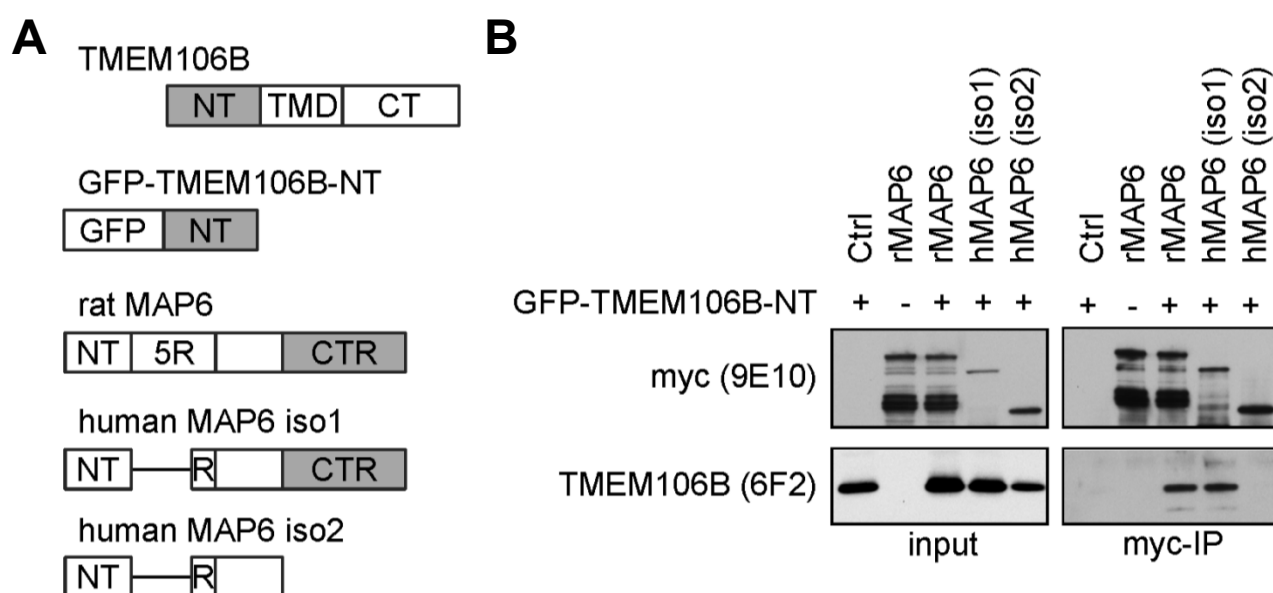


Figure 21: TMEM106B N-terminus binds to MAP6 C-terminus

(A) Deletion mutants of TMEM106B and MAP6 used for analysis of interaction domains. The cytoplasmic N-terminal domain (NT) of TMEM106B fused to GFP. Transmembrane domain (TMD) and C-terminal domain (CT) were removed to avoid aggregation. MAP6 contains a central repeat domain, consisting of five repeats (R) of a 46 amino acid motif in rat but only one repeat in humans. The shorter isoform 2 lacks the C-terminal repeat domain (CTR) consisting of up to 28 imperfect repeats. (B) GFP-TMEM106B-NT and the indicated myc-tagged MAP6 variants were co-expressed in HEK293FT cells. MAP6 variants were immunoprecipitated with myc-beads. Immunoblots with the indicated antibodies show coimmunoprecipitation of TMEM106B with CTR containing MAP6 variants. Figure 21B in collaboration with Christina M Lang.

5. MAP6 function in dendrites

5.1 MAP6 affects dendritic branching

In my previous experiments I could demonstrate that TMEM106B and MAP6 physically interact with each other. However, the functional relevance of this interaction remained elusive. In order to provide evidence for a functional cooperation, I transfected hippocampal neurons (DIV7+5) with a rat MAP6 overexpression construct and analyzed the morphology of the dendritic arbor as described before. Strikingly, MAP6 overexpression led to a substantial decrease in dendritic complexity to almost the same extent as TMEM106B knockdown (Figure 22A, compare Figure 12), as quantified by Sholl analysis (Figure 22B). Again, the most pronounced effect occurred in the proximal part of the dendrites. This similarity of MAP6 overexpression with TMEM106B knockdown suggested that the reduction of MAP6 would lead to the opposite effect. For this purpose, I generated a shRNA expression vector specific for rat MAP6. Lentiviral transduction of this shRNA in cortical neurons (DIV7+5) and subsequent immunoblotting clearly demonstrated a reduction of MAP6 protein level and confirmed the good knockdown efficiency of the short hairpin (Figure 23). However, loss of MAP6 in these neurons did not affect the protein level of TMEM106B (data not shown). Strikingly, knockdown of MAP6 in hippocampal neurons (DIV7+5) led to an increase in dendrite outgrowth compared to the control situation (Figure 22C and 22D).

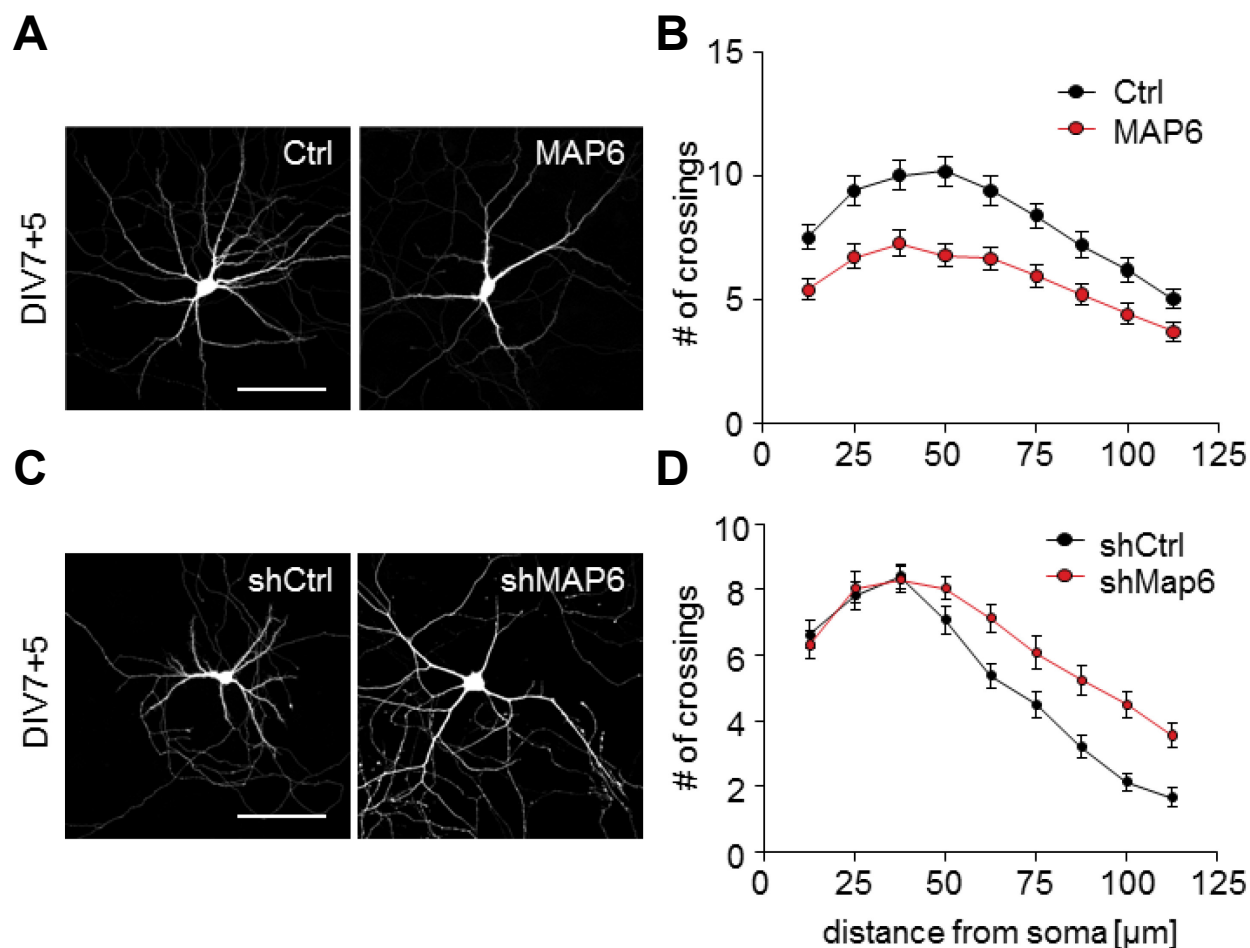


Figure 22: Effects of MAP6 overexpression and knockdown on dendritic branching

(A, B) Primary rat hippocampal neurons (DIV7+5) were cotransfected with either a MAP6 overexpression construct or an empty vector control and GFP. Dendritic arborization was analyzed by Sholl analysis as above. Neurons overexpressing MAP6 are significantly less branched than controls (at 12.5 μm , 25 μm , 75 μm and 87.5 μm radius $p < 0.05$, from 37.5 μm to 62.5 μm $p < 0.001$). $n > 40$ per condition, three independent experiments, mean \pm SEM, Two-way ANOVA. Scale bar represents 100 μm . (C, D) Primary rat hippocampal neurons (DIV7+5) were cotransfected with either with ctrl shRNA or MAP6 shRNA and GFP. Dendritic arborization was analyzed by Sholl analysis as above. MAP6 knockdown neurons are significantly more branched than controls in distal parts of dendrites (at 62.5 μm and 75 μm radius $p < 0.05$, at 87.5 μm and 112.5 μm $p < 0.01$, at 100 μm radius $p < 0.001$). $n > 40$ per condition, three independent experiments, mean \pm SEM, Two-way ANOVA. Scale bar represents 100 μm .

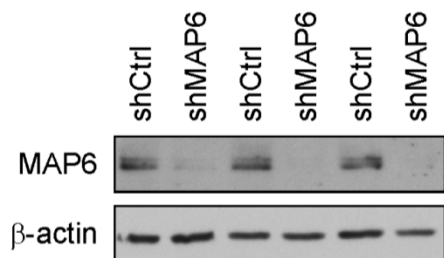


Figure 23: Knockdown of MAP6 in primary neurons

Primary hippocampal neurons (DIV7+5) were transduced with MAP6 shRNA or a Ctrl shRNA lentivirus. Immunoblot with the indicated antibodies indicates specific MAP6 knockdown.

To control also the MAP6 shRNA induced phenotype for unspecific off-target effects, I performed rescue experiments using the human MAP6 (isoform 1) overexpression construct, which is resistant to the shRNA targeting rat MAP6. Hence, I transfected hippocampal neurons with combinations of shCtrl or shMAP6 and human MAP6 or an empty vector control. Yet again, dendritic branching was measured by Sholl analysis in DIV7+5 neurons. While shMAP6 transfected neurons cotransfected with an empty vector control, showed as expected increased dendrite outgrowth (Figure 24A and 24B, compare to Figure 22C and D), the cotransfection of human MAP6 led to a loss of dendrites comparable to the transfection of human MAP6 alone. These results are a clear indication for the specificity of the MAP6 shRNA regarding the dendrite outgrowth phenotype.

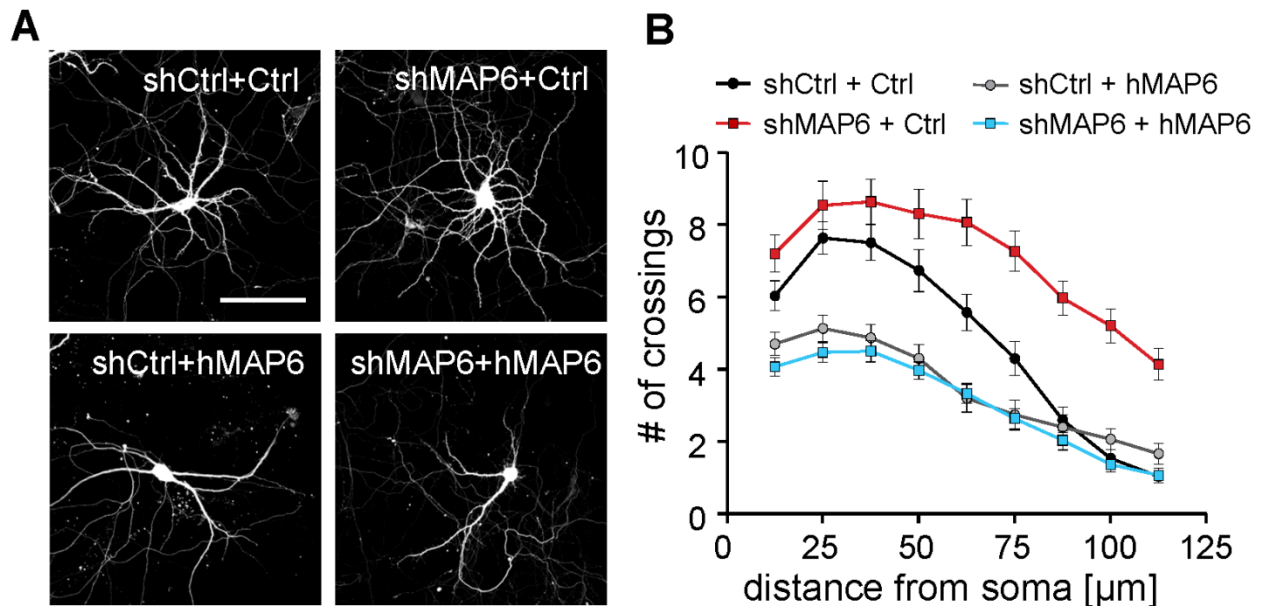


Figure 24: Validation of MAP6 shRNA using human MAP6

(A, B) Primary rat hippocampal neurons (DIV7+5) were cotransfected with combinations of control shRNA (shCtrl), shRNA targeting rat MAP6 (shMAP6) and human MAP6 (hMAP6) or an empty vector (Ctrl) together with GFP. Dendritic complexity was quantified using Sholl analysis as above. MAP6 knockdown increases distal branching while overexpression of human MAP6 prevents this effect (shCtrl+Ctrl vs shMAP6+Ctrl: 62.5 μm : $p < 0.05$, from 75 μm to 112.5 μm radius $p < 0.001$; shCtrl+Ctrl vs. shCtrl+hMAP6 at 25 μm , 50 μm and 62.5 μm radius $p < 0.05$, at 37.5 μm radius $p < 0.001$; shMAP6+Ctrl vs shMAP6+hMAP6: from 12.5 μm to 112.5 μm radius $p < 0.001$). $n = 25$ neurons per condition, 3 independent experiments, mean \pm SEM, two-way ANOVA. Scale bar represents 100 μm .

5.2 MAP6 depletion rescues TMEM106B knockdown phenotype

Since MAP6 knockdown increased dendritic branching, I further speculated that the combination of both shRNAs, shMAP6 and shT106b, should consequently alleviate the TMEM106B knockdown phenotype. For these shMAP6 rescue experiments, I cotransfected shT106B #2 or shCtrl together with shMAP6 or shCtrl in the same settings as above. Importantly, the coexpression of both, TMEM106B shRNA and MAP6 shRNA, led to a complete rescue of dendrite loss compared to only TMEM106B shRNA treated neurons. Moreover, shMAP6 expression increased distal branching in both groups (shCtrl + shMAP6 and shT106b + shMAP6) compared to control shRNA only expressing neurons (Figure 25A and 25B) and thereby led to an “overrescue” of the TMEM106B knockdown phenotype.

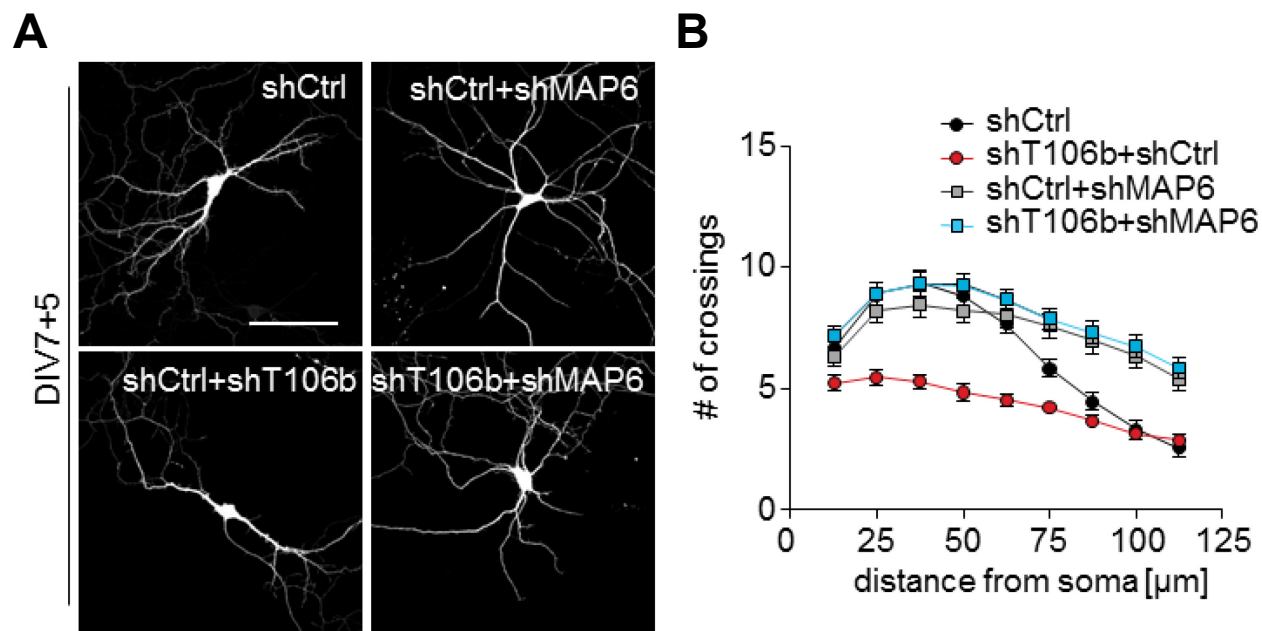


Figure 25: MAP6 knockdown rescues the branching effect of TMEM106B knockdown

(A, B) Primary rat hippocampal neurons (DIV7+5) were cotransfected with combinations of control shRNA (shCtrl), TMEM106B shRNA #2 (shT106b) and MAP6 shRNA (shMAP6) together with GFP. Sholl analysis as above. MAP6 knockdown restores branching in TMEM106B knockdown neurons (shCtrl vs shT106b#2+shCtrl: from 25 μm to 62.5 μm radius $p < 0.001$. shT106b#2+shCtrl vs shT106b#2+shMAP6: from 25 μm to 100 μm $p < 0.001$, at 112.5 μm $p < 0.05$. shCtrl vs shMAP6 + shCtrl: at 87.5 μm $p < 0.05$, from 100 μm to 112.5 μm $p < 0.001$). $n > 40$ per condition, 3 independent experiments, mean \pm SEM, two-way ANOVA. Scale bar represents 100 μm .

MAP6 belongs to the family of microtubule-associated proteins, among others responsible for the stabilization of microtubules. In order to test if the promotion of dendrite outgrowth is a common phenotype also seen upon loss of other microtubule stabilizing proteins, I analyzed dendrite arborization after shRNA mediated knockdown of the related microtubule-binding protein, MAP2. Hippocampal neurons (DIV7+5) were transfected with a shRNA targeting rat MAP2 and GFP to outline cellular morphology. Sholl analysis revealed that, in contrast to MAP6 knockdown, loss of MAP2 severely impaired dendrite outgrowth (compare Figure 20). Moreover, shMAP2 was not able to restore dendritic branching when cotransfected with the TMEM106B knockdown construct (Figure 26A and 26B).

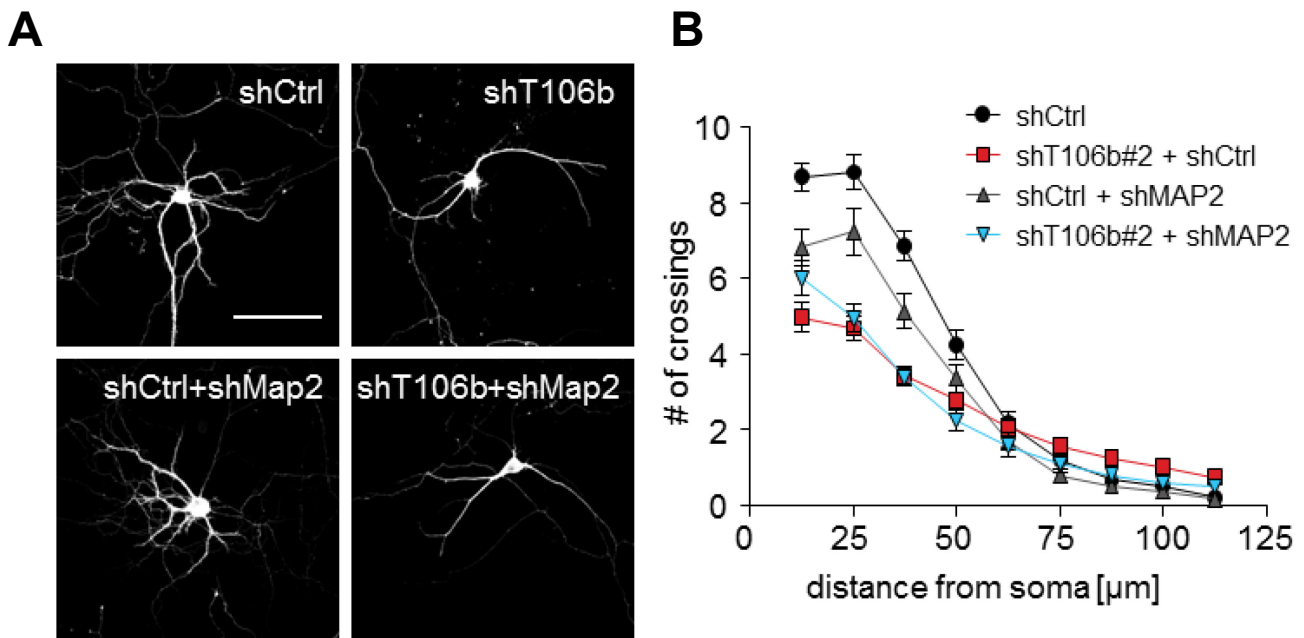


Figure 26: Validation of the specificity of shMAP6 rescue using shMAP2

(A, B) Primary rat hippocampal neurons (DIV7+5) were cotransfected with combinations of control shRNA (shCtrl), shRNA targeting rat MAP2 (shMAP2) and TMEM106B shRNA #2 together with GFP. Dendritic complexity was quantified using Sholl analysis as above. MAP2 knockdown decreased branching and combination of shMAP2 and shT106b#2 did not alleviate branching defects (shCtrl vs. shT106b#2 + shCtrl: from 12.5 μm to 37.5 μm radius $p < 0.001$, at 50 μm radius $p < 0.05$; shCtrl vs. shMAP2 + shCtrl: at 12.5 μm radius $p < 0.001$, at 25 μm radius $p < 0.05$, at 37.5 μm radius $p < 0.01$; shT106b#2 + shCtrl vs. shT106b#2 + shMAP2: no significant difference). $n = 40$ neurons per condition, 3 independent experiments, mean \pm SEM, two-way ANOVA. Scale bar represents 100 μm .

Taken together my data provides evidence for a specific function of TMEM106B interacting protein MAP6 in dendrite outgrowth and branching and thus for a functional interaction of both proteins in the same cellular pathway.

6. Role of TMEM106B in lysosomal Transport

6.1 TMEM106B knockdown affects lysosomal transport

Microtubules are the major tracks on which organelles are transported through the cell (Hirokawa and Takemura, 2005). Since the results presented above demonstrate that a lysosomal protein interacting with a microtubule-binding protein affects dendrite outgrowth, I speculated that TMEM106B and MAP6 might influence the microtubule dependent transport of dendritic lysosomes.

In order to test this hypothesis I performed live cell imaging experiments to analyze the movement of RAB7A-GFP labeled vesicles (late endosomes and lysosomes) in dendrites of hippocampal neurons. The neurons were cotransfected with RAB7A-GFP and TMEM106B shRNA #2 or the control shRNA on DIV6. Time laps movies were taken from single neurons three days later (DIV6+3). Path-time diagrams (kymographs) were generated for every recorded neuron depicting the movement of RAB7A-GFP-positive vesicles in several dendritic segments (Figure 27A). In these kymographs, the total number of RAB7A-GFP labeled vesicles, the number of moving or stationary RAB7A-GFP labeled vesicles and the direction of the respective transport events was analyzed. While the total number of RAB7A-labeled vesicles remained constant in dendrites of knockdown and control neurons, the number of moving vesicles was significantly increased in neurons devoid of TMEM106B (Figure 27B and 27C). In the control situation only about 10 % of all vesicle did move in the 5 min time frame, however, in shT106b #2 transfected neurons almost 30 % of vesicles were mobile. Interestingly, a specific increase in the number of retrogradely transported lysosomes was primarily responsible for the overall change while the number of anterogradely transported lysosomes and lysosomes without any net-movement remained almost unchanged (Figure 27D).

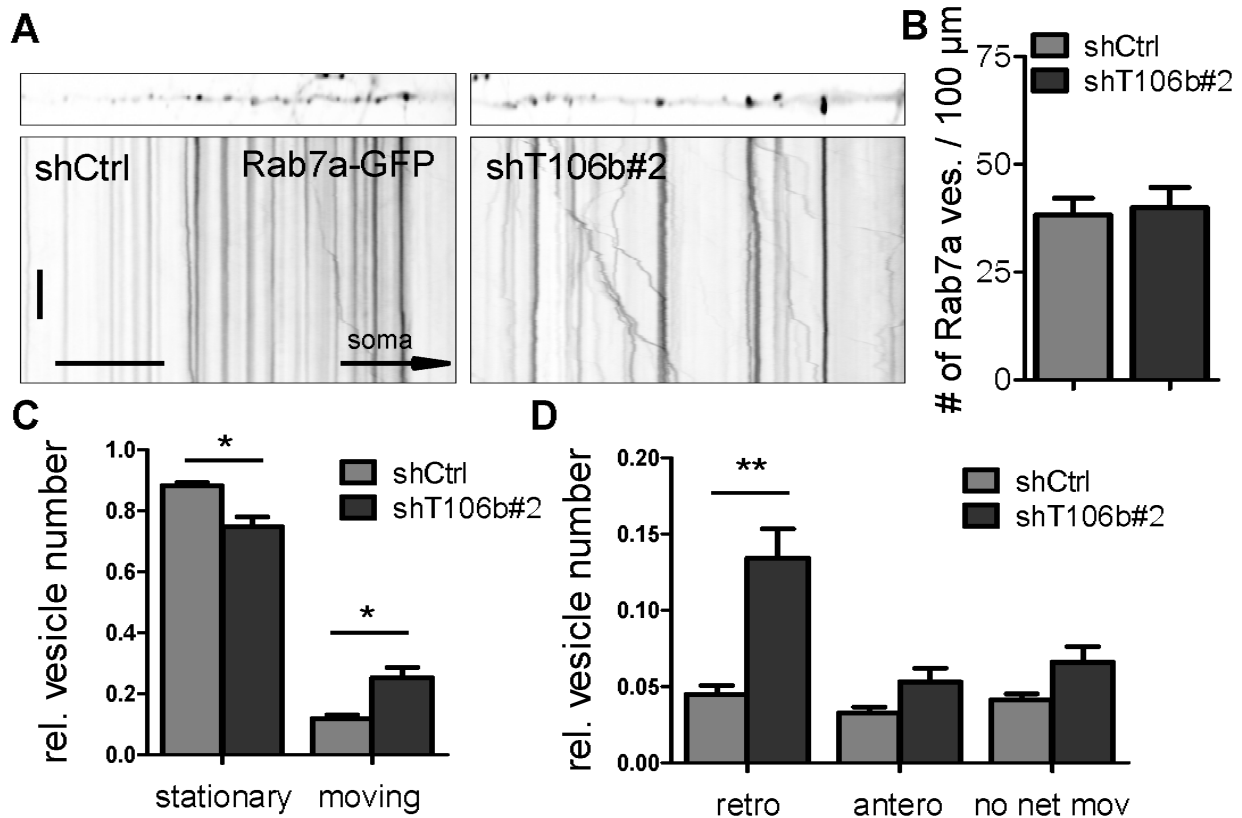


Figure 27: TMEM106B controls retrograde trafficking of dendritic late endosomes/lysosomes

(A) Primary hippocampal neurons (DIV6+3) were transfected with either TMEM106B shRNA #2 or a Ctrl shRNA and RAB7a-GFP to visualize late endosomal / lysosomal trafficking in dendrites and live imaged for 5 minutes with a frequency of 1 Hz. Dendrite segments and the corresponding representative kymographs of dendritic movement of RAB7a-GFP labeled vesicles are shown. Scale bar represents 60 s (vertical) and 20 μ m (horizontal). (B) Quantitative analysis of vesicle number in the dendrites of transfected neurons. The number of RAB7a-labeled vesicles per 100 μ m of dendrite length did not change. (C) Quantitative analysis of vesicle movement from 5 minute kymographs. Vesicles were manually classified according to their movement. TMEM106B knockdown significantly increased overall and specifically retrograde movement of RAB7a-GFP labeled vesicles. Between five and eleven neurons per condition were analyzed per experiment in at least three independent experiments, mean \pm SEM, unpaired t-test: * denotes $p < 0.05$, ** denotes $p < 0.01$.

To evaluate this process in more detail, velocity and run length of the RAB7A-GFP labeled vesicles was additionally determined from the kymographs. In the 5 min time frame of the movies, both parameters were increased upon loss of TMEM106B. Velocity of late endosomes / lysosomes increased from approximately 25 μ m/s to 34 μ m/s. Remarkably, this elevation by more than 35 % was primarily due to enhanced velocity in retrogradely transported vesicles (Figure 28A and 28B). The speed of

lysosomal movement is in the expected range for organelle transport in dendrites (Bannai et al., 2004; Kwinter et al., 2009; van Spronsen et al., 2013). The increase in run length upon TMEM106B knockdown was in a similar range (approx. 40 %, from 7.3 μm to 10.5 μm). Also in this case only the run length of retrogradely moving vesicles was increased while the run length of anterogradely moving vesicles did not change (Figure 28C and 28D).

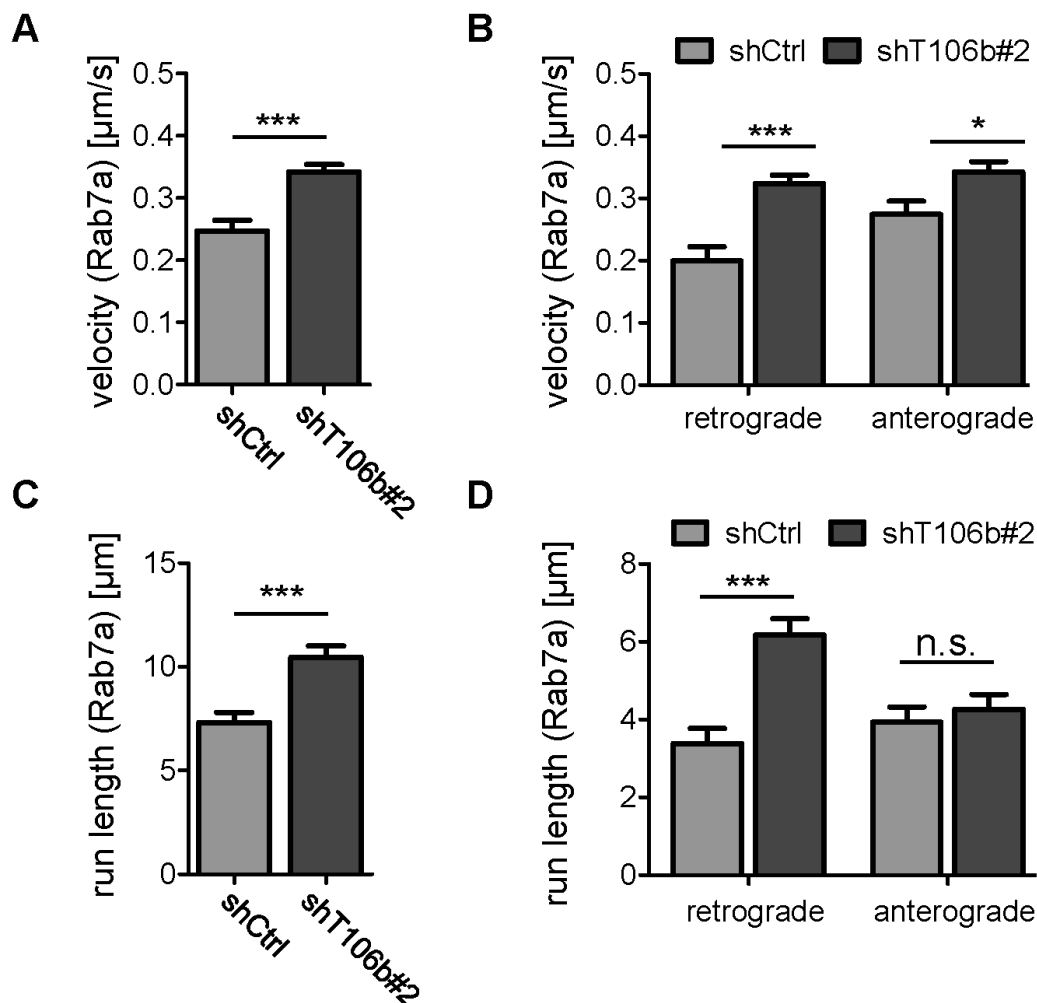


Figure 28: TMEM106B knockdown enhances retrograde movement of late endosomes/lysosomes

(A-C) Primary hippocampal neurons (DIV6+3) were transfected with either TMEM106B shRNA #2 or a Ctrl shRNA and RAB7a-GFP. Live cell imaging of RAB7a-GFP labeled vesicles was used to visualize late endosomal / lysosomal trafficking in dendrites. Velocity (A, B) and total run length (C, D) of individual moving vesicles in total (A, C) or separated for anterograde and retrograde movements (B, D) was analyzed from kymographs (compare Figure 17). At least 80 moving vesicles per condition were analyzed.

I tested the specificity of the TMEM106B shRNA additionally regarding the effect on dendritic trafficking of lysosomes. Similar to the rescue experiments before (compare Figure 13), the neurons were transduced with lentivirus expressing TMEM106b* or empty vector control one day before transfection of the shRNAs. Trafficking of RAB7A-GFP-labeled lysosomes was assessed as described above on DIV6+3. As expected, neurons expressing shT106b#2 and control virus showed an increased transport in retrograde direction compared to control neurons. However, viral expression of TMEM106b* together with shT106b#2 led to a complete rebalancing of anterograde and retrograde trafficking (Figure 29A and 29B).

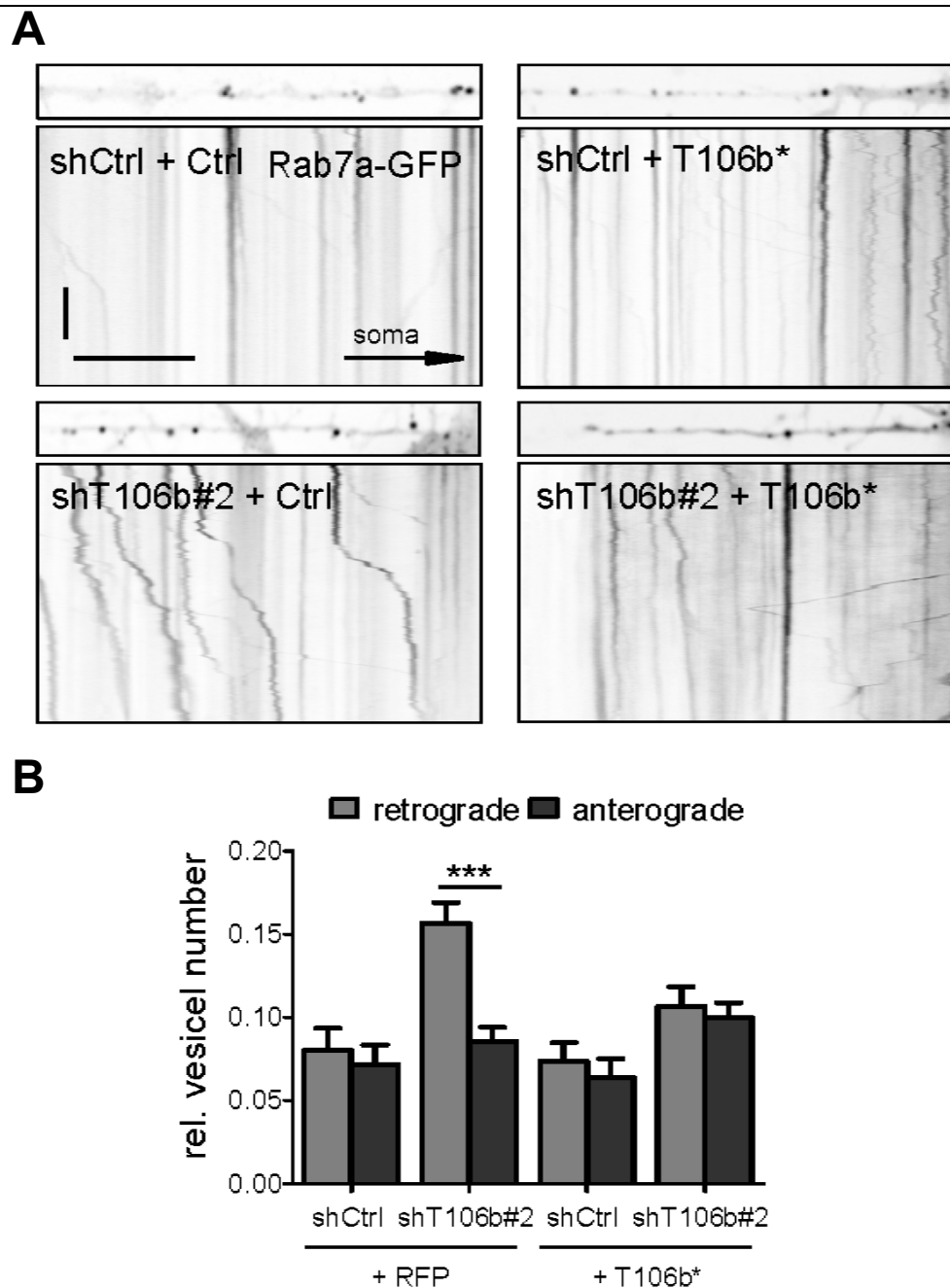


Figure 29: Reintroduction of shRNA-resistant TMEM106B rescues impaired lysosomal trafficking

(A) Primary rat hippocampal neurons were virally infected (DIV5) with either mCherry (RFP) or shRNA-resistant TMEM106B mutant (T106b*) and cotransfected (DIV6+3) with either a control shRNA or the indicated TMEM106B shRNA and RAB7a-GFP to visualize late endosomal / lysosomal trafficking. Dendrite segments and the corresponding representative kymographs of dendritic movement of RAB7a-GFP-labeled vesicles are shown. Scale bars represent 60 s and 15 μ m. (B) Quantitative analysis of vesicle movement from 5 min kymographs. Vesicles were manually classified according to their movement. Expression of the shRNA-resistant TMEM106B mutant prevents the induction of retrograde lysosomal transport. Between five and nine neurons per condition were analyzed per experiment in at least three independent experiments, mean \pm SEM, unpaired t-test: *** denotes $p < 0.001$.

As TMEM106B could be detected also in axons of primary neurons (compare Figure 9) and the length of the axons was altered in neurons devoid of the protein (compare Figure 16), I wanted to investigate if trafficking of RAB7A-GFP labeled neurons was changed as well. I used developing neurons (DIV0+4), because at this early stage of development axons could be easily traced and image acquisition at the same axonal region for every neuron could be ensured. The neurons were nucleofected as described above with shCtrl or shT106B #2 and RAB7A-GFP to identify the desired vesicles. The overall motility of late endosomes and lysosomes in axons was higher than the motility in dendrites for both groups. However, there was no difference in total, anterograde or retrograde movement between control and TMEM106B knockdown neurons (Figure 30A and 30B).

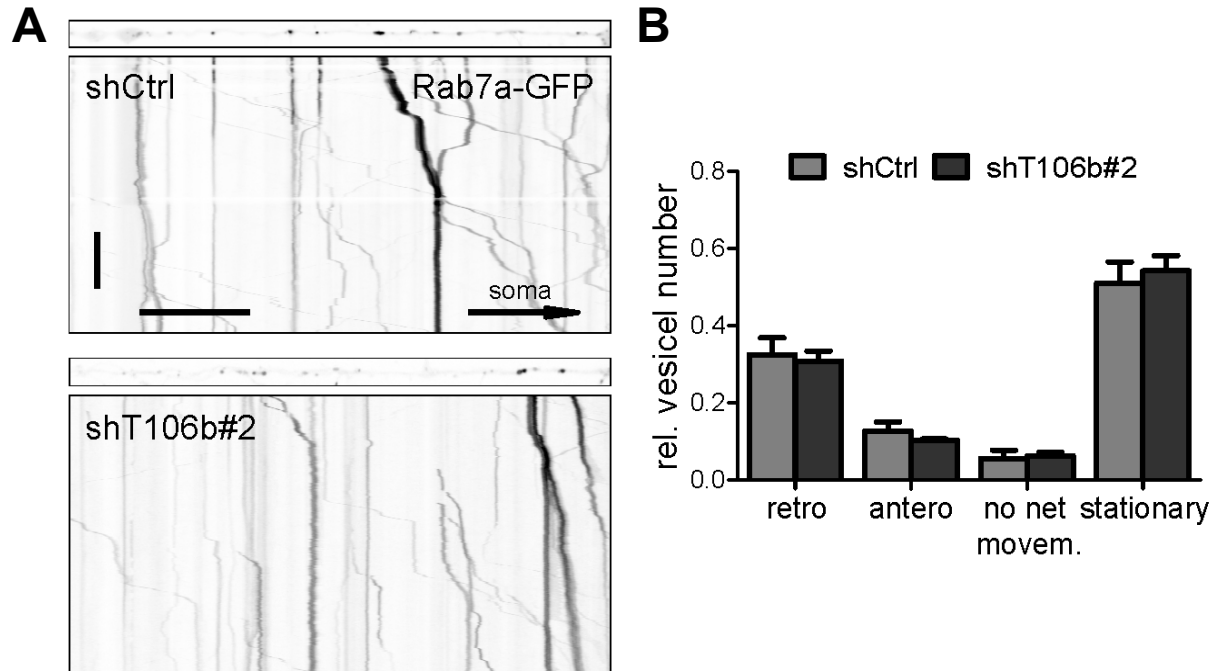


Figure 30: TMEM106B knockdown does not change trafficking of axonal lysosomes

(A) Primary hippocampal neurons (DIV0+4) were nucleofected with either TMEM106B shRNA #2 or a Ctrl shRNA and RAB7a-GFP to visualize late endosomal / lysosomal trafficking and live imaged every second for 5 minutes. Axonal segments and the corresponding representative kymographs of axonal movement of RAB7a-GFP labeled vesicles are shown. Scale bar represents 60 s (vertical) and 25 μ m (horizontal). (B) Quantitative analysis of vesicle movement from 5 minute kymographs. Vesicles were manually classified according to their movement. Overall motility and direction of transport does not change upon TMEM106B shRNA transfection. At least seven neurons per condition were analyzed per experiment in at least three independent experiments, mean \pm SEM.

As an additional control for a specific lysosomal effect of TMEM106B knockdown, the dendritic transport of mitochondria was analyzed. I visualized mitochondria in primary hippocampal neurons with a construct expressing the mitochondrial targeting sequence of cyclooxygenase 8 (COX8) fused to red fluorescent protein (RFP) (mitoRFP). In the 5 min time frame analyzed approximately 50 % of mitoRFP labeled mitochondria were moving in control shRNA transfected neurons whereas the other half remained stationary. In contrast to the dendritic transport, no change of this 1:1 ratio could be detected in shT106b #2 transfected neurons (Figure 31A and 31B). Moreover, the total number of mitochondria remained constant in both groups investigated (Figure 31C).

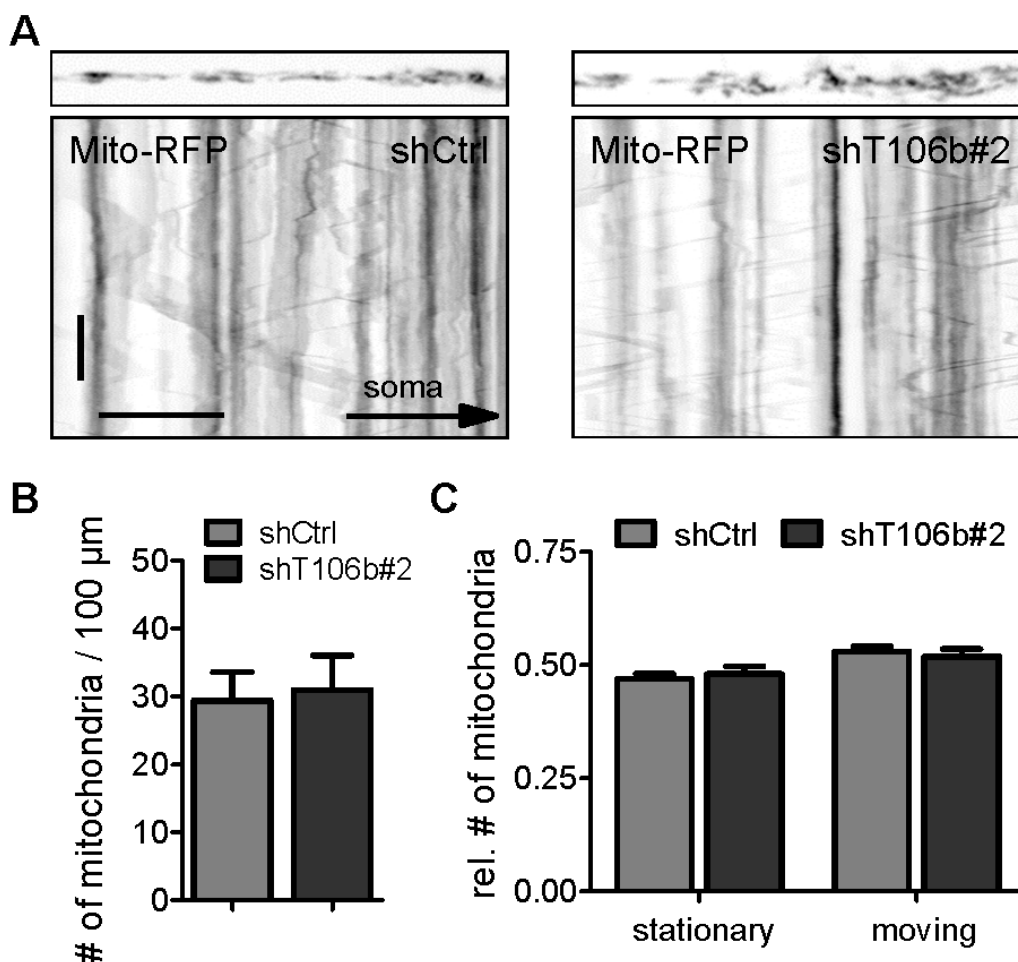


Figure 31: TMEM106B knockdown does not change mitochondrial trafficking in dendrites

(A) Primary rat hippocampal neurons were transfected (DIV6+3) with either a control shRNA or TMEM106B shRNA #2 and mito-dsRed to visualize mitochondrial trafficking in dendrites. Dendrite

segments and the corresponding representative kymographs of dendritic movement of mitochondria are shown. Scale bars represent 60 s and 25 μm . TMEM106B knockdown had no effect on mitochondrial density (B) and movement (C) in dendrites. At least seven neurons per condition were analyzed per experiment in at least three independent experiments, mean \pm SEM.

Taken together I demonstrated that the dendritic trafficking of lysosomes is affected by TMEM106B knockdown. Particularly the number of retrogradely transported RAB7A-GFP labeled vesicles is increased, as is the speed and length of their individual movements. In contrast, movement of mitochondria in dendrites as well as late endosomes / lysosomes in axons is not changed upon TMEM106B knockdown.

6.2 MAP6 affects lysosomal transport

Since TMEM106B and its interaction partner MAP6 both regulate dendrite outgrowth and knockdown of MAP6 even compensates for loss of TMEM106B, the question arose if overexpression of MAP6 would also phenocopy the impact of TMEM106B knockdown on lysosomal trafficking. Therefore, I transfected hippocampal neurons (DIV6+3) with rat MAP6 or an empty vector control and RAB7A-GFP to identify late endosomes and lysosomes. The trafficking of these vesicles was analyzed as described above. Strikingly, the number of retrogradely transported vesicles was similarly increased by almost two-fold, reminiscent of the TMEM106B knockdown effect. However, in the case of MAP6 overexpression the overall movement of RAB7A-GFP labeled vesicles in dendrites showed only a slight and non-significant elevation. This discrepancy to TMEM106B knockdown could be explained by the slight decrease observed in anterograde trafficking (Figure 32A, 32C and 32D). Also in these experiments, similar to the situation in TMEM106B knockdown neurons, the total number of RAB7A-GFP labeled vesicles in dendrites remained constant for both groups (Figure 32B, compare Figure 27).

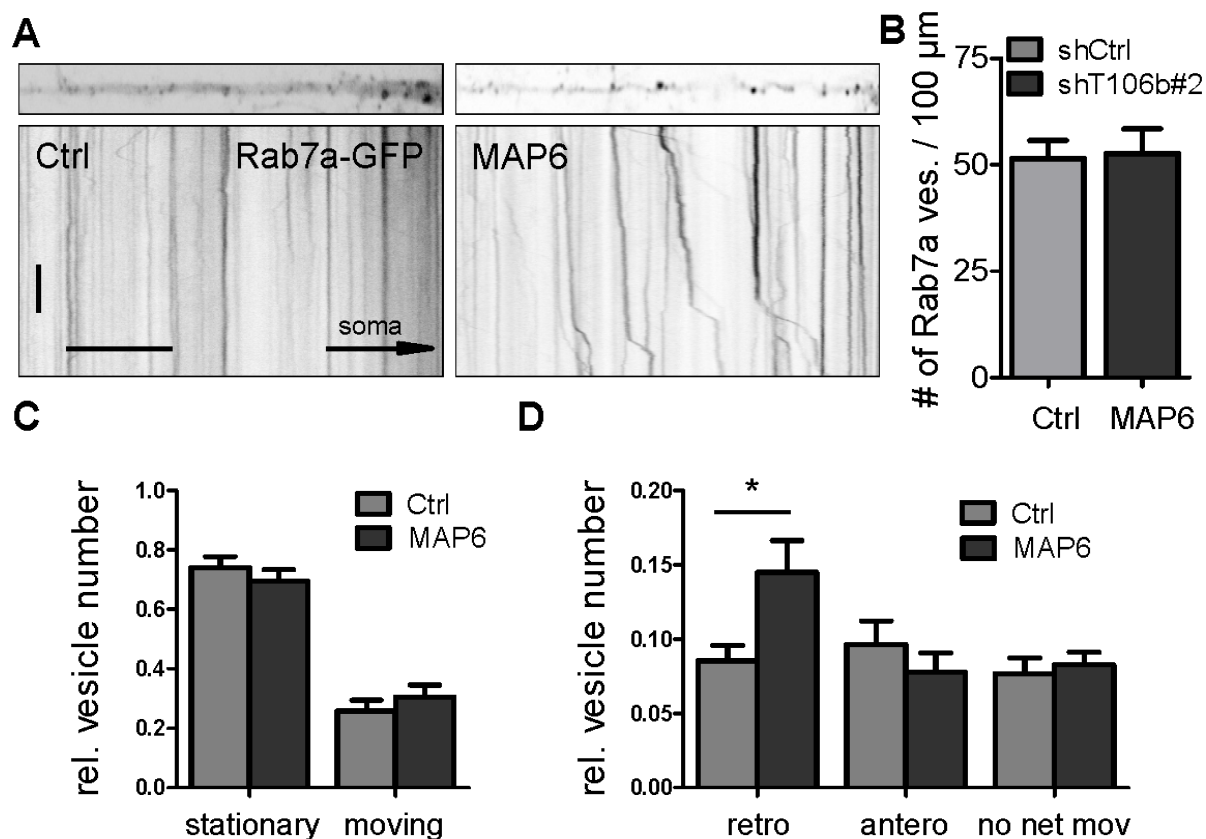


Figure 32: MAP6 regulates retrograde trafficking of late endosomes / lysosomes in dendrites

(A) Primary hippocampal neurons were transfected (DIV6+3) with either rat MAP6 or empty vector and RAB7a-GFP to visualize late endosome / lysosome trafficking in dendrites. Dendrite segments and the corresponding representative kymographs are shown. Scale bar represents 60 s and 20 μm. (B) Quantitative analysis of vesicle number in the dendrites of transfected neurons. The number of RAB7a-labeled vesicles per 100 μm of dendrite length did not change. (C) Analysis of RAB 7a-positive vesicle movement as above. Expression of MAP6 enhances retrograde mobility of RAB7a-GFP labeled vesicles. Between five and eleven neurons per condition were analyzed per experiment in at least three independent experiments, mean +/- SEM, unpaired t-test: * denotes $p < 0.05$, ** denotes $p < 0.01$.

6.3 MAP6 depletion rescues TMEM106B knockdown effect on lysosomal transport

Next, I tested if knockdown of MAP6 could - similar to the rescue of the dendrite outgrowth phenotype - also compensate for the enhanced retrograde trafficking in TMEM106B knockdown neurons. Hippocampal neurons (DIV6+3) were either transfected with shCtrl, shT106b#2 or shMAP6 individually or in combinations. RAB7A-GFP was used to visualize late endosomes and lysosomes in the dendritic compartment. On the one hand, neurons transfected with shT106b#2 alone exhibited

enhanced retrograde transport of the fluorescently labeled vesicles when compared to control neurons, as expected from the previous experiments. On the other hand, MAP6 knockdown alone slightly increased trafficking of both retrogradely and anterogradely transported vesicles. Strikingly, co-transfection of TMEM106B and MAP6 shRNA increased anterograde transport of late endosomes / lysosomes when compared to TMEM106B knockdown alone, thereby rebalancing the ratio of both directions (Figure 33A and 33B).

Altogether, these results further strengthen the connection between TMEM106B and MAP6 as they provide another cellular function affected by both proteins. Moreover, MAP6 knockdown also compensates the unbalanced dendritic trafficking of lysosome upon TMEM106B knockdown.

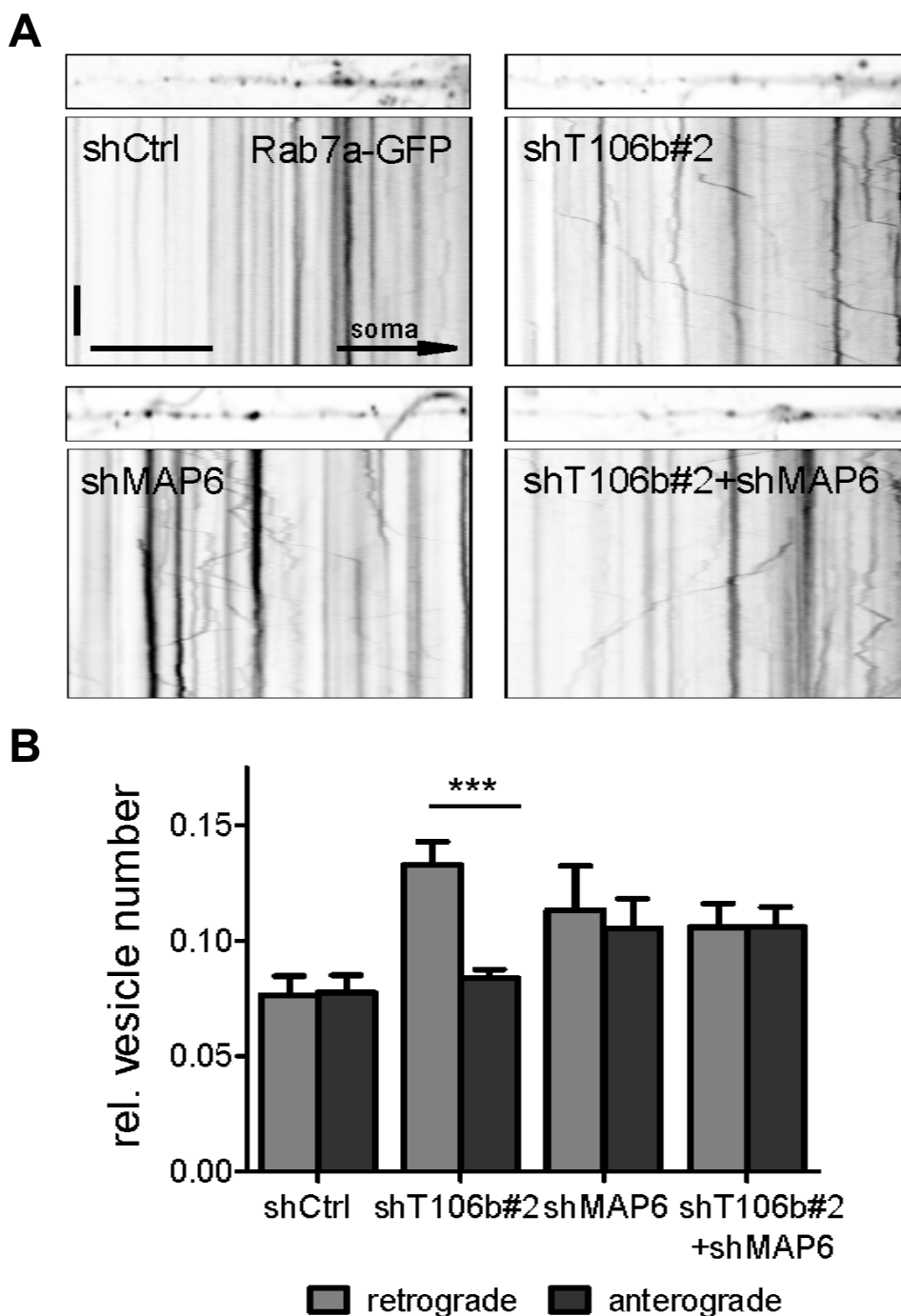


Figure 33: MAP6 knockdown rebalances lysosomal trafficking in TMEM106B knockdown neurons

(A) Primary hippocampal neurons (DIV6+3) were transfected with either shCtrl, shT106b#2+shCtrl, shCtrl+shMAP6 or shT106b#2+shMAP6 and RAB7a-GFP to visualize late endosomal / lysosomal trafficking. Dendrite segments and the corresponding representative kymographs of dendritic movement of RAB7a-GFP-labeled vesicles are shown. Scale bars represent 60 s and 20 μ m. (B) Quantitative analysis of vesicle movement from 5 min kymographs. Vesicles were manually classified according to their movement. Coexpression of MAP6 shRNA rebalances altered retrograde trafficking upon TMEM106B

knockdown. Between six and ten neurons per condition were analyzed per experiment in at least three independent experiments, mean +/- SEM, unpaired t-test: * denotes $p < 0.05$, *** denotes $p < 0.001$.

6.4 Overexpressed MAP6 co-migrates with dendritic lysosomes

My results indicate that TMEM106B and MAP6 together regulate late endosomal / lysosomal transport in dendrites and thereby influence dendrite morphology. This mechanism would require close contact of TMEM106B and MAP6 on microtubule and / or lysosomes. Above, I have already demonstrated that both proteins physically interact and that they are present in the same subcellular fraction as RAB7 (compare Figures 17, 18 and 20). Remarkably, live imaging of MAP6-GFP and LAMP1-RFP coexpressed in primary neurons (DIV6+3) displayed comigration of MAP6-GFP with some LAMP1-RFP-positive lysosomes in dendrites (Figure 34A). Although endogenous MAP6 shows - as expected for a microtubule-binding protein - a wide-spread distribution in axons and dendrites (Figure 34B), the comigration of MAP6-GFP with a fraction of moving lysosomes indicated that excess, non-MT-bound MAP6 can still bind to TMEM106B on lysosomes. This suggests a dominant negative effect of overexpressed MAP6.

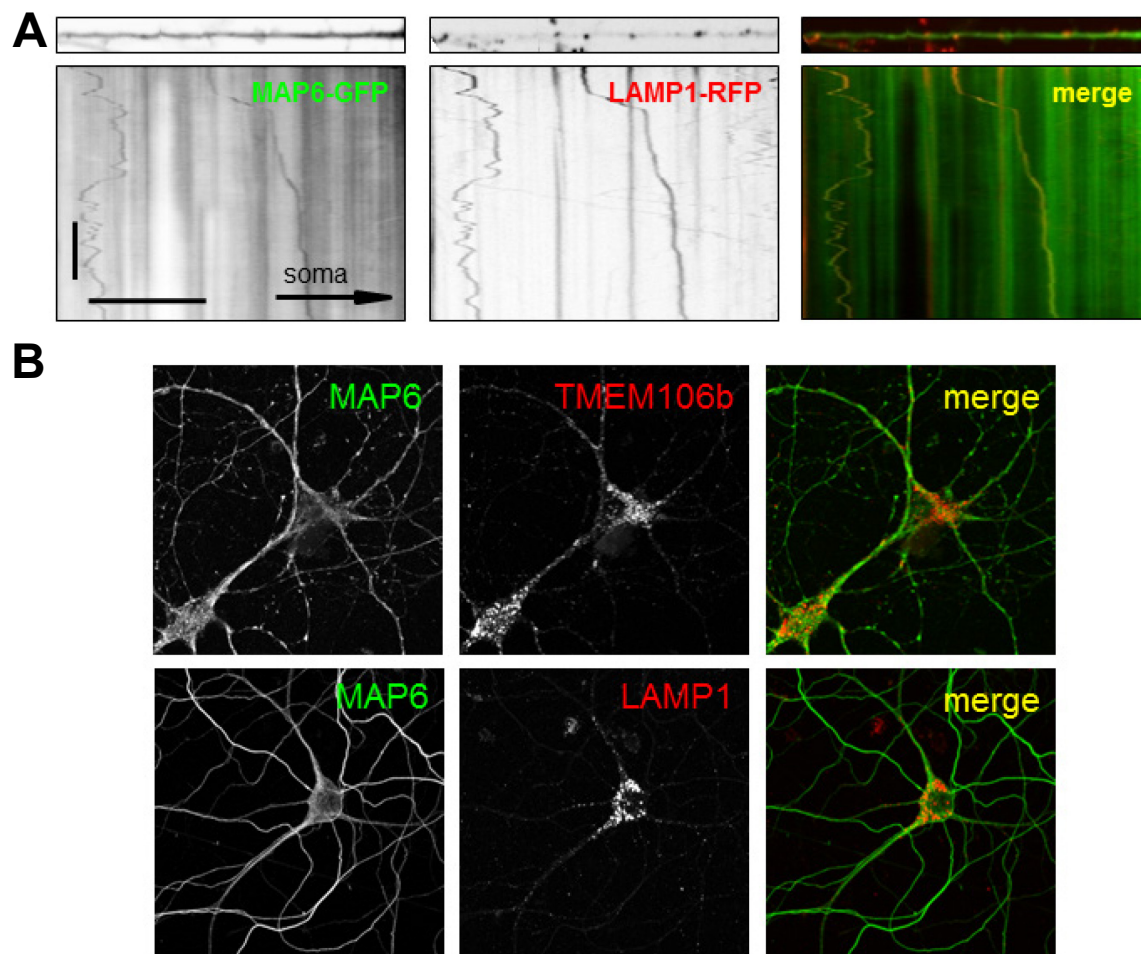


Figure 34: MAP6-GFP comigrates with some LAMP1-RFP-positive lysosomes in dendrites

(A) Primary hippocampal neurons (DIV6+3) were transfected with MAP6-GFP and LAMP1-RFP and live cell imaged for 5 min with a frequency of 1 Hz to visualize movement of the fluorescently tagged proteins. Dendrite segments and the corresponding representative kymographs are shown. Merged images show excess MAP6 bound to moving LAMP1-positive late-endosomes/lysosomes in dendrites. Scale bars represent 60 s and 15 μm. (B) Primary rat hippocampal neurons (DIV12) were immunostained with antibodies against MAP6 (green) and TMEM106B (red) or LAMP1 (red). A commercial mouse monoclonal and a home-made rabbit polyclonal anti-MAP6 antibody were used in the upper and lower panel, respectively. Confocal images show cytoskeletal staining in dendrites and axon and some vesicular staining in the soma for MAP6 and vesicular staining pattern for TMEM106B and LAMP1. Scale bar represents 50 μm.

6.5 Low dose Nocodazole rebalances lysosomal trafficking and partially rescues dendrite withering

Since it was reported that stabilizing the microtubule network is a major function of MAP6 (Bosc et al., 1996), it seems likely that reduction of the protein would increase the dynamics of the very same network. Thus, pharmacological enhancement of microtubule dynamics might also rescue lysosomal trafficking defects and the dendrite loss upon TMEM106B knockdown. Nocodazole is an anti-neoplastic agent, which inhibits polymerization of microtubules and thereby destroys the cytoskeletal network. However, Giannakakou and colleagues could demonstrate that subtherapeutical doses of nocodazole apparently enhance the dynamics of microtubules without destroying them, thus enhancing nucleus directed (that is retrograde) transport of adenovirus particles (Giannakakou et al., 2002).

With this in mind, I tried to restore the alterations in dendritic trafficking of lysosomes as well as the deficiency in dendrite outgrowth and maintenance upon loss of TMEM106B with chronic treatment of low dose nocodazole. Neurons (DIV6+3) were transfected with either a shRNA against TMEM106B or a control shRNA. Both groups were treated either with DMSO or 10 nM nocodazole every 36 h starting with transfection. The relative number of anterogradely and retrogradely moving RAB7A-GFP labeled vesicles was measured as described above. Again, vesicles in shCtrl transfected neurons exhibited an evenly balanced ratio of both types of movements whereas shT106b#2 transfected neurons showed an increase in retrograde trafficking (compare Figure 27). Upon addition of nocodazole, the balanced ratio between anterograde and retrograde movement was restored (Figure 35A and 35B), comparable to MAP6 knockdown.

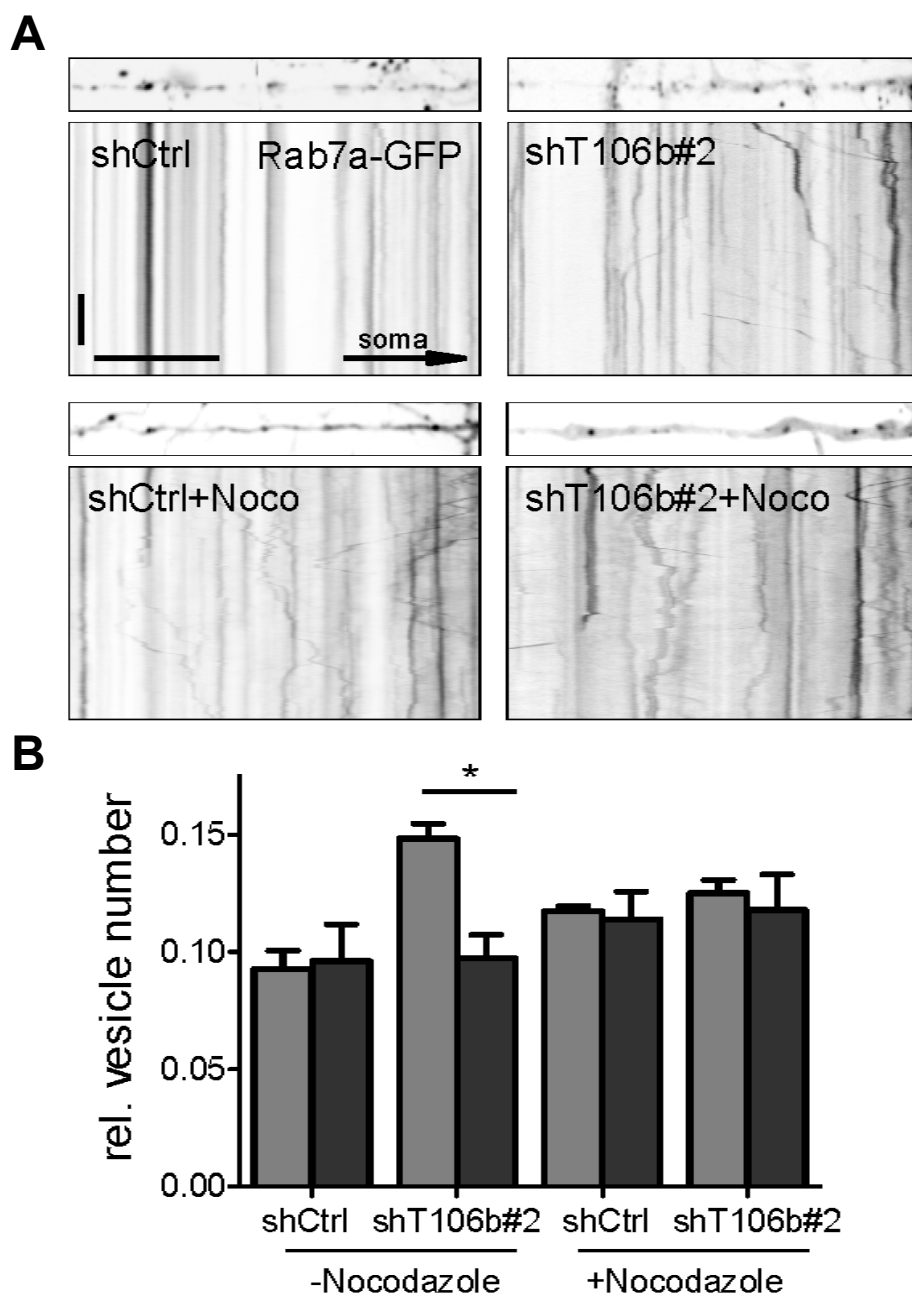


Figure 35: Nocodazole treatment rebalances lysosomal trafficking in TMEM106B knockdown neurons

(A) Primary hippocampal neurons (DIV6+3) were transfected with either shCtrl or shT106b#2 and RAB7a-GFP. After transfection fresh nocodazole (10nM) was added every 36 hours to neurons of the treatment group. Dendrite segments and the corresponding representative kymographs of RAB7a-labeled vesicle movement are shown. (B) Quantitative analysis of vesicle movement from 5 min kymographs. Vesicles were manually classified according to their movement. Low dose nocodazole treatment rebalances altered retrograde lysosomal trafficking upon TMEM106B knockdown. Between six and ten neurons per condition were analyzed per experiment in at least three independent experiments, mean \pm SEM, unpaired t-test: * denotes $p < 0.05$

If both phenotypes – dendritic vesicle trafficking and dendrite outgrowth – were in fact connected, rebalancing anterograde and retrograde transport would naturally lead also to an attenuation of the deficits in arborization. In order to test this, hippocampal neurons were transfected on DIV7 with shCtrl or shT106b #2 for five days. All shRNA transfected neurons co-expressed EGFP to visualize the dendritic morphology. As described above, images of individual neurons were taken and dendritic branching quantified by Sholl analysis. Neurons transfected with shRNA against TMEM106B showed deficits in dendritic arborization, as expected. Remarkably, neurons additionally treated with 10 nM nocodazole every 36 h, showed an alleviation of this phenotype albeit not a full restoration (Figure 36A and 36B).

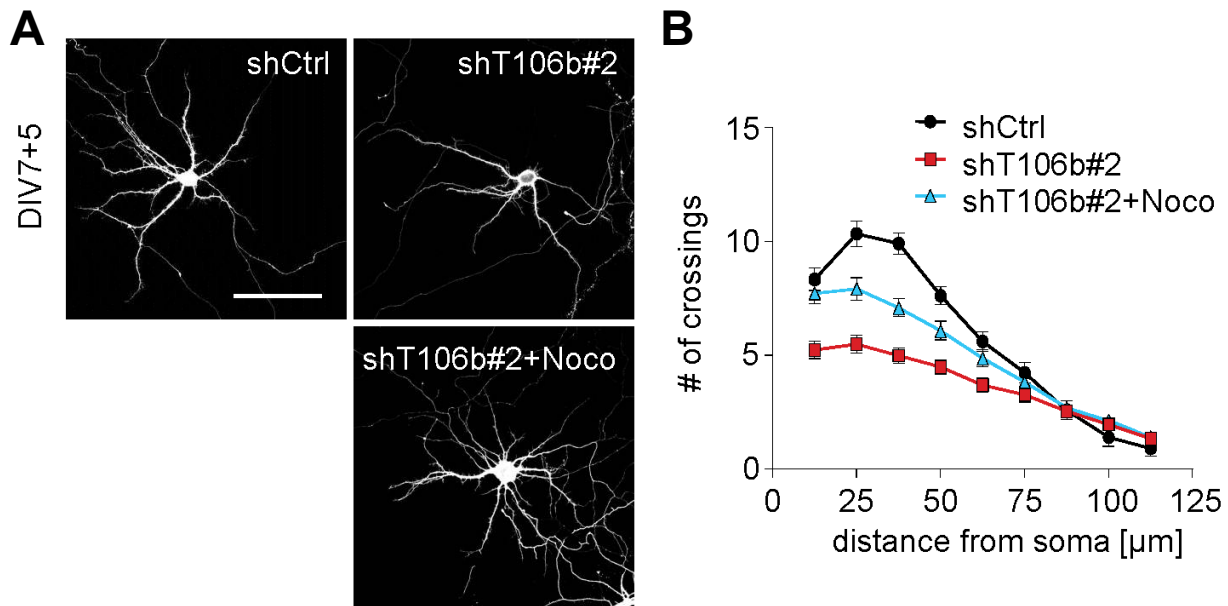


Figure 36: Nocodazole treatment rescues the branching effect of TMEM106B knockdown

(A, B) Primary rat hippocampal neurons (DIV7+5) were cotransfected with either shCtrl or shT106b#2 and GFP to visualize dendritic morphology. 10 nM nocodazole was added freshly every 36 hours for a total of 5 days to the neurons in the treatment group. Nocodazole-treated neurons branched significantly more than untreated T106b#2 transfected neurons (shCtrl vs shT106b#2: from 12.5 μm to 50 μm $p < 0.001$, 62.5 μm $p < 0.05$. shT106b#2 vs shT106b#2+Noco: from 12.5 μm to 25 μm $p < 0.001$, at 37.5 μm $p < 0.01$). $n > 40$ cells per condition, three independent experiments, mean \pm SEM, two-way ANOVA. Scale bar represent 100 μm .

Taken together, enhancing microtubule dynamics pharmacologically by low dose treatment with nocodazole is able to rebalance lysosomal trafficking and restore dendritic outgrowth in TMEM106B knockdown neurons comparable to MAP6 knockdown.

6.6 Enhancing anterograde transport by dnRILP stimulates dendrite growth and rescues TMEM106B knockdown phenotype

Endosomal and lysosomal trafficking, microtubule dynamics and dendrite morphology are tightly connected (Conde and Caceres, 2009; Dehmelt and Halpain, 2005; Kapitein and Hoogenraad, 2011; Villarroel-Campos et al., 2014). Therefore it is tempting to speculate that in the case of TMEM106B knockdown the misbalanced dendritic transport of lysosomes causes the decreased dendrite arborization. In order to provide evidence that such a mechanism is responsible for the observed phenotypes I searched for a way to manipulate lysosomal trafficking independent of TMEM106B and MAP6 and studied the subsequent impact on dendrite outgrowth. I took advantage of the dominant negative c-terminal fragment of Rab-Interacting-Lysosomal-Protein (RILP). Several studies have demonstrated that upon expression of wild-type RILP, dynein-dynactin motor protein complexes are recruited to lysosomes. As a consequence, this recruitment induces trafficking toward the minus-end of microtubules and the MTOC whereas the expression of dnRILP leads to dispersion of lysosomes throughout the cell (Cantalupo et al., 2001; Jordens et al., 2001).

In my experimental context (DIV6+3), overexpression of dnRILP increases the number of anterograde moving RAB7A-GFP labeled vesicles. In contrast, the number of late endosomes / lysosomes which moved retrogradely or exhibited no net movement did not change (Figure 37A and 37B). Next, I analyzed dendrite branching in hippocampal neurons (DIV7+5) upon dnRILP expression. Strikingly, neurons transfected with dnRILP showed a significantly higher complexity of the dendritic arbor compared to control transfected cells as quantified by Sholl analysis (Figure 37C and 37D), indicating that anterograde lysosomal transport promotes dendritic branching.

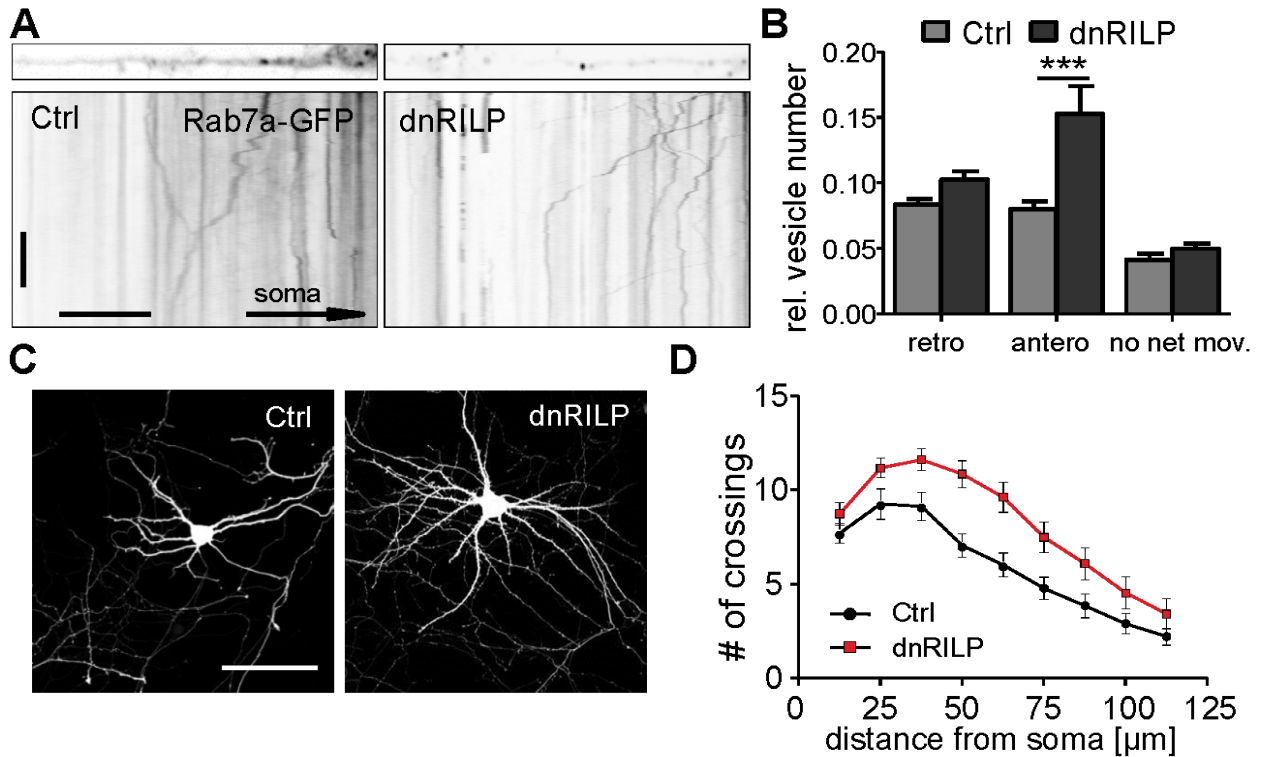


Figure 37: Overexpression of dominant negative RILP increases anterograde movement of lysosomes and dendritic branching

(A) Primary hippocampal neurons (DIV6+3) were transfected with either empty vector (Ctrl) or dnRILP and RAB7a-GFP to visualize late endosomal / lysosomal trafficking in dendrites and live imaged every second for 5 minutes. Dendrite segments and the corresponding representative kymographs of dendritic movement of RAB7a-GFP labeled vesicles are shown. Scale bar represents 60 s (vertical) and 15 μ m (horizontal). (B) Quantitative analysis of vesicle movement from 5 minute kymographs. Vesicles were manually classified according to their movement. Anterograde movement of RAB7a-GFP labeled vesicles is increased upon dnRILP expression. Mean \pm SEM, unpaired t-test: *** denotes $p < 0.001$. (C, D) Primary hippocampal neurons (DIV7+5) were cotransfected with an empty vector (Ctrl) or dnRILP together with GFP. Sholl analysis as above to quantify dendritic complexity which is increased upon dnRILP expression (50 μ m $p < 0.001$, 62.5 μ m $p < 0.01$, 75 μ m $p < 0.05$). $n = 25$ per condition, 3 independent experiments, mean \pm SEM, two-way ANOVA Scale bar represents 100 μ m.

Therefore, I asked whether promoting anterograde transport with dnRILP may rescue impaired branching in TMEM106B knockdown neurons. ShRNA-mediated knockdown of TMEM106B in hippocampal neurons (DIV6+3) led to the expected induction of lysosomal transport (compare Figure 23). Remarkably, the coexpression of dnRILP in these cells restored the increased number of retrogradely transported late endosomes / lysosomes to the control level. Coexpression of dnRILP with

shCtrl even slightly increased the number of anterogradely transported late endosomes / lysosomes, similar to the effect of shMAP6 (Figure 38A and 38B). Importantly, the coexpression of dnRILP in TMEM106B knockdown neurons (DIV7+5) alleviated the branching defect in line with my proposed mechanism (Figure 38C and 38D).

Taken together, the functional rescue with dnRILP implicates that dendritic trafficking of late endosomes / lysosomes is indeed directly controlling dendrite outgrowth.

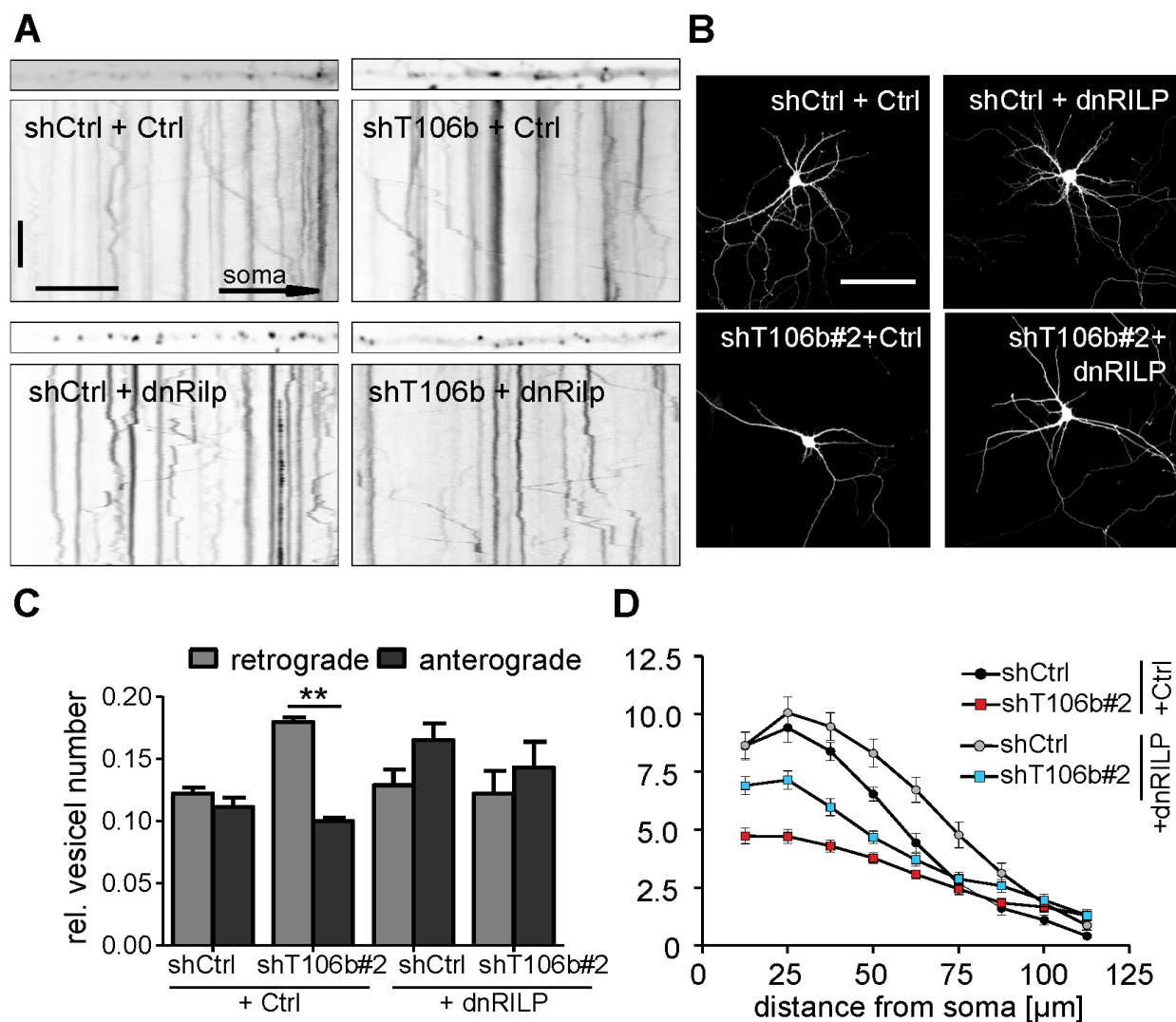


Figure 38: dnRILP restores dendritic branching in TMEM106B knockdown neurons.

(A) Primary hippocampal neurons (DIV6+3) were transfected with combinations of control shRNA (shCtrl) or TMEM106B shRNA#2 (shT106b) and dnRILP or an empty vector (Ctrl) and RAB7a-GFP to visualize late endosomal / lysosomal trafficking in dendrites. Dendrite segments and the corresponding

representative kymographs are shown. Scale bars represent 60 s and 15 μm . (F) Quantitative analysis of vesicle movement from 5 min kymographs. Vesicles were manually classified according to their movement. Coexpression of dnRILP restores balance of anterograde and retrograde vesicle movement in TMEM106B knockdown neurons. At least seven neurons per condition were analyzed per experiment in at least three independent experiments, mean \pm SEM, unpaired t-test: ** denotes $p < 0.01$. (G, H) Primary rat hippocampal neurons (DIV7+5) were cotransfected with combinations of control shRNA (shCtrl) or TMEM106B shRNA#2 (shT106b) and dnRILP or an empty vector (Ctrl) together with GFP. Sholl analysis as above to quantify dendritic complexity. Coexpression of dnRILP ameliorates the branching phenotype upon TMEM106B knockdown (shCtrl+Ctrl vs shT106b#2+Ctrl: from 12.5 μm to 50 μm radius $p < 0.001$. shT106b#2+Ctrl vs shT106b#2+dnRILP: from 12.5 μm $p < 0.001$, 25 μm $p < 0.01$. shCtrl+Ctrl vs shCtrl+dnRILP: from 62.5 μm to 75 μm $p < 0.01$). $n > 25$ per condition, 3 independent experiments, mean \pm SEM, two-way ANOVA. Scale bar represents 100 μm .

In summary, I could show on a biochemical and cell biological level that the FTL D risk factor TMEM106B functionally interacts with microtubule-associated-protein 6 (MAP6) at the lysosome. Together, both proteins regulate dendrite outgrowth and maintenance by controlling lysosomal trafficking in dendrites. Moreover, I could corroborate this causal link between trafficking and outgrowth by manipulating lysosomal transport independent of TMEM106B/MAP6.

V. Discussion

1. Genome-wide association study identified *TMEM106B* risk variants

The identification of *TMEM106B* as a risk factor for FTLN-TDP was based on a genome-wide association study (GWAS) (Van Deerlin et al., 2010). This type of study links certain SNPs in and around a gene to a disease, a syndrome or clinical symptoms. However, identified SNPs do not necessarily provide a direct and causal link between the gene and the disease but are sometimes only marker for other, still unidentified alterations (Manolio, 2010). The first genome-wide association study was conducted in 2005 in patients with aged-related macular degeneration (ARMD) and successfully identified two SNPs which exhibit altered allele frequency compared to controls (Haines et al., 2005). The challenge of such studies consists in the translation of a genetic association between a genomic region and a disease into mechanistic insight in the disease and benefit for the patient. Thus following the identification of genes in the GWAS, candidate based studies are needed to address such questions. Nevertheless, sceptics criticize the often small odd ratios thus the consequentially small impact of the SNP on the disease penetrance (Ku et al., 2010) and that associations rather exist between the disease and a certain genetic haploblock and not necessarily a distinct gene. However, several GWAS have been successfully transformed into better understanding the disease (Budarf et al., 2009). Moreover, other results have already been adopted in the clinics for example in the prevention of adverse effects of widely used remedies such as antiviral drugs and statins (Fellay et al., 2010; Maggo et al., 2011). Hence linking *TMEM106B* to FTLN was the first step of a long process that may lead eventually to the development of new, evidence-based pharmaceuticals. The study presented here is an effort to clarify the physiological role of the encoded protein and linking it also mechanistically to the disease.

2. Neuronal Phenotype: Loss of *TMEM106B* impairs dendrite and spine growth and maintenance

Previous work in cell lines uncovered basic biochemical properties as protein topology and glycosylation pattern (Lang et al., 2012) but neuronal function of

TMEM106B remained largely unknown. In this study I combined knock-down experiments in primary neuron culture, proteomics and live cell imaging to investigate the physiological role of TMEM106B and tie it to cellular functions affected in FTLN (reviewed in (Ling et al., 2013)). I demonstrate that TMEM106B is almost completely localized in late endosomes and lysosomes in primary neurons. This confinement to the late endocytic pathway was also reported in several other publications (Brady et al., 2013; Chen-Plotkin et al., 2012; Lang et al., 2012; Nicholson et al., 2013). Some of these studies claim that overexpression of TMEM106B influences lysosomal properties – for example an increase in lysosomal pH leading to impairment in maturation of lysosomal proteases or an enlarged and altered morphology (Brady et al., 2013; Chen-Plotkin et al., 2012). However, accumulation and probably aggregation of TMEM106B in lysosomes has been observed in neurons upon overexpression of the protein probably causing the lysosomal phenotype (Chen-Plotkin et al., 2012). Also in my hands plasmid-based overexpression of TMEM106B in primary neurons led to the formation of aggregates, especially in dendrites. Moreover, shRNA-mediated knockdown of the protein did not affect the aforementioned lysosomal features, both pointing towards an unphysiological effect of the highly overexpressed protein. TMEM106B similar to many other transmembrane proteins (Kopito, 2000) tends to aggregate when overexpressed due to its hydrophobic transmembrane domain thus questioning the relevance of the published findings. Therefore, I titrated the protein carefully back to endogenous protein levels in all rescue experiments to avoid unphysiological TMEM aggregation.

Overexpression and knockdown of many FTLN related proteins as TDP-43, FUS, and TAU lead to marked toxicity in cellular or animals models (Igaz et al., 2011; Shahani et al., 2006; Sun et al., 2011; Zhang et al., 2009b). However, loss of TMEM106B in primary neurons did not affect cellular viability in a metabolic assay. This finding and the increase in axonal length, despite the loss of dendrites, argue for a modifying role of TMEM106B on FTLN pathogenesis rather than a direct impact on neuronal survival.

The most obvious phenotype upon knockdown of TMEM106B was a pronounced loss of dendrites. The morphology of the dendrites was evaluated with Sholl

analysis, which measures the dendritic complexity combining length and branching (Sholl, 1953). The experiments in younger neurons and mature neurons with an already completely established dendritic arbor show that TMEM106B is required both for the growth and maintenance of dendrites. The decrease in dendrite complexity was especially marked in proximal dendrites in TMEM106B knockdown neurons while the main dendrite was in all cases protected from the shRNA treatment and even was increased in its length. This was not entirely unexpected as the main dendrite seems to be particularly resilient (Hoogenraad et al., 2005).

Emerging evidence points to an involvement of endosomes and lysosomes in neurite outgrowth and maintenance (Sann et al., 2009), for instance impairing the function of recycling endosomes by dominant negative RAB11 caused a collapse of developing axons in drosophila larvae (Bhuin and Roy, 2009). In order to confirm that lysosomes are indeed involved in neurite outgrowth, I inhibited lysosomal biogenesis by expressing dominant-negative RAB7 and observed a defect in dendritic arborization. Effectively, these experiments prove that compromising lysosomal function is actually able to impair dendrite architecture. Importantly, enhancing transport of lysosomes by dominant-negative RILP, a binding partner of RAB7, increased dendritic branching compared to control conditions. Together these findings point towards a direct impact of TMEM106B on dendrite morphology by modulating dendritic trafficking of lysosomes.

In line with the often observed phenomenon that function and morphology of dendrites and spines are regulated through overlapping pathways (reviewed in (Koleske, 2013)), a dramatic decrease in spine number is seen upon TMEM106B knockdown. Moreover the remaining dendritic protrusions are much smaller and thinner than their control counterparts. The density and morphology of spines correlates with synaptic strength and is often used as surrogate marker for a functional neuronal transmission (reviewed in (Hering and Sheng, 2001; Lamprecht and LeDoux, 2004)). I also observed a reduction of pre- and postsynaptic marker proteins, which corroborates the morphological findings on a biochemical level. Dysfunction and loss of synapses is a major hallmark of many neurodegenerative diseases such as AD (Davies et al., 1987; Masliah et al., 2001; Spires-Jones and Knafo, 2012), and might be also a common feature in FTLD (Petkau et al., 2012).

However, the role of synapses and synaptic plasticity still needs to be studied more comprehensively in this disease.

Taken together the data obtained in primary neurons clearly demonstrate that loss of the lysosomal protein TMEM106B lead to severely blunted dendrites and reduced spines number and dimensions without mediating obvious toxicity at the time point the experiments were done.

3. Interaction of TMEM106B with MAP6

To link TMEM106B to known cellular pathways and to the morphological phenotype observed, I sought to identify interacting proteins by coimmunoprecipitation and subsequent LC-MS/MS analysis of individual Coomassie stained bands that were enriched compared to the negative control. The only protein found in all three experiments was the microtubule-binding protein MAP6. Importantly, I could confirm the interaction by immunoblotting afterwards. Furthermore, I managed to map the interaction to the cytoplasmic N-terminus of TMEM106B and the C-terminal region of MAP6 by using deletion mutants and different isoforms of the proteins. The binding on the cytoplasmic part of TMEM106B excludes the possibility that intravesicular MAP6, designated for lysosomal degradation, mediates the interaction. Subcellular fractionations showing MAP6 and TMEM106B in the same (RAB7 and LAMP1 positive lysosomal) fractions further corroborate the interaction of these proteins in the lysosomal compartment. Interestingly, MAP6 was found to interact with another vesicular protein, the endocytic adaptor intersectin 1 (ITSN1) (Morderer et al., 2012). Moreover, depending on posttranslational modifications MAP6 is associated with other non-MT compartments such as the Golgi apparatus, actin rich spines and dendritic branch points (Baratier et al., 2006; Gory-Faure et al., 2006).

Moreover, I also provide evidence for a functional cooperation of TMEM106B and MAP6. While the overexpression of MAP6 phenocopies the blunted dendritic arborization, the additional knockdown of MAP6 in TMEM106B shRNA transfected neurons is able to rescue the knockdown effect and even increase dendritic branching. Although the main cellular function of MAP6 is regulating microtubule

stability, a study by Arama and colleagues demonstrates, in line with my results, a role for the protein in the regulation of cell morphology (Arama et al., 2012). Furthermore, MAP6 was found to coaggregate in spheroid neurofilaments in ALS patients already providing a connection to neurodegenerative diseases (Letournel et al., 2003).

Drawing a functional link between MAP6 and the control of dendrite outgrowth is very appealing, since microtubule-dependent processes and neurite outgrowth are tightly connected (reviewed in (Georges et al., 2008)). There is ample evidence of a huge impact of other structural MAPs such as MAP1B and MAP2 on both microtubule dynamics and neurite outgrowth (Caceres et al., 1992; Meixner et al., 2000). Moreover, axonal growth is a direct consequence arising from the ability of Collapsin Response Mediator Protein-2 (CRMP2) to bind and stabilize microtubules (Hensley et al., 2011). Notably, I provided additional experimental evidence for the connection of both processes, since I was able to rescue dendrite loss in TMEM106B knockdown neurons also by pharmacological enhancement of microtubule dynamics with low doses of nocodazole. However, whole proteome analysis of TMEM106B immunoprecipitate will probably reveal additional interacting proteins which may also contribute to the TMEM106B dependent regulation of dendritic outgrowth. Taken together I provide here ample evidence for a physical and functional interaction of TMEM106B with the microtubule-binding protein MAP6.

4. Dendritic trafficking of lysosomes is affected by TMEM106B and MAP6

Microtubules and vesicles converge on the level of microtubule dependent organelle transport, a tightly regulated process influencing almost all functions in neurons (reviewed in (Hirokawa et al., 2010)). Thus it was intuitive to analyze this crucial process in the context of TMEM106B knockdown in primary neurons, especially as experiments from TMEM106B siRNA treated HeLa-cells show lysosomal clustering at the MTOC ((Schwenk et al., 2014) data by Christina Lang).

I analyzed lysosomal transport in dendrites by acquiring time-laps movies from RAB7-GFP labeled vesicles that were converted into kymographs (path-time diagrams) (Chen et al., 2012; Zhang et al., 2013). Previously, little was known on

the mechanisms of dendritic trafficking of lysosomes and no data on direction and velocity was available. However, my results (0.24 $\mu\text{m/s}$ for control and 0.35 $\mu\text{m/s}$ for TMEM106B knockdown neurons) fall in the range of values reported for comparable transport events such as endosome movement in axons or mitochondrial movement in dendrites (Bannai et al., 2004; Kwinter et al., 2009; van Spronsen et al., 2013). Soon after transfection, at a time point before dendrite blunting became apparent, lysosomal trafficking in TMEM106B knockdown neurons was enhanced compared to controls. However, I observed not only an increase in the number of moving vesicles but also in the mean velocity and distance traveled. Interestingly, the increased vesicle trafficking could be attributed to enhanced retrograde transport (to the soma) whereas anterograde transport (to the dendrite tip) and transport events without net movement stayed roughly the same. Under control conditions the ratio of directions was balanced, while under knockdown conditions up to three times more vesicles moved towards the soma. The observed increase in organelle transport is a most unexpected finding in a neurodegenerative disease, as usually reduced organelle transport is found under pathological conditions (reviewed in (Franker and Hoogenraad, 2013; Millecamps and Julien, 2013)). Consistent with a functional interaction of MAP6 with TMEM106B, MAP6 overexpression had also an effect on lysosomal transport in dendrites. Similar to TMEM106B knockdown, retrograde transport was increased three days after transfection thus already before dendrite loss became apparent. In line with that, double knockdown of TMEM106B and MAP6 ameliorated this effect and reestablished the balance between anterograde and retrograde trafficking. The same was true for treatment with low doses of nocodazole which also rebalanced directed transport of lysosomes in TMEM106B knockdown neurons. Higher amounts of the anti-cancer drug nocodazole inhibit the polymerization of microtubules thus blocking MT-dependent transport (Samson et al., 1979). However, a study by Giannakakou et al. finds that subtherapeutical doses of this compound enhances transport presumably by increasing the dynamics of MT without causing complete collapse (Giannakakou et al., 2002). Moreover, knockdown of MAP6 or nocodazole treatment not only rebalanced the direction of lysosomal transport but mildly increased the number of total transport events in both directions.

The control of lysosomal trafficking and dendrite outgrowth by the same factors and the chronological order of the two phenotypes (lysosomal trafficking before dendrite withering), suggests that the first causes the latter. Neurite outgrowth relies heavily on the secretory and endocytic pathway (Horton et al., 2005; Jan and Jan, 2010; Sann et al., 2009) and also the involvement of lysosomes has been reported (Martinez-Arca et al., 2000). Furthermore, the fusion of lysosomes with the plasma membrane during lysosomal exocytosis provides lipids and other membrane components during cell growth and wound sealing (Chakrabarti et al., 2003; Huynh et al., 2004; Reddy et al., 2001). Moreover, ALS causing mutations in VABP, an ER targeted protein, diminish membrane delivery to dendrites and by that restrain dendritic outgrowth (Kuijpers et al., 2013; Nishimura et al., 2004). Thus, imbalance and the shift of lysosomal transport to the soma in the case of TMEM106B knockdown might affect the membrane and protein turnover in the dendrites and dendritic protrusions and directly lead to the observed loss of dendrites and spines.

To corroborate a causal link between misbalanced lysosomal transport and dendrite growth, I manipulated lysosomal movement in neurons independently of TMEM106B/MAP6 with dnRILP. When overexpressed in cell-lines, wild-type RILP leads to lysosomal clustering near the nucleus, while dnRILP disperses lysosomes throughout the cell body (Cantalupo et al., 2001; Jordens et al., 2001). In contrast to TMEM106B knockdown, dnRILP promotes anterograde transport of lysosomes in dendrites and consequently elevates the complexity of the dendritic arbor compared to control cells. Importantly, in a functional rescue experiment I could reestablish the equilibrium of directed transport in TMEM106B knockdown neurons with dnRILP and by this achieve a partial rescue of the dendritic withering.

Taken together I provide here several lines of evidence supporting that TMEM106B knockdown impairs dendritic arborization by enhancing retrograde trafficking of lysosomes in dendrites: First, The interaction partners TMEM106B and MAP6 influence both phenotypes, trafficking and outgrowth. Second, lysosomal transport defects precede the dendrite loss. Third, altering directed lysosomal transport independently of TMEM106B and MAP6 changes dendrite growth.

It is of course not possible to exclude that additional factors influence this process. Lysosomal misrouting might affect growth factor signaling such as GRN signaling

via sortilin and tumor necrosis factor receptor (TNFR) (Hu et al., 2010; Tang et al., 2011) or nerve growth factor (NGF) via neurotrophic tyrosine kinase receptor type 1 (TrKA) (Snider, 1988) by impairing the availability of the respective receptors on the cell surface. Furthermore, MAP6 might play an additional role in intracellular transport by its binding to MTs and the Golgi apparatus or by directly affecting MT-stability (Gory-Faure et al., 2006). In line with this assumption MAP6 interacts with ITSN1, a protein which affects endocytosis and signal transduction by receptor tyrosine kinases (Morderer et al., 2012; Tsyba et al., 2011).

5. Axonal phenotype

Fast axonal transport of organelles is one of the most widely studied transport process in neurons and neurodegenerative disorders (reviewed in (Hinckelmann et al., 2013; Millecamps and Julien, 2013)). Thus investigating the effect of TMEM106B on axonal transport was only consequential given the dramatic changes in dendritic trafficking of lysosomes. Colocalization experiments revealed that TMEM106B is present in axonal lysosomes as well, even though to a lesser extent than in dendritic lysosomes. Surprisingly, I could not detect any changes in the total number and more important in the direction of lysosomes transported in axons upon knockdown of TMEM106B, although at this time point, axons were 40 % longer than in controls. Several reasons could explain that discrepancy. First, dendrites and axons rely on largely different mechanisms to promote their growth. While axons are strongly dependent on guidance cues, dendritic growth is mainly regulated by limited membrane supply from the secretory and the endocytic pathway (Ye et al., 2007). Second, different motor proteins and regulatory factors are needed for organelle transport in axons and dendrites (Kapitein and Hoogenraad, 2011). Thus, it might be possible that, while TMEM106B and MAP6 control outgrowth in dendrites, other proteins regulate axonal growth by a comparable mechanism. Third, due to the fast growth of axons, I analyzed axonal length and axonal transport in still developing neurons at DIV4, when dendrites are not yet established. It might be possible that axonal transport or axonal morphology is regulated differently in older neurons, at a time the dendritic phenotypes were observed. However, this scenario is

not very likely as the crucial machinery for axonal growth is already established early in neurodevelopment (da Silva and Dotti, 2002; Neukirchen and Bradke, 2011).

6. Model

All findings in this study combined are compatible with a model describing TMEM106B as a molecular brake for the retrograde transport of lysosomes in dendrites thereby regulating dendrite growth and maintenance: TMEM106B – at the lysosomal membrane – binds with its cytoplasmic N-terminus to the C-terminus of microtubule-bound MAP6. This interaction apparently inhibits transport and stalls most dendritic lysosomes to the microtubule. Thus, only a limited amount of vesicles move retrogradely through the dendrite under control conditions (Figure 39A). In the case of TMEM106B knockdown, this interaction is not possible any more and more lysosomes move undisturbed towards the soma. In the case of MAP6 overexpression, the protein has a dominant negative effect. Excess MAP6 molecules, not attached to the saturated binding sites on the microtubule, will bind to TMEM106B impeding its interaction with microtubule-bound MAP6. This dominant negative effect of overexpressed MAP6 thus mimics TMEM106B knockdown. This hypothesis is corroborated by live cell imaging experiments demonstrating that overexpressed MAP6-GFP occasionally moves together with lysosomes along dendrites. In contrast, anterograde transport, presumably regulated by different factors, remains constant upon manipulation of TMEM106B or MAP6. Due to the shift towards retrograde lysosomal transport, a net loss of lipid membranes and protein may occur that leads to loss of dendrite and spines (Figure 39B). Knockdown of MAP6 mildly enhances dendritic trafficking of lysosomes in both directions but maintains the balance of anterograde and retrograde movement. Therefore, dendrite arborization is restored despite the loss of TMEM106B (Figure 39C). Why loss of MAP6 also enhances anterograde transport is not completely clear, but may involve other interaction partners of MAP6. Another important factor might be enhanced microtubule dynamics upon knockdown of MAP6 - a widely reported phenomenon (Bosc et al., 1996; Delphin et al., 2012). This is supported by the fact that also nocodazole, a drug that decreases microtubule stability, is able to

increase both retrograde and anterograde lysosomal transport. Such additional factors might also explain why the overexpression of dominant-negative RILP only partially rescues the TMEM106B knockdown phenotype although lysosomal transport is completely rebalanced.

A similar brake mechanism has already been reported for the axonal transport of mitochondria. Syntaphilin, like TMEM106B an integral membrane protein, halts mitochondrial transport in axons. When syntaphilin is inserted in the mitochondrial outer membrane, it can interact with dynein light chain LC8 and thereby bind to the axonal cytoskeleton. This interaction which is completely independent of the motor function of LC8 stalls mitochondria at their current position on the microtubule (Chen et al., 2009; Kang et al., 2008).

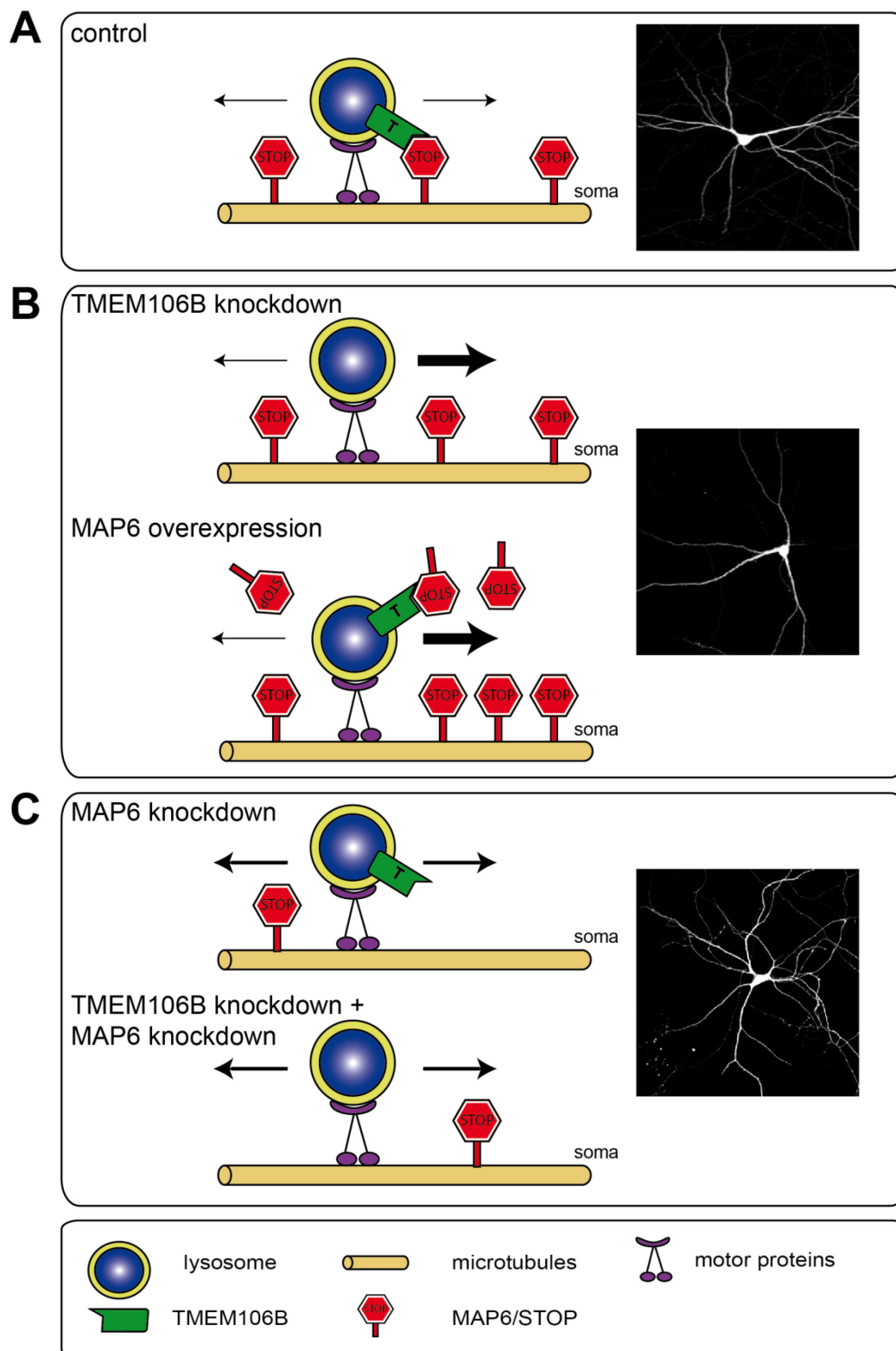


Figure 39 Model of the effects of TMEM106B and MAP6 on lysosomal transport

- (A) Interaction of TMEM106B and MAP6 inhibits retrograde transport of lysosomes in dendrites.
 (B) TMEM106B knockdown and MAP6 overexpression specifically enhance retrograde transport of lysosomes.
 (C) MAP6 knockdown moderately enhances trafficking of lysosomes in both direction and rescues TMEM106B knockdown.

None the less, the mechanism by which TMEM106B and MAP6 control vesicular transport and neurite outgrowth seems to be very specific for lysosomes and dendrites. On the one hand, dendritic trafficking of mitochondria is not affected upon TMEM106B knockdown, consistent with predominant lysosomal localization of the protein. On the other hand, no change in axonal transport of lysosomes could be detected. Additionally, knockdown of another microtubule stabilizing protein (microtubule-associated protein 2 (MAP2)) could not rescue the effect of TMEM106B knockdown on dendritic arborization but rather aggravated the branching defect.

7. Implications for FTLD and other neurodegenerative diseases

Although the association of TMEM106B with FTLD-TDP is now well accepted, the exact mechanism by which the lysosomal protein increases the risk of developing the disease is still unclear. Loss of neuronal TMEM106B does not obviously change the levels of FTLD associated proteins GRN, TDP-43, FUS and Tau. Although a slight elevation in GRN levels is reported for TMEM106B overexpression (Brady et al., 2013), this might also be caused by unspecific lysosomal impairment due to aberrant aggregation of the exogenous TMEM106B (Brady et al., 2013; Chen-Plotkin et al., 2012). Just recently, it was discovered that *TMEM106B* variants increase the risk of developing also other forms of FTLD and even different neurodegenerative disease such as late onset Alzheimer's disease (LOAD) (Gallagher et al., 2014; Lu et al., 2013; van Blitterswijk et al., 2014). Thus, it is likely that these variants rather render the neurons more vulnerable to general stress due to impaired protein homeostasis than induce direct neurotoxicity.

Although long debated at the beginning (van der Zee et al., 2011), emerging evidence suggest now that TMEM106B risk SNPs increase its mRNA and protein levels (Nicholson et al., 2013; Van Deerlin et al., 2010). Nevertheless, loss-of-function studies are an appropriate way to elucidate the physiological function of a protein and its potential role in the disease. With knockdown experiments I was able to demonstrate an important contribution of TMEM106B to the regulation of lysosomal trafficking. This finding fits perfectly into the emerging concept that

lysosomal dysfunction is an important part in the pathogenesis of FTLD per se and especially of cases with GRN involvement. Several lines of evidence support this hypothesis:

1. Mutations in the genes coding for VCP and CHMP2B, proteins involved in the maturation of endosomes and endolysosomal sorting and fusion events, are responsible for a small number of familial FTLD cases (FTLD-UPS) (Momeni et al., 2006a; Watts et al., 2004).
2. The v-type ATPase inhibitor bafilomycin A1 and other agents that inhibit lysosomal acidification increase GRN expression and secretion in *GRN*^{+/-} mice and lymphoblasts from *GRN* haploinsufficiency patients (Capell et al., 2011).
3. Homozygous *GRN* knockout mice exhibit apart from aberrantly phosphorylated TDP-43 and shorter life expectancy, a strong lysosomal dysfunction as mRNA and protein level of the lysosomal protease cathepsin D are highly elevated (Wils et al., 2012). Vice versa, in cathepsin D knockout mice, GRN mRNA level are almost doubled (Ahmed et al., 2010).
4. Additionally, severe accumulation of lipofuscin aggregates is found in the brain of the GRN knockout animals, suggesting an impairment of the lysosomal system (Ahmed et al., 2010). While heterozygous GRN mutations carriers develop FTLD-TDP, humans with homozygous *GRN* mutations thus complete loss of the protein develop, in line with the findings from the knockout mice, neuronal ceroid lipofuscinosis (NCL) a lysosomal storage disorder (Smith et al., 2012). Another juvenile onset form of this syndrome – Batten disease - is caused by mutations in CLN3 (Tuxworth et al., 2009). Expression of mutated CLN3 in HeLa cells induces perinuclear clustering of lysosomes (Uusi-Rauva et al., 2012), reminiscent of the clustering phenotype seen in HeLa cells, treated with TMEM106B siRNA ((Schwenk et al., 2014) data by Christina Lang).

All these facts argue for a strong lysosomal component in FTLD-TDP pathogenesis, especially in *GRN* mutation carriers, in whom TMEM106B SNPs have the strongest impact (Van Deerlin et al., 2010). Strikingly, TMEM106B, presumably together with lysosomes, accumulates in the soma and main dendrites of neurons in FTLD-

TDP patients with GRN mutation (Busch et al., 2013; Chen-Plotkin et al., 2012) supporting the data of the present study. The aforementioned connection between lysosomes and FTLN, together with the findings of this study strongly indicates that lysosomal dysfunction is a crucial step in the pathological cascade leading to the disease. This dysfunction may easily be aggravated by lysosomal misrouting in TMEM106B risk carriers.

8. Summary, open questions and future perspectives

Taken together I demonstrated that the FTLN-TDP risk factor TMEM106B is located in late endosomes and lysosomes in primary neurons. Together with its interaction partner MAP6, TMEM106B acts as a molecular brake controlling the retrograde transport of lysosomes in the dendrite. Releasing that brake by knockdown of TMEM106B or the dominant negative effect of overexpressed MAP6 leads to increased transport of lysosomes to the soma and thus presumably to a higher and faster membrane and protein turnover in dendrites and spines. This could lead to a net loss of membranes and ultimately to pronounced withering of dendrites and spines. However, rebalancing the lysosomal transport by knockdown of MAP6, overexpression of dominant-negative RILP or treatment with low dose nocodazole can overcome the TMEM106B knockdown effect and restore dendritic branching.

However, many questions remain:

1. Further cell culture experiments are needed to clarify if and how altered microtubule dynamics contributes to the regulation of lysosomal transport by TMEM106B as suggested by rescue experiments with nocodazole. Moreover, it remains unclear if also other vesicular organelles (apart from lysosomes) are affected by TMEM106B or if comparable regulatory mechanisms exist which are affected in other familial forms of the disease. And although initial studies have been conducted to elucidate the role of TMEM106B in protein degradation and autophagy (Brady et al., 2013; Lang et al., 2012), it is unclear how the misrouting of lysosomes influences both processes.
2. Electrophysiology experiments in primary neurons and slice cultures from disease models will need to confirm whether the transport phenotype by

TMEM106B knockdown indeed affects neurotransmission and synaptic strength as predicted by the loss of dendrites and spines. These model systems might also be helpful to identify and validate additional interaction partner for TMEM106B or MAP6 to generate a more complete insight into the mechanism by which the two proteins regulate vesicular transport and neuron morphology.

3. TMEM106B knock-out animal models should be generated to confirm the findings from cell lines and primary neurons *in vivo* and identify additional phenotypes. Another useful approach to model the role of TMEM106B in the disease might be to introduce the T185S variant at the endogenous *TMEM106B* locus (Barger, 2013). A full examination including especially the analysis of lysosomal transport and function will eventually reveal if the knock-in is already enough to trigger certain disease related symptoms and if crossing with other FTLD models, such as the *GRN* knockout mouse, aggravates their symptoms.
4. More studies in patients are needed to clarify the role of TMEM106B SNP in other sub classes of FTLD and in different neurodegenerative diseases (Lu et al., 2013; van Blitterswijk et al., 2014). Larger studies should also resolve the controversy how the risk variants affect RNA and protein levels of TMEM106B and GRN (Van Deerlin et al., 2010; van der Zee et al., 2011). Careful neuropathological assessment of patient brain samples is needed to evaluate the exact impact of the risk variants on vesicular localization and neuron morphology in affected brain regions. State-of-the-art techniques such as proteomics and transcriptomics from serum or cerebrospinal fluid (CSF) might identify additional dysregulated pathways in risk carriers.
5. Finally, all approaches should focus on the identification of new rationale-based drugs which have to proof their efficacy and safety in large clinical trials.

In the end, mechanistic data from cell culture and animals, genetic and pathological data from patients and –omics data have to be combined to understand how

TMEM106B influences neurodegeneration in general and FTLN in particular and to diagnose and cure patients suffering from these devastating diseases.

VI. References

- Ahmed, Z., Sheng, H., Xu, Y.F., Lin, W.L., Innes, A.E., Gass, J., Yu, X., Wuertzer, C.A., Hou, H., Chiba, S., *et al.* (2010). Accelerated lipofuscinosis and ubiquitination in granulin knockout mice suggest a role for progranulin in successful aging. *Am J Pathol* *177*, 311-324.
- Akhmanova, A., and Hammer, J.A., 3rd (2010). Linking molecular motors to membrane cargo. *Curr Opin Cell Biol* *22*, 479-487.
- Akhmanova, A., and Steinmetz, M.O. (2010). Microtubule +TIPs at a glance. *J Cell Sci* *123*, 3415-3419.
- Al-Sarraj, S., King, A., Troakes, C., Smith, B., Maekawa, S., Bodi, I., Rogelj, B., Al-Chalabi, A., Hortobagyi, T., and Shaw, C.E. (2011). p62 positive, TDP-43 negative, neuronal cytoplasmic and intranuclear inclusions in the cerebellum and hippocampus define the pathology of C9orf72-linked FTLN and MND/ALS. *Acta neuropathologica* *122*, 691-702.
- Alzheimer, A. (1911). Ueber eigenartige Krankheitsfaelle des spaeten Alters. *Zeitschr für die gesamte Psychiatr und Neurol* 356-358
- Amos, L.A., and Schlieper, D. (2005). Microtubules and maps. *Advances in protein chemistry* *71*, 257-298.
- Andrieux, A., Salin, P.A., Vernet, M., Kujala, P., Baratier, J., Gory-Faure, S., Bosc, C., Pointu, H., Proietto, D., Schweitzer, A., *et al.* (2002). The suppression of brain cold-stable microtubules in mice induces synaptic defects associated with neuroleptic-sensitive behavioral disorders. *Genes Dev* *16*, 2350-2364.
- Arai, T., Hasegawa, M., Akiyama, H., Ikeda, K., Nonaka, T., Mori, H., Mann, D., Tsuchiya, K., Yoshida, M., Hashizume, Y., *et al.* (2006). TDP-43 is a component of ubiquitin-positive tau-negative inclusions in frontotemporal lobar degeneration and amyotrophic lateral sclerosis. *Biochem Biophys Res Commun* *351*, 602-611.
- Arama, J., Boulay, A.C., Bosc, C., Delphin, C., Loew, D., Rostaing, P., Amigou, E., Ezan, P., Wingertsmann, L., Guillaud, L., *et al.* (2012). Bmcc1s, a novel brain-isoform of Bmcc1, affects cell morphology by regulating MAP6/STOP functions. *PLoS ONE* *7*, e35488.
- Arantes, R.M., and Andrews, N.W. (2006). A role for synaptotagmin VII-regulated exocytosis of lysosomes in neurite outgrowth from primary sympathetic neurons. *The Journal of neuroscience : the official journal of the Society for Neuroscience* *26*, 4630-4637.
- Ash, P.E., Bieniek, K.F., Gendron, T.F., Caulfield, T., Lin, W.L., DeJesus-Hernandez, M., van Blitterswijk, M.M., Jansen-West, K., Paul, J.W., 3rd, Rademakers, R., *et al.* (2013). Unconventional Translation of C9ORF72 GGGGCC Expansion Generates Insoluble Polypeptides Specific to c9FTD/ALS. *Neuron*.

- Baas, P.W., and Black, M.M. (1990). Individual microtubules in the axon consist of domains that differ in both composition and stability. *J Cell Biol* *111*, 495-509.
- Baas, P.W., Deitch, J.S., Black, M.M., and Banker, G.A. (1988). Polarity orientation of microtubules in hippocampal neurons: uniformity in the axon and nonuniformity in the dendrite. *Proc Natl Acad Sci U S A* *85*, 8335-8339.
- Bagshaw, R.D., Mahuran, D.J., and Callahan, J.W. (2005). Lysosomal membrane proteomics and biogenesis of lysosomes. *Molecular neurobiology* *32*, 27-41.
- Baker, M., Mackenzie, I.R., Pickering-Brown, S.M., Gass, J., Rademakers, R., Lindholm, C., Snowden, J., Adamson, J., Sadovnick, A.D., Rollinson, S., *et al.* (2006). Mutations in progranulin cause tau-negative frontotemporal dementia linked to chromosome 17. *Nature* *442*, 916-919.
- Bannai, H., Inoue, T., Nakayama, T., Hattori, M., and Mikoshiba, K. (2004). Kinesin dependent, rapid, bi-directional transport of ER sub-compartment in dendrites of hippocampal neurons. *J Cell Sci* *117*, 163-175.
- Baratier, J., Peris, L., Brocard, J., Gory-Faure, S., Dufour, F., Bosc, C., Fourest-Lieuvin, A., Blanchoin, L., Salin, P., Job, D., *et al.* (2006). Phosphorylation of microtubule-associated protein STOP by calmodulin kinase II. *The Journal of biological chemistry* *281*, 19561-19569.
- Barger, S.W. (2013). TMEM106B and frontotemporal lobar degeneration: can over-expression tell us how reductions are beneficial? *Journal of neurochemistry* *126*, 696-698.
- Benajiba, L., Le Ber, I., Camuzat, A., Lacoste, M., Thomas-Anterion, C., Couratier, P., Legallic, S., Salachas, F., Hannequin, D., Decousus, M., *et al.* (2009). TARDBP mutations in motoneuron disease with frontotemporal lobar degeneration. *Ann Neurol* *65*, 470-473.
- Bhuin, T., and Roy, J.K. (2009). Rab11 is required for embryonic nervous system development in *Drosophila*. *Cell and tissue research* *335*, 349-356.
- Bolte, S., and Cordelieres, F.P. (2006). A guided tour into subcellular colocalization analysis in light microscopy. *J Microsc* *224*, 213-232.
- Borroni, B., Bonvicini, C., Alberici, A., Buratti, E., Agosti, C., Archetti, S., Papetti, A., Stuani, C., Di Luca, M., Gennarelli, M., *et al.* (2009). Mutation within TARDBP leads to frontotemporal dementia without motor neuron disease. *Hum Mutat* *30*, E974-983.
- Bosc, C., Andrieux, A., and Job, D. (2003). STOP proteins. *Biochemistry* *42*, 12125-12132.
- Bosc, C., Cronk, J.D., Pirollet, F., Watterson, D.M., Haiech, J., Job, D., and Margolis, R.L. (1996). Cloning, expression, and properties of the microtubule-stabilizing protein STOP. *Proc Natl Acad Sci U S A* *93*, 2125-2130.

- Bosc, C., Frank, R., Denarier, E., Ronjat, M., Schweitzer, A., Wehland, J., and Job, D. (2001). Identification of novel bifunctional calmodulin-binding and microtubule-stabilizing motifs in STOP proteins. *The Journal of biological chemistry* 276, 30904-30913.
- Bouvrais-Veret, C., Weiss, S., Hanoun, N., Andrieux, A., Schweitzer, A., Job, D., Hamon, M., Giros, B., and Martres, M.P. (2008). Microtubule-associated STOP protein deletion triggers restricted changes in dopaminergic neurotransmission. *Journal of neurochemistry* 104, 745-756.
- Boxer, A.L., Lipton, A.M., Womack, K., Merrilees, J., Neuhaus, J., Pavlic, D., Gandhi, A., Red, D., Martin-Cook, K., Svetlik, D., *et al.* (2009). An open-label study of memantine treatment in 3 subtypes of frontotemporal lobar degeneration. *Alzheimer disease and associated disorders* 23, 211-217.
- Bradke, F., and Dotti, C.G. (2000). Changes in membrane trafficking and actin dynamics during axon formation in cultured hippocampal neurons. *Microscopy research and technique* 48, 3-11.
- Brady, O.A., Zheng, Y., Murphy, K., Huang, M., and Hu, F. (2013). The frontotemporal lobar degeneration risk factor, TMEM106B, regulates lysosomal morphology and function. *Human molecular genetics* 22, 685-695.
- Brenner, E., Sonnewald, U., Schweitzer, A., Andrieux, A., and Nehlig, A. (2007). Hypoglutamatergic activity in the STOP knockout mouse: a potential model for chronic untreated schizophrenia. *J Neurosci Res* 85, 3487-3493.
- Brettschneider, J., Van Deerlin, V.M., Robinson, J.L., Kwong, L., Lee, E.B., Ali, Y.O., Safren, N., Monteiro, M.J., Toledo, J.B., Elman, L., *et al.* (2012). Pattern of ubiquilin pathology in ALS and FTL indicates presence of C9ORF72 hexanucleotide expansion. *Acta neuropathologica* 123, 825-839.
- Breuer, A.C., Lynn, M.P., Atkinson, M.B., Chou, S.M., Wilbourn, A.J., Marks, K.E., Culver, J.E., and Fleegler, E.J. (1987). Fast axonal transport in amyotrophic lateral sclerosis: an intra-axonal organelle traffic analysis. *Neurology* 37, 738-748.
- Bucci, C., Thomsen, P., Nicoziani, P., McCarthy, J., and van Deurs, B. (2000). Rab7: a key to lysosome biogenesis. *Mol Biol Cell* 11, 467-480.
- Budarf, M.L., Labbe, C., David, G., and Rioux, J.D. (2009). GWA studies: rewriting the story of IBD. *Trends in genetics : TIG* 25, 137-146.
- Busch, J.I., Martinez-Lage, M., Ashbridge, E., Grossman, M., Van Deerlin, V.M., Hu, F., Lee, V.M., Trojanowski, J.Q., and Chen-Plotkin, A.S. (2013). Expression of TMEM106B, the frontotemporal lobar degeneration-associated protein, in normal and diseased human brain. *Acta Neuropathol Commun* 1, 36.
- Caceres, A., Mautino, J., and Kosik, K.S. (1992). Suppression of MAP2 in cultured cerebellar macroneurons inhibits minor neurite formation. *Neuron* 9, 607-618.

- Cantalupo, G., Alifano, P., Roberti, V., Bruni, C.B., and Bucci, C. (2001). Rab-interacting lysosomal protein (RILP): the Rab7 effector required for transport to lysosomes. *Embo J* 20, 683-693.
- Canuel, M., Libin, Y., and Morales, C.R. (2009). The interactomics of sortilin: an ancient lysosomal receptor evolving new functions. *Histology and histopathology* 24, 481-492.
- Capell, A., Liebscher, S., Fellerer, K., Brouwers, N., Willem, M., Lammich, S., Gijssels, I., Bittner, T., Carlson, A.M., Sasse, F., *et al.* (2011). Rescue of progranulin deficiency associated with frontotemporal lobar degeneration by alkalizing reagents and inhibition of vacuolar ATPase. *The Journal of neuroscience : the official journal of the Society for Neuroscience* 31, 1885-1894.
- Cenik, B., Sephton, C.F., Kutluk Cenik, B., Herz, J., and Yu, G. (2012). Progranulin: a proteolytically processed protein at the crossroads of inflammation and neurodegeneration. *The Journal of biological chemistry* 287, 32298-32306.
- Chakrabarti, S., Kobayashi, K.S., Flavell, R.A., Marks, C.B., Miyake, K., Liston, D.R., Fowler, K.T., Gorelick, F.S., and Andrews, N.W. (2003). Impaired membrane resealing and autoimmune myositis in synaptotagmin VII-deficient mice. *J Cell Biol* 162, 543-549.
- Chang, D.T., Honick, A.S., and Reynolds, I.J. (2006). Mitochondrial trafficking to synapses in cultured primary cortical neurons. *The Journal of neuroscience : the official journal of the Society for Neuroscience* 26, 7035-7045.
- Chen-Plotkin, A.S., Unger, T.L., Gallagher, M.D., Bill, E., Kwong, L.K., Volpicelli-Daley, L., Busch, J.I., Akle, S., Grossman, M., Van Deerlin, V., *et al.* (2012). TMEM106B, the risk gene for frontotemporal dementia, is regulated by the microRNA-132/212 cluster and affects progranulin pathways. *The Journal of neuroscience : the official journal of the Society for Neuroscience* 32, 11213-11227.
- Chen, X.Q., Wang, B., Wu, C., Pan, J., Yuan, B., Su, Y.Y., Jiang, X.Y., Zhang, X., and Bao, L. (2012). Endosome-mediated retrograde axonal transport of P2X3 receptor signals in primary sensory neurons. *Cell research* 22, 677-696.
- Chen, Y.M., Gerwin, C., and Sheng, Z.H. (2009). Dynein light chain LC8 regulates syntaphilin-mediated mitochondrial docking in axons. *The Journal of neuroscience : the official journal of the Society for Neuroscience* 29, 9429-9438.
- Condeelis, C.S., and Caceres, A. (2009). Microtubule assembly, organization and dynamics in axons and dendrites. *Nat Rev Neurosci* 10, 319-332.
- Conus, S., and Simon, H.U. (2008). Cathepsins: key modulators of cell death and inflammatory responses. *Biochemical pharmacology* 76, 1374-1382.
- Coy, D.L., Hancock, W.O., Wagenbach, M., and Howard, J. (1999). Kinesin's tail domain is an inhibitory regulator of the motor domain. *Nat Cell Biol* 1, 288-292.

Cruchaga, C., Graff, C., Chiang, H.H., Wang, J., Hinrichs, A.L., Spiegel, N., Bertelsen, S., Mayo, K., Norton, J.B., Morris, J.C., *et al.* (2011). Association of TMEM106B gene polymorphism with age at onset in granulin mutation carriers and plasma granulin protein levels. *Archives of neurology* 68, 581-586.

Cruts, M., Gijssels, I., van der Zee, J., Engelborghs, S., Wils, H., Pirici, D., Rademakers, R., Vandenberghe, R., Dermaut, B., Martin, J.J., *et al.* (2006). Null mutations in progranulin cause ubiquitin-positive frontotemporal dementia linked to chromosome 17q21. *Nature* 442, 920-924.

da Silva, J.S., and Dotti, C.G. (2002). Breaking the neuronal sphere: regulation of the actin cytoskeleton in neuritogenesis. *Nat Rev Neurosci* 3, 694-704.

Davies, C.A., Mann, D.M., Sumpter, P.Q., and Yates, P.O. (1987). A quantitative morphometric analysis of the neuronal and synaptic content of the frontal and temporal cortex in patients with Alzheimer's disease. *J Neurol Sci* 78, 151-164.

Dehmelt, L., and Halpain, S. (2005). The MAP2/Tau family of microtubule-associated proteins. *Genome Biol* 6, 204.

DeJesus-Hernandez, M., Mackenzie, I.R., Boeve, B.F., Boxer, A.L., Baker, M., Rutherford, N.J., Nicholson, A.M., Finch, N.A., Flynn, H., Adamson, J., *et al.* (2011). Expanded GGGGCC hexanucleotide repeat in noncoding region of C9ORF72 causes chromosome 9p-linked FTD and ALS. *Neuron* 72, 245-256.

Delotterie, D., Ruiz, G., Brocard, J., Schweitzer, A., Roucard, C., Roche, Y., Suaud-Chagny, M.F., Bressand, K., and Andrieux, A. (2010). Chronic administration of atypical antipsychotics improves behavioral and synaptic defects of STOP null mice. *Psychopharmacology* 208, 131-141.

Delphin, C., Bouvier, D., Seggio, M., Couriol, E., Saoudi, Y., Denarier, E., Bosc, C., Valiron, O., Bisbal, M., Arnal, I., *et al.* (2012). MAP6-F is a temperature sensor that directly binds to and protects microtubules from cold-induced depolymerization. *The Journal of biological chemistry* 287, 35127-35138.

Denarier, E., Fourest-Lieuvin, A., Bosc, C., Pirollet, F., Chapel, A., Margolis, R.L., and Job, D. (1998). Nonneuronal isoforms of STOP protein are responsible for microtubule cold stability in mammalian fibroblasts. *Proc Natl Acad Sci U S A* 95, 6055-6060.

Deng, H.X., Chen, W., Hong, S.T., Boycott, K.M., Gorrie, G.H., Siddique, N., Yang, Y., Fecto, F., Shi, Y., Zhai, H., *et al.* (2011). Mutations in UBQLN2 cause dominant X-linked juvenile and adult-onset ALS and ALS/dementia. *Nature* 477, 211-215.

Dormann, D., and Haass, C. (2011). TDP-43 and FUS: a nuclear affair. *Trends Neurosci* 34, 339-348.

Dormann, D., and Haass, C. (2013). Fused in sarcoma (FUS): an oncogene goes awry in neurodegeneration. *Mol Cell Neurosci* 56, 475-486.

Dormann, D., Rodde, R., Edbauer, D., Bentmann, E., Fischer, I., Hruscha, A., Than, M.E., Mackenzie, I.R., Capell, A., Schmid, B., *et al.* (2010). ALS-associated fused in sarcoma (FUS) mutations disrupt Transportin-mediated nuclear import. *Embo J* 29, 2841-2857.

Eskelinen, E.L., Tanaka, Y., and Saftig, P. (2003). At the acidic edge: emerging functions for lysosomal membrane proteins. *Trends Cell Biol* 13, 137-145.

Feiguin, F., Godena, V.K., Romano, G., D'Ambrogio, A., Klima, R., and Baralle, F.E. (2009). Depletion of TDP-43 affects Drosophila motoneurons terminal synapsis and locomotive behavior. *FEBS Lett* 583, 1586-1592.

Fellay, J., Thompson, A.J., Ge, D., Gumbs, C.E., Urban, T.J., Shianna, K.V., Little, L.D., Qiu, P., Bertelsen, A.H., Watson, M., *et al.* (2010). ITPA gene variants protect against anaemia in patients treated for chronic hepatitis C. *Nature* 464, 405-408.

Finch, N., Carrasquillo, M.M., Baker, M., Rutherford, N.J., Coppola, G., Dejesus-Hernandez, M., Crook, R., Hunter, T., Ghidoni, R., Benussi, L., *et al.* (2011). TMEM106B regulates progranulin levels and the penetrance of FTL in GRN mutation carriers. *Neurology* 76, 467-474.

Fournet, V., Jany, M., Fabre, V., Chali, F., Orsal, D., Schweitzer, A., Andrieux, A., Messanvi, F., Giros, B., Hamon, M., *et al.* (2010). The deletion of the microtubule-associated STOP protein affects the serotonergic mouse brain network. *Journal of neurochemistry* 115, 1579-1594.

Franker, M.A., and Hoogenraad, C.C. (2013). Microtubule-based transport - basic mechanisms, traffic rules and role in neurological pathogenesis. *J Cell Sci* 126, 2319-2329.

Fujii, R., Okabe, S., Urushido, T., Inoue, K., Yoshimura, A., Tachibana, T., Nishikawa, T., Hicks, G.G., and Takumi, T. (2005). The RNA binding protein TLS is translocated to dendritic spines by mGluR5 activation and regulates spine morphology. *Curr Biol* 15, 587-593.

Fujita, K., Ito, H., Nakano, S., Kinoshita, Y., Wate, R., and Kusaka, H. (2008). Immunohistochemical identification of messenger RNA-related proteins in basophilic inclusions of adult-onset atypical motor neuron disease. *Acta neuropathologica* 116, 439-445.

Gajdusek, D.C. (1985). Hypothesis: interference with axonal transport of neurofilament as a common pathogenetic mechanism in certain diseases of the central nervous system. *N Engl J Med* 312, 714-719.

Gallagher, M.D., Suh, E., Grossman, M., Elman, L., McCluskey, L., Van Swieten, J.C., Al-Sarraj, S., Neumann, M., Gelpi, E., Ghetti, B., *et al.* (2014). TMEM106B is a genetic modifier of frontotemporal lobar degeneration with C9orf72 hexanucleotide repeat expansions. *Acta neuropathologica*.

Galvez, T., Gilleron, J., Zerial, M., and O'Sullivan, G.A. (2012). SnapShot: Mammalian Rab proteins in endocytic trafficking. *Cell* 151, 234-234 e232.

- Gass, J., Lee, W.C., Cook, C., Finch, N., Stetler, C., Jansen-West, K., Lewis, J., Link, C.D., Rademakers, R., Nykjaer, A., *et al.* (2012). Progranulin regulates neuronal outgrowth independent of sortilin. *Mol Neurodegener* 7, 33.
- Georges, P.C., Hadzimichalis, N.M., Sweet, E.S., and Firestein, B.L. (2008). The yin-yang of dendrite morphology: unity of actin and microtubules. *Molecular neurobiology* 38, 270-284.
- Giannakakou, P., Nakano, M., Nicolaou, K.C., O'Brate, A., Yu, J., Blagosklonny, M.V., Greber, U.F., and Fojo, T. (2002). Enhanced microtubule-dependent trafficking and p53 nuclear accumulation by suppression of microtubule dynamics. *Proc Natl Acad Sci U S A* 99, 10855-10860.
- Gijssels, I., Van Langenhove, T., van der Zee, J., Sleegers, K., Philtjens, S., Kleinberger, G., Janssens, J., Bettens, K., Van Cauwenberghe, C., Pereson, S., *et al.* (2012). A C9orf72 promoter repeat expansion in a Flanders-Belgian cohort with disorders of the frontotemporal lobar degeneration-amyotrophic lateral sclerosis spectrum: a gene identification study. *Lancet Neurol* 11, 54-65.
- Gitcho, M.A., Bigio, E.H., Mishra, M., Johnson, N., Weintraub, S., Mesulam, M., Rademakers, R., Chakraverty, S., Cruchaga, C., Morris, J.C., *et al.* (2009). TARDBP 3'-UTR variant in autopsy-confirmed frontotemporal lobar degeneration with TDP-43 proteinopathy. *Acta neuropathologica* 118, 633-645.
- Goldman, J.S., Adamson, J., Karydas, A., Miller, B.L., and Hutton, M. (2007). New genes, new dilemmas: FTL D genetics and its implications for families. *American journal of Alzheimer's disease and other dementias* 22, 507-515.
- Goldman, J.S., Farmer, J.M., Wood, E.M., Johnson, J.K., Boxer, A., Neuhaus, J., Lomen-Hoerth, C., Wilhelmsen, K.C., Lee, V.M., Grossman, M., *et al.* (2005). Comparison of family histories in FTL D subtypes and related tauopathies. *Neurology* 65, 1817-1819.
- Gorno-Tempini, M.L., Hillis, A.E., Weintraub, S., Kertesz, A., Mendez, M., Cappa, S.F., Ogar, J.M., Rohrer, J.D., Black, S., Boeve, B.F., *et al.* (2011). Classification of primary progressive aphasia and its variants. *Neurology* 76, 1006-1014.
- Gory-Faure, S., Windscheid, V., Bosc, C., Peris, L., Proietto, D., Franck, R., Denarier, E., Job, D., and Andrieux, A. (2006). STOP-like protein 21 is a novel member of the STOP family, revealing a Golgi localization of STOP proteins. *The Journal of biological chemistry* 281, 28387-28396.
- Haass, C., and Mandelkow, E. (2010). Fyn-tau-amyloid: a toxic triad. *Cell* 142, 356-358.
- Haines, J.L., Hauser, M.A., Schmidt, S., Scott, W.K., Olson, L.M., Gallins, P., Spencer, K.L., Kwan, S.Y., Nouredine, M., Gilbert, J.R., *et al.* (2005). Complement factor H variant increases the risk of age-related macular degeneration. *Science* 308, 419-421.

- Harvey, R.J., Skelton-Robinson, M., and Rossor, M.N. (2003). The prevalence and causes of dementia in people under the age of 65 years. *J Neurol Neurosurg Psychiatry* 74, 1206-1209.
- He, Z., and Bateman, A. (2003). Progranulin (granulin-epithelin precursor, PC-cell-derived growth factor, acrogranin) mediates tissue repair and tumorigenesis. *Journal of molecular medicine* 81, 600-612.
- Hensley, K., Venkova, K., Christov, A., Gunning, W., and Park, J. (2011). Collapsin response mediator protein-2: an emerging pathologic feature and therapeutic target for neurodegenerative disease indications. *Molecular neurobiology* 43, 180-191.
- Hering, H., and Sheng, M. (2001). Dendritic spines: structure, dynamics and regulation. *Nat Rev Neurosci* 2, 880-888.
- Hinckelmann, M.V., Zala, D., and Saudou, F. (2013). Releasing the brake: restoring fast axonal transport in neurodegenerative disorders. *Trends Cell Biol* 23, 634-643.
- Hirokawa, N., Niwa, S., and Tanaka, Y. (2010). Molecular motors in neurons: transport mechanisms and roles in brain function, development, and disease. *Neuron* 68, 610-638.
- Hirokawa, N., and Takemura, R. (2005). Molecular motors and mechanisms of directional transport in neurons. *Nat Rev Neurosci* 6, 201-214.
- Hoogenraad, C.C., and Bradke, F. (2009). Control of neuronal polarity and plasticity--a renaissance for microtubules? *Trends Cell Biol* 19, 669-676.
- Hoogenraad, C.C., Milstein, A.D., Ethell, I.M., Henkemeyer, M., and Sheng, M. (2005). GRIP1 controls dendrite morphogenesis by regulating EphB receptor trafficking. *Nat Neurosci* 8, 906-915.
- Horton, A.C., Racz, B., Monson, E.E., Lin, A.L., Weinberg, R.J., and Ehlers, M.D. (2005). Polarized secretory trafficking directs cargo for asymmetric dendrite growth and morphogenesis. *Neuron* 48, 757-771.
- Hu, F., Padukkavidana, T., Vaegter, C.B., Brady, O.A., Zheng, Y., Mackenzie, I.R., Feldman, H.H., Nykjaer, A., and Strittmatter, S.M. (2010). Sortilin-mediated endocytosis determines levels of the frontotemporal dementia protein, progranulin. *Neuron* 68, 654-667.
- Hu, X., Viesselmann, C., Nam, S., Merriam, E., and Dent, E.W. (2008). Activity-dependent dynamic microtubule invasion of dendritic spines. *The Journal of neuroscience : the official journal of the Society for Neuroscience* 28, 13094-13105.
- Hutton, M., Lendon, C.L., Rizzu, P., Baker, M., Froelich, S., Houlden, H., Pickering-Brown, S., Chakraverty, S., Isaacs, A., Grover, A., *et al.* (1998). Association of missense and 5'-splice-site mutations in tau with the inherited dementia FTDP-17. *Nature* 393, 702-705.

- Huynh, C., Roth, D., Ward, D.M., Kaplan, J., and Andrews, N.W. (2004). Defective lysosomal exocytosis and plasma membrane repair in Chediak-Higashi/beige cells. *Proc Natl Acad Sci U S A* *101*, 16795-16800.
- Ichihara, M., Murakumo, Y., Masuda, A., Matsuura, T., Asai, N., Jijiwa, M., Ishida, M., Shinmi, J., Yatsuya, H., Qiao, S., *et al.* (2007). Thermodynamic instability of siRNA duplex is a prerequisite for dependable prediction of siRNA activities. *Nucleic Acids Res* *35*, e123.
- Igaz, L.M., Kwong, L.K., Lee, E.B., Chen-Plotkin, A., Swanson, E., Unger, T., Malunda, J., Xu, Y., Winton, M.J., Trojanowski, J.Q., *et al.* (2011). Dysregulation of the ALS-associated gene TDP-43 leads to neuronal death and degeneration in mice. *J Clin Invest* *121*, 726-738.
- Ishigaki, S., Masuda, A., Fujioka, Y., Iguchi, Y., Katsuno, M., Shibata, A., Urano, F., Sobue, G., and Ohno, K. (2012). Position-dependent FUS-RNA interactions regulate alternative splicing events and transcriptions. *Scientific reports* *2*, 529.
- Ittner, L.M., Ke, Y.D., Delerue, F., Bi, M., Gladbach, A., van Eersel, J., Wolfing, H., Chieng, B.C., Christie, M.J., Napier, I.A., *et al.* (2010). Dendritic function of tau mediates amyloid-beta toxicity in Alzheimer's disease mouse models. *Cell* *142*, 387-397.
- Jan, Y.N., and Jan, L.Y. (2010). Branching out: mechanisms of dendritic arborization. *Nat Rev Neurosci* *11*, 316-328.
- Jaworski, J., Kapitein, L.C., Gouveia, S.M., Dortland, B.R., Wulf, P.S., Grigoriev, I., Camera, P., Spangler, S.A., Di Stefano, P., Demmers, J., *et al.* (2009). Dynamic microtubules regulate dendritic spine morphology and synaptic plasticity. *Neuron* *61*, 85-100.
- Joachim, C.L., Morris, J.H., Kosik, K.S., and Selkoe, D.J. (1987). Tau antisera recognize neurofibrillary tangles in a range of neurodegenerative disorders. *Ann Neurol* *22*, 514-520.
- Johnson, B.S., Snead, D., Lee, J.J., McCaffery, J.M., Shorter, J., and Gitler, A.D. (2009). TDP-43 is intrinsically aggregation-prone, and amyotrophic lateral sclerosis-linked mutations accelerate aggregation and increase toxicity. *The Journal of biological chemistry* *284*, 20329-20339.
- Johnson, J.K., Diehl, J., Mendez, M.F., Neuhaus, J., Shapira, J.S., Forman, M., Chute, D.J., Roberson, E.D., Pace-Savitsky, C., Neumann, M., *et al.* (2005). Frontotemporal lobar degeneration: demographic characteristics of 353 patients. *Archives of neurology* *62*, 925-930.
- Jolly, A.L., and Gelfand, V.I. (2011). Bidirectional intracellular transport: utility and mechanism. *Biochemical Society transactions* *39*, 1126-1130.
- Jordan, M.A., and Wilson, L. (2004). Microtubules as a target for anticancer drugs. *Nat Rev Cancer* *4*, 253-265.
- Jordens, I., Fernandez-Borja, M., Marsman, M., Dusseljee, S., Janssen, L., Calafat, J., Janssen, H., Wubbolts, R., and Neefjes, J. (2001). The Rab7 effector protein RILP controls lysosomal transport by inducing the recruitment of dynein-dynactin motors. *Curr Biol* *11*, 1680-1685.

- Josephs, K.A., Hodges, J.R., Snowden, J.S., Mackenzie, I.R., Neumann, M., Mann, D.M., and Dickson, D.W. (2011). Neuropathological background of phenotypical variability in frontotemporal dementia. *Acta neuropathologica* *122*, 137-153.
- Kang, J.S., Tian, J.H., Pan, P.Y., Zald, P., Li, C., Deng, C., and Sheng, Z.H. (2008). Docking of axonal mitochondria by syntaphilin controls their mobility and affects short-term facilitation. *Cell* *132*, 137-148.
- Kapitein, L.C., and Hoogenraad, C.C. (2011). Which way to go? Cytoskeletal organization and polarized transport in neurons. *Mol Cell Neurosci* *46*, 9-20.
- Kapitein, L.C., Schlager, M.A., Kuijpers, M., Wulf, P.S., van Spronsen, M., MacKintosh, F.C., and Hoogenraad, C.C. (2010). Mixed microtubules steer dynein-driven cargo transport into dendrites. *Curr Biol* *20*, 290-299.
- Kaushik, S., and Cuervo, A.M. (2012). Chaperone-mediated autophagy: a unique way to enter the lysosome world. *Trends Cell Biol* *22*, 407-417.
- Kayasuga, Y., Chiba, S., Suzuki, M., Kikusui, T., Matsuwaki, T., Yamanouchi, K., Kotaki, H., Horai, R., Iwakura, Y., and Nishihara, M. (2007). Alteration of behavioural phenotype in mice by targeted disruption of the progranulin gene. *Behav Brain Res* *185*, 110-118.
- Kneussel, M., and Wagner, W. (2013). Myosin motors at neuronal synapses: drivers of membrane transport and actin dynamics. *Nat Rev Neurosci* *14*, 233-247.
- Koleske, A.J. (2013). Molecular mechanisms of dendrite stability. *Nat Rev Neurosci* *14*, 536-550.
- Kopito, R.R. (2000). Aggresomes, inclusion bodies and protein aggregation. *Trends Cell Biol* *10*, 524-530.
- Kornfeld, S., and Mellman, I. (1989). The biogenesis of lysosomes. *Annual review of cell biology* *5*, 483-525.
- Ku, C.S., Loy, E.Y., Pawitan, Y., and Chia, K.S. (2010). The pursuit of genome-wide association studies: where are we now? *Journal of human genetics* *55*, 195-206.
- Kuhn, P.H., Wang, H., Dislich, B., Colombo, A., Zeitschel, U., Ellwart, J.W., Kremmer, E., Rossner, S., and Lichtenthaler, S.F. (2010). ADAM10 is the physiologically relevant, constitutive alpha-secretase of the amyloid precursor protein in primary neurons. *Embo J* *29*, 3020-3032.
- Kuijpers, M., Yu, K.L., Teuling, E., Akhmanova, A., Jaarsma, D., and Hoogenraad, C.C. (2013). The ALS8 protein VAPB interacts with the ER-Golgi recycling protein YIF1A and regulates membrane delivery into dendrites. *Embo J* *32*, 2056-2072.

- Kwiatkowski, T.J., Jr., Bosco, D.A., Leclerc, A.L., Tamrazian, E., Vanderburg, C.R., Russ, C., Davis, A., Gilchrist, J., Kasarskis, E.J., Munsat, T., *et al.* (2009). Mutations in the FUS/TLS gene on chromosome 16 cause familial amyotrophic lateral sclerosis. *Science* 323, 1205-1208.
- Kwinter, D.M., Lo, K., Mafi, P., and Silverman, M.A. (2009). Dynactin regulates bidirectional transport of dense-core vesicles in the axon and dendrites of cultured hippocampal neurons. *Neuroscience* 162, 1001-1010.
- Lagier-Tourenne, C., Polymenidou, M., Hutt, K.R., Vu, A.Q., Baughn, M., Huelga, S.C., Clutario, K.M., Ling, S.C., Liang, T.Y., Mazur, C., *et al.* (2012). Divergent roles of ALS-linked proteins FUS/TLS and TDP-43 intersect in processing long pre-mRNAs. *Nat Neurosci* 15, 1488-1497.
- Lamb, C.A., Yoshimori, T., and Tooze, S.A. (2013). The autophagosome: origins unknown, biogenesis complex. *Nat Rev Mol Cell Biol* 14, 759-774.
- Lamprecht, R., and LeDoux, J. (2004). Structural plasticity and memory. *Nat Rev Neurosci* 5, 45-54.
- Lang, C.M., Fellerer, K., Schwenk, B.M., Kuhn, P.H., Kremmer, E., Edbauer, D., Capell, A., and Haass, C. (2012). Membrane orientation and subcellular localization of transmembrane protein 106B (TMEM106B), a major risk factor for frontotemporal lobar degeneration. *The Journal of biological chemistry* 287, 19355-19365.
- Laplante, M., and Sabatini, D.M. (2012). mTOR signaling in growth control and disease. *Cell* 149, 274-293.
- Letournel, F., Bocquet, A., Dubas, F., Barthelaix, A., and Eyer, J. (2003). Stable tubule only polypeptides (STOP) proteins co-aggregate with spheroid neurofilaments in amyotrophic lateral sclerosis. *J Neuropathol Exp Neurol* 62, 1211-1219.
- Ling, S.C., Polymenidou, M., and Cleveland, D.W. (2013). Converging mechanisms in ALS and FTD: disrupted RNA and protein homeostasis. *Neuron* 79, 416-438.
- Liu-Yesucevitz, L., Bilgutay, A., Zhang, Y.J., Vanderweyde, T., Citro, A., Mehta, T., Zaarur, N., McKee, A., Bowser, R., Sherman, M., *et al.* (2010). Tar DNA binding protein-43 (TDP-43) associates with stress granules: analysis of cultured cells and pathological brain tissue. *PLoS ONE* 5, e13250.
- Lu, R.C., Wang, H., Tan, M.S., Yu, J.T., and Tan, L. (2013). TMEM106B and APOE polymorphisms interact to confer risk for late-onset Alzheimer's disease in Han Chinese. *Journal of neural transmission*.
- Luebke, J.I., Weaver, C.M., Rocher, A.B., Rodriguez, A., Crimins, J.L., Dickstein, D.L., Wearne, S.L., and Hof, P.R. (2010). Dendritic vulnerability in neurodegenerative disease: insights from analyses of cortical pyramidal neurons in transgenic mouse models. *Brain structure & function* 214, 181-199.

Mackenzie, I.R., Neumann, M., Bigio, E.H., Cairns, N.J., Alafuzoff, I., Kril, J., Kovacs, G.G., Ghetti, B., Halliday, G., Holm, I.E., *et al.* (2010). Nomenclature and nosology for neuropathologic subtypes of frontotemporal lobar degeneration: an update. *Acta neuropathologica* 119, 1-4.

Maggo, S.D., Kennedy, M.A., and Clark, D.W. (2011). Clinical implications of pharmacogenetic variation on the effects of statins. *Drug safety : an international journal of medical toxicology and drug experience* 34, 1-19.

Mandell, J.W., and Banker, G.A. (1996). A spatial gradient of tau protein phosphorylation in nascent axons. *The Journal of neuroscience : the official journal of the Society for Neuroscience* 16, 5727-5740.

Manolio, T.A. (2010). Genomewide association studies and assessment of the risk of disease. *N Engl J Med* 363, 166-176.

Manoochehri, M., and Huey, E.D. (2012). Diagnosis and management of behavioral issues in frontotemporal dementia. *Current neurology and neuroscience reports* 12, 528-536.

Martinez-Arca, S., Alberts, P., Zahraoui, A., Louvard, D., and Galli, T. (2000). Role of tetanus neurotoxin insensitive vesicle-associated membrane protein (TI-VAMP) in vesicular transport mediating neurite outgrowth. *J Cell Biol* 149, 889-900.

Masliah, E., Mallory, M., Alford, M., DeTeresa, R., Hansen, L.A., McKeel, D.W., Jr., and

Morris, J.C. (2001). Altered expression of synaptic proteins occurs early during progression of Alzheimer's disease. *Neurology* 56, 127-129.

McGinnis, S.M. (2012). Neuroimaging in neurodegenerative dementias. *Seminars in neurology* 32, 347-360.

Meixner, A., Haverkamp, S., Wassle, H., Fuhrer, S., Thalhammer, J., Kropf, N., Bittner, R.E., Lassmann, H., Wiche, G., and Propst, F. (2000). MAP1B is required for axon guidance and is involved in the development of the central and peripheral nervous system. *J Cell Biol* 151, 1169-1178.

Mendez, M.F. (2009). Frontotemporal dementia: therapeutic interventions. *Frontiers of neurology and neuroscience* 24, 168-178.

Mijaljica, D., Prescott, M., and Devenish, R.J. (2011). Microautophagy in mammalian cells: revisiting a 40-year-old conundrum. *Autophagy* 7, 673-682.

Millecamps, S., and Julien, J.P. (2013). Axonal transport deficits and neurodegenerative diseases. *Nat Rev Neurosci* 14, 161-176.

Mindell, J.A. (2012). Lysosomal acidification mechanisms. *Annual review of physiology* 74, 69-86.

- Momeni, P., Bell, J., Duckworth, J., Hutton, M., Mann, D., Brown, S.P., and Hardy, J. (2006a). Sequence analysis of all identified open reading frames on the frontal temporal dementia haplotype on chromosome 3 fails to identify unique coding variants except in CHMP2B. *Neurosci Lett* 410, 77-79.
- Momeni, P., Rogaeva, E., Van Deerlin, V., Yuan, W., Grafman, J., Tierney, M., Huey, E., Bell, J., Morris, C.M., Kalaria, R.N., *et al.* (2006b). Genetic variability in CHMP2B and frontotemporal dementia. *Neuro-degenerative diseases* 3, 129-133.
- Morderer, D., Nikolaienko, O., Skrypkina, I., Cherkas, V., Tsyba, L., Belan, P., and Rynditch, A. (2012). Endocytic adaptor protein intersectin 1 forms a complex with microtubule stabilizer STOP in neurons. *Gene* 505, 360-364.
- Mori, K., Arzberger, T., Grasser, F.A., Gijssels, I., May, S., Rentzsch, K., Weng, S.M., Schludi, M.H., van der Zee, J., Cruets, M., *et al.* (2013a). Bidirectional transcripts of the expanded C9orf72 hexanucleotide repeat are translated into aggregating dipeptide repeat proteins. *Acta neuropathologica* 126, 881-893.
- Mori, K., Lammich, S., Mackenzie, I.R., Forne, I., Zilow, S., Kretschmar, H., Edbauer, D., Janssens, J., Kleinberger, G., Cruets, M., *et al.* (2013b). hnRNP A3 binds to GGGGCC repeats and is a constituent of p62-positive/TDP43-negative inclusions in the hippocampus of patients with C9orf72 mutations. *Acta neuropathologica*.
- Mori, K., Weng, S.M., Arzberger, T., May, S., Rentzsch, K., Kremmer, E., Schmid, B., Kretschmar, H.A., Cruets, M., Van Broeckhoven, C., *et al.* (2013c). The C9orf72 GGGGCC Repeat Is Translated into Aggregating Dipeptide-Repeat Proteins in FTL/ALS. *Science*.
- Morris, H.R., Waite, A.J., Williams, N.M., Neal, J.W., and Blake, D.J. (2012). Recent advances in the genetics of the ALS-FTLD complex. *Current neurology and neuroscience reports* 12, 243-250.
- Morris, M., Maeda, S., Vossel, K., and Mucke, L. (2011). The many faces of tau. *Neuron* 70, 410-426.
- Mukhopadhyay, A., Funato, K., and Stahl, P.D. (1997). Rab7 regulates transport from early to late endocytic compartments in *Xenopus* oocytes. *The Journal of biological chemistry* 272, 13055-13059.
- Muller, M.J., Klumpp, S., and Lipowsky, R. (2008). Tug-of-war as a cooperative mechanism for bidirectional cargo transport by molecular motors. *Proc Natl Acad Sci U S A* 105, 4609-4614.
- Munoz, D.G., Neumann, M., Kusaka, H., Yokota, O., Ishihara, K., Terada, S., Kuroda, S., and Mackenzie, I.R. (2009). FUS pathology in basophilic inclusion body disease. *Acta neuropathologica* 118, 617-627.

Neary, D., Snowden, J.S., Gustafson, L., Passant, U., Stuss, D., Black, S., Freedman, M., Kertesz, A., Robert, P.H., Albert, M., *et al.* (1998). Frontotemporal lobar degeneration: a consensus on clinical diagnostic criteria. *Neurology* *51*, 1546-1554.

Neukirchen, D., and Bradke, F. (2011). Neuronal polarization and the cytoskeleton. *Seminars in cell & developmental biology* *22*, 825-833.

Neumann, M., Bentmann, E., Dormann, D., Jawaid, A., DeJesus-Hernandez, M., Ansorge, O., Roeber, S., Kretzschmar, H.A., Munoz, D.G., Kusaka, H., *et al.* (2011). FET proteins TAF15 and EWS are selective markers that distinguish FTLD with FUS pathology from amyotrophic lateral sclerosis with FUS mutations. *Brain : a journal of neurology* *134*, 2595-2609.

Neumann, M., Rademakers, R., Roeber, S., Baker, M., Kretzschmar, H.A., and Mackenzie, I.R. (2009). A new subtype of frontotemporal lobar degeneration with FUS pathology. *Brain : a journal of neurology* *132*, 2922-2931.

Neumann, M., Sampathu, D.M., Kwong, L.K., Truax, A.C., Micsenyi, M.C., Chou, T.T., Bruce, J., Schuck, T., Grossman, M., Clark, C.M., *et al.* (2006). Ubiquitinated TDP-43 in frontotemporal lobar degeneration and amyotrophic lateral sclerosis. *Science* *314*, 130-133.

Nicholson, A.M., Finch, N.A., Wojtas, A., Baker, M.C., Perkerson, R.B., 3rd, Castanedes-Casey, M., Rousseau, L., Benussi, L., Binetti, G., Ghidoni, R., *et al.* (2013). TMEM106B p.T185S regulates TMEM106B protein levels: implications for frontotemporal dementia. *Journal of neurochemistry* *126*, 781-791.

Nicholson, A.M., Gass, J., Petrucelli, L., and Rademakers, R. (2012). Progranulin axis and recent developments in frontotemporal lobar degeneration. *Alzheimers Res Ther* *4*, 4.

Nishimura, A.L., Mitne-Neto, M., Silva, H.C., Richieri-Costa, A., Middleton, S., Cascio, D., Kok, F., Oliveira, J.R., Gillingwater, T., Webb, J., *et al.* (2004). A mutation in the vesicle-trafficking protein VAPB causes late-onset spinal muscular atrophy and amyotrophic lateral sclerosis. *Am J Hum Genet* *75*, 822-831.

Nixon, R.A. (2013). The role of autophagy in neurodegenerative disease. *Nat Med* *19*, 983-997.

Ohya, T., Miaczynska, M., Coskun, U., Lommer, B., Runge, A., Drechsel, D., Kalaidzidis, Y., and Zerial, M. (2009). Reconstitution of Rab- and SNARE-dependent membrane fusion by synthetic endosomes. *Nature* *459*, 1091-1097.

Orozco, D., Tahirovic, S., Rentzsch, K., Schwenk, B.M., Haass, C., and Edbauer, D. (2012). Loss of fused in sarcoma (FUS) promotes pathological Tau splicing. *EMBO Rep* *13*, 759-764.

Pan, X.D., and Chen, X.C. (2013). Clinic, neuropathology and molecular genetics of frontotemporal dementia: a mini-review. *Translational neurodegeneration* *2*, 8.

Pesiridis, G.S., Lee, V.M., and Trojanowski, J.Q. (2009). Mutations in TDP-43 link glycine-rich domain functions to amyotrophic lateral sclerosis. *Human molecular genetics* *18*, R156-162.

- Petkau, T.L., Neal, S.J., Milnerwood, A., Mew, A., Hill, A.M., Orban, P., Gregg, J., Lu, G., Feldman, H.H., Mackenzie, I.R., *et al.* (2012). Synaptic dysfunction in progranulin-deficient mice. *Neurobiol Dis* 45, 711-722.
- Pfeffer, S.R. (1994). Rab GTPases: master regulators of membrane trafficking. *Curr Opin Cell Biol* 6, 522-526.
- Pick, A. (1892). Über die beziehungen der senilen hirnatrophie zue aphasie. *Prager Medicinische Wochenschrift* 17, 165-167.
- Powell, K.J., Hori, S.E., Leslie, R., Andrieux, A., Schellinck, H., Thorne, M., and Robertson, G.S. (2007). Cognitive impairments in the STOP null mouse model of schizophrenia. *Behavioral neuroscience* 121, 826-835.
- Praprotnik, D., Smith, M.A., Richey, P.L., Vinters, H.V., and Perry, G. (1996). Filament heterogeneity within the dystrophic neurites of senile plaques suggests blockage of fast axonal transport in Alzheimer's disease. *Acta neuropathologica* 91, 226-235.
- Proudfoot, M., Gutowski, N.J., Edbauer, D., Hilton, D.A., Stephens, M., Rankin, J., and Mackenzie, I.R. (2014). Early dipeptide repeat pathology in a frontotemporal dementia kindred with C9ORF72 mutation and intellectual disability. *Acta neuropathologica* 127, 451-458.
- Rademakers, R., Cruts, M., and van Broeckhoven, C. (2004). The role of tau (MAPT) in frontotemporal dementia and related tauopathies. *Hum Mutat* 24, 277-295.
- Rademakers, R., Neumann, M., and Mackenzie, I.R. (2012). Advances in understanding the molecular basis of frontotemporal dementia. *Nature reviews Neurology* 8, 423-434.
- Rao, S.K., Huynh, C., Proux-Gillardeaux, V., Galli, T., and Andrews, N.W. (2004). Identification of SNAREs involved in synaptotagmin VII-regulated lysosomal exocytosis. *The Journal of biological chemistry* 279, 20471-20479.
- Rascovsky, K., Hodges, J.R., Knopman, D., Mendez, M.F., Kramer, J.H., Neuhaus, J., van Swieten, J.C., Seelaar, H., Dopper, E.G., Onyike, C.U., *et al.* (2011). Sensitivity of revised diagnostic criteria for the behavioural variant of frontotemporal dementia. *Brain : a journal of neurology* 134, 2456-2477.
- Ravikumar, B., Sarkar, S., Davies, J.E., Futter, M., Garcia-Arencibia, M., Green-Thompson, Z.W., Jimenez-Sanchez, M., Korolchuk, V.I., Lichtenberg, M., Luo, S., *et al.* (2010). Regulation of mammalian autophagy in physiology and pathophysiology. *Physiol Rev* 90, 1383-1435.
- Reddy, A., Caler, E.V., and Andrews, N.W. (2001). Plasma membrane repair is mediated by Ca(2+)-regulated exocytosis of lysosomes. *Cell* 106, 157-169.

- Renton, A.E., Majounie, E., Waite, A., Simon-Sanchez, J., Rollinson, S., Gibbs, J.R., Schymick, J.C., Laaksovirta, H., van Swieten, J.C., Myllykangas, L., *et al.* (2011). A hexanucleotide repeat expansion in C9ORF72 is the cause of chromosome 9p21-linked ALS-FTD. *Neuron* *72*, 257-268.
- Ringholz, G.M., Appel, S.H., Bradshaw, M., Cooke, N.A., Mosnik, D.M., and Schulz, P.E. (2005). Prevalence and patterns of cognitive impairment in sporadic ALS. *Neurology* *65*, 586-590.
- Rodriguez, A., Webster, P., Ortego, J., and Andrews, N.W. (1997). Lysosomes behave as Ca²⁺-regulated exocytic vesicles in fibroblasts and epithelial cells. *J Cell Biol* *137*, 93-104.
- Rogelj, B., Easton, L.E., Bogu, G.K., Stanton, L.W., Rot, G., Curk, T., Zupan, B., Sugimoto, Y., Modic, M., Haberman, N., *et al.* (2012). Widespread binding of FUS along nascent RNA regulates alternative splicing in the brain. *Scientific reports* *2*, 603.
- Rollinson, S., Mead, S., Snowden, J., Richardson, A., Rohrer, J., Halliwell, N., Usher, S., Neary, D., Mann, D., Hardy, J., *et al.* (2011). Frontotemporal lobar degeneration genome wide association study replication confirms a risk locus shared with amyotrophic lateral sclerosis. *Neurobiol Aging* *32*, 758 e751-757.
- Rutherford, N.J., Carrasquillo, M.M., Li, M., Bisceglia, G., Menke, J., Josephs, K.A., Parisi, J.E., Petersen, R.C., Graff-Radford, N.R., Younkin, S.G., *et al.* (2012). TMEM106B risk variant is implicated in the pathologic presentation of Alzheimer disease. *Neurology* *79*, 717-718.
- Saftig, P., and Klumperman, J. (2009). Lysosome biogenesis and lysosomal membrane proteins: trafficking meets function. *Nat Rev Mol Cell Biol* *10*, 623-635.
- Sahenk, Z., and Brady, S.T. (1987). Axonal tubulin and microtubules: morphologic evidence for stable regions on axonal microtubules. *Cell Motil Cytoskeleton* *8*, 155-164.
- Salmon, P., and Trono, D. (2007). Production and titration of lentiviral vectors. *Current protocols in human genetics / editorial board, Jonathan L Haines [et al]* *Chapter 12*, Unit 12 10.
- Samson, F., Donoso, J.A., Heller-Bettinger, I., Watson, D., and Himes, R.H. (1979). Nocodazole action on tubulin assembly, axonal ultrastructure and fast axoplasmic transport. *The Journal of pharmacology and experimental therapeutics* *208*, 411-417.
- Sancak, Y., Bar-Peled, L., Zoncu, R., Markhard, A.L., Nada, S., and Sabatini, D.M. (2010). Regulator-Rag complex targets mTORC1 to the lysosomal surface and is necessary for its activation by amino acids. *Cell* *141*, 290-303.
- Sann, S., Wang, Z., Brown, H., and Jin, Y. (2009). Roles of endosomal trafficking in neurite outgrowth and guidance. *Trends Cell Biol* *19*, 317-324.
- Sardiello, M., Palmieri, M., di Ronza, A., Medina, D.L., Valenza, M., Gennarino, V.A., Di Malta, C., Donaudy, F., Embrione, V., Polishchuk, R.S., *et al.* (2009). A gene network regulating lysosomal biogenesis and function. *Science* *325*, 473-477.

- Schlager, M.A., and Hoogenraad, C.C. (2009). Basic mechanisms for recognition and transport of synaptic cargos. *Molecular brain* 2, 25.
- Schwartz, S.L., Cao, C., Pylypenko, O., Rak, A., and Wandinger-Ness, A. (2007). Rab GTPases at a glance. *J Cell Sci* 120, 3905-3910.
- Schwenk, B.M., Lang, C.M., Hogg, S., Tahirovic, S., Orozco, D., Rentzsch, K., Lichtenthaler, S.F., Hoogenraad, C.C., Capell, A., Haass, C., *et al.* (2014). The FTL risk factor TMEM106B and MAP6 control dendritic trafficking of lysosomes. *Embo J*.
- Setou, M., Seog, D.H., Tanaka, Y., Kanai, Y., Takei, Y., Kawagishi, M., and Hirokawa, N. (2002). Glutamate-receptor-interacting protein GRIP1 directly steers kinesin to dendrites. *Nature* 417, 83-87.
- Settembre, C., Di Malta, C., Polito, V.A., Garcia Arencibia, M., Vetrini, F., Erdin, S., Erdin, S.U., Huynh, T., Medina, D., Colella, P., *et al.* (2011). TFEB links autophagy to lysosomal biogenesis. *Science* 332, 1429-1433.
- Shahani, N., Subramaniam, S., Wolf, T., Tackenberg, C., and Brandt, R. (2006). Tau aggregation and progressive neuronal degeneration in the absence of changes in spine density and morphology after targeted expression of Alzheimer's disease-relevant tau constructs in organotypic hippocampal slices. *The Journal of neuroscience : the official journal of the Society for Neuroscience* 26, 6103-6114.
- Shevchenko, A., Tomas, H., Havlis, J., Olsen, J.V., and Mann, M. (2006). In-gel digestion for mass spectrometric characterization of proteins and proteomes. *Nat Protoc* 1, 2856-2860.
- Sholl, D.A. (1953). Dendritic organization in the neurons of the visual and motor cortices of the cat. *J Anat* 87, 387-406.
- Sieben, A., Van Langenhove, T., Engelborghs, S., Martin, J.J., Boon, P., Cras, P., De Deyn, P.P., Santens, P., Van Broeckhoven, C., and Cruts, M. (2012). The genetics and neuropathology of frontotemporal lobar degeneration. *Acta neuropathologica* 124, 353-372.
- Slaughter, T., and Black, M.M. (2003). STOP (stable-tubule-only-polypeptide) is preferentially associated with the stable domain of axonal microtubules. *Journal of neurocytology* 32, 399-413.
- Sleegers, K., Cruts, M., and Van Broeckhoven, C. (2010). Molecular pathways of frontotemporal lobar degeneration. *Annu Rev Neurosci* 33, 71-88.
- Smith, K.R., Damiano, J., Franceschetti, S., Carpenter, S., Canafoglia, L., Morbin, M., Rossi, G., Pareyson, D., Mole, S.E., Staropoli, J.F., *et al.* (2012). Strikingly different clinicopathological phenotypes determined by progranulin-mutation dosage. *Am J Hum Genet* 90, 1102-1107.
- Snider, W.D. (1988). Nerve growth factor enhances dendritic arborization of sympathetic ganglion cells in developing mammals. *The Journal of neuroscience : the official journal of the Society for Neuroscience* 8, 2628-2634.

- Song, A.H., Wang, D., Chen, G., Li, Y., Luo, J., Duan, S., and Poo, M.M. (2009). A selective filter for cytoplasmic transport at the axon initial segment. *Cell* *136*, 1148-1160.
- Song, Y., Kirkpatrick, L.L., Schilling, A.B., Helseth, D.L., Chabot, N., Keillor, J.W., Johnson, G.V., and Brady, S.T. (2013). Transglutaminase and polyamination of tubulin: posttranslational modification for stabilizing axonal microtubules. *Neuron* *78*, 109-123.
- Soppina, V., Rai, A.K., Ramaiya, A.J., Barak, P., and Mallik, R. (2009). Tug-of-war between dissimilar teams of microtubule motors regulates transport and fission of endosomes. *Proc Natl Acad Sci U S A* *106*, 19381-19386.
- Spinosa, M.R., Progida, C., De Luca, A., Colucci, A.M., Alifano, P., and Bucci, C. (2008). Functional characterization of Rab7 mutant proteins associated with Charcot-Marie-Tooth type 2B disease. *The Journal of neuroscience : the official journal of the Society for Neuroscience* *28*, 1640-1648.
- Spires-Jones, T., and Knafo, S. (2012). Spines, plasticity, and cognition in Alzheimer's model mice. *Neural plasticity* *2012*, 319836.
- Stenmark, H. (2009). Rab GTPases as coordinators of vesicle traffic. *Nat Rev Mol Cell Biol* *10*, 513-525.
- Strong, M.J., Grace, G.M., Freedman, M., Lomen-Hoerth, C., Woolley, S., Goldstein, L.H., Murphy, J., Shoesmith, C., Rosenfeld, J., Leigh, P.N., *et al.* (2009). Consensus criteria for the diagnosis of frontotemporal cognitive and behavioural syndromes in amyotrophic lateral sclerosis. *Amyotroph Lateral Scler* *10*, 131-146.
- Sun, Z., Diaz, Z., Fang, X., Hart, M.P., Chesi, A., Shorter, J., and Gitler, A.D. (2011). Molecular determinants and genetic modifiers of aggregation and toxicity for the ALS disease protein FUS/TLS. *PLoS Biol* *9*, e1000614.
- Synofzik, M., Maetzler, W., Grehl, T., Prudlo, J., Vom Hagen, J.M., Haack, T., Rebassoo, P., Munz, M., Schols, L., and Biskup, S. (2012). Screening in ALS and FTD patients reveals 3 novel UBQLN2 mutations outside the PXX domain and a pure FTD phenotype. *Neurobiol Aging* *33*, 2949 e2913-2947.
- Tai, A.W., Chuang, J.Z., Bode, C., Wolfrum, U., and Sung, C.H. (1999). Rhodopsin's carboxy-terminal cytoplasmic tail acts as a membrane receptor for cytoplasmic dynein by binding to the dynein light chain Tctex-1. *Cell* *97*, 877-887.
- Tamaoka, A., Arai, M., Itokawa, M., Arai, T., Hasegawa, M., Tsuchiya, K., Takuma, H., Tsuji, H., Ishii, A., Watanabe, M., *et al.* (2010). TDP-43 M337V mutation in familial amyotrophic lateral sclerosis in Japan. *Internal medicine* *49*, 331-334.
- Tang, W., Lu, Y., Tian, Q.Y., Zhang, Y., Guo, F.J., Liu, G.Y., Syed, N.M., Lai, Y., Lin, E.A., Kong, L., *et al.* (2011). The growth factor progranulin binds to TNF receptors and is therapeutic against inflammatory arthritis in mice. *Science* *332*, 478-484.

- Trojanowski, J.Q., Duff, K., Fillit, H., Koroshetz, W., Kuret, J., Murphy, D., Refolo, L., and Frontotemporal Dementia Working Group on, F.T.D.D.D. (2008). New directions for frontotemporal dementia drug discovery. *Alzheimer's & dementia : the journal of the Alzheimer's Association* 4, 89-93.
- Tsyba, L., Nikolaienko, O., Dergai, O., Dergai, M., Novokhatska, O., Skrypkina, I., and Rynditch, A. (2011). Intersectin multidomain adaptor proteins: regulation of functional diversity. *Gene* 473, 67-75.
- Tuxworth, R.I., Vivancos, V., O'Hare, M.B., and Tear, G. (2009). Interactions between the juvenile Batten disease gene, CLN3, and the Notch and JNK signalling pathways. *Human molecular genetics* 18, 667-678.
- Untergasser, A., Nijveen, H., Rao, X., Bisseling, T., Geurts, R., and Leunissen, J.A. (2007). Primer3Plus, an enhanced web interface to Primer3. *Nucleic Acids Res* 35, W71-74.
- Uusi-Rauva, K., Kyttala, A., van der Kant, R., Vesa, J., Tanhuanpaa, K., Neefjes, J., Olkkonen, V.M., and Jalanko, A. (2012). Neuronal ceroid lipofuscinosis protein CLN3 interacts with motor proteins and modifies location of late endosomal compartments. *Cell Mol Life Sci* 69, 2075-2089.
- Vallee, R.B., Williams, J.C., Varma, D., and Barnhart, L.E. (2004). Dynein: An ancient motor protein involved in multiple modes of transport. *J Neurobiol* 58, 189-200.
- van Blitterswijk, M., Mullen, B., Nicholson, A.M., Bieniek, K.F., Heckman, M.G., Baker, M.C., Dejesus-Hernandez, M., Finch, N.A., Brown, P.H., Murray, M.E., *et al.* (2014). TMEM106B protects C9ORF72 expansion carriers against frontotemporal dementia. *Acta neuropathologica*.
- Van Damme, P., Van Hoecke, A., Lambrechts, D., Vanacker, P., Bogaert, E., van Swieten, J., Carmeliet, P., Van Den Bosch, L., and Robberecht, W. (2008). Progranulin functions as a neurotrophic factor to regulate neurite outgrowth and enhance neuronal survival. *J Cell Biol* 181, 37-41.
- Van Deerlin, V.M., Sleiman, P.M., Martinez-Lage, M., Chen-Plotkin, A., Wang, L.S., Graff-Radford, N.R., Dickson, D.W., Rademakers, R., Boeve, B.F., Grossman, M., *et al.* (2010). Common variants at 7p21 are associated with frontotemporal lobar degeneration with TDP-43 inclusions. *Nat Genet* 42, 234-239.
- van der Zee, J., Van Langenhove, T., Kleinberger, G., Slegers, K., Engelborghs, S., Vandenberghe, R., Santens, P., Van den Broeck, M., Joris, G., Brys, J., *et al.* (2011). TMEM106B is associated with frontotemporal lobar degeneration in a clinically diagnosed patient cohort. *Brain : a journal of neurology* 134, 808-815.
- Van Langenhove, T., van der Zee, J., and Van Broeckhoven, C. (2012). The molecular basis of the frontotemporal lobar degeneration-amyotrophic lateral sclerosis spectrum. *Ann Med* 44, 817-828.

- van Spronsen, M., Mikhaylova, M., Lipka, J., Schlager, M.A., van den Heuvel, D.J., Kuijpers, M., Wulf, P.S., Keijzer, N., Demmers, J., Kapitein, L.C., *et al.* (2013). TRAK/Milton motor-adaptor proteins steer mitochondrial trafficking to axons and dendrites. *Neuron* 77, 485-502.
- Vance, C., Rogelj, B., Hortobagyi, T., De Vos, K.J., Nishimura, A.L., Sreedharan, J., Hu, X., Smith, B., Ruddy, D., Wright, P., *et al.* (2009). Mutations in FUS, an RNA processing protein, cause familial amyotrophic lateral sclerosis type 6. *Science* 323, 1208-1211.
- Vass, R., Ashbridge, E., Geser, F., Hu, W.T., Grossman, M., Clay-Falcone, D., Elman, L., McCluskey, L., Lee, V.M., Van Deerlin, V.M., *et al.* (2011). Risk genotypes at TMEM106B are associated with cognitive impairment in amyotrophic lateral sclerosis. *Acta neuropathologica* 121, 373-380.
- Villaruel-Campos, D., Gastaldi, L., Conde, C., Caceres, A., and Gonzalez-Billault, C. (2014). Rab-mediated trafficking role in neurite formation. *Journal of neurochemistry* 129, 240-248.
- Vossel, K.A., and Miller, B.L. (2008). New approaches to the treatment of frontotemporal lobar degeneration. *Current opinion in neurology* 21, 708-716.
- Ward, M.E., and Miller, B.L. (2011). Potential mechanisms of progranulin-deficient FTL. *Journal of molecular neuroscience* : MN 45, 574-582.
- Watts, G.D., Wymer, J., Kovach, M.J., Mehta, S.G., Mumm, S., Darvish, D., Pestronk, A., Whyte, M.P., and Kimonis, V.E. (2004). Inclusion body myopathy associated with Paget disease of bone and frontotemporal dementia is caused by mutant valosin-containing protein. *Nat Genet* 36, 377-381.
- Westermann, S., and Weber, K. (2003). Post-translational modifications regulate microtubule function. *Nat Rev Mol Cell Biol* 4, 938-947.
- Wheaton, M.W., Salamone, A.R., Mosnik, D.M., McDonald, R.O., Appel, S.H., Schmolck, H.I., Ringholz, G.M., and Schulz, P.E. (2007). Cognitive impairment in familial ALS. *Neurology* 69, 1411-1417.
- Wils, H., Kleinberger, G., Pereson, S., Janssens, J., Capell, A., Van Dam, D., Cuijt, I., Joris, G., De Deyn, P.P., Haass, C., *et al.* (2012). Cellular ageing, increased mortality and FTL-TDP-associated neuropathology in progranulin knockout mice. *J Pathol* 228, 67-76.
- Ye, B., Zhang, Y., Song, W., Younger, S.H., Jan, L.Y., and Jan, Y.N. (2007). Growing dendrites and axons differ in their reliance on the secretory pathway. *Cell* 130, 717-729.
- Yin, F., Dumont, M., Banerjee, R., Ma, Y., Li, H., Lin, M.T., Beal, M.F., Nathan, C., Thomas, B., and Ding, A. (2010). Behavioral deficits and progressive neuropathology in progranulin-deficient mice: a mouse model of frontotemporal dementia. *Faseb J* 24, 4639-4647.
- Zhang, K., Fishel Ben Kenan, R., Osakada, Y., Xu, W., Sinit, R.S., Chen, L., Zhao, X., Chen, J.Y., Cui, B., and Wu, C. (2013). Defective axonal transport of Rab7 GTPase results in

dysregulated trophic signaling. *The Journal of neuroscience : the official journal of the Society for Neuroscience* *33*, 7451-7462.

Zhang, M., Chen, L., Wang, S., and Wang, T. (2009a). Rab7: roles in membrane trafficking and disease. *Bioscience reports* *29*, 193-209.

Zhang, Y.J., Xu, Y.F., Cook, C., Gendron, T.F., Roettges, P., Link, C.D., Lin, W.L., Tong, J., Castanedes-Casey, M., Ash, P., *et al.* (2009b). Aberrant cleavage of TDP-43 enhances aggregation and cellular toxicity. *Proc Natl Acad Sci U S A* *106*, 7607-7612.

Zhu, G.D., Salazar, G., Zlatic, S.A., Fiza, B., Doucette, M.M., Heilman, C.J., Levey, A.I., Faundez, V., and L'Hernault S, W. (2009). SPE-39 family proteins interact with the HOPS complex and function in lysosomal delivery. *Mol Biol Cell* *20*, 1223-1240.

Zhu, J., Nathan, C., Jin, W., Sim, D., Ashcroft, G.S., Wahl, S.M., Lacomis, L., Erdjument-Bromage, H., Tempst, P., Wright, C.D., *et al.* (2002). Conversion of proepithelin to epithelins: roles of SLPI and elastase in host defense and wound repair. *Cell* *111*, 867-878.

Zinchuk, V., and Grossenbacher-Zinchuk, O. (2011). Quantitative colocalization analysis of confocal fluorescence microscopy images. *Current protocols in cell biology / editorial board, Juan S Bonifacino [et al] Chapter 4, Unit4* 19.

Zu, T., Gibbens, B., Doty, N.S., Gomes-Pereira, M., Huguet, A., Stone, M.D., Margolis, J., Peterson, M., Markowski, T.W., Ingram, M.A., *et al.* (2011). Non-ATG-initiated translation directed by microsatellite expansions. *Proc Natl Acad Sci U S A* *108*, 260-265.

VII. Acknowledgements

DANKE...

...**Eddie** (Aka Prof. Dr. Dieter Edbauer) für deine Ideen, deinen Einsatz, dein Wissen, deine ständige Unterstützung, dafür dass du deine Feiertage für uns an der Bench verbringst wenn die Deadline näher rückt und dafür, dass ich dir drei Bierkästen Fangprämie wert war obwohl du mich nicht kanntest. Dafür dass du mehr als nur ein Chef bist.

...**Prof. Dr. Christian Haass** für Ihren wissenschaftlichen Input, dafür, dass sie als offizieller Doktorvater zur Verfügung stehen, uns nie das Gefühl gaben nicht zu Ihrer Gruppe zu gehören und Ihr stets offenes Ohr für die Anliegen der Doktoranden.

...Allen **Mitgliedern meiner Prüfungskommission** die zum Zeitpunkt des Drucks noch nicht feststanden.

...Meinen Labormitgliedern für die angenehme Stimmung, all den Spaß und die Unterstützung in den letzten vier Jahren und euren wissenschaftlichen Input: **Kristin Rentsch** für deine tollen Klonierungen und all die Platten die du für uns coatest! **Lorenz Dreßen** für die Midis. **Carina Lehmer**: Willkommen! **Martin Schludi** dafür, dass ich nicht mehr der einzige Mann und Chaot im Labor bin. Den Großvenediger schaffen wir schon noch! **Stephanie May** für deine gute Laune, deine Begeisterung für Fußball und deinen Einsatz für die Doktoranden! **Denise Orozco** für 4 gemeinsame Jahre mit Höhen und Tiefen in denen wir viel gelacht, gelitten und gelernt haben! Ich komm dich besuchen in deiner Villa am Strand, versprochen! *¡vive tu sueño!*

...Meinen ehemaligen Labormitglieder: **Dr. Julia Banzhaf-Strathmann** für wissenschaftliche Diskussionen und unsere 10 h morgens Kaffee-Pausen. **Dr. ShihMing (Jonas) Weng**, **Franziska Boneberg**, und **Claudia Lehrmer** für die gute Atmosphäre im Labor.

...Der TMEM106B-Gruppe **Christina Lang** und **Dr. Anja Capell** für eine harmonische Zusammenarbeit statt Konkurrenzdrucks. Meinen weiteren Kollaborationspartnern **Prof. Dr. Caspar Hoogenraad**, **Dr. Sabina Tahirovic**, **Stephanie Kunath**, **Andrea Wenninger-Weinzierl**, **Nagore Astola**, **Dr. Sebastian Hogl** und **Prof. Dr. Stefan Lichtenthaler** ohne die diese Arbeit nicht möglich gewesen wäre.

...**Daniel Fleck**, **Matthias Voss**, **Dr. Eva Bentmann**, **Caro Schweimer**, **Maria Sadic**, **Dr. Katrin Müller-Rischart** und **Dr. Anna Pils** für Kaffee, Kickern, Winnetou, den täglichen Irrsinn beim Mittagessen und ja sogar gelegentliche wissenschaftliche Diskussionen. Für die Tatsache dass aus Kollegen Freunde wurden

...Den **Fischmädel** und **Alex Hruscha** die uns im 7. Stock willkommen heißen haben und Freitag abends das „Besprechungszimmer“ zu einer der besten Locations der Stadt gemacht haben.

...**Dr. Anna Palsl** and **Dr. Katran Mallar-Raschart**, dass saa aanam anarfahranan Pharmazaatan daa Basacs galarnt haban und damat saana Bagaastarang far daa Labararbaat and dan Taschfassball gawackt haban.

...**Denise Orozco** und **Dr. Eva Bentmann** für das Korrekturlesen dieser Arbeit.

...**Dr. Ulf Dettmer** für die tolle Wohnung!

...Allen **Mitgliedern des Haass-Labs** für kritische Fragen, wissenschaftliche Diskussionen und die Hilfsbereitschaft. Besonders **Sabine Odoy** für ellenlange Primerbestellungen und dafür, dass der Laden läuft! Danke an die **Sekretärinnen**, v.a. **Irene Neumeier**, dafür das sie uns den administrativen „Kram“ vom Hals halten.

...**Sami** für deine unerschütterliche Zuversicht, viel Bier und viele gute Gespräche.

...Meinen Freunden (aka the Pharmadudes (und Mädels) und die Dachaurerer) **Christian, Raimund, Maren, Michael, Anja, Karl, Martin, Tom, Geoffrey** für eine tolle Zeit in München, viele lustige Abende, die Burns-Wochenenden, das Southside und dass ihr mich immer daran erinnert habt dass es noch so viel mehr gibt als die Arbeit!

...**Jocki, Feli und Tom**, auch wenn ich mal wieder 3 Monate nicht in Augsburg (oder im 3-Mühlenviertel) war und euch nicht gesehen habe, es ist jedes Mal als wär ich nur kurz vor der Tür gewesen. Danke für eure Freundschaft!

...**Meiner Familie** für die ständige Unterstützung, ohne die so vieles schwerer wäre! Dafür dass ihr mich meinen Weg gehen lassen habt, mich dazu gebracht habt auf eigen Füßen zu stehen und doch immer da seid wenn ich euch brauche!

...**C!!!**

Published online: December 19, 2013

Article



The FTLD risk factor TMEM106B and MAP6 control dendritic trafficking of lysosomes

Benjamin M. Schwenk¹, Christina M. Lang², Sebastian Hög¹, Sabina Tahirovic¹, Denise Orozco¹, Kristin Rentzsch¹, Stefan F. Lichtenthaler^{1,3,4}, Casper C. Hoogenraad⁵, Anja Capell², Christian Haass^{1,2,4} & Dieter Edbauer^{1,2,4,*}

Abstract

TMEM106B is a major risk factor for frontotemporal lobar degeneration with TDP-43 pathology. *TMEM106B* localizes to lysosomes, but its function remains unclear. We show that *TMEM106B* knockdown in primary neurons affects lysosomal trafficking and blunts dendritic arborization. We identify microtubule-associated protein 6 (MAP6) as novel interacting protein for *TMEM106B*. MAP6 overexpression inhibits dendritic branching similar to *TMEM106B* knockdown. MAP6 knockdown fully rescues the dendritic phenotype of *TMEM106B* knockdown, supporting a functional interaction between *TMEM106B* and MAP6. Live imaging reveals that *TMEM106B* knockdown and MAP6 overexpression strongly increase retrograde transport of lysosomes in dendrites. Downregulation of MAP6 in *TMEM106B* knockdown neurons restores the balance of anterograde and retrograde lysosomal transport and thereby prevents loss of dendrites. To strengthen the link, we enhanced anterograde lysosomal transport by expressing dominant-negative Rab7-interacting lysosomal protein (RILP), which also rescues the dendrite loss in *TMEM106B* knockdown neurons. Thus, *TMEM106B*/MAP6 interaction is crucial for controlling dendritic trafficking of lysosomes, presumably by acting as a molecular brake for retrograde transport. Lysosomal misrouting may promote neurodegeneration in patients with *TMEM106B* risk variants.

Keywords dendrites; frontotemporal lobar degeneration; lysosomes; microtubule-associated protein 6; *TMEM106B*

Subject Categories Neuroscience

DOI 10.1002/embj.201385857 | Received 31 June 2013 | Revised 7 October 2013 | Accepted 27 October 2013

Introduction

Frontotemporal lobar degeneration (FTLD) is the third most common neurodegenerative disease after Alzheimer's disease and

Parkinson's disease (reviewed in Rademakers *et al.*, 2012). The clinical presentation is diverse and the symptoms include dementia, behavioral changes, as well as speech and language impairment. Additional symptoms of upper or lower motoneuron disease are common and indicate a partial overlap with amyotrophic lateral sclerosis (ALS). Moreover, FTLD is heterogeneous in terms of pathology and genetics. The majority of cases show neuronal cytoplasmic aggregates of the nuclear DNA/RNA-binding protein TDP-43 (Neumann *et al.*, 2006). Pathogenic mutations in *TARDBP*, the gene coding for TDP-43 are rare and predominantly cause ALS (Sreedharan *et al.*, 2008). Familial forms of FTLD with TDP-43 pathology are mainly caused by hexanucleotide repeat expansion in *C9ORF72* (DeJesus-Hernandez *et al.*, 2011; Renton *et al.*, 2011) and dominant loss-of-function mutations in the growth factor programulin (*GRN*) (Cruts *et al.*, 2006).

A multicentric genome-wide association study identified *TMEM106B* as a risk factor for FTLD with TDP-43 pathology (Van Deerlin *et al.*, 2010). Three SNPs in linkage disequilibrium (LD) (rs1020004, rs6966915, and rs1990622) have been identified in coding and non-coding regions of *TMEM106B* with genome-wide significance. These SNPs conferred the strongest risk in patients also carrying a *GRN* mutation suggesting a functional interaction between *TMEM106B* and *GRN*. The genetic association of *TMEM106B* variants with FTLD-TDP was replicated with high confidence (Cruchaga *et al.*, 2011; Finch *et al.*, 2011; Van der Zee *et al.*, 2011). Homozygosity of the protective minor allele of the non-coding SNP rs1990622 (7 kb downstream of the gene) is observed only in 2.6% of patients and 19.1% of controls. This protective allele is associated with higher *GRN* levels in plasma (Finch *et al.*, 2011). The *TMEM106B* coding variant T185S, although not significantly associated with the risk of FTLD-TDP, but in perfect LD with rs1990622, seems to slightly increase *TMEM106B* protein levels (Nicholson *et al.*, 2013). Although *TMEM106B* variants are not associated with ALS per se, the risk allele is linked to cognitive impairment in these patients (Vass *et al.*, 2011). The minor allele of rs1990622 protects against hippocampal sclerosis and TDP-43

¹ German Center for Neurodegenerative Diseases (DZNE), Munich, Germany

² Biochemistry, Adolf Butenandt Institute, Ludwig-Maximilians University, Munich, Germany

³ Neuroproteomics, Klinikum rechts der Isar, Technische Universität München, Munich, Germany

⁴ Munich Cluster of Systems Neurology (SyNergy), Munich, Germany

⁵ Cell Biology, Faculty of Science, Utrecht University, Utrecht, The Netherlands

*Corresponding author. Tel: +49 (0)89 / 2180 - 75453; Fax: +49 (0) 89 / 2180 - 75415; E-mail: dieter.edbauer@dzne.de

pathology in Alzheimer patients suggesting a more general role in neurodegeneration independent of *GRN* (Rutherford et al, 2012).

TMEM106B is a type 2 transmembrane protein and primarily localizes to late endosomes and lysosomes (Brady et al, 2012; Chen-Plotkin et al, 2012; Lang et al, 2012). TMEM106B overexpression leads to aberrant vacuole formation and enlarged lysosomes that are less acidic, which may be accompanied by slightly enhanced *GRN* levels and thus argues against a gain-of-function role of TMEM106B risk variants in FTLD (Brady et al, 2012; Chen-Plotkin et al, 2012). Lysosomal and autophagosomal inhibitors increase TMEM106B expression (Brady et al, 2012; Lang et al, 2012). Thus, the increased TMEM106B expression observed in *GRN* mutation carriers may be due to impaired lysosomal/autophagosomal function, which has been described in *GRN* knockout mice (Ahmed et al, 2010; Chen-Plotkin et al, 2012; Wils et al, 2012). Interestingly, homozygous *GRN* mutations cause neuronal ceroid lipofuscinosis, a lysosomal storage disorder (Smith et al, 2012). Pathogenic mutations in *CHMP2B* and *VCP* further support a strong endo-lysosomal dysfunction component in FTLD, as they affect membrane fusion and vesicle sorting within the endo-lysosomal and autophagosomal system (Filimonenko et al, 2007; Ju et al, 2009; Urwin et al, 2010; Ritz et al, 2011).

Despite its lysosomal localization, none of the previous publications reported altered lysosomal function or morphology or any effect on *GRN* expression upon TMEM106B knockdown (Brady et al, 2012; Chen-Plotkin et al, 2012; Lang et al, 2012). The physiological role of TMEM106B is therefore unknown. Here, we combine loss-of-function experiments and proteomics to identify the microtubule-associated protein 6 (MAP6) as novel interacting protein for TMEM106B. We show that interaction of TMEM106B and MAP6 regulates dendritic trafficking of lysosomes and affects dendrite morphology.

Results

TMEM106B knockdown causes lysosomal clustering in HeLa cells

TMEM106B shows a predominantly lysosomal localization, but its function in lysosomes is unknown. Transfection of HeLa cells with siRNAs against TMEM106B strongly reduced TMEM106B protein expression without affecting the pH-dependent proteolytic maturation of the lysosomal protease Cathepsin B (Fig 1A). However, immunostaining of lysosomes against the marker protein LAMP2 revealed a striking change in lysosomal localization upon

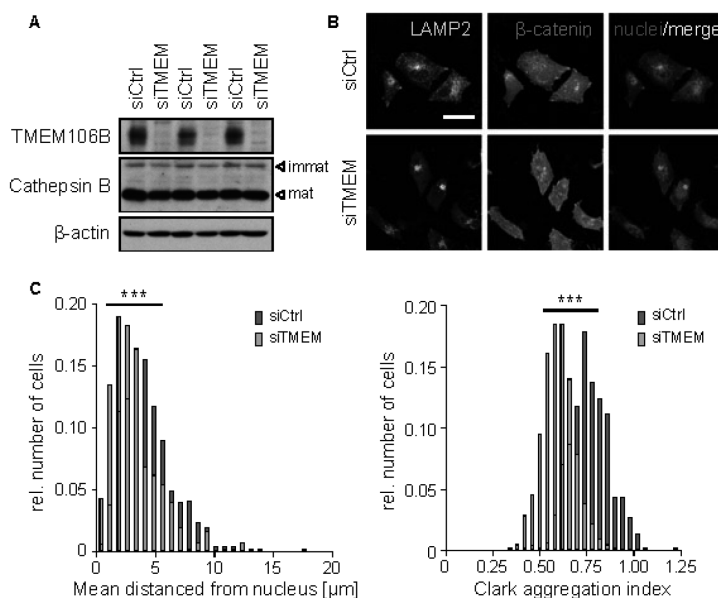


Figure 1. Knockdown of the late-endosomal/lysosomal localized protein TMEM106B does not change lysosomal properties, but lysosomal localization.

A HeLa cells were transfected with control siRNA (siCtrl) or siRNA against TMEM106B (siTMEM). Immunoblot detects TMEM106B at 51 kDa. Immature and processed mature Cathepsin B is detected at 40 kDa and 25 kDa, respectively. β-actin levels confirm equal loading.
B siRNA-transfected HeLa cells were immunostained with antibodies against LAMP2 (green) and β-catenin (red). Scale bar represents 25 μm.
C Quantification of lysosomal positioning and clustering upon TMEM106B knockdown in HeLa cells. Positioning of lysosomes was determined by measuring the mean distance of the lysosomes to the nucleus and clustering was quantified by using the Clark aggregation index (Clark & Evans, 1954). In three independent experiments, a total of 510 control cells and 422 TMEM106B knockdown cells were analyzed. Mann-Whitney-U-test, *** denotes $P < 0.001$.

TMEM106B knockdown (Fig 1B). Lysosomes were distributed throughout the cytoplasm in control-transfected cells, but appeared tightly clustered near the nucleus in cells devoid of TMEM106B, although the cell size was unaltered. Automated quantitative image analysis measuring the average distance of lysosomes to the nucleus and the lysosomal distribution using the Clark aggregation index (Clark & Evans, 1954) confirmed the shift of lysosomes towards the nucleus and the more compact subcellular distribution of lysosomes upon TMEM106B knockdown (Fig 1C). Overexpressing siRNA-resistant human TMEM106B (HA-HT106b*) in cells transfected with TMEM106B siRNA rescued normal lysosomal localization (compare HA-T106b*-expressing cell to the neighboring cells in supplementary Fig S1) thus confirming siRNA specificity. These data suggest that TMEM106B controls lysosomal localization and trafficking,

which may be particularly important in highly polarized cells such as neurons.

TMEM106B localizes to late-endosomes and lysosomes throughout the somatodendritic compartment in primary neurons

Since accumulation of lysosomes in the soma and proximal dendrites is a common finding in brain tissue of FTLD patients particularly with GRN mutations (Chen-Plotkin et al, 2012; Busch et al, 2013), we analyzed the localization of TMEM106B in rat primary hippocampal neurons. Consistent with previous reports (Chen-Plotkin et al, 2012; Lang et al, 2012), endogenous TMEM106B colocalized with LAMP1-positive late-endosomal/lysosomal vesicles in the cell body and in dendrites (Fig 2A). Quantitative correlation analysis

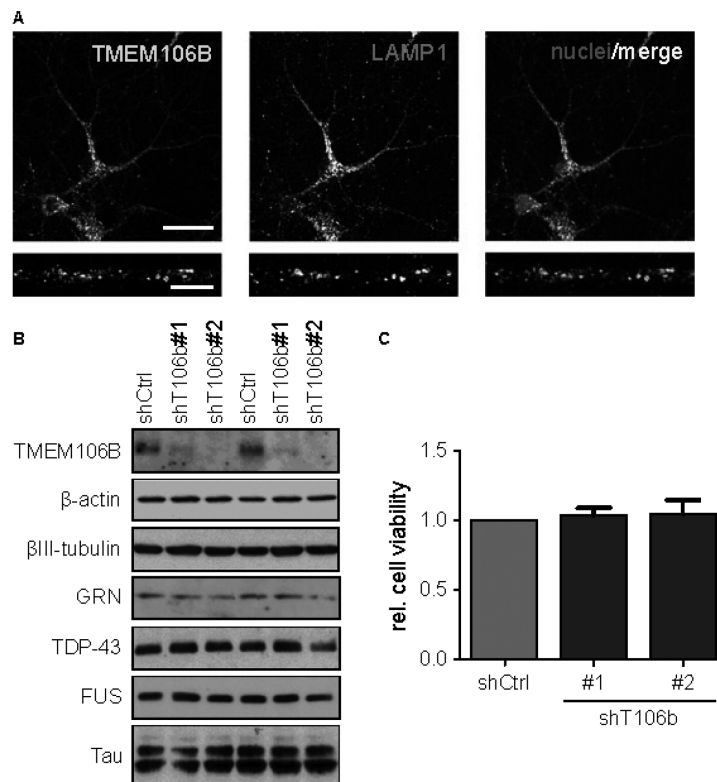


Figure 2. In neurons TMEM106B is localized to late endosomes/lysosomes in the somatodendritic compartment and knockdown does not affect general cell viability.

A Primary rat hippocampal neurons (DIV12) immunostained with antibodies against TMEM106B (green) and LAMP1 (red). Merged image indicates widespread colocalization in a single confocal plane. Scale bar represents 50 μ m (overview) or 10 μ m (dendrite segment).
 B Primary rat cortical neurons (DIV7+6) were transduced with lentiviruses expressing either TMEM106B shRNA #1 or #2 or (shT106b) a control shRNA (shCtrl). Immunoblots with the indicated antibodies.
 C Primary rat cortical neurons (DIV7+6) were transduced with the indicated lentiviruses. Cell viability upon TMEM106B knockdown was measured using an XTT assay. TMEM106B knockdown had no statistically significant effect (one-way ANOVA). n = 3 independent experiments, mean \pm s.e.m.

confirms good colocalization of TMEM106B with LAMP1 (Pearson's coefficient 0.66 ± 0.02), but not synaptic vesicles (labeled with SV2) and early or recycling endosomes (labeled with transferrin receptor TfR) (supplementary Fig S2A and B).

To investigate the role of TMEM106B in neurons, we took advantage of lentiviral knockdown using two specific shRNAs targeting TMEM106B (shT106b#1 and #2). Cortical neurons were transduced at day 7 *in vitro* (DIV7) with individual shRNAs for 5 days (DIV7+5). Both shRNAs strongly reduced TMEM106B expression compared to the control shRNA (shCtrl), without affecting the expression of β -actin, β III-tubulin or the FTLD-associated proteins GRN, TDP-43, FUS and Tau (Fig 2B). We detected no overt toxicity upon TMEM106B knockdown under these conditions using an XTT-based viability assay (Fig 2C) indicating that loss of TMEM106B alone does not cause neurodegeneration.

To analyze the morphology of individual cells by immunofluorescence, we transfected hippocampal neurons with shRNA constructs targeting TMEM106B. The punctate somatodendritic TMEM106B staining disappeared almost completely in neurons transfected with both TMEM106B-specific short hairpin constructs (supplementary Fig S3A). While the distribution of lysosomes showed only a subtle trend towards clustering in the soma of TMEM106B shRNA-transfected neurons (supplementary Fig S3B), the dendritic arborization appeared less complex suggesting TMEM106B may affect the function or distribution of lysosomes particularly in dendrites. Together, these data indicate that in neurons TMEM106B is localized to lysosomes throughout the somatodendritic compartment without grossly affecting their somatic distribution and neuronal viability.

TMEM106B is essential for dendrite branching and maintenance

We observed a blunted dendritic arborization in TMEM106B shRNA-transfected neurons compared to shCtrl-transfected cells (supplementary Fig S3A). To quantitatively assess these changes, we co-transfected hippocampal neurons at DIV7 or 14 with the shRNA constructs together with a GFP-expressing plasmid to outline cell morphology. Five days after transfection the most noticeable effect was significantly reduced complexity of the dendritic arbor (Fig 3A). We quantified this phenotype by Sholl analysis, which measures the number of dendrites crossing concentric circles around the cell body (Sholl, 1953). Despite the nearly normal number of primary dendrites in TMEM106B knockdown neurons, we observed a striking reduction in dendritic branching compared to control transfected neurons. This effect was similar for neurons transfected at DIV7 and 14 (Fig 3B), indicating that TMEM106B is also required for maintenance of already established dendritic arborization in mature neurons. While overall dendritic branching was less complex in TMEM106B knockdown neurons, we found that the remaining principal dendrite was longer in the shRNA-treated cells (supplementary Fig S4A). To exclude off-target effects, we used lentiviral co-expression of shRNA-resistant rat TMEM106B (T106b*) in knockdown neurons to restore basal TMEM106B levels (Fig 3C), while avoiding TMEM106B aggregation seen at higher expression levels (Brady *et al.*, 2012; Chen-Plotkin *et al.*, 2012). Expression of shRNA-resistant T106b* in TMEM106B shRNA-transfected hippocampal neurons restored dendritic arborization (Fig 3D and E) almost to control levels, while the expression of T106b* together with the control shRNA had no effect on dendritic arborization.

To further characterize whether impairment of lysosomal function inhibits dendritic branching we transfected hippocampal neurons (DIV7+5) with wild-type Rab7a, constitutively active Rab7a (Q67L) or dominant-negative Rab7a (T22N), which blocks cargo transport from early to late endosomes and lysosomes and inhibits lysosomal biogenesis (Mukhopadhyay *et al.*, 1997; Press *et al.*, 1998; Bucci *et al.*, 2000). Neurons transfected with wild-type or constitutively active Rab7a appeared normal. In contrast, dendrites in neurons expressing the dominant-negative Rab7a showed a less complex branching pattern reminiscent of TMEM106B knockdown suggesting that proper lysosomal function is required for dendrite development (supplementary Fig S4B and C, compare to Fig 3A and B).

Moreover, compared to the abundant mushroom-shaped spines in control neurons, the dendritic protrusions in TMEM106B knockdown cells appeared less dense and thinner (supplementary Fig S4D). Reduction of the pre- and post-synaptic marker proteins (synaptophysin and PSD-95) in cortical neurons transfected with TMEM106B knockdown virus corroborate synapse loss at a biochemical level (supplementary Fig S4E and F).

We detected some endogenous TMEM106B also in the axonal compartment in developing neurons at DIV4 (supplementary Fig S5A), which allows better morphological analysis of axons than in mature neurons. Interestingly, developmental TMEM106B knockdown (DIV0+4) increased axon length by 40% (supplementary Fig S5B and C), confirming that TMEM106B knockdown has no general toxic effect, but differentially affects axons, dendrites and synapses. Due to its predominant somatodendritic localization, we focused our further analysis on the dendritic phenotype.

Taken together, the late endosomal/lysosomal protein TMEM106B is required for proper maintenance of all except the primary dendrites possibly through a specific effect on lysosomes in the dendritic compartment.

TMEM106B interacts with the microtubule-binding protein MAP6 in the brain

In order to tie TMEM106B function to known cellular pathways, we performed immunoprecipitation experiments from P15 rat brain to identify interacting proteins using a proteomics approach. In three independent experiments with a total of five replicates the only common protein specifically identified in TMEM106B immunoprecipitates under these conditions was the microtubule-associated protein 6 (MAP6), also known as stable tubule-only polypeptide (STOP) (Bosc *et al.*, 1996). Apart from microtubules, MAP6 is known to interact with the actin cytoskeleton and the Golgi apparatus (Baratier *et al.*, 2006; Gory-Faure *et al.*, 2006). LC-MS/MS analysis identified a total of 11 peptides unique for MAP6 (23% sequence coverage) in TMEM106B immunoprecipitates, but none in controls (supplementary Fig S6A). To confirm the proteomics data, we repeated the experiment and analyzed TMEM106B and MAP6 immunoprecipitates by immunoblotting. Coimmunoprecipitation in both directions corroborates the specific interaction of TMEM106B and MAP6 (Fig 4A and B).

To determine the interacting domains we transfected variants of MAP6 and TMEM106B in HEK293 cells. We expressed only the cytoplasmic N-terminus of TMEM106B tagged with GFP to avoid aggregation of the full-length construct. We could robustly detect GFP-N-TMEM106B in immunoprecipitates of rat MAP6 and the long neuron-enriched isoform 1 of human MAP6, but not in the

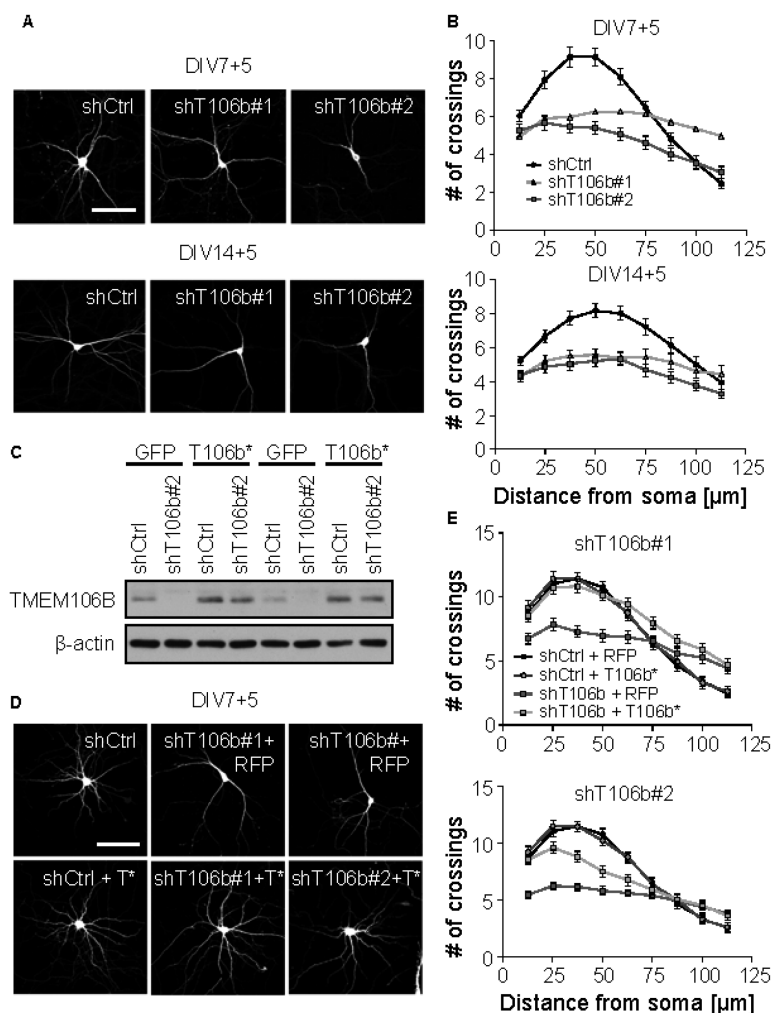


Figure 3. TMEM106B knockdown impairs dendrite branching and maintenance.

A, B Primary rat hippocampal neurons (DIV7+5 and DIV14+5) were cotransfected with the indicated shRNAs and GFP to visualize cell morphology. The dendritic arborization was quantified manually and blinded to the experimental condition by Sholl analysis using MetaMorph software. Neurons transfected with either TMEM106B shRNA#1 or #2 are significantly different from control shRNA transfected cells (at DIV7 + 5: shT106b#1: from 25 to 62.5 μm radius $P < 0.001$, 100 and 112.5 μm $P < 0.001$; shT106b#2: from 25 to 75 μm $P < 0.001$. Analysis at DIV14+5: shT106b#1: from 37.5 to 62.5 μm $P < 0.001$, at 75 μm $P < 0.05$; shT106b#2: 37.5 to 62.5 μm $P < 0.001$, at 25 and 87.5 μm $P < 0.05$). $n > 38$ neurons per condition, three independent experiments, mean \pm s.e.m. Two-way ANOVA. Scale bar represents 100 μm .

C Primary rat cortical neurons (DIV7+6) were cotransduced with a shRNA-expressing lentivirus (shT106b #2) and a lentivirus expressing shRNA-resistant TMEM106B (T106b*) or GFP as control to titrate TMEM106B expression. Immunoblots with the indicated antibodies.

D, E Primary rat hippocampal neurons were virally infected (DIV6) with either mCherry (RFP) or shRNA-resistant TMEM106B mutant (T106b*) and cotransfected (DIV7) with either a control shRNA or the indicated TMEM106B shRNA and GFP to outline neuron morphology for additional 5 days. Sholl analysis as above. shRNA-resistant TMEM106B overexpression fully rescued the phenotype of the less potent TMEM106B shRNA #1 (shCtrl+RFP versus shT106b+RFP: from 25 to 50 μm $P < 0.001$, shT106b+RFP versus shT106b+T106b*: 25 and 62.5 μm $P < 0.05$, 37.5 and 50 μm $P < 0.001$) and partially rescued the more potent shRNA #2 (shCtrl+RFP versus shT106b+RFP: from 12.5 to 50 μm $P < 0.001$, shT106b+RFP versus shT106b+T106b*: from 12.5 to 25 μm $P < 0.001$, at 37.5 μm $P < 0.05$). $n > 38$ neurons per condition, three independent experiments, mean \pm s.e.m., two-way ANOVA. Scale bar represents 100 μm .

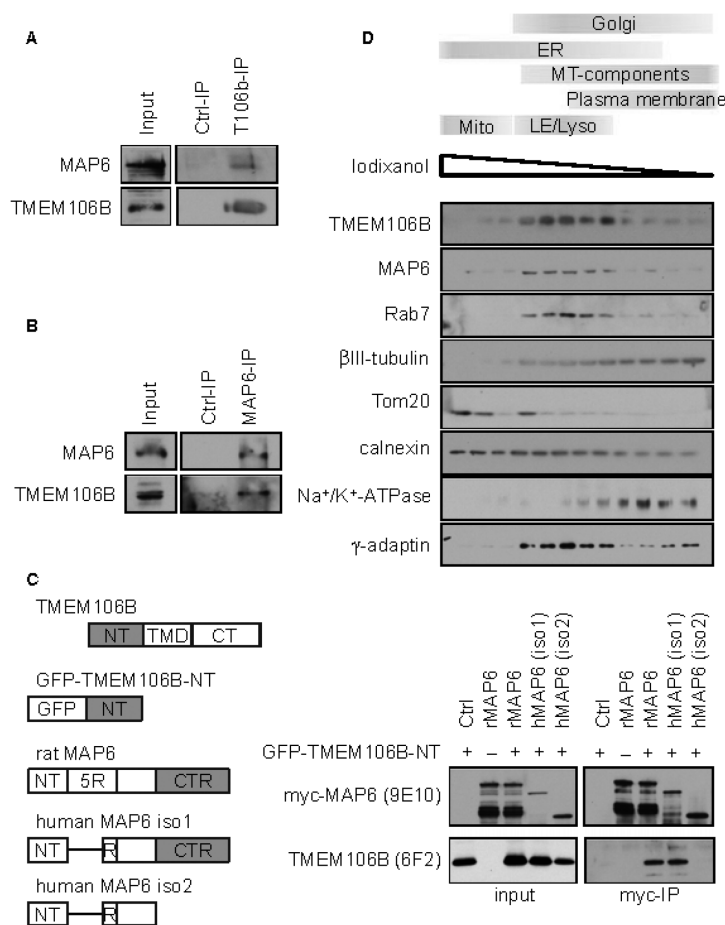


Figure 4. TMEM106B interacts with MAP6 in rat brain.

A, B TMEM106B (A) and MAP6 (B) were immunoprecipitated from P15 rat brain. Immunoblots with the indicated antibodies.
 C Interacting domains of TMEM106B and MAP6. The cytoplasmic N-terminal domain (NT) of TMEM106B fused to GFP. Transmembrane domain (TMD) and C-terminal domain (CT) were removed to avoid aggregation. MAP6 contains a central repeat domain, consisting of five repeats (R) of a 46 amino acid motif in rat but only one repeat in humans. The shorter isoform 2 lacks the C-terminal repeat domain (CTR) consisting of up to 28 imperfect repeats. The right panel shows coimmunoprecipitation of TMEM106B and MAP6 variants. GFP-TMEM106B-NT and the indicated myc-tagged MAP6 variants were co-expressed in HEK293FT cells. MAP6 variants were immunoprecipitated with myc-beads. Immunoblots with the indicated antibodies.
 D Subcellular compartments from rat brain were fractionated using discontinuous iodixanol density gradient (2.5–30%). Immunoblots with the indicated antibodies.

C-terminally truncated isoform 2, indicating that the C-terminal domain of MAP6 interacts with the TMEM106B N-terminus (Fig 4C).

Consistent with previous observations (Baratier *et al*, 2006; Gory-Faure *et al*, 2006), double immunofluorescence shows predominant microtubule-like staining of MAP6 in dendrites and axons and vesicular staining in the soma with some overlap with TMEM106B-positive vesicles (supplementary Fig S6B).

To further support the biological relevance of the interaction between TMEM106B and MAP6, we performed subcellular fraction-

ation of rat brain on a discontinuous iodixanol density gradient. While β III-tubulin was broadly distributed over the whole gradient, TMEM106B and MAP6 levels peaked in endosomal/lysosomal fractions (marker protein Rab7) supporting close contact of the two proteins in the same cellular compartment (Fig 4D).

Together, our data establish the physical interaction of TMEM106B and MAP6 and imply a role of TMEM106B in microtubule-dependent processes, which are central to neurite development and maintenance (Hoogenraad & Bradke, 2009).

MAP6 knockdown rescues TMEM106B knockdown

Since TMEM106B knockdown strongly reduced dendritic branching, we asked whether MAP6 and the interaction between TMEM106B and MAP6 in particular affects dendrite morphology. Interestingly, MAP6 overexpression in hippocampal neurons (DIV7+5) strongly

reduced dendrite branching and thus phenocopies the effect of TMEM106B knockdown (Fig 5A and B). We generated a shRNA construct against MAP6 to perform loss-of-function studies (supplementary Fig S6C). MAP6 knockdown enhanced dendritic complexity and particularly the distal branching (supplementary

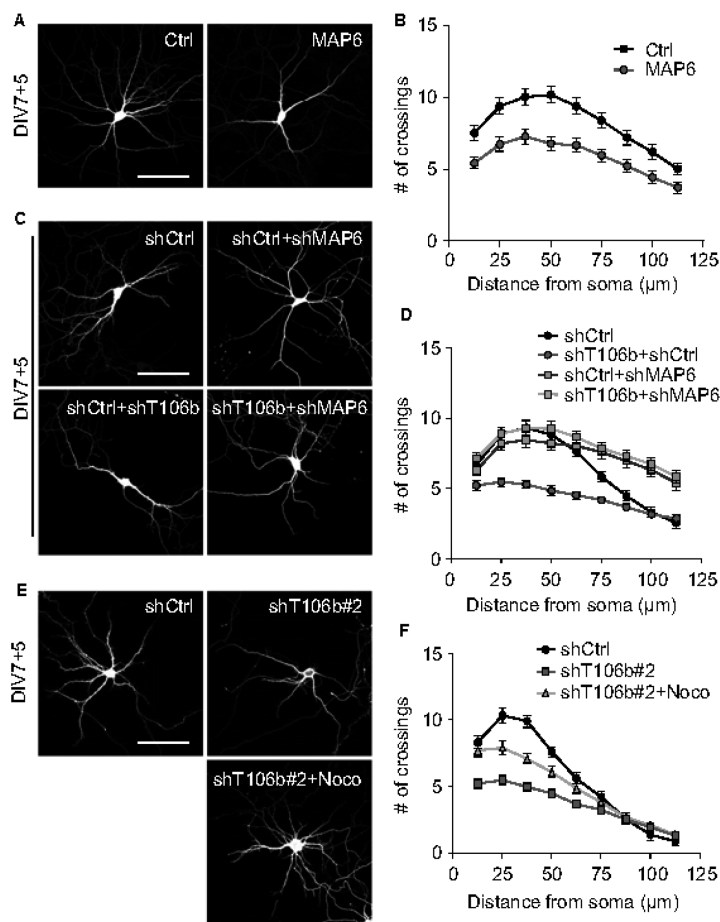


Figure 5. MAP6 knockdown and nocodazole treatment rescue the branching effect of TMEM106B knockdown.

A, B Primary rat hippocampal neurons (DIV7+5) were cotransfected with either a MAP6 overexpression construct or an empty vector control and CFP. Quantification of dendritic arborization by Sholl analysis. Neurons overexpressing MAP6 are significantly less branched than controls ($n > 40$ per condition; three independent experiments, mean \pm s.e.m., at 12.5, 25, 75 and 87.5 μ m radius $P < 0.05$, from 37.5 to 62.5 μ m $P < 0.001$). Scale bar represents 100 μ m.

C, D Primary rat hippocampal neurons (DIV7+5) were cotransfected with combinations of control shRNA (shCtrl), TMEM106B shRNA (shT106b) and MAP6 shRNA (shMAP6) together with CFP. Sholl analysis as above. MAP6 knockdown restores branching in TMEM106B knockdown neurons ($n > 40$ per condition; 3 independent experiments, mean \pm s.e.m., two-way ANOVA: shCtrl versus shT106b#2 + shCtrl: from 25 to 62.5 μ m radius $P < 0.001$. shT106b#2 + shCtrl versus shT106b#2 + shMAP6: from 25 to 100 μ m $P < 0.001$, at 112.5 μ m $P < 0.05$. shCtrl versus shMAP6 + shCtrl: at 87.5 μ m $P < 0.05$, from 100 to 112.5 μ m $P < 0.001$). Scale bar represents 100 μ m.

E, F Primary rat hippocampal neurons (DIV7+5) were cotransfected with either shCtrl or shT106b#2 and CFP. 10 nM nocodazole was added to neurons in the treatment group freshly every 36 h for a total of 5 days. Nocodazole-treated neurons branched significantly more than untreated T106b#2-transfected neurons ($n > 40$ cells per condition; three independent experiments, mean \pm SEM, two-way ANOVA: shCtrl versus shT106b#2: from 12.5 to 50 μ m $P < 0.001$, 62.5 μ m $P < 0.05$. shT106b#2 versus shT106b#2 + Noco: from 12.5 to 25 μ m $P < 0.001$, at 37.5 μ m $P < 0.01$). Scale bar represent 100 μ m.

Fig S7A and B). This effect was fully rescued by overexpressing shRNA-resistant human MAP6 indicating a specific effect of the MAP6 shRNA.

We therefore speculated that MAP6 knockdown might alleviate the impact of TMEM106B knockdown. MAP6 knockdown alone enhanced branching preferentially in the distal part of the dendrite (Fig 5 C and D, but see also supplemental Fig S7A and B). Strikingly, combined knockdown of MAP6 and TMEM106B fully restored also proximal dendritic branching compared to TMEM106B knockdown alone suggesting the two interacting proteins act in a common pathway (Fig 5C and D).

Since MAP6 knockdown is predicted to enhance microtubule dynamics (Bosc *et al*, 1996), we also tested if pharmacological destabilization of microtubules associated with enhanced dynamics could rescue the TMEM106B knockdown phenotype. Prolonged treatment with low concentrations of nocodazole (10 nM, added fresh every 36 h) for 5 days after transfection partially rescued the blunted dendritic morphology in TMEM106B shRNA transfected neurons (Fig 5E and F). The slight difference in the rescue capacity of MAP6 knockdown and nocodazole treatment might be due to additional effects apart from changing lysosomal transport and microtubule dynamics.

We conclude that the dendrite loss by TMEM106B knockdown can be rescued by additionally reducing MAP6 expression or by increasing microtubule dynamics pharmacologically, which strongly suggests that the functional interaction of TMEM106B and MAP6 is microtubule-dependent.

TMEM106B and MAP6 regulate retrograde lysosomal trafficking in dendrites

Vesicular trafficking in dendrites and axons strongly relies on microtubules and microtubule-associated proteins (Dehmelt & Halpain, 2005; Kapitein & Hoogenraad, 2011). To test whether the interaction between TMEM106B and MAP6 affects lysosomal trafficking in dendrites we performed live imaging of late endosomes and lysosomes labeled with Rab7a-GFP. We analyzed TMEM106B knockdown neurons at a time point before dendritic loss becomes apparent to exclude secondary effects (DIV6+3). Accelerated movies of lysosomal trafficking revealed a population of highly mobile lysosomes in the dendrites of TMEM106B knockdown neurons that was not present in controls (supplementary Movies S1 and S2). Quantitative analysis of kymographs visualizing the trafficking of dendritic lysosomes showed a more than two-fold increase in the number of mobile vesicles in the dendrites of TMEM106B knockdown neurons (Fig 6A and B). This effect was predominantly due to enhanced retrograde motility while the number of anterogradely transported vesicles and vesicles without net-movement (during the 5 min recording time) remained unaffected (Fig 6B). This imbalance towards retrograde transport implies a progressive net loss of lipid membranes from distal dendrites which may be the cause of progressive dendrite loss. Reintroduction of TMEM106B by viral overexpression of shRNA-resistant T106b* fully restored the balance of anterograde and retrograde movement and thereby excludes off-target effects of the TMEM10B shRNA (supplementary Fig S7C and D). Both the total distance a mobile vesicle traveled and the average velocity in the 5 min interval were increased upon TMEM106B knockdown (supplementary Fig S8A and B). This effect was primarily due to increased speed and distance of retrogradely transported

lysosomes. The overall density of dendritic Rab7a-positive vesicles was not affected by TMEM106B knockdown (supplementary Fig S8C).

To exclude unspecific effects on dendritic trafficking in general, we analyzed the transport of mitochondria using dsRed fused to a mitochondrial targeting sequence. Importantly, TMEM106B knockdown had no effect on mitochondrial density and motility in dendrites supporting a specific effect of TMEM106B on lysosomal trafficking (supplementary Fig S8D and E).

As a further control for the specificity of TMEM106B knockdown on dendritic trafficking of lysosomes, we analyzed the movement of Rab7a-GFP labeled vesicles in axons. Hippocampal neurons were nucleofected directly before plating and analyzed by live imaging at DIV4. We found no apparent difference in the number or the direction of moving lysosomes (supplementary Fig S5D and E).

Since overexpression of MAP6 reduced dendritic arborization similar to knockdown of TMEM106B, we asked whether lysosomal trafficking is similarly affected under both conditions. Indeed, overexpression of MAP6 accelerated retrograde transport of Rab7a vesicles comparable to TMEM106B knockdown without affecting anterograde transport (Fig 6C and D) and overall vesicle density (supplementary Fig S8F). Interestingly, live imaging of co-expressed MAP6-GFP and LAMP1-RFP revealed that some moving lysosomes are labeled with MAP6-GFP, indicating that excess MAP6-GFP that can no longer bind to microtubules may still bind to TMEM106B on lysosomes (supplementary Fig S9). This implies a dominant-negative effect of MAP6 overexpression. Thus, TMEM106B and MAP6 both regulate retrograde transport of lysosomes along dendritic microtubules.

MAP6 knockdown and nocodazole treatment rescue TMEM106B knockdown phenotype by rebalancing lysosomal transport in dendrites

MAP6 knockdown or treatment with low doses of nocodazole rescued the branching deficit in TMEM106B knockdown neurons (see Fig 5). To test whether MAP6 knockdown could also correct the enhanced retrograde transport of lysosomes, we cotransfected TMEM106B shRNA #2 together with MAP6 shRNA and performed live cell imaging of Rab7a-GFP labeled vesicles. Surprisingly, MAP6 knockdown alone as well as double knockdown of TMEM106B and MAP6 (Fig 7A and C) enhanced lysosome motility. However, retrograde and anterograde transport were both increased to an equal level, suggesting balanced lysosomal transport is important for dendrite development and maintenance.

Similar results were obtained for the rescue with low-dose nocodazole treatment. While untreated TMEM106B knockdown neurons showed an increased number of retrogradely moving vesicles, neurons which were additionally treated with 10 nM nocodazole for 5 days showed enhanced movement in both directions (Fig 7B and D). Thus, genetic or pharmacologic re-balancing of dendritic transport of lysosomes rescues dendrite loss in TMEM106B knockdown neurons.

Enhancing anterograde transport of lysosomes promotes dendritic branching and rescues the TMEM106B phenotype

To further confirm that TMEM106B and MAP6 affect dendritic branching through their effect on lysosomal trafficking we aimed to manipulate lysosomal transport independent of TMEM106B and

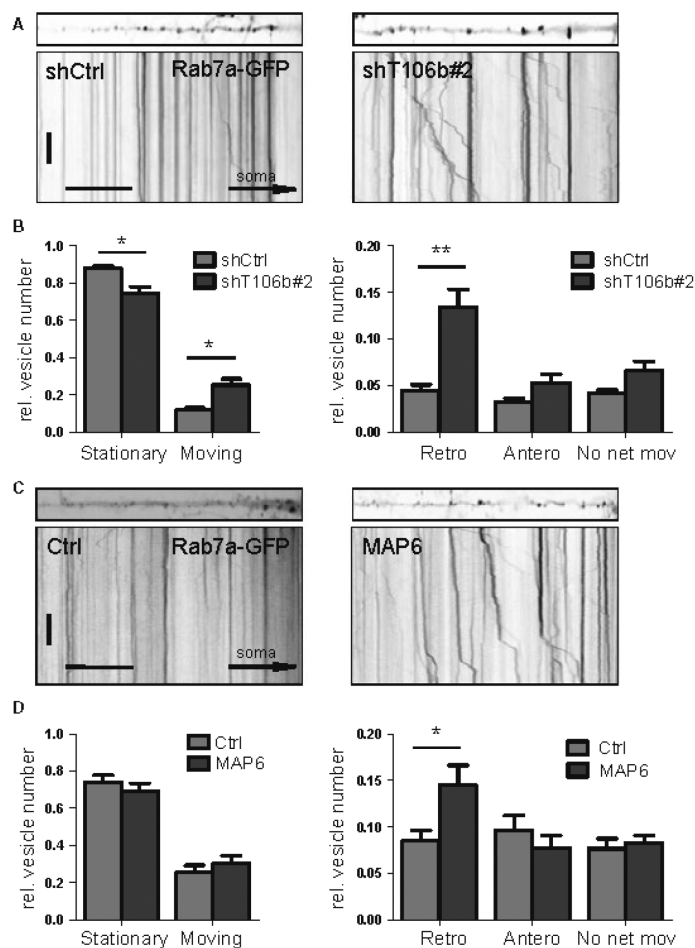


Figure 6. TMEM106B and MAP6 regulate retrograde trafficking of late endosomes / lysosomes in dendrites.
 A Primary hippocampal neurons (DIV6+3) were transfected with Rab7a-GFP and either TMEM106B shRNA #2 or a Ctrl shRNA and live imaged every second for 5 min to visualize late-endosomal/lysosomal trafficking in dendrites. Dendrite segments and kymographs of dendritic movement of Rab7a-GFP labeled vesicles. Scale bar represents 60 s (vertical) and 20 μ m (horizontal).
 B Quantitative analysis of vesicle movement from 5 min kymographs. Vesicles were manually classified according to their movement.
 C Primary hippocampal neurons were transfected with either rat MAP6 or empty vector and Rab7a-GFP. Scale bar represents 60 s and 20 μ m.
 D Analysis of Rab7a-positive vesicle movement as above.
 Data information: In (B) and (D), between five and 11 neurons per condition were analyzed per experiment in at least three independent experiments, mean \pm s.e.m., unpaired t-test: * denotes $P < 0.05$, ** denotes $P < 0.01$.

MAP6. Rab7-interacting lysosomal protein (RILP) is known to recruit dynein-dynactin motor complexes to lysosomes and thus promotes trafficking towards the minus end of microtubules (Cantalupo et al, 2001; Jordens et al, 2001). To investigate how RILP affects lysosomes in neurons, we co-expressed the dominant-negative C-terminal fragment of RILP together with Rab7-GFP and

quantified lysosomal trafficking in dendrites. dnRILP expression specifically enhanced anterograde movement, without affecting retrograde motility (Fig 9A and B). Moreover, prolonged expression of dnRILP resulted in enhanced dendritic complexity indicating that anterograde lysosomal transport is required for dendritic branching (Fig 8C and D).

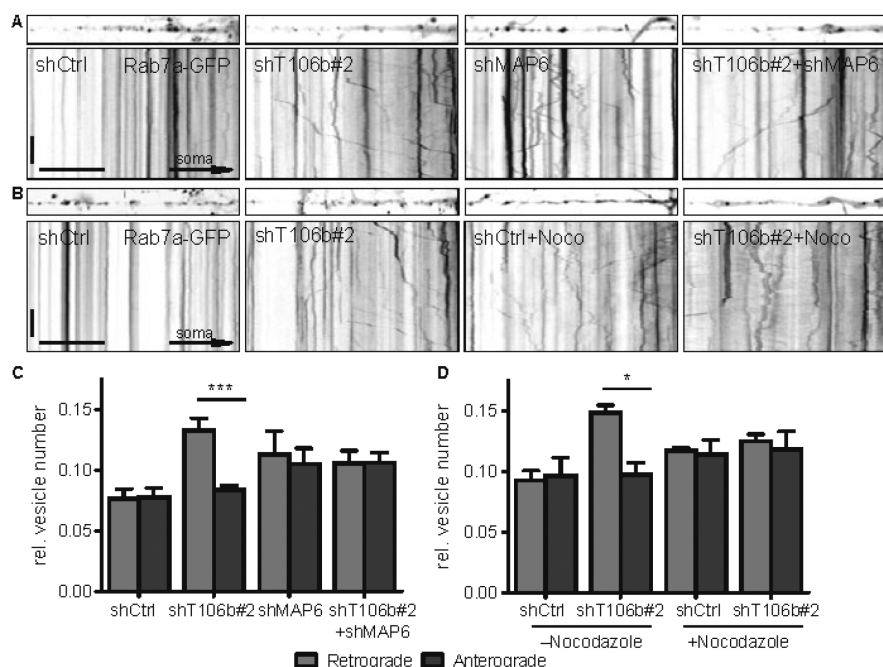


Figure 7. MAP6 knockdown and nocodazole treatment rebalance lysosomal trafficking in TMEM106B knockdown neurons.

A Primary hippocampal neurons were transfected with either shCtrl, shT106b#2 + shCtrl, shCtrl+shMAP6 or shT106b#2 + shMAP6 and Rab7a-GFP to visualize late endosomal/lysosomal trafficking. Dendrite segment and kymographs of dendritic movement of Rab7a-GFP-labeled vesicles. Scale bars represent 60 s and 20 μ m.
B Primary hippocampal neurons were transfected with either shCtrl or shT106b#2 and Rab7a-GFP. Fresh nocodazole (30 nM) was added to neurons of the treatment group every 36 h.
C, D Quantitative analysis of vesicle movement from 5 min kymographs. Vesicles were manually classified according to their movement. Between six and 10 neurons per condition were analyzed per experiment in at least three independent experiments, mean \pm s.e.m., unpaired t-test: * denotes $P < 0.05$, *** denotes $P < 0.001$.

We therefore asked whether promoting anterograde lysosomal transport may rescue the impaired branching in TMEM106B knockdown neurons. Expression of dnRILP restored the balance of anterograde and retrograde lysosomal transport in neurons transfected with TMEM106B shRNA (Fig 8E and F). Importantly, dnRILP expression also enhanced dendritic complexity in TMEM106B knockdown neurons (Fig 8G and H). The functional rescue of TMEM106B knockdown by promoting anterograde lysosomal transport indicates that the misbalanced lysosomal trafficking directly reduces dendrite complexity.

Discussion

Together, our data implicate TMEM106B in dendrite morphogenesis and maintenance by controlling lysosomal trafficking through its novel interacting partner MAP6. Vesicular trafficking, microtubule dynamics, and neurite development and maintenance are tightly connected and all have been linked to neurodegeneration (Garcia &

Cleveland, 2001; Hoogenraad & Bradke, 2009). Thus, TMEM106B risk variants may contribute to FTLD pathogenesis through lysosomal misrouting particularly in GRN mutation carriers.

Neuronal phenotype of TMEM106B knockdown

Our data confirm the predominant localization of TMEM106B to late-endosomes/lysosomes in primary neurons (Brady *et al*, 2012; Chen-Plotkin *et al*, 2012; Lang *et al*, 2012). TMEM106B overexpression is reported to inhibit lysosomal function (Brady *et al*, 2012). We find that TMEM106B knockdown has no effect on the maturation of the lysosomal protease Cathepsin B indicating that lysosomal acidification is normal in the absence of TMEM106B. Thus, impaired lysosomal function upon TMEM106B overexpression may be attributed to the pronounced TMEM106B aggregation seen upon strong overexpression (Brady *et al*, 2012). To avoid unspecific effects, we carefully titrated the TMEM106B levels back to endogenous levels for rescue experiments in HeLa cells and neurons.

TMEM106B knockdown dramatically alters the neuronal architecture without affecting viability. While axon length in immature

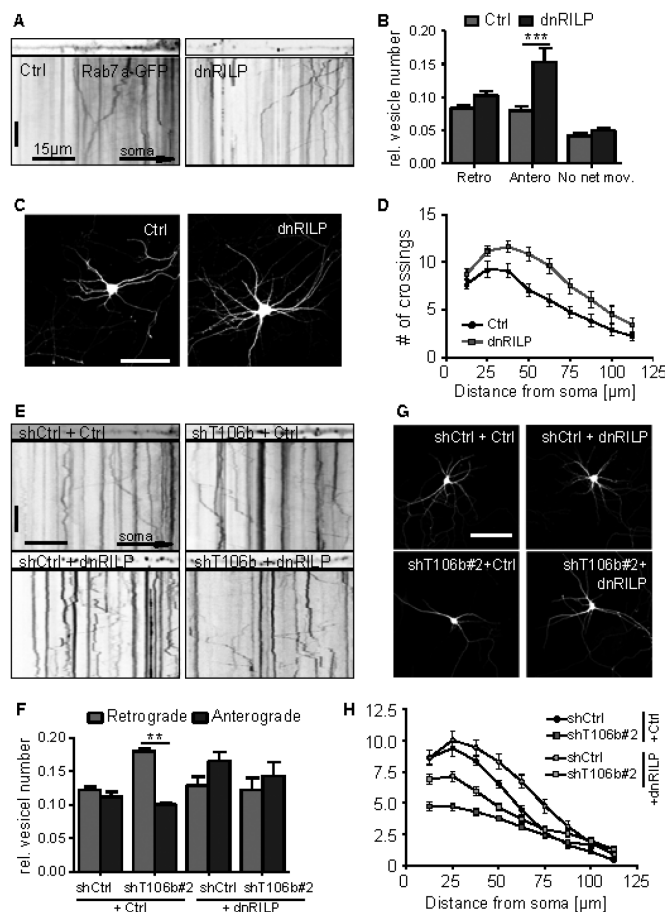


Figure 8. Overexpression of dominant-negative RILP increases anterograde movement of lysosomes and restores dendritic branching in TMEM106B knockdown neurons.

neurons is increased by 40%, dendritic arborization is severely blunted in mature neurons. The dominant-negative Rab7a T22N inhibits lysosomal biogenesis and leads to dendrite loss similar to TMEM106B knockdown showing that functional lysosomes are required for dendritic arborization. In contrast, enhancing anterograde transport of lysosomes in dendrites by expression of dnRILP promotes dendritic growth. Moreover, dendritic spines appear less mature and the levels of synaptic marker proteins are reduced in TMEM106B knockdown neurons, which has also been observed in the brains of FTLN patients (Clare *et al*, 2010). These changes imply weakened synaptic strength and impaired synaptic plasticity, which are common attributes of neurodegenerative diseases and awaits further study in FTLN/ALS (Tackenberg *et al*, 2009; Petkau *et al*, 2012). These findings argue for an important role of TMEM106B in regulating neuronal morphology through subtle alteration in lysosomal function, most likely through altered transport.

TMEM106B/MAP6 interaction

We identified MAP6 as TMEM106B interacting partner by mass spectrometry and confirmed the interaction using bidirectional coimmunoprecipitation, immunoblotting and live imaging of lysosomal trafficking. The C-terminal repeat region of the neuron-enriched splice variant of MAP6 binds to the cytoplasmic N-terminus of TMEM106B preferentially. MAP6 is a microtubule-associated protein that has been implicated in the cold-stability of microtubules, cellular morphology, cognition and mood (Bosc *et al*, 1996; Andrieux *et al*, 2002; Arama *et al*, 2012; Fournet *et al*, 2012). Posttranslational modifications, such as phosphorylation and palmitoylation, as well as overall protein levels have been shown to regulate MAP6 localization and target the protein also to cellular compartments other than microtubules i.e. Golgi apparatus, dendritic branch points and spines (Baratier *et al*, 2006; Gory-Faure *et al*, 2006). Moreover, MAP6 coaggregates with neurofilaments in spheroid axonal aggregates in ALS (Letourneil *et al*, 2003). Given the dramatic changes upon TMEM106B knockdown on dendritic arborization, linking TMEM106B to microtubules is intriguing. We show that overexpressing MAP6 phenocopies the effect of TMEM106B knockdown on dendrite morphology and that knockdown of MAP6 fully restores dendritic arborization upon TMEM106B knockdown, suggesting these morphological changes depend on the interaction of TMEM106B with MAP6.

Lysosome trafficking in dendrites

TMEM106B knockdown and MAP6 overexpression increase the number and speed of retrogradely moving lysosomes in dendrites suggesting this may be the common cause for the impaired dendritic branching. In HeLa cells, altered trafficking even leads to dramatic perinuclear clustering of lysosomes at the microtubule-organizing center, where most of the microtubules nucleate in these cells (Akhanova & Steinmetz, 2008; Tamura & Draviam, 2012). Restoring the balance of dendritic trafficking of lysosomes through MAP6 knockdown and nocodazole treatment rescue dendritic branching. Interestingly, comparable low concentrations of nocodazole also enhance transport of adenovirus particles (Giannakakou *et al*, 2002). Moreover, promoting anterograde lysosomal transport in dendrites independent of TMEM106B and MAP6 also rescues dendritic branching in TMEM106B knockdown cells, indicating that imbalanced lysosomal transport causes this phenotype.

Ample evidence suggests that an imbalance between anterograde and retrograde transport of lysosomes may impair protein and membrane turnover in the distal dendrites and thus impair dendrite and spine maintenance. The secretory pathway in general and endosomal/lysosomal trafficking in particular are important for neurite outgrowth (Horton *et al*, 2005; Sann *et al*, 2009; Jan & Jan, 2010). Interestingly, ALS-causing mutants in the ER-targeted protein VAPB impair membrane delivery to dendrites through its interacting protein YIF1A and thereby inhibit dendritic branching (Nishimura *et al*, 2004; Kuipers *et al*, 2013). These findings further support overlapping pathomechanisms in the FTLN/ALS disease spectrum. Moreover, fusion of lysosomes with the plasma membrane (and secretion of lysosomal content) supplies membrane components during wound sealing and cell growth (Reddy *et al*, 2001; Chakrabarti *et al*, 2003; Huynh *et al*, 2004). Promoting anterograde lysosomal transport using dnRILP strongly enhances dendritic complexity. Thus, a shift towards retrograde transport of lysosomes may contribute to dendrite withering through loss of lipid membranes in distal dendrites in TMEM106B knockdown neurons.

Additionally, disturbed lysosomal trafficking may impair growth factor signaling through altered transport of receptors, such as the signaling of GRN via sortilin or tumor necrosis factor receptor (Hu *et al*, 2010; Tang *et al*, 2011). Intriguingly, MAP6 was recently also reported to interact with Intersectin1 (Morderer *et al*, 2012), a protein important for endocytosis and signal transduction, suggesting MAP6 may play a broader role in endosomal and lysosomal trafficking. Altered signal transduction may also contribute to increased axonal length upon TMEM106B knockdown, since axons are less dependent on membrane supply through the secretory pathway than dendrites but strongly respond to guidance cues (Ye *et al*, 2007).

Model

We propose the following model for TMEM106B action centered on its role on lysosomal trafficking (Fig 9). Under normal conditions, binding of lysosomal TMEM106B to microtubule-attached MAP6 inhibits active retrograde transport of lysosomes along dendrites (Fig 9A). Upon TMEM106B knockdown, retrogradely moving vesicles no longer bind to MAP6 and are transported with increased speed and fewer stops along the dendrites. This imbalance in late-endosomal/lysosomal trafficking with a shift towards the somatic compartment may impair dendrite and synapse stability through loss of membranes (Fig 9B). Overexpression of MAP6 saturates the binding sites on microtubules and excess MAP6 binds to TMEM106B on lysosomes without anchoring them to microtubules which causes a dominant-negative effect mimicking the knockdown of TMEM106B and leads to enhanced retrograde transport (Fig 9B). This model is supported by live imaging experiments showing MAP6-GFP moving together with LAMP1-RFP labeled lysosomes (Fig S9). Knockdown of MAP6 alone or double knockdown of TMEM106B and MAP6 slightly accelerates lysosome trafficking, but affects retrograde and anterograde trafficking to the same extent, thus preventing membrane loss in the dendrite (Fig 9C). Therefore, additional mechanisms (such as the interaction of Rab7a and RILP) likely control bidirectional transport of lysosomes in dendrites. Enhanced microtubule dynamics upon MAP6 knockdown (Bosc *et al*, 1996) may add to this effect because increasing microtubule dynamics with nocodazole also enhances overall motility of lysosomes and restores the balance of retrograde

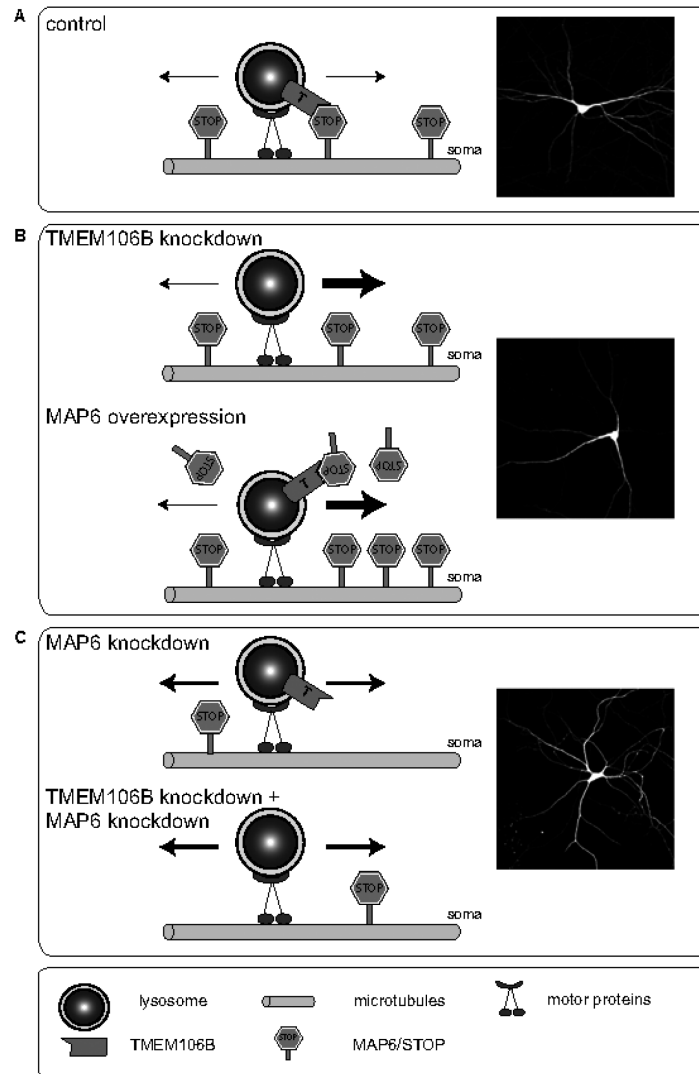


Figure 9. Model of the effects of TMEM106B and MAP6 on lysosomal transport.

- A Interaction of TMEM106B and MAP6 inhibits retrograde transport of lysosomes in dendrites.
- B TMEM106B knockdown and MAP6 overexpression specifically enhance retrograde transport of lysosomes.
- C MAP6 knockdown moderately enhances trafficking of lysosomes in both direction and rescues TMEM106B knockdown.

and anterograde trafficking in TMEM106B knockdown neurons. Thus, low concentrations of the anti-cancer drug Vincristine, which also enhances microtubule dynamics, may be beneficial for patients with TMEM106B variants or GRN mutations, where lysosomes accumulate in the soma and proximal dendrites (Chen-Plotkin et al, 2012).

A similar transport mechanism has already been shown for the docking of mitochondria to the axonal cytoskeleton. Interaction of the mitochondrial protein Syntaphilin with dynein light chain LC8 (independently of its motor function) stalls mitochondrial transport along axonal microtubules (Kang et al, 2008; Chen et al, 2009). Our data suggest that TMEM106B together with its binding partner

MAP6 act as a molecular brake for retrogradely moving late endosomes and lysosomes in a similar manner without affecting mitochondrial transport. Since TMEM106B is predominantly localized in the late-endosomal/lysosomal compartment, the trafficking function of MAP6/TMEM106B is likely specific to this compartment.

Disease implication

We and others find no effect of TMEM106B knockdown on the expression of FTLD-associated proteins GRN, TDP-43, FUS and Tau or neuronal viability suggesting that *TMEM106B* risk variants may sensitize neurons to GRN or TDP-43-dependent pathomechanisms, rather than causing neurodegeneration directly (Lang et al, 2012). Emerging pathological and genetic evidence supports lysosomal impairment in FTLD, particularly in patients with *GRN* mutations in whom *TMEM106B* variants confer the strongest risk (Van Deerlin et al, 2010). Homozygous loss of *GRN* in mice and patients leads to lipofuscin accumulation, a common feature of lysosomal dysfunction (Ahmed et al, 2010; Smith et al, 2012). Moreover, *CLN3* mutations that cause juvenile onset neuronal ceroid lipofuscinosis induce perinuclear clustering of lysosomes similar to the phenotype of TMEM106B knockdown in HeLa cells (Tuxworth et al, 2009; Uusi-Rauva et al, 2012). Interestingly, TMEM106B and presumably lysosomes accumulate in the soma and proximal dendrites in FTLD patients, most prominently in those with *GRN* mutations (Chen-Plotkin et al, 2012). Thus, lysosomal misrouting may be a common pathomechanism of FTLD that is further boosted by *TMEM106B* risk variants.

We identified a molecular interaction partner and a very specific function in lysosomal transport for TMEM106B, a protein of previously unknown function, opening new therapeutic strategies for FTLD treatment.

Materials and Methods

Antibodies and reagents

Rabbits were immunized with an MBP-TMEM106B-NT fusion protein (rat amino acids 1–91) or with MBP-MAP6-CT (amino acids 793–952 according to NP_058900). The serum was purified with corresponding GST fusion proteins cross-linked to glutathione sepharose with Bis(sulfosuccinimidyl)suberate (BS3; Pierce, Rockford, IL, USA), eluted by pH shift (0.1 M glycine 0.5 M NaCl, pH 2.5) and immediately neutralized (1/10 volume 1 M Tris, pH 9.5). The monoclonal TMEM106B antibody (6F2) was described previously (Lang et al, 2012). Antibodies for LAMP1 (Enzo Life Sciences, Lörrach, Germany), LAMP2 (Developmental Studies Hybridoma Bank), β -catenin (Sigma-Aldrich, St. Louis, MO, USA), Cathepsin B (Santa-Cruz Biotechnology, Dallas, TX, USA), myc (9E10, Santa-Cruz Biotechnology), HA (3F10; Roche Applied Science, Mannheim, Germany), GFP (Neuromab, Davis, CA, USA), Rab7 (Cell Signaling Technologies, Danver, MA, USA), MAP6 (Cell Signaling Technologies and Abcam), β III-tubulin (Sigma-Aldrich), β -actin (Sigma-Aldrich), FUS (Bethyl), TDP-43 (Cosmo Bio, Tokyo, Japan), total-Tau (Dako, Hamburg, Germany), Tau-1 (Millipore, Billerica, MA, USA), Synaptophysin (Millipore), PSD-95 (Neuromab), Na^+/K^+ -ATPase (Developmental Studies Hybridoma Bank), Tom-20 (Santa-Cruz Biotechnology), calnexin (Enzo Life Sciences), γ -adaptin (BD Transduction Laboratories, San Jose, CA, USA), TfR (Invitrogen, Grand

Island, NY, USA), SV2 (Developmental Studies Hybridoma Bank) are commercially available. Nocodazole was from Sigma-Aldrich.

DNA constructs and lentivirus production

Rat TMEM106B cDNA was expressed from a lentiviral vector driven by human synapsin promoter. shRNAs were cloned into pSUPER (target sequences: TMEM106B #1 GCAGATTGATTATACGGTA, TMEM106B #2 GTGGAAGGAACACGACTTA, MAP6 GGTGCAGATC AGCGTGACA and luciferase control CGTACGCGGAATACTTCGA). For lentiviral knockdown the H1 promoter shRNA cassette was subcloned in a modified pLentilox 3.7 with a GFP-cassette driven by human synapsin promoter (Edbauer et al, 2010). The TMEM106B N-terminal fragment (AA 1–93) was cloned into the pEGFP-C1 vector. Rat MAP6 (NP_058900.1), human Map6 (isoform 1: NP_149052.1, isoform 2: NP_997460.1) and dnRILP (rat AA 201–401) were cloned into GW1-myc expression vector driven by the CMV promoter (British Biotechnology, Oxford, UK). All constructs were verified by sequencing. siRNA against human TMEM106B was purchased from Thermo Scientific (Waltham, MA, USA) (target sequence GATCAGAGATTAA GGCCAA).

Lentivirus was produced in HEK293FT cells cotransfected with psPAX2, pVSVg and the respective overexpression or knockdown constructs (Orozco et al, 2012). After harvest, the supernatant was concentrated by ultracentrifugation and the virus particles resuspended in Neurobasal medium.

Cell culture and transfection

Hippocampal and cortical neurons were prepared from embryonic day 18 Sprague–Dawley rats and transfected with Lipofectamine 2000 or transduced with lentivirus as described before (Orozco et al, 2012). For the analysis of axonal morphology and lysosomal trafficking in axons, hippocampal neurons were held on astrocyte feeder cultures using N2 medium and transfected before plating with an Amaxa 4D-Nucleofector (Lonza, Basel, Switzerland) with primary culture kit P3 (Orozco et al, 2012). Immunofluorescence and immunoblotting was performed as described previously (Orozco et al, 2012). Images were taken on Zeiss LSM 510 or 710 laser scanning microscopes (Zeiss, Jena, Germany) using 40 \times and 63 \times objectives with 1 Airy unit pinhole. HeLa cells were transfected with X-tremeGENE 9 DNA Transfection Reagent (Roche Applied Science) for 72 h and either processed for immunoblotting or immunocytochemistry as described before (Lang et al, 2012). For immunoprecipitation experiments, HEK293FT cells were transfected with Lipofectamine 2000 according to the manufacturer's instructions.

Cell viability assay

Neurons were plated in 96-well plates and transduced with the indicated lentiviruses for 5 days. XTT assay (Roche Applied Science) was performed according to the manufacturer's instructions.

Quantitative analysis of colocalization

The amount of colocalization of two fluorescent signals in a confocal image was analyzed using Pearson's coefficient estimated with the JaCoP plugin (Bolte & Cordelières, 2006) of ImageJ.

Live cell imaging and quantification of organelle movement

Time lapse images were taken on a Zeiss Cell observer SD spinning-disc microscope with an air-cooled Evolve 512 EMCCD camera at

1 Hz for 5 min. Neurons were kept in a climate chamber (37°C, 5% CO₂) during image acquisition. Kymographs of vesicular movement from the axon or 3–5 dendrite segments per cell were generated and manually analyzed using ImageJ software (Multiple Kymograph plugin by J. Rietdorf and A. Seitz). For the analysis of average run length and velocity only vesicles with more than 2.5 μm run length were included.

Morphological analysis

For the automatic analysis of lysosomes, projected images were segmented with Definiens Developer XD (version 2.02; Definiens AG, Munich, Germany). Nuclei regions were identified in the DAPI channel by automatic thresholding. Touching objects were separated by using the shape split function and subsequent erosion and dilation of the nucleus objects. Cell regions were identified based on β-catenin staining by a watershed algorithm using nucleus objects as seeds. Cell borders were smoothed by subsequent erosion and dilation. Lysosome region was identified in each cell object by automatic thresholding of the LAMP2 channel. The mean distance of lysosomes from nucleus was calculated by averaging the distance of each pixel belonging to the lysosome region to nucleus border. Aggregation of lysosomes was quantified with the Clark aggregation index (CAI). For each object, $D(x)$ denotes the spatial distance to the next neighbor of pixels belonging to the lysosome region, $N(x)$ denotes the number of pixels belonging to the lysosome region and A denotes the number of pixels of the cell object. The CAI is defined as $[\text{sum}(D(x))/N(x)] * \sqrt{N(x)/A}$.

Dendritic complexity was quantified using manual Sholl analysis using MetaMorph software (Molecular Devices, Sunnyvale, CA, USA). Concentric circles were laid around the cell soma from 12.5 to 112.5 μm (in 12.5 μm intervals) from the soma. The number of dendrites crossing each circle was counted. For morphological analysis of axons, the length of the tau-1 positive neurite was measured using the AxioVision software. All image acquisition and quantification for morphological analyses were done blind to the experimental conditions.

Immunoprecipitation from rat brain

P15 Sprague-Dawley-rat brains were homogenized in 0.32 M sucrose, 4 mM Hepes, 2 mM EDTA (pH 7.4). After centrifugation (75 600 g, 30 min) the pellet was lysed with 1% Triton X-100 in PBS for 20 min at 4°C. Subsequently, the soluble fraction (100 000 g, 20 min) was subjected to immunoprecipitation with TMEM106B, MAP6 or an unspecific control antibody (anti-GST) coupled (BS3; Thermo Scientific) to Dynabeads (Life-Technologies, Carlsbad, CA, USA) for 1.5 h at room temperature. After several washing steps with lysis buffer protein was eluted from the beads with 50 mM glycine, pH 2.8 for Coomassie staining (NOVEK colloidal blue staining kit; Invitrogen) and subsequent LC-MS/MS analysis, or directly boiled in sample buffer (4% SDS, 20% glycerol, 5% β-mercaptoethanol, 200 mM sodium phosphate pH 7.4) for immunoblotting. Protease and phosphatase inhibitor were present in all steps of the immunoprecipitation.

Coimmunoprecipitation from HEK293FT cells

HEK293FT (Invitrogen) cells were transfected with the respective constructs for 48 h using Lipofectamine 2000 (Invitrogen). Cells were washed with PBS, lysed with 1% Triton X-100 in PBS and

the lysate centrifuged (40 min, 17 000 g). The supernatant was diluted with PBS to 0.5% Triton X-100, precleared for 30 min with Protein A sepharose beads and afterwards subjected to immunoprecipitation with 30 μl myc-agarose beads (Sigma-Aldrich). Samples were washed four times with 0.5% Triton X-100 in PBS before loading. In all steps, protease and phosphatase inhibitors were present.

Mass spectrometry

Tryptic in-gel digestion of the proteins was performed as described (Shevchenko *et al*, 2006). Peptides were analyzed by an LC-MS/MS set-up coupling a Proxeon Easy nLCII (Thermo Fisher Scientific) with in-house packed 15 cm columns (2.4 μm C18 beads, Dr. Maisch GmbH) to an LTQ Velos Orbitrap mass spectrometer (Thermo Scientific). A bilinear gradient of 60 to 85 min was applied for peptide separation; collision induced dissociation (CID) was applied for fragmentation of TOP14 peptides. Data analysis was performed using the Proteome Discoverer 1.2 (Thermo Scientific) with the embedded SEQUEST algorithm for peptide identification. The International Protein Index database for rat (version 3.87) was used for the database search with carbamidomethylation of cysteine as a static and oxidation of methionine as a dynamic modification. Only full tryptic peptides with a maximum of 2 missed cleavages and an FDR below 5% were allowed.

Subcellular fractionation

An adult rat brain was homogenized in 20 ml buffer (10 mM Hepes, 1 mM EDTA, 0.32 M sucrose, pH 7.4). Postnuclear supernatant (1500 g, 10 min) was centrifuged (100 000 g, 30 min) and the membrane fraction was resuspended in homogenization buffer (10 mM Hepes, 1 mM EDTA, 0.25 M sucrose, pH 7.4). 1/10 volume was loaded on a step gradient (2.5, 5, 7.5, 10, 12.5, 15, 17.5, 20 and 30% iodixanol in homogenization buffer). After centrifugation (40,000 rpm, 2.5 h in a TH-641 rotor) 1 ml fractions were collected by needle puncture at the bottom.

Supplementary information for this article is available online: <http://emboj.embopress.org>

Acknowledgements

We thank J. Banzhaf-Strathmann, Eva Bentmann, S. Hassan, B. Schmid and C. Wahl-Schott for critical comments. We thank Andrea Wenninger-Weinzierl, and Nagore Astola for technical assistance. Automated image analysis was performed by C. Moehl at the DZNE light microscopy facility. CML was supported by a fellowship of the Hans and Ilse Breuer Foundation. DE was supported by the Helmholtz Young Investigator program HZ-NG-607. We thank the Competence Network for Neurodegenerative Diseases (KNDD) of the Bundesministerium für Bildung und Forschung (BMBF) for support to CH and SFL. The research leading to these results has received funding from the European Research Council under the European Union's Seventh Framework Programme (FP7/2007-2013) / ERC grant agreement no. 321366-Amyloid to CH. SFL was supported by the JPN-D-RIMOD program.

Author contributions

BMS and DE conceived the experiments. BMS performed and analyzed most experiments in neurons and rat brain. CML performed the analysis in heterologous cells. SH and SFL performed mass spectrometry analyses. DO and ST analyzed the axonal phenotype. KR and DE generated reagents. CCH, AC, CH

and DE supervised research. BMS and DE wrote the manuscript with input from all coauthors.

Conflict of interest

The authors declare that they have no conflict of interest.

References

- Ahmed Z, Sheng H, Xu YF, Lin WL, Innes AE, Gass J, Yu X, Wuertzer CA, Hou H, Chiba S, Yamanouchi K, Leissring M, Petrucelli L, Nishihara M, Hutton ML, McGowan E, Dickson DW, Lewis J (2010) Accelerated lipofuscinosis and ubiquitination in granulin knockout mice suggest a role for progranulin in successful aging. *Am J Pathol* 177: 311–324
- Akhmanova A, Steinmetz MO (2008) Tracking the ends: a dynamic protein network controls the fate of microtubule tips. *Nat Rev Mol Cell Biol* 9: 309–322
- Andrieux A, Salin PA, Vernet M, Kujala P, Barotier J, Gory-Faure S, Bosc C, Pointu H, Proietto D, Schweitzer A, Denarier E, Klumperman J, Job D (2002) The suppression of brain cold-stable microtubules in mice induces synaptic defects associated with neuroleptic-sensitive behavioral disorders. *Genes Dev* 16: 2350–2364
- Arama J, Boulay AC, Bosc C, Delphin C, Loew D, Rostaing P, Amigou E, Ezan P, Wingertsmann L, Guillaud L, Andrieux A, Giaume C, Cohen-Salmon M (2012) Bmcc1, a novel brain-isoform of Bmcc1, affects cell morphology by regulating MAP6/STOP functions. *PLoS ONE* 7: e35488
- Barotier J, Peris L, Brocard J, Gory-Faure S, Dufour F, Bosc C, Fourest-Lieuvin A, Blanchoin L, Salin P, Job D, Andrieux A (2006) Phosphorylation of microtubule-associated protein STOP by calmodulin kinase II. *J Biol Chem* 281: 19561–19569
- Bolte S, Cordelieres FP (2006) A guided tour into subcellular colocalization analysis in light microscopy. *J Microsc* 224: 213–232
- Bosc C, Cronk JD, Pirolet F, Watterson DM, Haiech J, Job D, Margolis RL (1996) Cloning, expression, and properties of the microtubule-stabilizing protein STOP. *Proc Natl Acad Sci USA* 93: 2125–2130
- Brady OA, Zheng Y, Murphy K, Huang M, Hu F (2012) The frontotemporal lobar degeneration risk factor, TMEM106B, regulates lysosomal morphology and function. *Hum Mol Genet* 22: 685–695
- Bucci C, Thomsen P, Nicoziani P, McCarthy J, van Deurs B (2000) Rab7: a key to lysosome biogenesis. *Mol Biol Cell* 11: 467–480
- Busch J, Martinez-Lage M, Ashbridge E, Grossman M, Van Deerlin V, Hu F, Lee V, Trojanowski J, Chen-Plotkin A (2013) Expression of TMEM106B, the frontotemporal lobar degeneration-associated protein, in normal and diseased human brain. *Acta Neuropathol Commun* 1: 36
- Cantalupo C, Alifano P, Roberti V, Bruni CB, Bucci C (2001) Rab-interacting lysosomal protein (RILP): the Rab7 effector required for transport to lysosomes. *EMBO J* 20: 683–693
- Chakrabarti S, Kobayashi KS, Flavell RA, Marks CB, Miyake K, Liston DR, Fowler KT, Gorelick FS, Andrews NW (2003) Impaired membrane resealing and autoimmune myositis in synaptotagmin VII-deficient mice. *J Cell Biol* 162: 543–549
- Chen YM, Gerwin C, Sheng ZH (2009) Dynein light chain LC8 regulates syntaphilin-mediated mitochondrial docking in axons. *J Neurosci* 29: 9429–9438
- Chen-Plotkin AS, Unger TL, Gallagher MD, Bill E, Kwong LK, Volpicelli-Daley L, Busch JI, Akle S, Grossman M, Van Deerlin V, Trojanowski JQ, Lee VM (2012) TMEM106B, the risk gene for frontotemporal dementia, is regulated by the microRNA-132/212 cluster and affects progranulin pathways. *J Neurosci* 32: 11213–11227
- Clare R, King VC, Wirenfeldt M, Vinters HV (2010) Synapse loss in dementias. *J Neurosci Res* 88: 2083–2090
- Clark PJ, Evans FC (1954) Distance to nearest neighbor as a measure of spatial relationships in populations. *Ecology* 35: 445–453
- Cruchaga C, Graff C, Chiang HH, Wang J, Hinrichs AL, Spiegel N, Bertelsen S, Mayo K, Norton JB, Morris JC, Goate A (2011) Association of TMEM106B gene polymorphism with age at onset in granulin mutation carriers and plasma granulin protein levels. *Arch Neurol* 68: 581–586
- Cruts M, Gijssels I, van der Zee J, Engelborghs S, Wils H, Pirici D, Rademakers R, Vandenbergh R, Dermaut B, Martin JJ, van Duijn C, Peeters K, Sciot R, Santens P, De Pooter T, Mattheijssens M, Van den Broeck M, Cuijt I, Vennekens K, De Deyn PP et al (2006) Null mutations in progranulin cause ubiquitin-positive frontotemporal dementia linked to chromosome 17q21. *Nature* 442: 920–924
- Dehmelt L, Halpain S (2005) The MAP2/Tau family of microtubule-associated proteins. *Genome Biol* 6: 204
- DeJesus-Hernandez M, Mackenzie IR, Boeve BF, Boxer AL, Baker M, Rutherford NJ, Nicholson AM, Finch NA, Flynn H, Adamson J, Kouri N, Wojtas A, Sengdy P, Hsiung CY, Karydas A, Seeley WW, Josephs KA, Coppola G, Geschwind DH, Wszolek ZK et al (2011) Expanded GGGCC hexanucleotide repeat in noncoding region of C9ORF72 causes chromosome 9p-linked FTD and ALS. *Neuron* 72: 245–256
- Edbauer D, Neilson JR, Foster KA, Wang CF, Seeburg DP, Batterton MN, Tada T, Dolan BM, Sharp PA, Sheng M (2010) Regulation of synaptic structure and function by FMRP-associated microRNAs miR-125b and miR-132. *Neuron* 65: 373–384
- Filimonenko M, Stuffers S, Raiborg C, Yamamoto A, Malerod L, Fisher EM, Isaacs A, Brech A, Stenmark H, Simonsen A (2007) Functional multivesicular bodies are required for autophagic clearance of protein aggregates associated with neurodegenerative disease. *J Cell Biol* 179: 485–500
- Finch N, Carrasquillo MM, Baker M, Rutherford NJ, Coppola G, DeJesus-Hernandez M, Crook R, Hunter T, Ghidoni R, Benussi L, Crook J, Finger E, Hantantaa KJ, Karydas AM, Sengdy P, Gonzalez J, Seeley WW, Johnson N, Beach TG, Mesulam M et al (2011) TMEM106B regulates progranulin levels and the penetrance of FTD in GRN mutation carriers. *Neurology* 76: 467–474
- Fournet V, de Lavilleon C, Schweitzer A, Giros B, Andrieux A, Martres MP (2012) Both chronic treatments by epothilone D and fluoxetine increase the short-term memory and differentially alter the mood status of STOP/ MAP6 KO mice. *J Neurochem* 123: 982–996
- Garcia ML, Cleveland DW (2001) Going new places using an old MAP: tau, microtubules and human neurodegenerative disease. *Curr Opin Cell Biol* 13: 41–48
- Giannakakou P, Nakano M, Nicolaou KC, O'Brate A, Yu J, Blagosklonny MV, Greber UF, Fojo T (2002) Enhanced microtubule-dependent trafficking and p53 nuclear accumulation by suppression of microtubule dynamics. *Proc Natl Acad Sci USA* 99: 10855–10860
- Gory-Faure S, Windscheid V, Bosc C, Peris L, Proietto D, Franck R, Denarier E, Job D, Andrieux A (2006) STOP-like protein 21 is a novel member of the STOP family, revealing a Colgi localization of STOP proteins. *J Biol Chem* 281: 28387–28396
- Hoogenraad CC, Bradke F (2009) Control of neuronal polarity and plasticity: a renaissance for microtubules? *Trends Cell Biol* 19: 669–676

- Horton AC, Racz B, Monson EE, Lin AL, Weinberg RJ, Ehlers MD (2005) Polarized secretory trafficking directs cargo for asymmetric dendrite growth and morphogenesis. *Neuron* 48: 757–771
- Hu F, Padukkavidana T, Vaegter CB, Brady OA, Zheng Y, Mackenzie IR, Feldman HH, Nykjaer A, Strittmatter SM (2010) Sortilin-mediated endocytosis determines levels of the frontotemporal dementia protein, progranulin. *Neuron* 68: 654–667
- Huynh C, Roth D, Ward DM, Kaplan J, Andrews NW (2004) Defective lysosomal exocytosis and plasma membrane repair in Chediak-Higashi/beige cells. *Proc Natl Acad Sci USA* 101: 16795–16800
- Jan YN, Jan LY (2010) Branching out: mechanisms of dendritic arborization. *Nat Rev Neurosci* 11: 316–328
- Jordens I, Fernandez-Borja M, Marsman M, Dusseljee S, Janssen L, Calafat J, Janssen H, Wubbolts R, Neeftjes J (2001) The Rab7 effector protein RILP controls lysosomal transport by inducing the recruitment of dynein-dynactin motors. *Curr Biol* 11: 1680–1685
- Ju JS, Fuentealba RA, Miller SE, Jackson E, Pivnick-Worms D, Baloh RH, Wehl CC (2009) Valosin-containing protein (VCP) is required for autophagy and is disrupted in VCP disease. *J Cell Biol* 187: 875–888
- Kang JS, Tian JH, Pan PY, Zald P, Li C, Deng C, Sheng ZH (2008) Docking of axonal mitochondria by syntaphilin controls their mobility and affects short-term facilitation. *Cell* 132: 137–148
- Kapitein LC, Hoogenraad CC (2011) Which way to go? Cytoskeletal organization and polarized transport in neurons. *Mol Cell Neurosci* 46: 9–20
- Kuijpers M, Yu KL, Teuling E, Akhmanova A, Jaarsma D, Hoogenraad CC (2013) The ALS8 protein VAPB interacts with the ER-Golgi recycling protein YIF1A and regulates membrane delivery into dendrites. *EMBO J* 32: 2056–2072
- Lang CM, Fellerer K, Schwenk BM, Kuhn PH, Kremmer E, Edbauer D, Capell A, Haass C (2012) Membrane orientation and subcellular localization of transmembrane protein 106B (TMEM106B), a major risk factor for frontotemporal lobar degeneration. *J Biol Chem* 287: 19355–19365
- Letourneau F, Bocquet A, Dubas F, Bartheleix A, Eyer J (2003) Stable tubule only polypeptides (STOP) proteins co-aggregate with spheroid neurofilaments in amyotrophic lateral sclerosis. *J Neuropathol Exp Neurol* 62: 1211–1219
- Morderer D, Nikolaenko O, Skrypkina I, Cherkas V, Tsyba L, Belan P, Rynditch A (2012) Endocytic adaptor protein intersectin 1 forms a complex with microtubule stabilizer STOP in neurons. *Gene* 505: 360–364
- Mukhopadhyay A, Funato K, Stahl PD (1997) Rab7 regulates transport from early to late endocytic compartments in *Xenopus* oocytes. *J Biol Chem* 272: 13055–13059
- Neumann M, Sampathu DM, Kwong LK, Truax AC, Micsenyi MC, Chou TT, Bruce J, Schuck T, Grossman M, Clark CM, McCluskey LF, Miller BL, Masliah E, Mackenzie IR, Feldman H, Feiden W, Kretzschmar HA, Trojanowski JQ, Lee VM (2006) Ubiquitinated TDP-43 in frontotemporal lobar degeneration and amyotrophic lateral sclerosis. *Science* 314: 130–133
- Nicholson AM, Finch NA, Wojtas A, Baker MC, Perkerson RB III, Castaneda-Casey M, Rousseau L, Benussi L, Binetti G, Ghidoni R, Hsiung CY, Mackenzie IR, Finger E, Boeve BF, Ertekin-Taner N, Graff-Radford NR, Dickson DW, Rademakers R (2013) TMEM106B p.T185S regulates TMEM106B protein levels: implications for frontotemporal dementia. *J Neurochem* 126: 781–791
- Nishimura AL, Mitne-Neto M, Silva HC, Richieri-Costa A, Middleton S, Cascio D, Kok F, Oliveira JR, Gillingwater T, Webb J, Skehel P, Zatz M (2004) A mutation in the vesicle-trafficking protein VAPB causes late-onset spinal muscular atrophy and amyotrophic lateral sclerosis. *Am J Hum Genet* 75: 822–831
- Orozco D, Tahirovic S, Rentzsch K, Schwenk BM, Haass C, Edbauer D (2012) Loss of fused in sarcoma (FUS) promotes pathological Tau splicing. *EMBO Rep* 13: 759–764
- Petkau TL, Neal SJ, Milnerwood A, Mew A, Hill AM, Orban P, Gregg J, Lu C, Feldman HH, Mackenzie IR, Raymond LA, Leavitt BR (2012) Synaptic dysfunction in progranulin-deficient mice. *Neurobiol Dis* 45: 711–722
- Press B, Feng Y, Hoflack B, Wandinger-Ness A (1998) Mutant Rab7 causes the accumulation of cathepsin D and cation-independent mannose 6-phosphate receptor in an early endocytic compartment. *J Cell Biol* 140: 1075–1089
- Rademakers R, Neumann M, Mackenzie IR (2012) Advances in understanding the molecular basis of frontotemporal dementia. *Nat Rev Neurol* 8: 423–434
- Reddy A, Caler EV, Andrews NW (2001) Plasma membrane repair is mediated by Ca(2+)-regulated exocytosis of lysosomes. *Cell* 106: 157–169
- Renton AE, Majounie E, Waite A, Simon-Sanchez J, Rollinson S, Gibbs JR, Schymick JC, Laaksovirta H, van Swieten JC, Myllykangas L, Kalimo H, Paetau A, Abramzon Y, Remes AM, Kaganovich A, Scholz SW, Duckworth J, Ding J, Harmer DW, Hernandez DG et al (2011) A hexanucleotide repeat expansion in C9ORF72 is the cause of chromosome 9p21-linked ALS-FTD. *Neuron* 72: 257–268
- Ritz D, Vuk M, Kirchner P, Bug M, Schutz S, Hayer A, Bremer S, Lusk C, Baloh RH, Lee H, Glatter T, Gstaiger M, Aebersold R, Wehl CC, Meyer H (2011) Endolysosomal sorting of ubiquitinated caveolin-1 is regulated by VCP and UBXD1 and impaired by VCP disease mutations. *Nat Cell Biol* 13: 1116–1123
- Rutherford NJ, Carrasquillo MM, Li M, Bisceglia G, Menke J, Josephs KA, Parisi JE, Petersen RC, Graff-Radford NR, Younkin SG, Dickson DW, Rademakers R (2012) TMEM106B risk variant is implicated in the pathologic presentation of Alzheimer disease. *Neurology* 79: 717–718
- Sann S, Wang Z, Brown H, Jin Y (2009) Roles of endosomal trafficking in neurite outgrowth and guidance. *Trends Cell Biol* 19: 317–324
- Shevchenko A, Tomas H, Havlis J, Olsen JV, Mann M (2006) In-gel digestion for mass spectrometric characterization of proteins and proteomes. *Nat Protoc* 1: 2856–2860
- Sholl DA (1953) Dendritic organization in the neurons of the visual and motor cortices of the cat. *J Anat* 87: 387–406
- Smith KR, Damiano J, Franceschetti S, Carpenter S, Canafoglia L, Morbin M, Rossi G, Pareyson D, Mole SE, Staropoli JF, Sims KB, Lewis J, Lin WL, Dickson DW, Dahl HH, Bahlo M, Berkovic SF (2012) Strikingly different clinicopathological phenotypes determined by progranulin-mutation dosage. *Am J Hum Genet* 90: 1102–1107
- Sreedharan J, Blair IP, Tripathi VB, Hu X, Vance C, Rogelj B, Ackerley S, Durnall JC, Williams KL, Buratti E, Baralle F, de Bellerocche J, Mitchell JD, Leigh PN, Al-Chalabi A, Miller CC, Nicholson G, Shaw CE (2008) TDP-43 mutations in familial and sporadic amyotrophic lateral sclerosis. *Science* 319: 1668–1672
- Tackenberg C, Chori A, Brandt R (2009) Thin, stubby or mushroom: spine pathology in Alzheimer's disease. *Curr Alzheimer Res* 6: 261–268
- Tamura N, Draviam VM (2012) Microtubule plus-ends within a mitotic cell are 'moving platforms' with anchoring, signalling and force-coupling roles. *Open Biol* 2: 120132
- Tang W, Lu Y, Tian QY, Zhang Y, Cuo FJ, Liu CY, Syed NM, Lai Y, Lin EA, Kong L, Su J, Yin F, Ding AH, Zanin-Zhorov A, Dustin ML, Tao J, Craft J, Yin Z,

- Feng JQ, Abramson SB et al (2011) The growth factor progranulin binds to TNF receptors and is therapeutic against inflammatory arthritis in mice. *Science* 332: 478–484
- Tuxworth RI, Vivancos V, O'Hare MB, Tear G (2009) Interactions between the juvenile Batten disease gene, CLN3, and the Notch and JNK signalling pathways. *Hum Mol Genet* 18: 667–678
- Urwin H, Authier A, Nielsen JE, Metcalf D, Powell C, Froud K, Malcolm DS, Holm I, Johannsen P, Brown J, Fisher EM, van der Zee J, Bruylant M, Van Broeckhoven C, Collinge J, Brandner S, Futter C, Isaacs AM (2010) Disruption of endocytic trafficking in frontotemporal dementia with CHMP2B mutations. *Hum Mol Genet* 19: 2228–2238
- Uusi-Rauva K, Kytälä A, van der Kant R, Vesa J, Tanhuanpää K, Neefjes J, Olkkonen VM, Jalanko A (2012) Neuronal ceroid lipofuscinosis protein CLN3 interacts with motor proteins and modifies location of late endosomal compartments. *Cell Mol Life Sci* 69: 2075–2089
- Van Deerlin VM, Sleiman PM, Martinez-Lage M, Chen-Plotkin A, Wang LS, Graff-Radford NR, Dickson DW, Rademakers R, Boeve BF, Grossman M, Arnold SE, Mann DM, Pickering-Brown SM, Seelaar H, Heutink P, van Swieten JC, Murrell JR, Ghetti B, Spina S, Grafman J et al (2010) Common variants at 7p21 are associated with frontotemporal lobar degeneration with TDP-43 inclusions. *Nat Genet* 42: 234–239
- Van der Zee J, Van Langenhove T, Kleinberger G, Sleegers K, Engelborghs S, Vandenberghe R, Santens P, Van den Broeck M, Joris G, Brys J, Mattheijssens M, Peeters K, Cras P, De Deyn PP, Cruts M, Van Broeckhoven C (2011) TMEM106B is associated with frontotemporal lobar degeneration in a clinically diagnosed patient cohort. *Brain* 134: 808–815
- Vass R, Ashbridge E, Geser F, Hu WT, Grossman M, Clay-Falcone D, Elman L, McCluskey L, Lee VM, Van Deerlin VM, Trojanowski JQ, Chen-Plotkin AS (2011) Risk genotypes at TMEM106B are associated with cognitive impairment in amyotrophic lateral sclerosis. *Acta Neuropathol* 121: 373–380
- Wils H, Kleinberger G, Pereson S, Janssens J, Capell A, Van Dam D, Cuijt I, Joris G, De Deyn PP, Haass C, Van Broeckhoven C, Kumar-Singh S (2012) Cellular ageing, increased mortality and FTLD-TDP-associated neuropathology in progranulin knockout mice. *J Pathol* 228: 67–76
- Ye B, Zhang Y, Song W, Younger SH, Jan LY, Jan YN (2007) Growing dendrites and axons differ in their reliance on the secretory pathway. *Cell* 130: 717–729

